Systems Biology of Mitosis

seit 1558

Dissertation

to receive the degree Dr. rer. nat from the

Friedrich-Schiller-University Jena

by

Bashar Ibrahim

Born on August 28, 1976 in Mosul

Examiners:
1. PD Dr. Peter Dittrich (Jena Centre for Bioinformatics & FSU Jena)
2. Prof. Dr. Stephan Diekmann (Fritz-Lipmann-Institute Jena)
3. Dr. Andrea Musacchio (European Institute of Oncology)

Oral examination : July 30, 2008
Public defence : September 15, 2008

Systems Biologie der Mitose

seit 1558

Dissertation zur Erlangung des akademischen Grades doctor rerum naturalium (Dr. rer. nat.) vorgelegt dem Rat der Fakultät für Mathematik und Informatik der Friedrich-Schiller-Universität Jena

von

Bashar Ibrahim

geboren am 28.08.1976 in Mosul

Gedruckt mit Unterstützung des Deutschen Akademischen Austauschdienstes

Gutachter:
1. PD Dr. Peter Dittrich (Jenaer Centrum für Bioinformatik & FSU Jena)
2. Prof. Dr. Stephan Diekmann (Fritz-Lipmann-Institut Jena)
3. Dr. Andrea Musacchio (Europäisch Institut für Onkologie)

Tag der letzten Prüfung des Rigorosums: 30. Juli 2008
Tag der öffentlichen Verteidigung: 15. September 2008

To the loving memory of my FATHER,
who passed away on March 14th, 2005.

I've no words to describe him.

I am so proud of his gentle, beautiful ways.

I did see his love. He presented me with it, and it filled my heart with loyalty and dignity.

I dedicate this work to him, to honor these filial remembrances.

... And to my MOTHER.

Her support, encouragement, and constant love have sustained me throughout my entire life.

Acknowledgements

I am deeply indebted to the German Academic Exchange Service (DAAD) for providing me with a high-quality research opportunity to carry out my PhD research in Germany.

I would like to express my gratitude to my advisor, Peter Dittrich, whose research expertise, comprehensive understanding of our work, and patience, added considerable knowledge to my graduate experience. I am most thankful, and indebted to him in all possible ways.

Stephan Diekmann made crucial contributions in the context of this thesis. He became a virtual co-adviser of my research, and provided us with critical knowledge on all the biological aspects of this work.

I am grateful to Eberhard Schmitt for his important and very much welcomed contributions on many mathematical aspects of this work.

I would also like to thank Clemens Beckstein for his unconditional support to our work.

My sincere thanks also go to Rodulf Gorenflo and Martin Hermann, who initially supported my research, and to Mrs. Margret Steuernagel and Mrs. Birgit Klaes (DAAD), who took care of many important aspects related to my wonderful experience in Germany.

I would like to express my profound gratitude to my friends, Mariana Gil and Rodrigo De Marco; their extraordinary love and support were of immeasurable value to me.

I feel a deep sense of gratitude to my family who formed part of my vision and taught me the good things that really matter in life. The happy memory of my father still provides a persistent inspiration for

my journey in this life. I am grateful for my beloved brothers for rendering me the sense and the value of brotherhood. I am glad to be one of them.

Finally, it is my belief that quite a number of people contributed to and supported my work in many different ways. It would virtually be impossible to refer to all of them, and to emphasize their roles and specific contributions. They will, I think forgive me if I name only the two whose contribution proved most far-reaching and decisive: Thorsten Lenser and Heiko Lochas.

Abstract

In mitosis, 'surveillance control mechanisms' regulate transitions across the several stages of cell division. The so called '**M**itotic-**S**pindle-**A**ssembly-**C**heckpoint (^{M}SAC)' and '**E**xit-**F**rom-**M**itosis (EFM)' are examples of such mechanisms. ^{M}SAC ensures the correct segregation of chromosomes by preventing cell-cycle progression until all chromosomes have made proper bipolar attachments to the mitotic spindle through their kinetochores. EFM ensures that each of the two daughter nuclei receives one copy of each chromosome. Both mechanisms are seemingly regulated by the so called 'Anaphase-Promoting-Complex (APC)', bound, in turn, to either 'Cdc20' or 'Cdh1', which are associated regulatory proteins. APC remains inactive during metaphase. In the transition from metaphase to anaphase, and only after all chromosomes are attached, a newly formed 'APC:Cdc20' complex mediates the ubiquitination and degradation of the protein 'Securin'; this leads, in turn, to the activation of the protein 'Separase', the dissolution of the so called 'Cohesin Complex', and, eventually, to chromatid separation. 'APC:Cdc20' also mediates the initial phase of 'Cyclin B' proteolysis. In the transition from anaphase to telophase, APC:Cdh1 completely ubiquitinates 'Cyclin B', thus inactivating a protein called 'CyclinB:Cdk1-Mitotic-Kinase' and triggering the exit from mitosis. Both ^{M}SAC and EFM prevent chromosome miss-segregation and aneuploidy, and their failure eventually leads to cell death; both mechanisms have been implicated in cancer. Our understanding of mitotic regulatory mechanisms has significantly improved in recent years. Yet, ^{M}SAC and EFM remain poorly understood. Hence, we benefited from *in-silico* modeling and simulation approaches embedded in a cross-disciplinary framework, typically referred to as Systems

Biology, in order to contribute to a deeper understanding of these mitotic regulatory mechanisms. We first focused on the question how 'Cdc20' availability is controlled prior to the attachments of all chromosomes; or, in other words, how 'APC:Cdc20' formation is eventually prevented. It had been proposed that Cdc20 remains fully sequestered until the last chromosome is attached. By using a Systems Biology approach to this question, we built-up and tested predictions from a series of dynamic models fed with empirical data (Ibrahim et al., 2008b,c). According to our results, cells are unable to completely sequester Cdc20 until the last chromosome is attached. Next, we asked whether a complex called 'MCC' might be able to fully prevent 'APC:Cdc20' formation by binding APC, thereby sequestering it fully, prior to the attachment of all chromosomes. To tackle this question, we built-up a combined *in-silico* model fed with empirical data on APC levels prior to chromosome attachment (Ibrahim et al., 2008a). Our results then showed that MCC can fully sequester APC prior to chromosome attachment. This would eventually prevent 'APC:Cdc20' activity. From the later results, one still needs to ask how a complex like 'MCC:APC' would fall apart after chromosome attachment. In order to address this question, we constructed two equally suitable model variants, called the "Dissociation" and "Convey" models, and validated them by means of mutation experiments (Ibrahim et al., 2008a). Moreover, we also developed and tested the robustness of a qualitative model of ^{M}SAC (Ibrahim et al., 2007). Finally, we incorporated an adapted 'EFM-model' involving 'APC:Cdh1' activity into an integrative model involving APC:Ccd20 activity, thereby addressing simultaneously the functioning of both transition control mechanisms, ^{M}SAC and EFM.

Deutsche Zusammenfassung

Die Übergänge zwischen den einzelnen Phasen der Mitose werden durch 'surveillance control mechanisms' reguliert. Zwei Beispiele hierfür sind der '**M**itotic-**S**pindle-**A**ssembly-**C**heckpoint (^{M}SAC)' und der '**E**xit-**F**rom-**M**itosis (EFM)'. ^{M}SAC sichert die korrekte Teilung der Chromosomen, indem der Fortschritt des Zellzyklus angehalten wird, bis alle Chromosomen durch ihre Kinetochore fest mit dem mitotischen Spindelapparat verbunden sind. EFM stellt sicher, dass jeder der beiden Zellkerne nach der Teilung über genau eine Kopie eines jeden Chromosomes verfügt.

Beide Mechanismen werden anscheinend durch den 'Anaphase-Promoting-Complex (APC)' reguliert, welcher wiederum an die regulativen Proteine 'Cdc20' und 'Cdh1' gebunden ist. APC bleibt inaktiv während der Metaphase. Beim Übergang von der Metaphase zur Anaphase, nachdem alle Chromosomen an den Spindelapparat gekoppelt sind, katalysiert der neu geformte 'APC:Cdc20' Komplex die Ubiquitination und Degradierung des Proteins 'Securin'; dies wiederum führt zur Aktivierung des Proteins 'Separase', zur Auflösung des 'Cohesin Komplexes' und zur Trennung der Chromatide.

'APC:Cdc20' katalysiert auch die Frühphase der Proteolyse des 'Cyclin B'. Beim Übergang von Anaphase zu Telophase wird 'Cyclin B' komplett durch APC:Cdh1 ubiquitiniert, was zur Inaktivierung des Proteins 'CyclinB:Cdk1-Mitotic-Kinase' und schließlich zum Austritt aus der Mitose führt. Sowohl ^{M}SAC als auch EFM verhindern fehlerhafte Chromosomenteilung und Aneuploidie, ihr Versagen führt zum Zelltod. Beide Mechanismen sind mit der Entstehung von Krebserkrankungen in Verbindung gebracht worden.

In den letzten Jahren hat sich unser Verständnis der regulativen Mechanismen in der Mitose drastisch verbessert, aber ^{M}SAC und EFM sind weiterhin schlecht verstanden. *In silico* Modellierungs- und Simulationsansätze - eingebettet in die interdisziplinäre Systembiologie - können

uns helfen, ein tieferes Verständnis dieser regulativen Mechanismen zu erreichen.

Wir haben uns zuerst auf die Frage konzentriert, wie die Verfügbarkeit von 'Cdc20' vor dem Andocken der Chromosomen kontrolliert wird, oder in anderen Worten, wie die Bildung von 'APC:Cdc20' verhindert wird. Ein bestehender Vorschlag besagt, dass Cdc20 vollständig festgehalten wird bis das letzte Chromosom angedockt ist. In einem systembiologischen Zugang zu dieser Fragestellung haben wir eine Reihe von dynamischen Modellen erstellt, basierend auf empirischen Daten (Ibrahim et al., 2008b,c), um Vorhersagen zu erstellen und zu testen. Unsere Ergebnisse implizieren, dass Zellen Cdc20 nicht komplett bis zum Andocken des letzten Chromosomes festhalten können.

Als nächstes fragten wir, ob der sogenannte 'MCC' Komplex in der Lage sein könnte, die Bildung von 'APC:Cdc20' vor dem Andocken aller Chromosome vollständig zu verhindern, indem er APC bindet und festhält. Um diese Frage zu attackieren, haben wir ein kombiniertes *in silico* Model erstellt und mit empirischen Daten über APC Levels vor dem Andocken der Chromosomen gefüttert (Ibrahim et al., 2008a). Unsere Ergebnisse zeigen, dass MCC APC vollständing festhalten kann, was die Aktivität von 'APC:Cdc20' verhindern würde.

Aufbauend auf diesem Resultat stellt sich nun die Frage, wie der 'MCC:APC' Komplex nach dem Andocken der Chromosome auseinanderfällt. Um diese Frage zu addressieren, haben wir zwei Modellvarianten erstellt - die sogenannten "Dissociation" und "Convey" Modelle - und diese mit Hilfe von Mutationsexperimenten validiert (Ibrahim et al., 2008a). Darüber hinaus haben wir ein qualitatives Modell von ^{M}SAC erstellt und dessen Robustheit untersucht (Ibrahim et al., 2007).

Zum Abschluss haben wir ein 'EFM' Modell, welches 'APC:Cdh1' Aktivität mitbeachtet, in ein integratives Modell inklusive APC:Cdc20 eingefügt. Das entstandene Modell enthält nun gleichzeitig die Funktion von ^{M}SAC und EFM, der beiden Mechanismen der Transitionskontrolle.

Contents

"Mathematics, rightly viewed, possesses not only truth, but supreme beauty - a beauty cold and austere, like that of sculpture". Bertrand Russell (1872 - 1970)

"Biologists must constantly keep in mind that what they see was not designed, but rather evolved".

Francis Crick, *What Mad Pursuit*, 1990, p.138.

Chapter 1

Orientation, Motivation and Aim of the study

Contents

1.1 Why to use a Systems Biology Approach to Mitosis Transition Controls?

The renowned theoretical and applied mathematician Norbert Wiener stated that living organisms can be thought of as systems governed by feedback and regulatory mechanisms, which are, in turn, plausible of being understood (Wiener, 1948). The study of both complexity (Holland, 1995) and control theory (von Bertalanffy, 1968) now receives increasing attention by scientists following the so called "Systems Biology" approach to research. Some refer to Systems Biology as an emergent field that "studies cells as spatiotemporal networks of interacting molecules using an integrative approach of theory (mathematics, physics, engineering), experimental biology (genetics, molecular biology, physiology), and quantitative network-wide analytical measurement (analytical biochemistry, imaging) (Bruggeman, 2007)." Systems Biology therefore deals with modeling and simulation, and involves concepts from mathematics, computer science, physics, biochemistry, and engineering.

Living systems are undoubtedly complex. They exhibit organizational principles, chemical uniqueness, variability, genetic programs, and historical nature, properties embedded in the concepts of pleiotropy and polygeny (Mayr, 1982). It follows that only systems, or subsystems, that show their own dynamics, but not their isolated, constitutive elements, can be thought of as the subject matter of functional biology (Núñez and Marco, 2007). We need to examine the structure and dynamics of biological functions, rather than the characteristics of the isolated parts of a cell or organism. In the context of cell biology, this may have a major impact on the future of biological and medical research (Kitano, 2002b,a). There is a need which drives Systems Biology. It relies on an increasing knowledge on a cell's constitutive elements, accompanied by a simultaneous lack of comparable knowledge on the ensuing interactions and organizing principles that govern them. Computer science already proved fruitful in biology, and it now appears as increasingly difficult to study complex cellular functions without the help of computational, modeling approaches.

1.1 Why to use a Systems Biology Approach to Mitosis Transition Controls?

Mitosis can be thought of as a finely regulated and exceedingly complex process. During the process of cell division, a cell's chromosomes are eventually distributed between two daughter nuclei. Molecular biologists typically characterize the activity, aggregation and interactions of tens of cellular elements involved in mitosis, although the relation between such interacting elements and their respective environment remains still elusive. Predictions, therefore, are not straightforward. There is a need for a system-level understating of the regulatory mechanisms involved in mitosis. This might be of major relevance for medical research, as well as for a better understating of other cellular processes. We shall refer to our work as to "Systems Biology of Mitosis". Our focus is on human cells, and we benefit from modeling and simulation approaches embedded in a cross-disciplinary framework, in order to contribute to a deeper understanding of mitotic regulatory mechanisms. Below there is a list of items that may help in illustrating what we can gain from a Systems Biology approach to mitosis.

Identifying a System's Structure: Understanding the functioning of a biochemical network demands identifying its underlying pathways. One can obtain knowledge about the several elements involved in the mechanisms controlling mitosis, as well as information on their -isolated- interactions. Yet, one also needs to ask whether and how these elements and interactions are topologically organized. This would eventually allow understanding a system's functional structure by means of accessible network models. Analyzing these networks would lead, in turn, to the development of new, testable hypotheses. (e.g., Appendix A, Section A.2)

Capturing a System's Behavior: Modeling and simulation approaches allow qualitative as well as quantitative analyzes of a system's behaviour. They permit to capture not only the dynamics of an evolving system, but also its specific state at any given time on the basis of kinetic data. To this end, one uses deterministic (ODEs), stochastic (particle simulation), or even mixed (SDEs) modeling approaches. (See Chapters 3-7)

Evaluating a System's Intrinsic Properties: A Systems Biology approach to mitosis allows predictions based on stability and sensitivity analyzes. It also allows capturing the effects of noise, bifurcations, and chaotic attractors.

Chapter 6 helps in illustrating the relevance of these intrinsic properties in the context of a qualitative model of anaphase initiation.

Capturing a System's Signalling Pathways: The functioning of the transition control mechanisms depends upon regulating signals; a Systems Biology account of such signals would eventually lead to a deeper understanding of the entire process of mitosis. (e.g., Chapter 5).

3D-Modeling: A Systems Biology approach to mitosis allows evaluating specific effects of a three-dimensional 'environment' on those interactions occurring among the several elements of a network. The term 'environment' here refers to variations arising from diffusion effects, the movements of microtubules, changes in the cell volume, localization and binding specificities, etc. This is important because the functioning of the several networks controlling mitosis influences the cellular space, and vice versa; there is a cross-talk between a given environment and the functional processes embedded in it (Figure 1.1). To tackle the effects of such a phenomenon, one benefits from partial differential equations (PDEs), cellular automate, or even mixed approaches like stochastic partial differential equations (SPDEs). By means of such tools, rich dynamics and powerful predictions are within reach.

Mutual Benefits Across Disciplines: Systems Biology demands a fusion of concepts from several disciplines, thereby integrating different computational instruments into a general computational infrastructure. In the present context, new concepts arise from well-established and tested results from mathematics, computer science, molecular biology, and biochemistry. It is sometimes difficult to handle data arising from such an inter-disciplinary approach. As a by-product of the present work, a software tool, called "Mitosis Arena", is being developed to help in visualizing and interpreting the flood of data related to mitosis transitions control mechanisms (Figure 1.1). Such a tool would eventually be integrated and communicated via SBML (Systems Biology Markup Language).

A cross-talk between theoretical and empirical accounts of mitosis: Biological research can sometimes be the subject of ontological reductionism;

Systems Biology aims to counterbalance such a tendency. We suggest that a Systems Biology approach to mitosis would prove fruitful in proposing testable hypotheses, simply because it gives off useful predictions based on the countless interactions among the various cellular elements whose behaviors cannot simultaneously be addressed in the laboratory. (See, for example, Chapter 5)

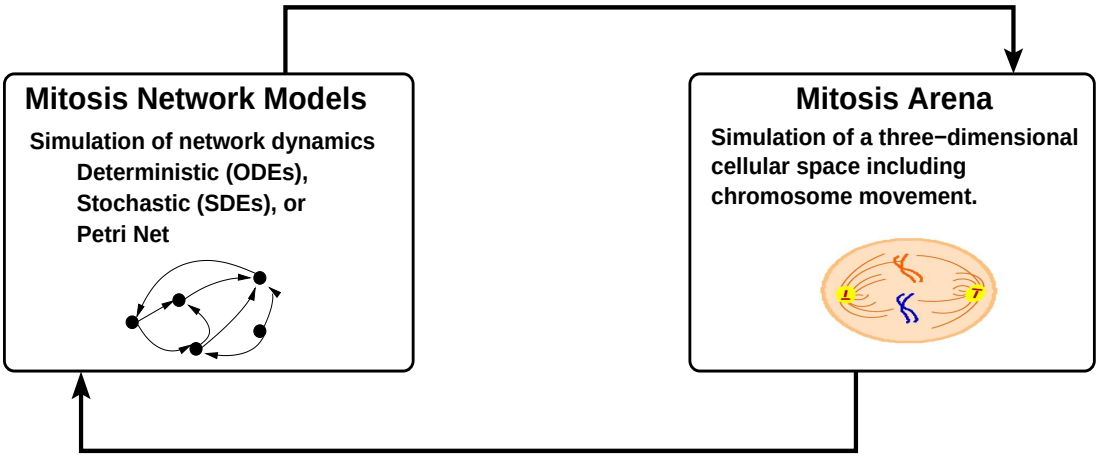

Figure 1.1: Schematic diagram of the simulation environment. The new tool called Mitosis Arena will allow to load a network model (SBML) describing the bio-chemical reaction mechanism. The simulation includes the three-dimensional movement of the chromosomes, which influences the bio-chemical dynamics through a changing topology and which in turn is influenced by the state of the bio-chemical network species. This tool is necessary, because understanding the network controlling mitosis requires also to consider a changing cellular space whose topological change is influenced by the biochemical network, and vice versa where the spatial structure influences the dynamics of the biochemical system.

1.2 Background, Specific Problems, and Results

In the present context, our emphasize is on two different, still connected mitosis transition control mechanisms, namely, the **M**itotic **S**pindle **A**ssembly **C**heckpoint **(MSAC)** and **E**xit **F**rom **M**itosis **(EFM)**. MSAC ensures the correct segregation of chromosomes by restraining cell-cycle progression from entering anaphase until all chromosomes have made proper bipolar attachments to the mitotic spindle. MSAC thus ensures the fidelity of chromosome segregation; its failure leads to aneuploidy (Kim and Kao, 2005; Steuerwald, 2005), for example, and might contribute to cancer (Compton, 2006; Gupta et al., 2003). In principle, MSAC controls the activity of a complex of proteins called "Anaphase Promoting Complex", or APC, during the transition from metaphase to anaphase, when chromosomes are not yet attached. MSAC becomes inactive once all chromosomes are attached. At this time, APC interacts with its co-activator, a protein called "Cell Division Cycle", or Cdc20. The active, ensuing complex "APC:Cdc20" has two functions. First, it activates a protein called "Separase", involved in breaking-up the so called "Cohesion ring", which eventually leads to the separation of the sister chromatids. Second, APC:Cdc20 is involved in the partial degradation of "Cyclin B", the mitotic cyclin. Mitosis then progresses, and becomes the subject of the second transition control mechanism, the Exit From Mitosis mechanism. Generally speaking, EFM ensures that each of the two daughter nuclei receives one copy of each chromosome. Its main role is to guarantee a full degradation of Cyclin B via the activity of the complex "APC:Cdh1", formed by APC and its second co-activator, a protein called Cdh1. After the full degradation of Cyclin B, the process of cell division progresses into cytokinesis.

Both MSAC and EFM are complex mechanisms involving numerous interacting elements. They are the subject of complex dynamics, in addition. Therefore their functional and topological structures remain still poorly understood. At present, no model provides a satisfactory account of how MSAC actually works. In contrast, there are several models describing how EFM works, all them based on data from yeast. These two mechanisms have not yet been integrated into a

single model. Here we aim to contribute towards an integrative model explaining both ^{M}SAC and EFM in human cells.

We first focused on the question how the availability of Cdc20 is controlled prior to the attachments of all chromosomes. In other words, how APC:Cdc20 formation is eventually prevented. It has been proposed that Cdc20 remains fully sequestered until the last chromosome is attached. The first candidate thought to fully sequester Cdc20 appeared to be a ^{M}SAC -protein called "Mad2"(e.g., Luo et al., 2002; Sironi et al., 2001a). Two basic models, called "Exchange" (Luo et al., 2004) and "Template" (DeAntoni et al., 2005a), have been developed on the basis of such hypothesis. By using a Systems Biology approach to this question, we built-up a series of dynamic models, fed them with empirical data, and tested predictions from both the Template and the Exchange models. Our results indicate that Mad2 is not sufficient to fully sequester Cdc20, and that only the Template model appears to be partially consistent with our simulations (See Chapter 3). It has also been proposed that a second protein, called "BubR1", can sequester Cdc20 prior to the attachment of all chromosomes (e.g., Bolanos-Garcia et al., 2005; Davenport et al., 2006). BubR1 binds Cdc20 within two seemingly different contexts. In the first context, it forms an isolated complex with Cdc20, whereas in the second it is part of a larger complex of proteins (BubR1, Cdc20, Mad2, Bub3) called "Mitotic Checkpoint Complex", or MCC. We incorporated both contexts in two different models, and found that Cdc20 can be fully sequestered by BubR1 neither in the first nor in the second context. Moreover, it has been postulated that MCC formation can be either Kinetochore-independent (KIM) or Kinetochore-dependent (KDM) (Musacchio and Salmon, 2007; for details, see Chapter 4). We found that only the Kinetochore-dependent model can -partially- account for the availability of Cdc20 both before and after the attachment of all chromosomes. Next, we asked whether MCC might be able to fully prevent APC:Cdc20 formation by binding APC, thereby sequestering it fully, prior to the attachment of all chromosomes. To tackle this question, we built-up an *in-silico* model that combines the Template model, the MCC-Kinetochore-dependent formation model, and empirical data on APC levels prior to chromosome attachment. Our results show that MCC can fully sequester APC prior to chromosome attachment, thereby preventing

APC:Cdc20 activity. If this was the case in nature, one would also need to ask how such a complex as the MCC:APC complex would fall apart after chromosome attachment. Hence, we built-up two equally suitable model variants addressing this issue, called "Dissociation" and the "Convey" models, and validated them by means of mutation experiments (see Chapter 5). Moreover, we also developed a qualitative model of ^{M}SAC , and tested its robustness (see Chapter 6). Finally, we incorporated an adapted EFM model that involves the activity of APC:Cdh1 into an integrative model that also involves the activity of APC:Ccd20. Hence, we addressed simultaneously the functioning of both transition control mechanisms, ^{M}SAC and EFM. This integrative model is presented in Chapter 7.

Important questions still remain open. For example, how the checkpoint remains active until all kinetochores are attached? Answering this kind of questions, however, demands understanding how the mitosis transition control mechanisms work in three dimensions. For such an understanding to be achieved, new tools are needed. Therefore, we are currently developing a software tool called "Mitosis Arena", in order to test network models of mitosis within a 3-D framework. "Mitosis Arena" will be available to the scientific community, so that alternative models could easily be studied within a dynamical 3-D environment (Figure 1.1). It has been designed in accordance with standard languages (i.e., SBML), and would eventually be combined with other Systems Biology software tools.

1.3 This thesis is based on the following publications

Peer-reviewed articles in international journals

◇ Ibrahim, B., Dittrich, P., Diekmann, S., Schmitt, E. Mad2 binding is not sufficient for complete Cdc20 sequestering (an *in-silico* study). BioPhy Chem. Journal, 134, 93-100., 2008.

◇ Ibrahim, B., Schmitt, E., Dittrich, D., Diekmann, D. *In-silico* study of kinetochore control, amplification, and inhibition effects in MCC assembly. BioSystems Journal, 2008. (In press)

◇ Ibrahim, B., Diekmann, S., Schmitt, E., Dittrich, P. *In-silico* Modeling of the Mitotic Spindle Assembly Checkpoint. PLoS ONE Journal, 3(2): e1555, 2008.

◇ Ibrahim, B, Dittrich, P., Diekmann, S., Schmitt, E. Stochastic effects in a compartmental model for mitotic checkpoint regulation. Journal of Integrative Bioinformatics, 4(3):66, 2007.

Peer-reviewed articles in proceedings

◇ Rohn, H., Ibrahim, B., Lenser, T., Hinze, T., Dittrich., Enhancing Parameter Estimation of Biochemical Networks by Exponentially Scaled Search Steps. In: E. Marchiori and J. H. Moore (Eds.), Proceedings of the Sixth European Conference on Evolutionary Computation, Machine Learning and Data Mining in Bioinformatics (EvoBIO), Napoli, LNCS 4973, pp. 177-187, Springer Verlag, 2008.

◇ Lenser, T., Hinze, T., Ibrahim, B., Dittrich, P., Towards evolutionary network reconstruction tools for systems biology. In: E. Marchiori, J.H. Moore, J.C. Rajapakse (Eds.), Proceedings of the Fifth European Conference on Evolutionary Computation, Machine Learning and Data Mining in Bioinformatics (EvoBIO), Valencia, LNCS 4447, pp 132-142, Springer Verlag, 2007.

1. ORIENTATION, MOTIVATION AND AIM OF THE STUDY

"It is the weight, not numbers of experiments that is to be regarded". Isaac Newton (1642-1727)

"Biology will tell you a lot of things, but there are many that it can not explain and you need to look at physics instead". Walter Gilbert(1932-)

Chapter 2

Mitosis Transition Controls

Contents

2.1 Cell Division

Cell[1] division is accomplished by means of two different processes in eukaryotes: mitosis[2] and meiosis[3]. During mitosis, a somatic cell (and also eukaryotic unicellular organisms) divides to produce two genetically identical cells. In contrast, during meiosis, a sex cell undergoes two stages of cell division resulting in four haploid cells (gametes) each of which has only a single complement of chromosomes. In this thesis we will focus on transition control mechanisms of mitosis.

In an elaborate series of events known as "cell cycle", *chromosomes*[4,5] are replicated and then, together with other components, distributed into the two daughter cells. The cell cycle is composed of five distinct phases: G1 (Gap 1), S (Synthesis)-phase, G2 (Gap 2) (which are collectively called interphase), Mitosis and Cytokinesis (which are collectively called M-phase) (see Figure 2.1). During interphase, the rate of biosynthetic activity is high. During G1 various proteins are synthesised that are required in S-phase, for example those needed for DNA replication. G1's duration is highly variable; in humans it can take between 6-12 h. Most cells in G1 become committed to either continued division or exit from the cell cycle. A cell may pause for an extended period in G1 or may even enter in a non-dividing state called G0. In S-phase the DNA is replicated so that at the end of this phase the genome is duplicated from 2n to 4n. In human's cells, the S-phase lasts 6-8 h. The cell then enters into G2. Now proteins are synthesised which are for example involved in the production of microtubules required during mitosis. In humans G2 lasts 3-4h. Finally, after G2, the cell enters into M-phase, during which chromosomes are segregated into the two daughter cells. This process last

[1]**Robert Hooke** (1635 1703), an English polymath, was the first person to coined the term "cell" to describe the basic unit of life, after viewing slices of cork through a microscope in about 1663.

[2]**Mitosis** has been first identified by the anatomist Walther Flemming (1882).

[3]**Meiosis** has been first identified by the German embryologist Oscar Hertwig (1875).

[4]**Chromosomes** are organized structures of DNA and proteins. A chromosome contains a single continuous piece of DNA, which contains many genes, regulatory elements and other nucleotide sequences. Chromosomes also contain DNA-bound proteins, which serve to package the DNA and control its functions.

[5]**Karl Wilhelm von Ngeli** (1817 1891), a Swiss botanist, he discovered what would later become known as chromosomes.

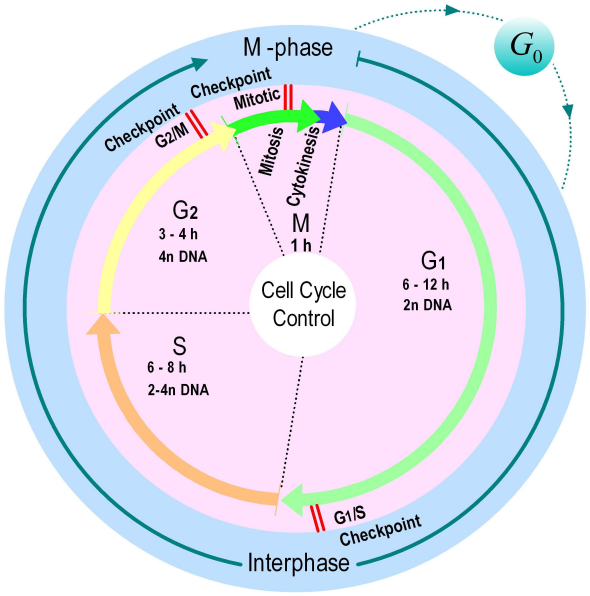

Figure 2.1: Cell cycle phases in eukaryotic cells. Interphase consisting of G1, S, and G2 -phases, is followed by M-phase, consists of mitosis (or could be meiosis) and cytokinesis. G0 refers to a pause period or an extended periods in G1 or even inter nondividing state. The time course is an example for the human cell cycle. G1, occurs before S-phase, whereas G2 occurs before M-phase. The DNA is 2n in both G0 and G1, and 4n in both G2 and M -phases. n is the number of DNA strands The figure also depict cell cycle checkpoints. In interphase, G1/S is the first checkpoint, followed by G2/M. In M-phase, the mitosis checkpoint " metaphase-to-anaphase transition checkpoint".

approximately 1 h in human cells. Chromosome segregation of newly replicated *sister chromatids*[1] into daughter cells is a critical and central event. It ensures that both of the newly divided cells receive a full complement of chromosomes. If this event is not properly completed, the newly divided cells will probably lack essential genes resulting in cellular malfunction.

From a technical point of view, cells behave like an oscillator. In mitosis, two new daughter cells are created from the mother cell. In G1, these daughter cells grow until they reach a mass which allows them to enter a new round of duplication. This new round begins with entry into the S-phase. Once genome duplication is

[1] **Sister chromatids** are identical copies of a chromosome. In other words, sister chromatids contain the same genes

completed, the cell prepares for division in G2. In mitosis, when a checkpoint has checked the correct state of the cell, the cell finally dives and creates new daughter cells. During this oscillation, the cell runs through kinetically very different states: static or semi-static, dynamic, intermediate and steady-states. When modeling the mitotic transition control, all input and output signals across these cell cycle phases must be incorporated as precisely as possible (see Appendix A). In doing this, the work can benefit from a deterministic and stochastic modeling base for biochemical reaction networks.

This work focuses on the mechanisms controlling human mitosis. The goal is to understand how chromosomes segregation is controlled by the mitotic checkpoint. Since the proteins carrying out these mechanisms were already identified in experimental laboratories, this work intends to tackle how these proteins interact with each other and which are the rules for their combined function. Ultimately, we intend to simulate empirical knowledge and formulate straight forward, useful predictions to be experimentally tested in the future. The goal is to determine the essential features of mitotic control of the meta- to anaphase transition.

2.2 Mitosis

The German anatomist Walther Flemming[1](1882), a pioneer of mitosis research, was one of the first scientists to give a detailed description of the numerous events during cell division in animals and named the division of somatic cells “mitosis”. He originally minted the term “mitosis” from the Greek word for thread, reflecting the shape of mitotic chromosomes. Mitosis is the most dramatic period of the cell cycle, involving a major reorganization of virtually all cell components. Although many of the details of mitosis vary among different organisms, the fundamental processes that ensure the faithful segregation of sister chromatids are conserved in all eukaryotes. These basic events of mitosis include chromosome condensation,

[1]**Walther Flemming**: (1843-1905) a founder of the science of cytogenetics (the study of the cell’s hereditary material, the chromosomes). He was the first to observe and describe systematically the behaviour of chromosomes in the cell nucleus during normal cell division (mitosis).

formation of the mitotic spindle, and attachment of chromosomes to the spindle *microtubules*[1]. Sister chromatids then separate from each other and move to opposite poles of the spindle, followed by the formation of daughter nuclei (see Figure 2.3).

Mitosis is simply described as having four stages: *prophase*, *metaphase*, *anaphase*,[2] and *telophase*[3]; these stages follow one to another as a continuous process without interruption. The entire four-stage division process in human cells lasts about one hour in average.

Prophase During prophase the chromosomes become condensed and key proteins bind the *kinetochores*[4] preparing for *spindle*[5] attachment. *Centrioles*[6] begin moving to opposite ends of the cell and fibers extend from the centrosomes. The nuclear membrane dissolves. Proteins link the multi-protein kinetochore complex at the centromeres with the microtubules and the chromosomes move to the equatorial plate. Sometimes, this stage is classified in two sub-stages, Prophase and late Prophase or Prometaphase (see Figure 2.3).

[1]**Microtubule**: Eukaryotic cells rely on self assembling array of microtubules (MTs) known as the spindle to effect chromosome segregation. MTs emanate from microtubule organizing centers (MTOCs) and form attachments with the cell cortex and with anti-parallel MTs from the opposite pole. Moreover, MTs attach to the chromosomes by binding to the kinetochore. A microtubule is a polymer of globular tubulin subunits, which are arranged in a cylindrical tube measuring about 25 nm in diameter (see Figure 2.2)

[2]**Prophase, metaphase and anaphase** were first coined by Eduard Strasburger in 1884.

[3]**Telophase** was first introduced by Martin Heidenhain in 1894

[4]**The kinetochore** is a large A multiprotein structure, positioned at the central constriction of each chromosome, contains two regions: an inner kinetochore, which is tightly associated with the centromere DNA; and an outer kinetochore, which interacts with microtubules (see Figures 2.2 and 2.8). Kinetochores consist of more than 45 different proteins. Many of these proteins are conserved throughout eukaryote species (see Figure 2.8).
The centromere is a single site on the chromosome that is responsible for assembling the kinetochore, which mediates chromosome attachment to the microtubule spindle and all chromosome movements.

[5]**Spindle** is a network of protein fibers that forms in the cytoplasm of a cell during cell division. The spindle grows forth from the centrosomes and attaches to the chromosomes after the latter have been replicated, and the nuclear membrane dissolves. Once attached, the spindle fibers contract, pulling the replicate chromosomes apart to opposite poles of the dividing cell. It often referred to as the mitotic spindle during mitosis and the meiotic spindle during meiosis.

[6]**Centrioles** are cylindrical structures, found in eukaryotic, that are composed of groupings of microtubules arranged in pattern. They help to organize the assembly of microtubules during cell division.

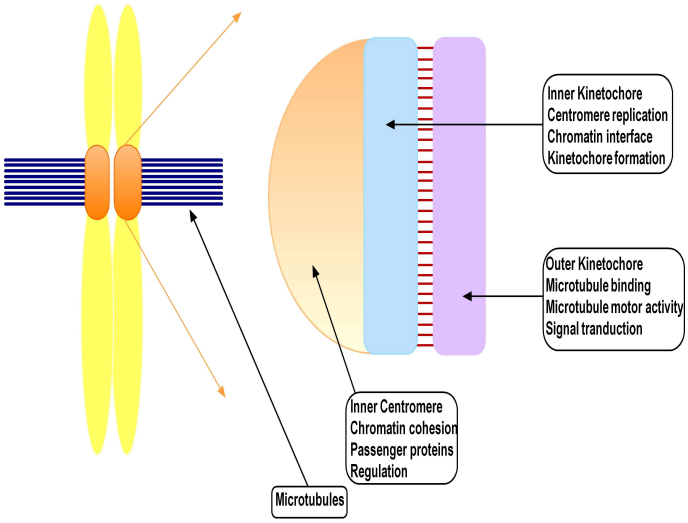

Figure 2.2: Organization of the kinetochore. A complex structure that specifies the attachments between the chromosomes and microtubules of the spindle and is thus essential for accurate chromosome segregation. The left hand side refers to the sister chromatids. The right hand side refers to the kinetochore structure. The eukaryotic kinetochore consists of an inner, gap, and outer regions. The blue stained material are the microtubules that form the mitotic spindle. The Navajo White color refers to the centromere

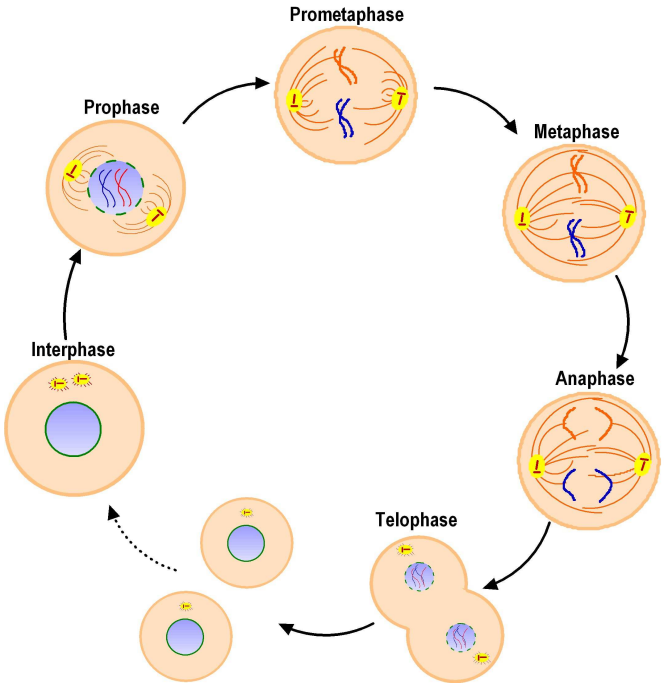

Figure 2.3: Depiction of the distinct stages of mitosis. Interphase is divided into G1-, S- and G2-phase, followed by M-phase, which is divided into mitosis and cytokinesis. Mitosis is simply described as having four stages: prophase, metaphase, anaphase, and telophase; the stages follow one another as a continuous process without interruption or pause.

Metaphase In this stage, chromosomes are attached to microtubule spindles via their kinetochores followed by alignment on the metaphase plate half way between the two spindle poles. This state is controlled by the mitotic checkpoint. Once all the chromosomes are aligned, mitosis can progress into the next stage.

Anaphase The paired chromosomes separate at the kinetochores and move to opposite sides of the cell. Motion results from a combination of kinetochore movement along the spindle microtubules and through the physical interaction of polar microtubules.

Telophase After successful segregation of the chromosomes, chromatids arrive at opposite poles of the cell and new membranes are formed around the daughter nuclei. The chromosomes disperse and are no longer visible under the light microscope. The spindle fibers disperse and partitioning of the cell begins.

Cytokinesis It is the final phase, the cell cytoplasm of the mother cell is physically divided in two daughter cells. Cytokinesis was one of the first cell cycle events observed by cell biological techniques (see Figure 2.3).

Two essential transition control mechanisms, namely, 'initiation of anaphase" and "exit from mitosis", govern mitosis. In the following sections, these mechanisms are described.

2.3 Checkpoints in Cell Cycle Regulation

Checkpoints are surveillance control mechanisms that monitor the progression of the cell cycle, so that in the case of malfunction the cell cycle can be arrested at a given stage by specific signals. The central components of the cell cycle control system are a family of enzymes called cyclin-dependent kinases (Cdks). Like others protein kinases, Cdks catalyze the covalent attachment of phosphate groups derived from ATP to protein substrates. This phosphorylation results in changes in the substrate's enzymatic activity or its interaction with other element species. A cyclin-dependent kinase is activated by association with a cyclin forming a cyclin-dependent kinase complex. Different types of cyclins are produced at different cell cycle phases. Cyclins and CDKs determine a cell's progress through the cell cycle (see Table 2.1). Malfunctions of any control during cell division might lead to serous diseases (see section 2.4.2). In order to avoid any failure, the cell verifies that proper conditions are satisfied at crucial steps in the division process. In general, cell cycle progression is governed by three major checkpoints (Figure 2.1).

- The first checkpoint control occurs in G1-phase, and is called the **G1/S checkpoint**. It checks the cell size, nutritional, status DNA/cellular damage mating status and growth factor availability. In case of damage during G1, it will delay the onset of S-phase and DNA replication.
- The second checkpoint control occurs in G2-phase, and is called the **G2/M checkpoint**. It monitors the completion of DNA replication and assures accurate transmission of genetic material and the completion of mitosis.
- The third checkpoint is the metaphase-to-anaphase transition control (mitotic, or chromosome segregation, or division control) named the **M**itotic **S**pindle **A**ssembly **C**heckpoint (**^{M}SAC**)(in order to differentiate it from the Meiosis checkpoint). The ^{M}SAC functions to ensure faithful chromosome segregation by delaying cell division until all chromosomes are correctly oriented on the mitotic spindle. It is an important element of mitosis transition control and thus, is a main focus of this thesis.

The Major Cyclins and Cdks

	Homo sapiens		Saccharomyces cerevisiae	
Cyclin:Cdk complex	**Cyclin**	**Cdk partner**	**Cyclin**	**Cdk partner**
G1-Cdk	Cyclin D*	Cdk4, Cdk6	Cln3	Cdk1**
G1/S-Cdk	Cyclin E	Cdk2	Cln1, 2	Cdk1
S-Cdk	Cyclin A	Cdk2	Clb5, 6	Cdk1
M-Cdk	**Cyclin B**	**Cdk1****	**Clb1, 2, 3,4**	**Cdk1**

Table 2.1: The major cyclins and Cdks for progression through the cell cycle in Homo sapiens and Budding Yeast. *There are three D cyclins in mammals (cyclins D1, D2, and D3), **The original name of Cdk1 was Cdc2 in both Homo sapiens and fission yeast, and Cdc28 in budding yeast. For S. pombe, the major cyclins are; Puc1, Cig2, Cdc13, and Puc1 for G1/S, S, M, and G1 -phases respectively. This table has been taken and modified from (Alberts et al., 2002). The bold line denotes mitosis cyclin, which is of our interest.

The following focusses on the human ^{M}SAC mechanism.

2.4 Anaphase Initiation Control

2.4.1 The Mitotic Spindle Assembly Checkpoint (^{M}SAC)

Chromosomes segregation of newly replicated sister chromatids into daughter cells during anaphase is a critical event of mitosis. ^{M}SAC ensures the correct segregation of chromosomes by restraining cell cycle progression from entering anaphase until all chromosomes have made proper bipolar attachments to the mitotic spindle and are aligned at the metaphase plate (for review see Musacchio and Salmon, 2007). Incorrect chromosome segregation may lead to cell death (Weaver and Cleveland, 2005; Heald, 2006) and aging (Baker et al., 2004), may also generate aneuploidy (Kim and Kao, 2005; Steuerwald, 2005; Mondal and Roychoudhury, 2003). Since deviation from euploidy is seen in 70-80% of all types of human cancers, errors in DNA segregation might facilitate tumorigenesis (Iwanaga et al., 2002; Kops et al., 2005b; Michel et al., 2004; Sotillo et al., 2007) and possibly contribute to cancer (Compton, 2006; Gupta et al., 2003; Mondal et al., 2007a) Thus, the ^{M}SAC mechanism guards the fidelity of chromosome segregation. Figure 2.4 illustrates how the ^{M}SAC mechanism seems to works. In early metaphase, those chromosomes not attached to the spindle, generate a signal that inhibits the transition from metaphase to anaphase. Once all kinetochores achieve bipolar attachment to the spindle's microtubules (in late metaphase) the ^{M}SAC is switched off and anaphase ensues. The Anaphase Promoting Complex (APC) is the target of the ^{M}SAC. It becomes active only after the attachment of the last kinetochore. Cdc20 is the co-activator of APC at the metaphase to anaphase transition. APC:Cdc20 mediated ubiquitination leads to activation of the separase, which cleaves the cohesins that maintain the linkage between sister chromatids (Peters, 2002), leading to sister chromatid separation and anaphase onset. Ubiquitination and degradation of cyclin B inactivates Cdk1, thereby permitting exit from mitosis (Nasmyth, 1993; Taylor, 1999).

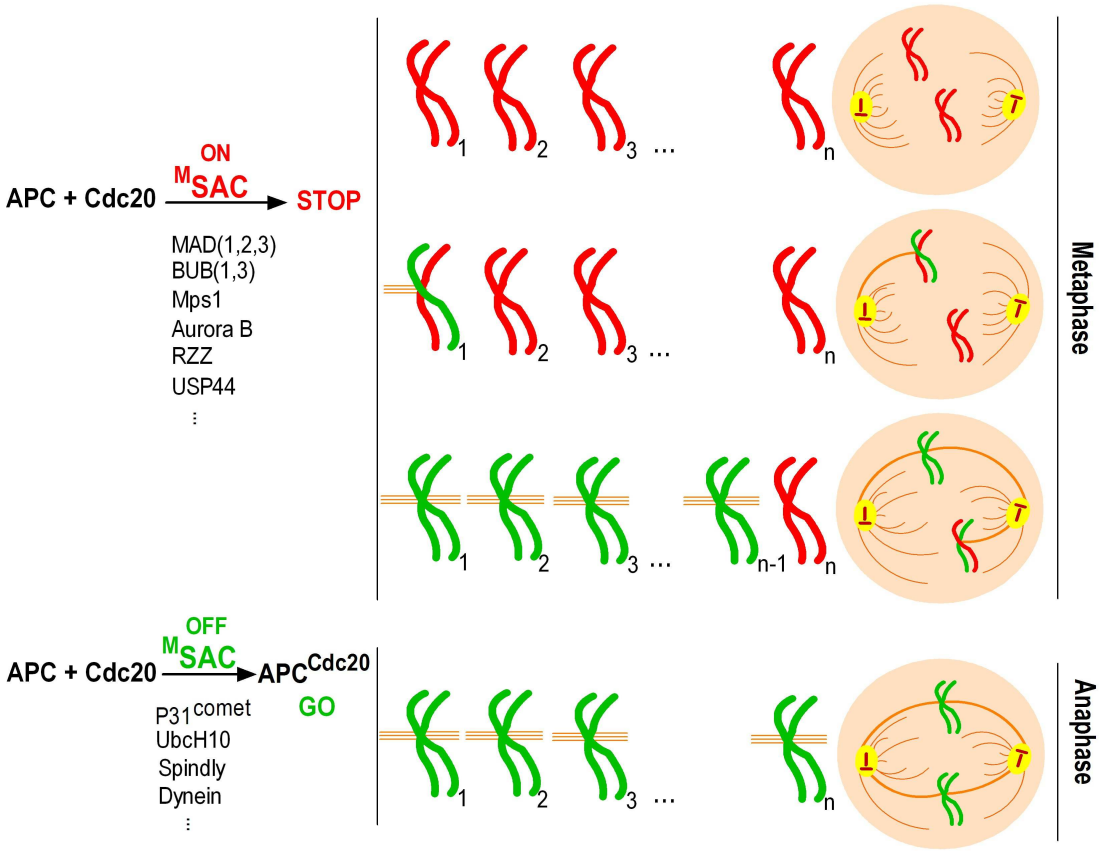

Figure 2.4: The ^{M}SAC , is the major cell cycle control mechanism in mitosis. It delays the transition from metaphase to anaphase until all chromosomes are correctly aligned at the metaphase spindle equator. In early metaphase, the chromosomes are not attached to the spindle of microtubules, while in late metaphase most chromosomes are attached. Once all kinetochores are attached, anaphase initiation is rapid. The subscript n denotes the number of chromosomes (e.g. $n = 46$ for human)

2.4.2 Experimental Studies on the ᴹSAC

ᴹSAC is a complex mechanism the elucidation of which is of high importance for cell biology and medical research. The following section summarizes recent progress toward the understanding of the functions of the ᴹSAC , as well as the mechanisms by which it activates the APC/C, and its regulation by phosphorylation and by association with its binding proteins.

Core Components of the ᴹSAC

The core proteins involved in ᴹSAC (Minshull et al., 1994) include MAD ("**M**itotic **A**rrest **D**eficient"; Mad1, Mad2, and Mad3 (in humans: BubR1)) (Li and Murray, 1991) and BUB ("**B**udding **U**ninhibited by **B**enzimidazole"; Bub1, and Bub3) (Hoyt et al., 1991), all of which are conserved among eukaryotes. A detailed list of the characteristics and proposed functions of the ᴹSAC core proteins in different organisms is shown in Table 2.2.

Structural domain and Functions of the Core ^{M}SAC Species

S.c.	S.p.	H. sapiens	Structural Feature	Functions in ^{M}SAC	References
Mad1	Mad1	Mad1	∼718 residue. coiled-coil	Bind to Mad2 and recruits it to unattached kinetochore Phosphorylated by Mps1 and Bub1 *in vitro* Essential for generation the Cdc20:Mad2 complex	(Hardwick and Murray, 1995; Chen et al., 1998, 1999a; Chung and Chen, 2002; Hardwick and Murray, 1995; Hardwick et al., 1996; Sironi et al., 2002, 2001b; Brady and Hardwick, 2000; Millband and Hardwick, 2002;
Mad2	Mad2	Mad2	∼205 residue. Horma domain	Binds Cdc20 and inhibits APC:Cdc20 activity Binds to Mad1	(Chen et al., 1998, 1999a; Yu, 2006; Sudakin et al., 2001; Li et al., 1997b; Poddar et al., 2005; Zhang and Lees, 2001a; Fang, 2002; Aravind and Koonin, 1998).
Mad3	Mad3	BubR1	∼1052 residue. GLEBS motif Serine/ threonine kinase	Bind to Bub3 constitutively. Binds to CENP-E Binds Cdc20 yeast Mad3 lacks the kinase domain	(Bharadwaj and Yu, 2004; Mao et al., 2003, 2005; Chen et al., 1998, 1999a; Davenport et al., 2006; Wang et al., 2001; Fraschini et al., 2001; Millband and Hardwick, 2002).
Bub1	Bub1	Bub1	∼1080 residue. GLEBS motif Serine/ threonine kinase	Phosphorylate Mad1 *in vitro* Requires for localization of Bub3 and BubR1	(Musacchio and Hardwick, 2002; Abrieu et al., 2001; Yamaguchi et al., 2003; Stucke et al., 2002; Gillett et al., 2004; Wang et al., 2001; Brady and Hardwick, 2000; Palframan et al., 2006; Taylor et al., 2001; Chen et al., 1999a; Hardwick et al., 1996).
Bub3	Bub3	Bub3	∼327 residue. Seven WD40 repeats	Binds to BubR1	(Taylor et al., 2004; Wang et al., 2001; Sharp-Baker and Chen, 2001; Sudakin et al., 2001).

Table 2.2: ^{M}SAC Core components: Domain structures and functions in different eukaryotic organisms (S.c., Saccharomyces cerevisiae; S.p., Schizosaccharomyces pombe; and H. sapiens, Homo sapiens), (reviewed in Zhou et al. (2003); Chan and Yen (2003); Hoyt (2001)).

Cdc20

The molecular understanding of the cell cycle began when Lee Hartwell and coworkers isolated **C**ell **D**ivision **C**ycle 20 homolog (Cdc20) mutants of S. cerevisiae that, despite continued cell growth, failed to execute or complete key cell-cycle events, such as DNA replication or mitosis (Hartwell et al., 1970).

Among the original Hartwell mutant collection were the Cdc20 mutants that arrest cell division in mitosis and fail to initiate anaphase and chromosome segregation (Hartwell et al., 1973). Cdc20 is a highly conserved WD40-repeat protein (Prinz et al., 1998; Pfleger and Kirschner, 2000a). Orthologs of Cdc20 were then discovered in various organisms (see Tables 2.3), including mammals and Drosophila (Weinstein et al., 1994; Dawson et al., 1995). In Drosophila, the Cdc20 ortholog, Fizzy, was shown to be required for the degradation of mitotic cyclins A and B (Dawson et al., 1995). However, the biochemical functions of Cdc20 remained obscure until the discovery of the Anaphase Promoting Complex/Cyclosome (King et al., 1995; Sudakin et al., 1995). (for review see Yu, 2007). Two main species, Mad2 and BubR1, can bind and sequester Cdc20.

APC

The downstream target of the ^{M}SAC is the **A**naphase **P**romoting **C**omplex/ **C**yclosome (APC/C or APC; an E3 ubiquitin ligase). APC is a multisubunit enzyme conserved from yeasts to humans, which is first identified independently by King et al. (1995) and Sudakin et al. (1995). The APC is composed of at least thirteen different subunits (see Table 2.3) which form two sub-complexes joined by the Apc1 subunit (see Figure 2.5). They remain tightly associated throughout the cell cycle.

APC activity is also strictly dependent on one of several co-activator proteins (see Table 2.3) that associate with APC during specific periods of the cell cycle. The best studied of these are Cdc20 and Cdh1, which are encoded by all known eukaryotic genomes. Additional meiosis-specific APC co-activators have been identified in yeasts and Drosophila.

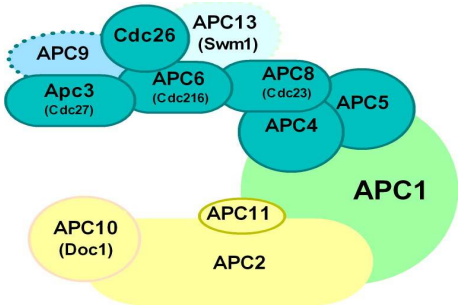

Figure 2.5: The APC subunits, The APC is composed of two sub-complexes joined by Apc1. This figure has been re-drown and modified from Peters (2006).

APC activity at metaphase-to-anaphase transition depends on the co-activator Cdc20. At the exit from mitosis, its activity depends on the co-activator Cdh1. Note that all APC co-activators contain a C-terminal WD40 domain[1] that is predicted to fold into a propeller-like structure, and that is now believed to recognize APC substrates by interacting with specific recognition elements in these substrates, called D[2]- (Glotzer et al., 1991), and KEN[3]-boxes (Pfleger and Kirschner, 2000b). Both Cdc20 and Cdh1 can recognize APC substrates that contain the D-box, but Cdh1 can also interact with a second motif, the KEN-box, thereby broadening the substrate specificity of the APC (Buschhorn and Peters, 2006; Pfleger et al., 2001; Eytan et al., 2006; Yamano et al., 2004; Pfleger and Kirschner, 2000a; Burton and Solomon, 2007; Chang et al., 2004).

The APC becomes active as APC:Cdc20 at the onset of anaphase just after ^{M}SAC is silenced. The APC:Cdc20 has two main functions:

- ◇ First, it catalyzes the ubiquitination of Securin which binds and inhibits the protease Separase (May and Hardwick, 2006). Subsequently, the Separase cleaves the cohesin subunit Scc1, which breaks the Cohesin ring (species details

[1]**WD40 domain**: A propeller-shaped protein domain that is composed of sequence repeats that are 40-amino-acid residues long and contain tryptophan (W) and aspartate (D) residues in conserved positions. In most cases, seven WD40 repeats fold into a seven-bladed propeller structure.

[2]**Destruction-box**: A sequence element (consensus RXXLXXXN) that was first discovered in the N terminus of mitotic cyclins that is required for their destruction. D-boxes can be recognized by APC:Cdc20 and by APC:Cdh1f. Where x is any amino acid

[3]**KEN-boxes**: A sequence element (consensus KEN) that is present in many APC substrates. KEN-boxes are preferentially, but not exclusively, recognized by APC:Cdh1.

are summarized in Table 2.3 and Table 2.4).

- Second, APC:Cdc20 is responsible for the first phase of Cyclin B proteolysis that occurs when cellular levels of the Cyclin B are high. Then the activated APC:Cdh1 mediates the second phase of Cyclin B destruction and triggers mitotic exit (Tan et al., 2005; Yeong et al., 2000).

APC subunits and co-activators in different organisms

S.c.	Mass (kDa)	D.m.	H. sapiens	C.e.	S.p.	A.n.	Structural Feature	Functions
Core subunits								
Apc1	196	CG9198/ Shattered	Apc1/Tsg24	Mat-2	Cut4	Bime	Rpn1/2 homology	- -
Apc2	96	CG3060/ Morula	Apc2	K06H7.6	SPBP23A10.04	-	Cullin homology	binding Apc11 & Doc1
Cdc27/Apc3	85	cdc27/Makos	Cdc27/Apc3	Mat-1	Nuc2	Bima	TPRs	Cdh1 binding
Apc4	73	CG4350	Apc4	Emb-30	Cut20/Lid1	-	WD40 repeats	-
Apc5	77	CG10850/lda	Apc5	M163.4	Apc5,spac959,09C	-	TPRs	-
Cdc16/Apc6	94	cdc16	Cdc16/Apc6	Emb-27	Cut9	Bimh	TPRs	-
-	-	-	Apc7	-	-	-	TPRs	-
Cdc23/Apc8	70	CG2508	Cdc23/Apc8	Mat-3	Cdc23/Apc8	-	TPRs	-
Apc9	30	-	-	-	-	-	-	-
Doc1/Apc10	26	CG11419	DOC1/Apc10	F15H10.3	Apc10	-	Doc domain	Substrate recognition
Apc11	19	Lmg (Lemming)	Apc11	F35G12.9	Apc11, SPAC343.03	-	Ring-H2 finger	E2 recruitment E3 activity
Cdc26	14	-	Cdc26	-	Hcn1	-	-	-
Apc13/Swm1	19	-	Swm1/Apc13	-	-	-	-	-
Mnd2	43	-	-	-	-	-	-	Ama1 inhibition
Co-activators								
Cdc20	68	Fizzy	Cdc20/$P55^{CDC}$	-	Slp1	-	WD40 repeats	Meta-to-anaphase
Cdh1/Hct1	64	Fizzy-related	Cdh1 A,B,C,D	FZR-1	Srw1/Ste9	-	WD40 repeats	Mitosis exit
Ama1	66	-	-	-	Mfr1	-	WD40 repeats	Meiosis

Table 2.3: APC: Subunits, Domain structures and functions (see (Peters, 2006, 2002; Passmore, 2004a; Zachariae et al., 1998b; Dube et al., 2005; Thornton et al., 2006; Harper et al., 2002; Melloy and Holloway, 2004; yong Huang and Raff, 2002; King et al., 1995; Sudakin et al., 1995; Blow and Tanaka, 2005)). S.c., Saccharomyces cerevisiae; D.m., Drosophila melanogaster; H. sapiens, Homo sapiens; C.e., Caenorhabditis elegans; S.p., Schizosaccharomyces pombe; and A.n., Aspergillus nidulans).

APC targets in different organisms

S.c.	S.p.	H. sapiens	Functions Feature	References
Pds1	Cut2	Securin/ PTTG	Binds and inhibits separase. ^{M}SAC activation prevents its ubiquitination by APC:Cdc20.	(Yu, 2002; Peters, 2002; May and Hardwick, 2006; Luo et al., 2000a; Fang, 2002; Palframan et al., 2006).
Esp1	Cut1	Separase	Degradation of securin releases separase to cleave cohesin and allow chromosomes to segregate.	(Uhlmann et al., 1999; May and Hardwick, 2006; Yu, 2002; Yanagida, 2000).
Clb2	Cdc13	Cyclin B	^{M}SAC prevents mitotic exit by inhibitin APC-mediated ubiquitination of cyclin B.	(Hagan et al., 1988; Nasmyth, 1993; Taylor, 1999).

Table 2.4: APC: Subunits, Domain structures and functions. S.c., Saccharomyces cerevisiae; S.p., Schizosaccharomyces pombe; and H. sapiens, Homo sapiens

Mad2 Function in Sequestering Cdc20

Mad1 forms a tight 2:2 complex with Mad2 (Sironi et al., 2001b, 2002). The binding of Mad2 to Mad1 triggers a conformational change of Mad2, in a similar way as does Cdc20 binding. Mad2 binds to Mad1 and Cdc20 in the same pocket with similar affinities (Luo et al., 2002; Yu, 2006). Mad2 can adopt two conformations: O-Mad2 and C-Mad2 (for "Open" and "Closed" respectively), which differ in the structure of its 50 residue C-terminal segment (Luo et al., 2002; Luo and Yu, 2005). The O-Mad2 is the physiological state of cytosolic Mad2 in the absence of Mad1 or Cdc20 (Luo et al., 2004; DeAntoni et al., 2005a). O-Mad2 refolds to C-Mad2 when bound to kinetochore receptor Mad1 or APC activator Cdc20 (Luo et al., 2002, 2000a). $p31^{comet}$ is a negative regulator of the spindle checkpoint. It prevents further Mad2 turnover on Mad1 and neutralizes the inhibitory activity of Cdc20-bound Mad2, leading to activation of the APC followed by degradation of Securin and Cyclin B (Habu et al., 2002; Xia et al., 2004; Mapelli et al., 2006).

Recently, intensive studies led to an improved understanding of Mad2 - Cdc20 binding. Accordingly, two alternative mechanistic models were proposed: the "Exchange" (Luo et al., 2004) and the "Template" model (DeAntoni et al., 2005a; reviewed by Lénárt and Peters, 2006; Nasmyth, 2005; Hardwick, 2005; Hagan and Sorger, 2005).

- ◇ In the Exchange model (see Figure 2.6), Mad1 recruits O-Mad2 at the kinetochore and transforms its conformation from O-Mad2 to C-Mad2. Then, C-Mad2 dissociates from Mad1 and binds Cdc20. This model was criticized because it is unable to explain additional experimental data (DeAntoni et al., 2005a,b; Vink et al., 2006; Mapelli et al., 2006) and assumes that Mad1 competes with Cdc20 for Mad2 binding.
- ◇ According to the alternative Mad2 Template model (see Figure 2.6), Mad1 and C-Mad2 form a stable 2:2 complex at unattached kinetochores (DeAntoni et al., 2005a). This quadromer complex then, binds additional molecules of O-Mad2 through formation of conformational heterodimers between the C-Mad2 subunit of the Mad1:C-Mad2 complex and O-Mad2. Upon Mad1:C-Mad2 binding, O-Mad2 adopts an intermediate conformation (O-Mad2*) that can quickly and

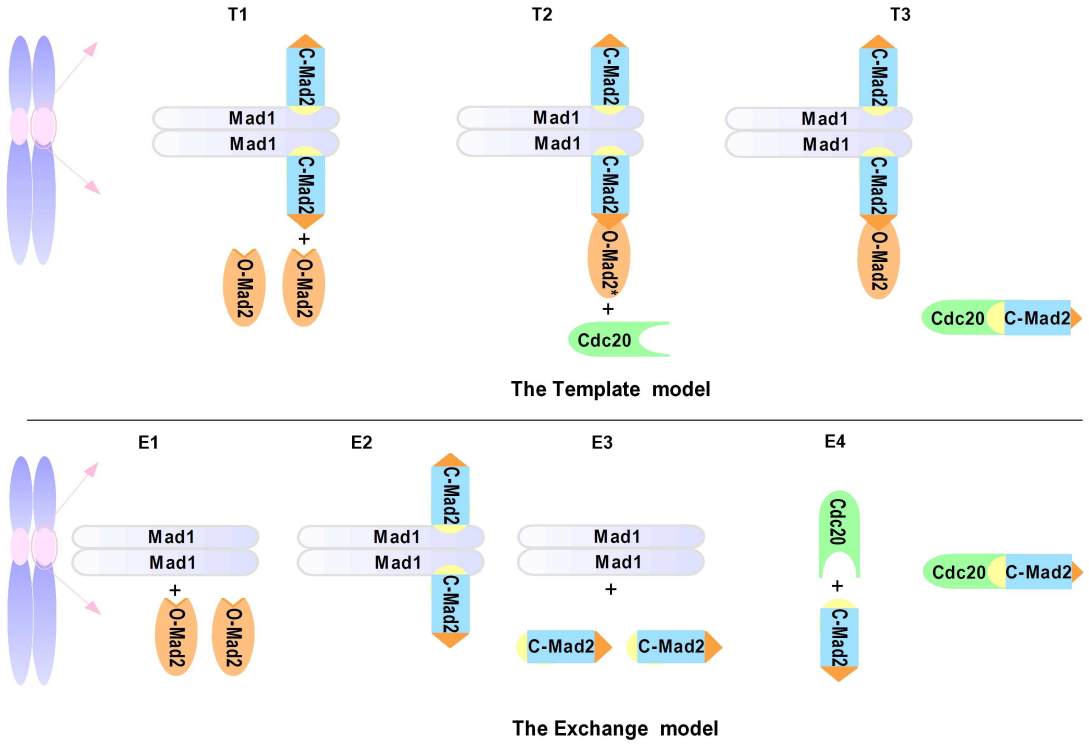

Figure 2.6: Schematic drawing of the Mad2 Template and the Mad2 Exchange models. The Template model (upper part of the figure) assumes that Mad1 and C-Mad2 form a stable core complex at unattached kinetochores. This core then binds additional molecules of O-Mad2 through formation of conformational heterodimers between the C-Mad2 subunit of the Mad1:C-Mad2 complex and O-Mad2. Cdc20 binding to this complex leads to the conversion of O-Mad2 to C-Mad2 resulting in the formation of Cdc20:C-Mad2, which in turn is assumed then to dissociate off Mad1:C-Mad2. Upon Mad1:C-Mad2 binding, O-Mad2 adopts an intermediate conformation (O-Mad2*) that can quickly and efficiently bind Cdc20 and switch to the C-conformation. The Exchange (lower part of the figure) assumes that Mad1 recruits open Mad2 (O-Mad2) at the kinetochore and transforms its conformation from O-Mad2 to closed Mad2 (C-Mad2). C-Mad2 then dissociates from Mad1 and binds Cdc20.

efficiently bind Cdc20 and switch to the C-conformation. The binding of Cdc20 to this complex leads to the conversion of O-Mad2 to C-Mad2, resulting in the formation of C-Mad2:Cdc20 which then dissociates from Mad1:C-Mad2 (Fang, 2002). The Template model describes Mad2:Cdc20 complexation, which is the seeding reaction of MCC (*M*itotic *C*heckpoint *C*omplex) formation.

There are still open questions related to the role of Mad2 that are critical to understanding the ^{M}SAC mechanism. These questions will be discussed in the conclusion section of this chapter as well as in chapter 3. In the following section, MCC formation will be analyzed.

MCC Formation

The highly conserved proteins Mad2 and BubR1 are essential for Cdc20 binding. They form the Mitotic Checkpoint Complex (MCC). In HeLa[1] cells, MCC contains Mad2, Bub3, BubR1 and Cdc20 in apparently equal stoichiometries (Sudakin et al., 2001). A similar complex was identified in budding (Hardwick et al., 2000) and fission (Millband and Hardwick, 2002) yeasts and in Xenopus (Chung and Chen, 2003).

Bub3 associates with BubR1 (Taylor et al., 1998a; Sudakin et al., 2001). This interaction is constitutive and is required for the localization of BubR1 to the kinetochores during mitosis. In prometaphase, CENP-E activates the kinase activity of BubR1 at unattached kinetochores. It is unclear whether BubR1 activation is required for ^{M}SAC function (Chen, 2002a; Mao et al., 2003). The kinase activity of BubR1 might not be required in the MCC, however, it might control other aspects of kinetochore signaling or chromosome alignment (Ditchfield et al., 2003; Lampson and Kapoor, 2005) (reviewed by Musacchio and Salmon, 2007). BubR1 activity is switched off upon microtubule attachment (Mao et al., 2005; Braunstein et al., 2007). BubR1 cannot bind Mad2 directly (Fang, 2002). Moreover, BubR1 does not form a ternary complex with Mad2 and Cdc20. Two Cdc20 binding sites

[1]**HeLa cell**: cancerous cell belonging to a strain continuously cultured since its isolation in 1951 from a patient suffering from uterine cervical carcinoma. The designation HeLa is derived from the name of the patient (Henrietta Lacks (August 18, 1920 October 4, 1951)). HeLa cells have been widely used in laboratory studies.

were identified on BubR1 (Bolanos-Garcia et al., 2005; Davenport et al., 2006). Binding of the N-terminal region of BubR1 to Cdc20 requires prior binding of Mad2 to Cdc20 (Davenport et al., 2006). The other site (between residues 490 and 560) can bind Cdc20 tightly regardless of Mad2 being bound to Cdc20 (Davenport et al., 2006). Thus, BubR1 can form a ternary complex with Bub3 and Cdc20 which however has no inhibitory activity at the APC (unpublished data by Sudakin et al., 2001). In addition, *in vivo* inhibition of Cdc20 for mitotic function is a two-step process in which prior binding of Mad2 to Cdc20 is required to make Cdc20 sensitive for BubR1 binding (Davenport et al., 2006).

Localization of all ^{M}SAC proteins at unattached kinetochores in mitosis provides a catalytic platform and contributes to MCC formation. The MCC is also detectable in normal metaphase-arrested cells in which the ^{M}SAC is inactive. This indicates that MCC formation does not require checkpoint activation (Poddar et al., 2005). Moreover, the MCC is also detectable in checkpoint defective cells (Poddar et al., 2005; Fraschini et al., 2001). A detailed study (Meraldi et al., 2004) proposes that cytosolic Mad2-BubR1 is essential to restrain anaphase onset early in mitosis when kinetochores are still assembling. These arguments support the idea that the MCC (and its sub-complexes) might form in a kinetochore-independent manner (for review see Musacchio and Salmon, 2007).

The MCC binds to and inhibits the APC and is believed to be essential for ^{M}SAC function (Musacchio and Salmon, 2007). However, MCC inhibits only the mitotic and not the interphase APC (Pinsky and Biggins, 2005). The interaction between APC and MCC is quite labile in the absence of unattached kinetochores (Sudakin et al., 2001). How the MCC inhibits APC activity is poorly understood (Musacchio and Salmon, 2007). The MCC might bind to the APC as a pseudo-substrate due to a KEN-box motif in BubR1. This indicates that the MCC needs to disassemble from the APC at metaphase to elicit anaphase (Morrow et al., 2005; Fang, 2002). Bub1 and Aurora-B kinase contribute directly to the formation of a complex of the MCC with the APC (Morrow et al., 2005). Unattached kinetochores might sensitize the APC to inhibition by the MCC (Sudakin et al., 2001; Chan et al., 2005; Doncic et al., 2005; Sear and Howard, 2006).

In addition to kinetochore attachment, tension is important for ^{M}SAC inactivation (Nicklas et al., 1995; Nicklas, 1997). For example, if both sister kinetochores attach to microtubules from the same pole, not enough tension is generated and microtubule kinetochore attachment is destabilized to correct the problem (Musacchio and Salmon, 2007). This destabilization depends on Aurora-B kinase (Hauf et al., 2003; Pinsky and Biggins, 2005; Tanaka et al., 2002; Lampson et al., 2004). For sub-complex details see Table2.5.

^{M}SAC Complexes

Complex name	**Complex elements**	**Functions**	**References**
Mad1:C-Mad2	Mad1, C-Mad2	conversion of O-Mad2 into closed Mad2 bound to Cdc20.	(Sironi et al., 2001b, 2002; DeAntoni et al., 2005a).
Cdc20:C-Mad2	Cdc20, C-Mad2	Sequester Cdc20 and contribute to MCC formation	(Luo et al., 2002; Yu, 2006; DeAntoni et al., 2005a; Luo et al., 2004).
Bub3:BubR1	Bub3, BubR1	Contributes to MCC formation Sequester Cdc20	(Sudakin et al., 2001; Taylor et al., 1998a, 2004; Taylor et al., 2004; Davenport et al., 2006).
Bub3:BubR1:Cdc20	Bub3, BubR1, Cdc20	Partially sequester Cdc20	(Sudakin et al., 2001).
MCC	Cdc20, C-Mad2, Bub3, BubR1,	Binds and inhibits APC	(Sudakin et al., 2001; Hardwick et al., 2000; Millband and Hardwick, 2002; Chung and Chen, 2003).
MCC:APC	MCC, APC	Keep inhibiting of APC	(Sudakin et al., 2001; Fang et al., 1998a; Shannon et al., 2002; Tang et al., 2001; Hardwick et al., 2000; Fraschini et al., 2001; Poddar et al., 2005; Acquaviva et al., 2004; Morrow et al., 2005; D'Angiolella et al., 2003).
RZZ	Rod, Zw10, Zwilch	Localized dyneindynactin complex, and Mad1Mad2 complex.	(Karess, 2005; May and Hardwick, 2006; Buffin et al., 2007; Saffery et al., 2000a; Saffery et al., 2000b; Chan et al., 2000; Williams et al., 2003; Karess, 2005; Scholey et al., 2003; Raff et al., 2002; Kops et al., 2005a; Wang et al., 2004a)
APC:Cdc20	APC, Cdc20	Anaphase initiation, cyclin B first phase destruction More details in Table2.4	(Yu, 2002; Peters, 2002; Shirayama et al., 1999; Tan et al., 2005; D'Amours and Amon, 2004).
APC:Cdh1	APC, Cdh1	complete destruction of Cyclin B, inactivates APC:Cdc20	(Pfleger and Kirschner, 2000a; Prinz et al., 1998). (for details see Section.2.9)

Table 2.5: ^{M}SAC Complexes

Additional Components of the ᴹSAC

In addition to the four MCC proteins, the ᴹSAC also involves several other proteins that also are involved in essential aspects of this mechanism. Among these additional components are Aurora-B and the "Multipolar spindle-1" protein (Mps1). These components are required for ᴹSAC signal amplification and MCC formation (see Table 2.6). Moreover, several other proteins have recently been identified in higher eukaryotes that are also involved in carrying out essential aspects of the ᴹSAC mechanism e.g., localization or biochemical signaling: "Rough Deal" (Rod) (May and Hardwick, 2006; Buffin et al., 2007), ZW10 (Zeste White 10) (Saffery et al., 2000a,b; Chan et al., 2000; Scholey et al., 2003; Raff et al., 2002), Zwilch (Williams et al., 2003; Karess, 2005) , Zwint-1 (Kops et al., 2005a; Wang et al., 2004a) the RZZ complex (Karess, 2005), CENP-E ("Centromere associate Protein E", a member of the kinesin superfamily), and protein kinases like "Mitogen Activated Protein Kinase" (MAPK), CDK1, and cyclin-B.

Several core checkpoint proteins are recruited to unattached kinetochores in prometaphase including Mad1 (Campbell et al., 2001; Chung and Chen, 2002), Mad2 (Fang et al., 1998a; Lampson and Kapoor, 2005), BubR1 (Morrow et al., 2005; Hoffman et al., 2001), Bub1 (Taylor et al., 1998a; Chen, 2002b), Bub3 (Taylor et al., 1998a; Howell et al., 2004), and Mps1 (Stucke et al., 2004, 2002) (Figure 2.7). Obviously, the kinetochores serve as a platform for complex formation (cf. Figure 2.8). The Cdc20:Mad2 and Mad1:Mad2 complexes form in the absence of other proteins *in vitro* (BubR1 or Bub3 are dispensable) (Chung and Chen, 2002; Hwang et al., 1998; Martin-Lluesma et al., 2002; Luo et al., 2002; Fraschini et al., 2001). Upon microtubule attachment, many of these proteins deplete from the kinetochores (see for example Lampson and Kapoor, 2005; Wassmann et al., 2003; Shannon et al., 2002).

Structural domain and Functions of the additional ^{M}SAC Species

S.c.	S.p.	H. sapiens	Structural Feature	Functions in ^{M}SAC	References
Mps1	Mph1	Mps1 (hMps1)	Dual-specificity kinase	Role in recruitment of checkpoint proteins to kinetochores (Mad1/2) Requires for spindle pole Requires for centrosome replication	(Stucke et al., 2002, 2004; Abrieu et al., 2001; Hoffman et al., 2001; Howell et al., 2004; Fisk et al., 2004; Fisk and Winey, 2004, 2001; Liu et al., 2003; Tang et al., 2004; Vigneron et al., 2004).
Ipl1	Ark1	Aurora B	Serine/threonine kinase	Important for MCC bind APC proposed to sense tension at kinetochores Ensures bipolar orientation	(Morrow et al., 2005; Liu et al., 2006; Ducat and Zheng, 2004; Steuerwald, 2005; Cheeseman et al., 2002; Biggins and Murray, 2001; Murata-Hori and li Wang, 2002).
Bub2	Cdc16	TBC1 (tre-2 Bub2, cdc16)	GAP (GTPase activating-protein) coiled-coil	Regulates mitotic exit network in S. cerevisiae. Essential for cytokinesis in S. pombe.	(Hu and Elledge, 2002; Sklan et al., 2007; Martinu et al., 2004; Fraschini et al., 2001; Geymonat et al., 2003; Pereira et al., 2002).
-	-	CENP-E	∼2663 residues. Kinesin-like plus end-directed motor	Interacts with BubR1 and microtubules Essential for the stable bi-oriented attachments of chromosome to the MTs	(Yao et al., 2000; Zecevic et al., 1998; Chan et al., 1998, 1999; Neumann et al., 2006; Garcia-Saez et al., 2004. Mao et al., 2003, 2005; Vigneron et al., 2004; Morrow et al., 2005).

Table 2.6: ^{M}SAC additional components: Domain structures and functions in different eukaryotic organisms (S.c., Saccharomyces cerevisiae; S.p., Schizosaccharomyces pombe; and H. sapiens, Homo sapiens).

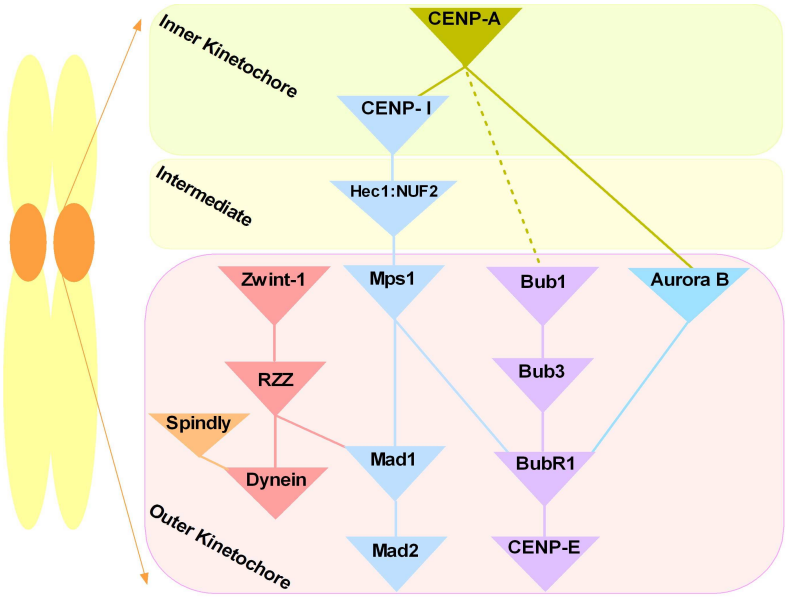

Figure 2.7: A hierarchical network of localization pathways. This figure has been re-drown modified from Liu et al. (2006), new species has been added like, Spindly, Bub3, and Dynein.

Biochemical Signaling

UbcH10 increases both, Cdc20 ubiquitination and the dissociation of Cdc20 from Mad2 and APC Reddy et al. (2007). Conversely, depletion of UbcH10 from HeLa cells decreases APC-mediated ubiquitination of Cdc20, stabilizes the Mad2-Cdc20 interaction, and delays anaphase initiation (Reddy et al., 2007). In an accompanying study, Stegmeier et al. (2007) have identified the ubiquitin-specific protease USP44 as a spindle checkpoint component through an RNA interference (RNAi) screen. Human cells depleted for USP44 by RNAi do not undergo mitotic arrest in the presence of spindle poisons. The checkpoint bypass of USP44 RNAi cells depends on APC, although Mad2 and BubR1 are localized normally in the kinetochores. Thus, in APC inhibition, USP44 acts downstream of Mad2 in APC inhibition. Furthermore, USP44 antagonizes APC-mediated ubiquitination of Cdc20 *in vivo*. Recombinant USP44 directly deubiquitinates Cdc20 *in vitro*. This study indicates that USP44 reduces Cdc20 autoubiquitination and protects the Cdc20:Mad2 checkpoint complexes from disassembly. Griffis

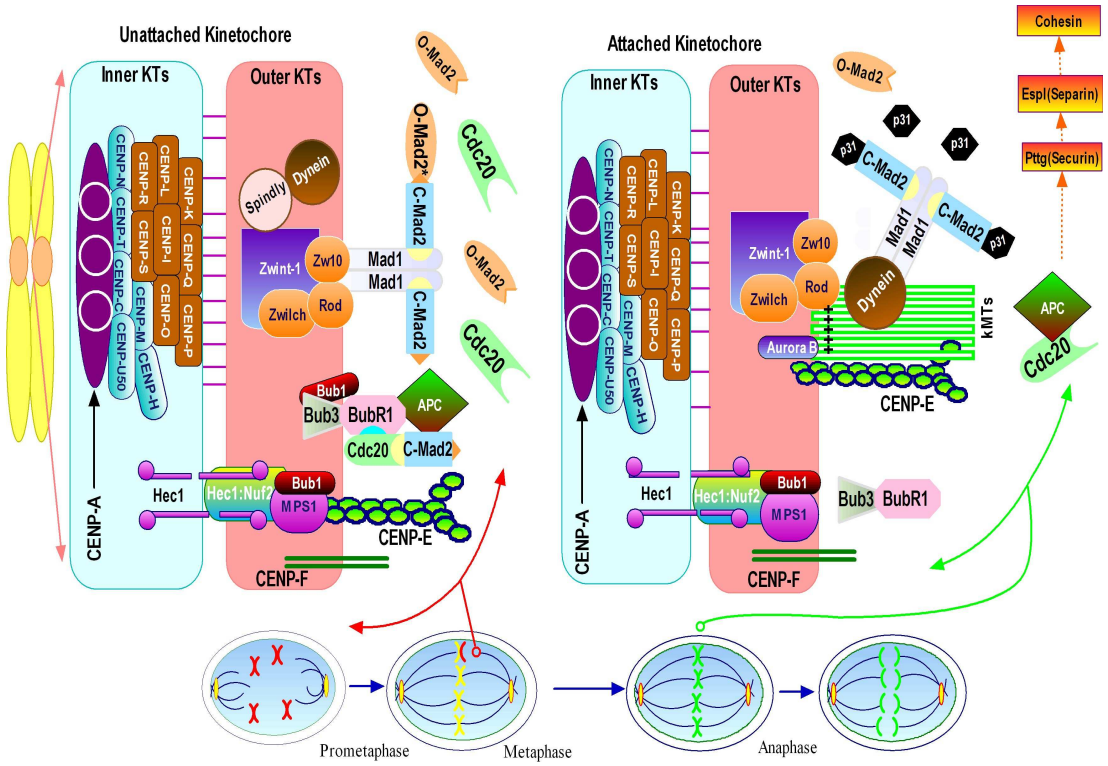

Figure 2.8: Structural features in the regulation of mitotic progression from metaphase to anaphase defining the model relations. The left part of the figure (unattached case) has been re-drown modified from Musacchio and Salmon (2007) and new species like Spindly and Dynein have been integrated. Before the attachment most species recruited to the kinetochore. The right hand port of the figure presented the kinetochore after attachment to the spindle microtubule. After the attachment, many species deplete from the kinetochore.

et al. (2007) have recently identified a new protein, called "Spindly". After the depletion of Spindly, dynein cannot target to kinetochores, and, as a result, cells arrest in metaphase with high levels of kinetochore-bound Mad2 and RZZ. They also identified a human homologue of Spindly that serves a similar function that accumulates on unattached kinetochores and is required for silencing the ^{M}SAC .

p31^{comet} (formerly CMT2) is a negative regulator of the spindle checkpoint. It prevents further Mad2 turnover on Mad1 and neutralizes the inhibitory activity of Cdc20-bound Mad2, leading to activation of APC (Habu et al., 2002; Xia et al., 2004; Mapelli et al., 2006). For details see Table 2.7.

^{M}SAC Signaling Species

Species	**Name (s)**	**Functions in ^{M}SAC**	**References**
UBE2C or UbcH10	ubiquitin-conjugating enzyme E2C	dissociation of Cdc20 from Mad2.	(Reddy et al., 2007; Townsley et al., 1997; Hershko et al., 1994; Aristarkhov et al., 1996; Yu et al., 1996; Seufert and Jentsch, 1990).
USP44	Ubiquitin specific protease 44	reduces Cdc20 autoubiquitination and protects the Cdc20 and Mad2 complex from disassembly.	(Stegmeier et al., 2007).
Dynein	Dynein	Remove Mad1:C-Mad2 from KTs	(Howell et al., 2001; Starr et al., 1998; Griffis et al., 2007).
Spindly	Spindly	Localized Dynein	(Griffis et al., 2007).
p31^{comet}	p31^{comet}	It prevents further Mad2 turnover on Mad1 and neutralizes the inhibitory activity of Cdc20-bound Mad2	(Habu et al., 2002; Xia et al., 2004; Mapelli et al., 2006; Yang et al., 2007).

Table 2.7: ^{M}SAC Signaling Species

2.4.3 Recent Models of the ^{M}SAC

For the cell cycle in general there exists already a large number of models, ranging from relative simple, low-dimensional models (Tyson, 1991; Goldbeter, 1991) to complex models taking into account a large number of molecular species (Chen et al., 2004).

Because most experimental studies of the spindle checkpoint are recent, the ^{M}SAC has not yet been modeled in a detailed molecular level. Doncic et al. (2005) compared several mechanisms that could account for the inhibition of the APC^{Cdc20} complex in yeast. They noticed that the design of the ^{M}SAC network is limited by physical constrains imposed by realistic diffusion constants and the relevant spatial and temporal dimensions in the yeast cell. By designing a simplified model of radial symmetry, they observed that amplifying the signal through the release of a diffusible inhibitory complex can describe the checkpoint function. Nevertheless, their model does not fully take into account the molecular complexity. A similar approach was presented by Sear and Howard (2006). They investigated two mechanisms for ^{M}SAC in metazoan cells:

- ◇ one involves free diffusion and sequestration of cell cycle regulators requiring a two-stage signal amplification cascade.
- ◇ The second mechanism involves spatial gradients of a short-lived inhibitory signal that propagates by diffusion and primarily by active transport along spindle microtubules.

Both mechanisms might act in parallel. Mathematical modeling of cell cycle control in budding yeast was analyzed in more details by Chen et al. (2004), however, this work is not focused on the ^{M}SAC. A model for the exit from mitosis (Ciliberto et al., 2005) describes the control of the checkpoint, however it not considers BubR1 (Mad3 in yeast) and the influence of spatial distribution and diffusion.

2.5 Mitotic Exit control

The second critical control mechanism during mitosis is a complex regulatory mechanism (called **E**xit **F**rom **M**itosis **(EFM)**) that allows cells to leave mitosis.

2.5.1 Exit From Mitosis (EFM) Mechanism

As described above, the APC plays an important role in the ubiquitination and destruction of both securin and cyclin B. The kinase activity of a cyclinB:Cdk1 complex promotes mitosis, whereas the destruction of the cyclin partner and loss of kinase activity is required for EFM (Su et al., 1998).

APC:Cdc20 is responsible for the first phase of Cyclin B proteolysis that occurs when cellular levels of the Cyclin B are high. Since ^{M}SAC is activated, Cdh1 is phosphorylated by Cdks and thereby kept inactive. After anaphase initiation (^{M}SAC inactivate), Cdh1 is dephosphorylated and thus, it is able to bind and activate the APC (Kramer et al., 2000; Zachariae et al., 1998a). APC:Cdh1 then ubiquitinates Cdc20 and thereby inactivates APC:Cdc20 (Pfleger and Kirschner, 2000a; Prinz et al., 1998). More precisely, APC:Cdh1 is activated once the degradation of cyclin B has been initiated by APC:Cdc20 (see Figure 2.9). The second phase of Cyclin B destruction is mediated by APC:Cdh1 which then trigger the exit from mitosis (Tan et al., 2005; Yeong et al., 2000; Bosl and Li, 2005; Morgan, 1999; King et al., 1996; Alexandru et al., 1999).

2.5.2 Analysis of the Recent Experimental Studies of the EFM

In all eukaryotes, EFM occurs through the inactivation of the Cdk1 in complex with mitotic cyclin. This complex is called Cdk1:cyclin B or Cdc28:Clb2 in budding yeast (Bloom and Cross, 2007). Two main events must occur before a cell is able to leave mitosis:

- ◇ The separation of sister chromatids
- ◇ The destruction of Cyclin B.

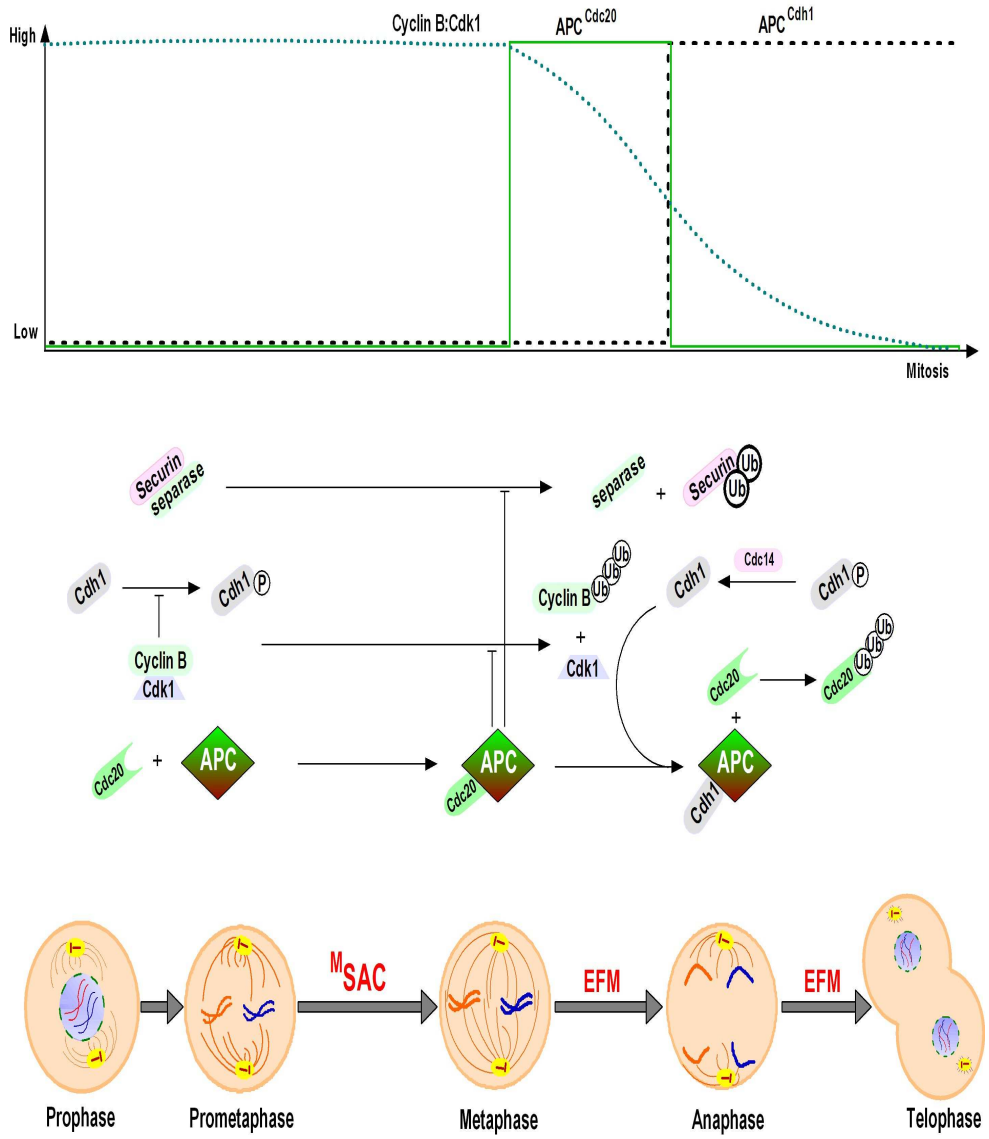

Figure 2.9: Activation of APC by Cdc20 and Cdh1 during mitosis. ^{M}SAC is activated at kinetochores that are not (or not fully) attached with microtubules. It inhibits the capability of APC:Cdc20 to ubiquitylate securin and cyclin B and thereby prevent anaphase. Once, all kinetochores are attached to microtubules, APC:Cdc20 is responsible for activates Separase and the first phase of Cyclin B proteolysis that occurs when cellular levels of the Cyclin B are high. Thereby Cdh1 is dephosphorylated (activated) and thus able to bind and activate the APC:Cdch1. Activated APC:Cdh1 then mediates the second phase of Cyclin B destruction and triggers EFM. The upper part of this figure explain the expected behavior of APC activity (with both Cdc20 and Cdh1)and cyclin B in mitosis. Then, an abstract reaction scheme explain active APC functions. The lower part of the figure explain the corresponding transition event of mitosis.

These late mitotic events are tightly regulated to occur only after the onset of anaphase (^{M}SAC inactivated) and prior to cytokinesis (Wolfe et al., 2006; Nasmyth et al., 2000). Several proteins and protein complexes are involved in these tasks; APC, Cdc20, Cdc14, Cdh1, Cdc15, Net1, Tem, Cyclin B complex, securin, separase and the cohesin complex. Some of these players are not observed in humans (e.g. Net1).

During anaphase, the phosphatase Cdc14 is activated. It dephosphorylates several targets of mitotic Cdk and promotes mitotic exit (D'Amours and Amon, 2004). Separase plays an essential role in Cdc14[1] activation (Queralt et al., 2006; Sullivan and Uhlmann, 2003). Cdc14 dephosphorylates (and thereby activates) a second APC co-activator called Cdh1[2] that promotes completion of cyclin destruction (Prinz et al., 1998). In higher eukaryotes, it has been shown that a homolog of Cdc14 can dephosphorylate Cdh1 *in vitro* (Bembenek and Yu, 2001b). Cdh1 dephosphorylation activates APC and forms the APC:Cdh1 complex, allowing cells to progressively accumulate mitotic cyclin Clb2 (in human Cyclin B) (Zachariae et al., 1998b; Yeong et al., 2000; Zachariae et al., 1998a; Huang et al., 2001). Then, APC:Cdh1 ubiquitinates Cdc20, and completely degrades Cyclin B. Additionally, APC:Cdh1 ubiquitinates other species, like Bub1 that are not required for EFM (Qi and Yu, 2007).

The mechanism of the activation of APC:Cdh1 and EFM is well characterized in budding yeast (Morgan, 1999). Mutations of a set of yeast genes, such as Tem1, Lte1, Cdc14, and Cdc15 stabilize mitotic cyclin Clb2p and cause late anaphase arrest, indicating that they are required for the EFM (Morgan, 1999; Jaspersen et al., 1998; Shou et al., 1999; Visintin et al., 1999). During most part of the cell cycle, Cdc14 is sequestered in the nucleolus due to its association with the regulatory subunit Net1 (also called Cfi1) (Shou et al., 1999; Visintin et al., 1999). The release of Cdc14 from the nucleolus and its accumulation in

[1] **hCdc14A** is the human homologue of Cdc14 (Lanzetti et al., 2007; Krasinska et al., 2007; Vazquez-Novelle et al., 2005). hCdc14A protein is 64% identical to yeast Cdc14 (Li et al., 1997a).

[2] **hCdc14A** was shown to dephosphorylate Cdh1 and reconstitute active APC:hCdh1 *in vitro* (Bembenek and Yu, 2001a). Additionally, human Cdc14 phosphorylates Cdc25 *in vitro* (Esteban et al., 2006). The later has important roles in other cell cycle phases.

the nucleus (and partially in the cytoplasm) during anaphase is thought to be important for activating APC:Cdh1 (Shirayama et al., 1999).

2.5.3 Recent Models of the EFM

Béla Novák and colleagues have proposed several models for EFM in budding yeast. Queralt et al. (2006) presented a new mathematical model for EFM focused only on the cell cycle transition from a stable state of high Cdk activity in mitosis, via anaphase and mitotic exit, to a stable state of low Cdk activity in G1. This transition corresponds to the window of the cell cycle that was analyzed by experiments in which cells arrested in metaphase because of Cdc20-deprivation, are able to enter in anaphase by re-addition of Cdc20 or by over-expression of separase. They described a wiring diagram of EFM and developed a quantitative model based on nonlinear differential equations. The model was analyzed by numerical simulations. The kinetic parameters were chosen to fit the experimental observations.

Toth et al. (2007) present a two dimensional model for the EFM in budding yeast. They use phase-plane analysis, which reveals two underlying bistable switches in the regulatory network. One bistable switch is caused by mutual activation (positive feedback) between Cdc14 activating MEN and Cdc14 itself. The mitosis-inducing Cdk1 activity inhibits the activation of this positive feedback loop and thereby controlling this switch. The other irreversible switch is generated by a double-negative feedback (mutual antagonism) between mitosis inducing Cdk1 activity and its degradation machinery (APC:Cdh1). The Cdc14 phosphatase helps turning this switch in favor of APC:Cdh1. Both of these bistable switches have characteristic thresholds, the first one for Cdk1 activity, and other for Cdc14 activity. The same authors show that the physiological behaviors of certain cell cycle mutants are suggestive for those Cdk1 and Cdc14 thresholds.

We built an integrative mathematical model for ^{M}SAC and EFM mechanism (M. Palm, 2008). Our model overlaps with the model developed by Toth et al. (2007).And will be introduced in detail in Chapter 7.

2.6 Concluding Remarks

Our focus in this chapter was on identifying open questions related to two different, still connected mitosis transition control mechanisms, namely, the **M**itotic **S**pindle **A**ssembly **C**heckpoint (**^{M}SAC**) and **E**xit **F**rom **M**itosis (**EFM**) mechanisms. These mechanisms involve a rather large number of biochemical species of elements, together with their corresponding interactions. Since of these elements serve multiple functions, in addition. Empirical data have proved fruitful in the understanding of these mechanisms, in the context of mitosis, a fact well documented by an increasing number of open questions. Yet, such data are typically limited by the complexity of such mechanisms.

The following are examples of open questions that are of most importance in this context. We know that both Mad2 and BubR1 sequester Cdc20, but how do these three elements interact? The Template model seems to explain some empirical data more accurately than the Exchange model does, but the question why this is so remains elusive. Is there any amplification phenomenon in the template model? MCC is formed in different organisms, but is MCC formation kinetochore dependent or independent? Moreover, MCC inhibits APC, but how? How an MCC:APC complex falls apart after attachments? How biochemical signals as $p31^{comet}$ and dynein actually work? How can we ponder the roles of localizations and diffusion in the context of ^{M}SAC ? Eventually, how does ^{M}SAC operate throughout the entire process of mitosis? These questions, as examples, relate to the ^{M}SAC mechanism, and comparable questions can be made in relation to the EFM mechanism.

We propose that theoretical accounts of mitosis transition controls based on modeling, simulation, and cross-disciplinary research (*In-Silico*) will be of significant help for better understanding of such a complex phenomenon as mitosis. This might well be an eye-opening trip a cross disciplines, a perspective belonging to the so called new science of Systems Biology. We shall refer to our work as to "Systems Biology of Mitosis". In the next chapter, we will introduce modeling approaches and classifications for systems biology. Some details and basic concepts will be presented for non modelers.

Entering to Anaphase

"Music is the pleasure the human mind experiences from counting without being aware that it is counting".

Gottfried Leibniz (1646 1716)

"Mathematics is the handwriting on the human consciousness of the very Spirit of Life itself".

Claude Bragdon (1866-1946)

Chapter 3

Modeling Mad2 Function in Sequestering Cdc20

Contents

3.1 Summary

For successful mitosis, metaphase has to be arrested until all centromeres are properly attached. The onset of anaphase, which is initiated by activating the APC, is controlled by the spindle assembly checkpoint ^{M}SAC . Mad2, which is a constitutive member of the ^{M}SAC , is supposed to inhibit the activity of the APC by sequestering away its co-activator Cdc20. Mad1 recruits Mad2 to unattached kinetochores and is compulsory for the establishment of the Mad2 and Cdc20 complexes. Recently, based on results from *in vivo* and *in vitro* studies, two biochemical models were proposed: the Template and the Exchange model. Here, we derive a mathematical description to compare the dynamical behavior of the two models. Our simulation analysis supports the Template model. Using experimentally determined values for the model parameters, the Cdc20 concentration is reduced down to only about half. Thus, although the Template model displays good metaphase-to-anaphase switching behavior, it is not able to completely describe ^{M}SAC regulation. This situation is neither improved by amplification nor by p31^{comet} inhibition. We speculate that either additional reaction partners are required for total inhibition of Cdc20 or an extended mechanism has to be introduced for ^{M}SAC regulation.

3.2 Introduction

To address the question, how Cdc20 concentration relates to anaphase onset and how it is regulated, we investigated the role of Mad1 in eliciting the formation of the Cdc20:Mad2 complex on the basis of two biochemical models, the exchange (Luo et al., 2004) and the template (DeAntoni et al., 2005a) model. To this end, we derived the reaction equations from the description in (Luo et al., 2004; DeAntoni et al., 2005a). Using standard principles of chemistry and thermodynamics, we converted the reaction equations into non-linear ordinary differential equations for the concentrations of the reactants. To simulate their dynamics in the course of time, the differential equations were integrated for different values of the kinetic constants involved. To find a behavior in concordance with experimental

results, we employed a minimization procedure. The purpose of this chapter is threefold. First, we show how to derive a mathematical model for the biochemically described Exchange and Template models. Then, as the main purpose, we compare the two models by mathematical simulations and show that the Exchange model is not able to realistically describe the metaphase-to-anaphase transition. Though the Template model in principle can show correct switching behavior for this transition, it is not able to sequester away Cdc20 completely whenever physiologically realistic kinetic constants are used. Therefore, in a third step, we investigate six further extensions of the Template model, based on recently described biochemical amplification and inhibition effects, especially considering the role of $p31^{comet}$. As total inhibition of Cdc20 activity during metaphase is the basis of most models for metaphase-to-anaphase transition (Ibrahim et al., 2007; Toth et al., 2007; Queralt et al., 2006), it is an important question, whether Mad2 is able to fully Cdc20 sequester (inhibition) or additional reaction partners are required or an extended ^{M}SAC regulation mechanism has to be introduced?

3.3 Methods: Definition and Simulation of the Models

For each model, we describe briefly the basic biochemical pathways and experimental findings. These experimental foundations are turned into chemical reaction equations. In some cases, reactions depend on the attachment of the microtubules to the kinetochore, which is described by a switching parameter u: before attachment, we set $u = 1$; and after attachment, $u = 0$. Formation of the Mad1:C-Mad2:OMad2* complex in the classical Template model is an example for this dependence (see Eq. (3.6)). The corresponding kinetic parameter α_T is therefore multiplied by u. Biochemically, the switching parameter u may represent the function of dynein, which after microtubule attachment removes the Mad1:C-Mad2 2:2 complex from the kinetochore site.

The reaction equations are converted into non-linear ordinary differential equations (ODEs) using the mass action kinetics (c.f. Appendix B B.1-B.5). Starting from

initial concentrations for all reaction partners taken from literature (cf. Table 3.1), the ODEs are integrated until steady state is reached before attachment (using $u = 1$). After switching u to 0, the equations are again integrated, until steady state is reached. The minimum concentration of Cdc20 before attachment and the recovery after attachment (level of Cdc20 increase and recovery time) are criteria to compare the models. As far as documented in the literature, experimental values are used for the kinetic constants. In all other cases, we select representative values for each parameter (cf. Table 3.1) exemplifying its whole physiologically possible range. The resulting concentration curves show the influence of the kinetic parameter on the behavior of the model. It can be clearly seen that the variation of the curves depends in a continuous manner on the variation of the parameters. Their influence on the behavior of the models is described in detail in the respective sections. In a more global approach, we fit optimal values to the model parameters by minimizing a Cdc20 concentration objective functional describing a minimal Cdc20 concentration before and a maximal concentration after switching (see Appendix B B.6). Minimization was performed by statistical approaches by selecting randomly starting values within the whole range of parameters. For the Cdc20 concentration functional, a minimal solution is in general not unique, as can be seen from the graphs with the example parameter settings. On the other hand, due to the continuous behavior of the system in dependence of the parameters, in some cases parameters tend to an asymptotic, often physiologically unrealistic, value. In other cases, the velocity of Cdc20 recovery after switching can help to define a possible parameter set. The details are explained in the respective model sections.

3.4 Biochemical Basis of the Models

The biochemical basis of the models are the binding kinetics of Mad1, Mad2, and Cdc20. Mad1 forms a tight 2:2 complex with Mad2 (Sironi et al., 2001a). Binding of Mad2 to Mad1 triggers a conformational change of Mad2, in a similar way as does Cdc20 binding: Mad2 binds to Mad1 and Cdc20 in the same pocket with similar affinities (Luo et al., 2002). Mad2 can adopt two conformations, O-Mad2

and C-Mad2, differing in the structure of its 50 residue C-terminal segment (Luo et al., 2002). The O-Mad2 is the physiological state of cytosolic Mad2 in the absence of Mad1 or Cdc20 (Luo et al., 2004). O-Mad2 refolds to C-Mad2 when bound to the kinetochore receptor Mad1 or the APC activator Cdc20 (Luo et al., 2004). Upon microtubule attachment, Mad1 (Campbell et al., 2001) remains detectable at kinetochores whereas Mad2 (Lampson and Kapoor, 2005) depletes from the kinetochores.

3.5 The Exchange Model

In order to explain the formation of the Mad1:Cdc20 complex, Luo et al. (2004) suggested the Mad2 Exchange model, based on a series of *in vitro* and *in vivo* experiments. It assumes that Mad1 recruits open Mad2 (O-Mad2) at the kinetochore and transforms its conformation from open Mad2 (O-Mad2) to closed Mad2 (C-Mad2). C-Mad2 then dissociates away from Mad1 and binds Cdc20. This model portrays Mad1 as a catalyst of the structural transition of O-Mad2 into C-Mad2. The reaction rules governing the Exchange model are (cf. Figure 3.1):

$$\text{O-Mad2} \underset{\mathrm{k}_{-1}}{\overset{k_1}{\rightleftharpoons}} \text{C-Mad2} \tag{3.1}$$

$$\text{Mad1} + \text{O-Mad2} \underset{\mathrm{k}_{-2}}{\overset{\alpha_E.u}{\rightleftharpoons}} \text{Mad1:C-Mad2} \tag{3.2}$$

$$\text{Mad1:C-Mad2} \underset{\mathrm{k}_{-3}}{\overset{k_3}{\rightleftharpoons}} \text{C-Mad2} + \text{Mad1} \tag{3.3}$$

$$\text{C-Mad2} + \text{Cdc20} \xrightarrow{k_E} \text{Cdc20:C-Mad2} \tag{3.4}$$

$$\text{Cdc20:C-Mad2} \xrightarrow{\eta_E} \text{Cdc20} + \text{O-Mad2} \tag{3.5}$$

which lead to the set of time dependent nonlinear ODEs listed in Appendix B B.1, Eqs. (B.1)-(B.6).

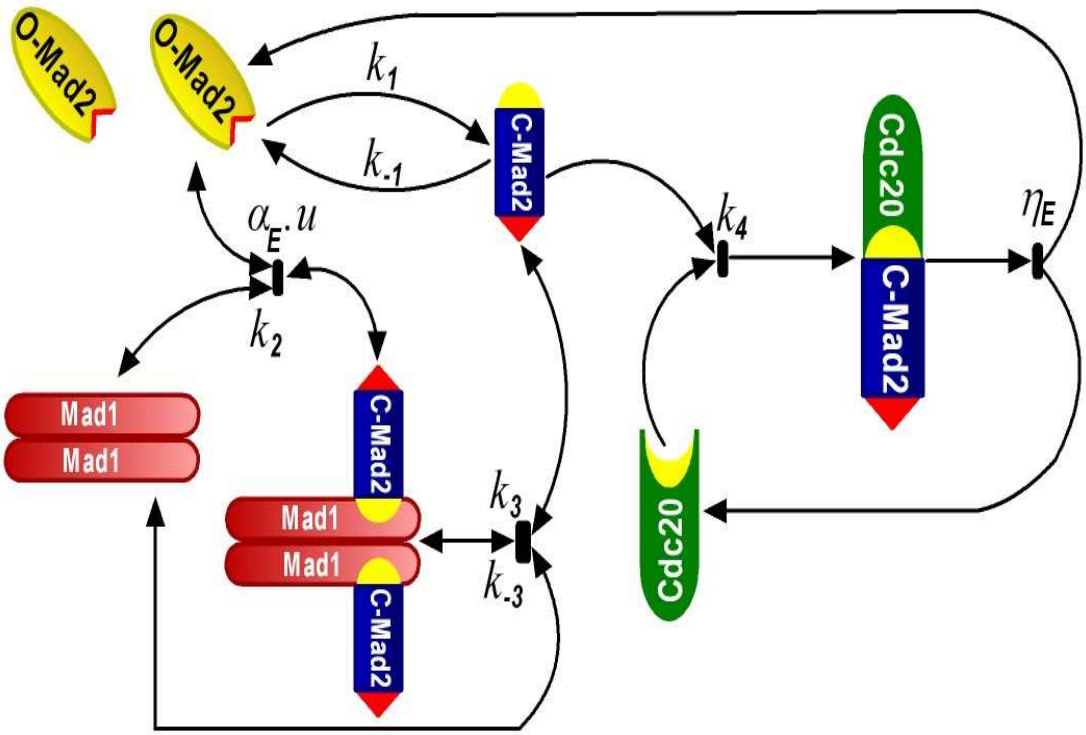

Figure 3.1: Schematic reaction network of the Exchange model. In the Exchange model (Luo et al., 2004), it is assumed that Mad1 recruits open Mad2 (O-Mad2) at the kinetochore and transforms its conformation from O-Mad2 to closed Mad2 (C-Mad2). C-Mad2 then dissociates from Mad1 and binds Cdc20. This model portrays Mad1 as a catalyst of the structural transition of O-Mad2 into C-Mad2. Already this purely biochemical description gave rise to several criticisms (Lénárt and Peters, 2006; Hardwick, 2005). Especially the question remained, why and how Mad2 first binds (as O-Mad2) to Mad1, but then dissociates off (as C-Mad2) (DeAntoni et al., 2005b).

The only parameter dependent on the kinetochore attachment status is α_E which therefore is multiplied by the switching parameter u. The reaction scheme contains the background reaction for O-Mad2 conversion to C-Mad2 (Eq. (3.1)) with very low rates k_1 and k_{-1} (Luo et al., 2004). For α_E, k_{-2}, k_3, and k_{-3} we used quantitative experimental data from (Luo et al., 2004) (see Table 3.1). The remaining two parameters k_E and η_E were varied within a realistic range (Luo et al., 2004; DeAntoni et al., 2005a; Fang, 2002): k_E between $10^5 \mathrm{M}^{-1}\mathrm{s}^{-1}$and $10^9 \mathrm{M}^{-1}\mathrm{s}^{-1}$and η_E between $3 * 10^{-5}\mathrm{s}^{-1}$and $10^{-2}\mathrm{s}^{-1}$. When analyzing this set of ODEs, we found that only for very small η_E ($3 * 10^{-5}\mathrm{s}^{-1}$) the initial Cdc20 concentration is clearly reduced to about half the initial value (Figure 3.2a) while for the higher values of η_E ($10^{-2}\mathrm{s}^{-1}$) the Cdc20 concentration hardly changed (Figure 3.2d). Our data indicate that the switching of u from 1 to 0 has little influence on Cdc20 concentration, smaller η_E (Figure 3.2 a) showing slightly larger effects than larger η_E (Figure 3.2 d). A large influence of u on Cdc20 concentration, however, is required for checkpoint function. While the $^{\mathrm{M}}$SAC is activated, the concentration of Cdc20 should be low, and should switch to large values when the kinetochores are attached. The Exchange model does not describe this behavior.

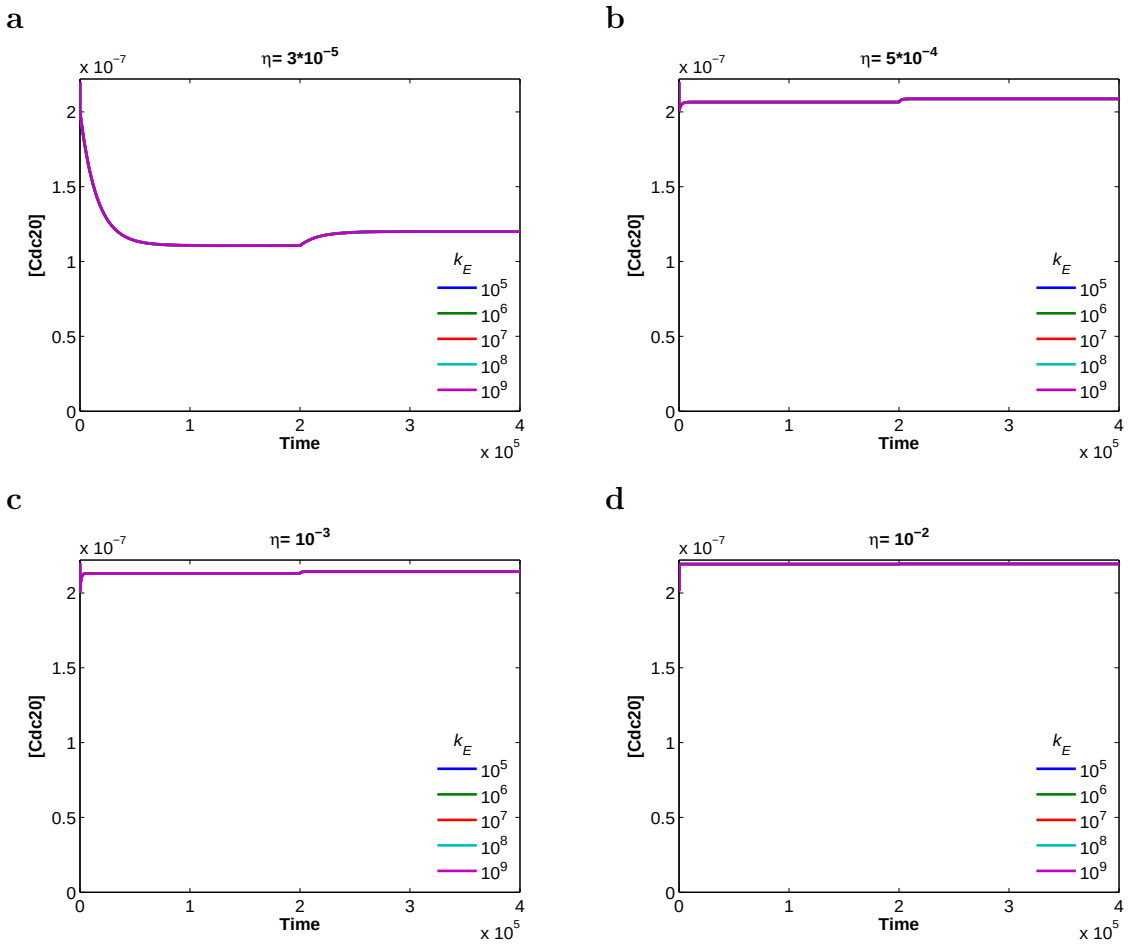

Figure 3.2: The dynamical behavior of the Exchange model with different values of k_4 and η_E. Color lines represent different values of k_4, which is without influence on the model behavior, as all line coincide. Switching of u from 0 to 1at time

3.6 The Template Model

In the Exchange model it remained unclear, how Mad2 first binds to Mad1 and then dissociates off by just adopting another conformation. In an experimental study, (DeAntoni et al., 2005a) provided information about the detailed reaction mechanism, which was finally condensed into the Mad2 Template model. It assumes that Mad1 and C-Mad2 form a stable core complex at unattached kinetochores (DeAntoni et al., 2005a). This core then binds additional molecules of O-Mad2 through formation of conformational heterodimers between the C-Mad2 subunit of the Mad1:C-Mad2 complex and O-Mad2. Cdc20 binding to this complex leads to the conversion of O-Mad2 to C-Mad2 resulting in the formation of Cdc20:C-Mad2, which in turn is assumed then to dissociate off Mad1:C-Mad2 (Fang, 2002). Upon Mad1:C-Mad2 binding, O-Mad2 adopts an intermediate conformation (O-Mad2*) that can quickly and efficiently bind Cdc20 and switch to the C-conformation (see Figure 3.3). The reaction rules covering the Template model are (cf. Appendix B B.2 for ODEs):

$$\text{Mad1:C-Mad2} + \text{O-Mad2} \underset{\beta_T}{\overset{\alpha_T.u}{\rightleftharpoons}} \text{Mad1:C-Mad2:O-Mad2}^* \tag{3.6}$$

$$\text{Mad1:C-Mad2:O-Mad2}^* + \text{Cdc20} \xrightarrow{\gamma_T.u} \text{Cdc20:C-Mad2} + \text{Mad1:C-Mad2} \tag{3.7}$$

$$\text{Cdc20:C-Mad2} \xrightarrow{\eta_T} \text{O-Mad2} + \text{Cdc20} \tag{3.8}$$

The kinetic constants α_T, β_T, and γ_T depend on the attachment state of the kinetochore and are thus multiplied by the variable u. We used quantitative data from FRAP experiments for α_T and β_T (Vink et al., 2006). The remaining two parameters γ_T and η_T were varied widely within realistic frames (Luo et al., 2004; DeAntoni et al., 2005a; Fang, 2002): η_T between $5 * 10^{-4}\text{s}^{-1}$and 10^{-1}s^{-1}, and γ_T between $10^5\text{M}^{-1}\text{s}^{-1}$and $10^9\text{M}^{-1}\text{s}^{-1}$(c.f. Table 3.1). Characteristic Cdc20 concentration curves were obtained as displayed in 3.4.

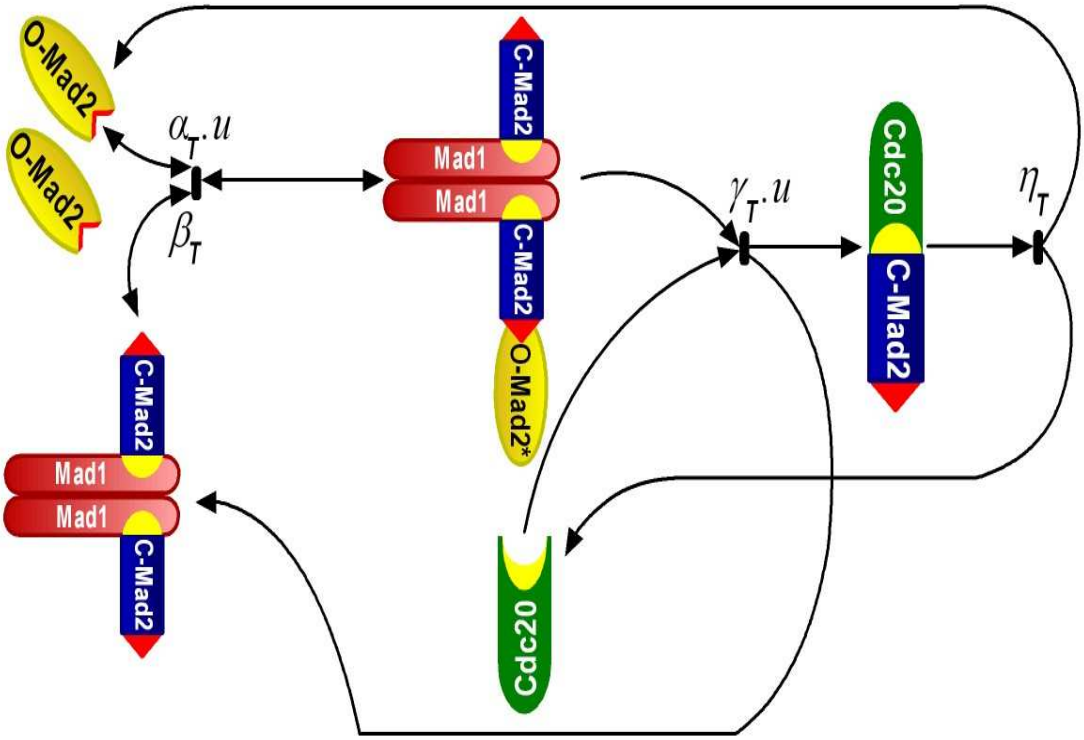

Figure 3.3: Schematic reaction network of the Template model. In a subsequent sophisticated experimental investigation, (DeAntoni et al., 2005a) could precise the reaction mechanism further and developed the biochemical Template model. Here, it is assumed that Mad1 and C-Mad2 form a stable core complex at unattached kinetochores. This core then binds additional molecules of O-Mad2 through formation of conformational heterodimers between the C-Mad2 subunit of the Mad1:C-Mad2 complex and O-Mad2. Cdc20 binding to this complex leads to the conversion of O-Mad2 to C-Mad2 resulting in the formation of Cdc20:C-Mad2, which in turn is assumed then to dissociate off Mad1:C-Mad2 (Fang, 2002). But even with this refined description, many questions remained open (Mapelli et al., 2006; Nezi et al., 2006), and a decision for one of the models to be more realistic could not be met Vink et al. (2006).

For η_T values smaller than $10^{-1}s^{-1}$, we observed a clear dependence of the Cdc20 concentration on the switching parameter u with the effect being larger for larger γ_T. In early mitosis ($u = 1$), for η_T values in the order of $10^{-3}s^{-1}$(clearly smaller than $10^{-2}s^{-1}$) and γ_T values larger than $10^6M^{-1}s^{-1}$, the Template model sequesters about half of the Cdc20 concentration (Figure 3.4) in quantitative agreement with experimental findings (Luo et al., 2004; Fang, 2002). However, within this frame of realistic parameter variations, Cdc20 is never completely inhibited as would be required for checkpoint function. η_T determines the rate of Cdc20 concentration recovery after u is switched to zero: small η_T values of about $10^{-3}s^{-1}$display slow recovery while values of $10^{-2}s^{-1}$and above show fast recovery (Figure 3.4).

Already Fang (2002) increased the Mad2 level 100fold (to 22.5 μM) to gain maximal Cdc20 inhibition. In our Template model simulation, an 8fold increase of free Mad2 concentration showed complete Cdc20 disappearance for small η_T ($< 10^{-1}s^{-1}$) and large γ_T ($> 10^6M^{-1}s^{-1}$) (see Figure 3.5). In addition, the rate of Cdc20 recovery becomes fast for larger values of η_T. However, this Mad2 concentration is far above experimentally observed values (Fang, 2002).

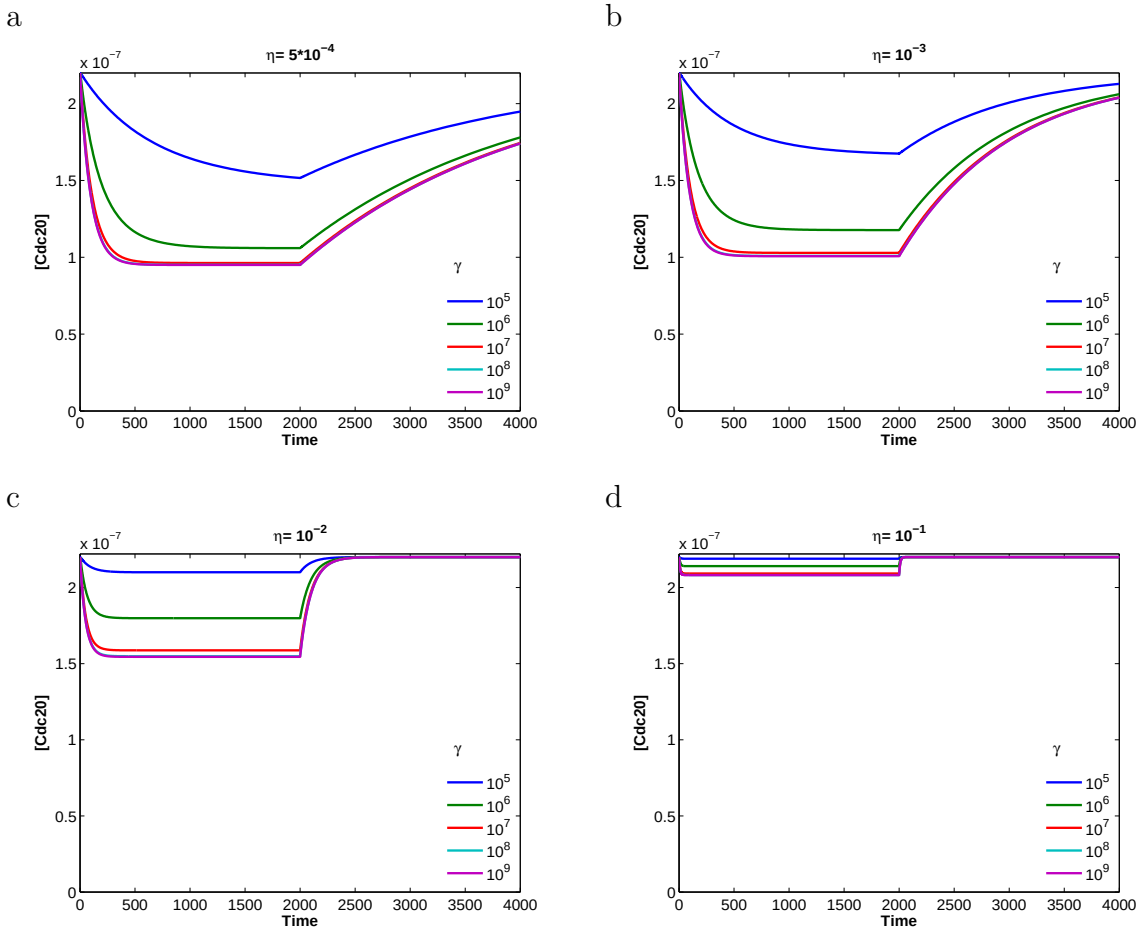

Figure 3.4: The dynamical behavior of the Template model with different values of γ_T and η_T. Figures a, b, c, and d for physiological data (see text), for increase Mad2 see Figure 3.5. Switching of u from 0 to 1 at time 2000 s

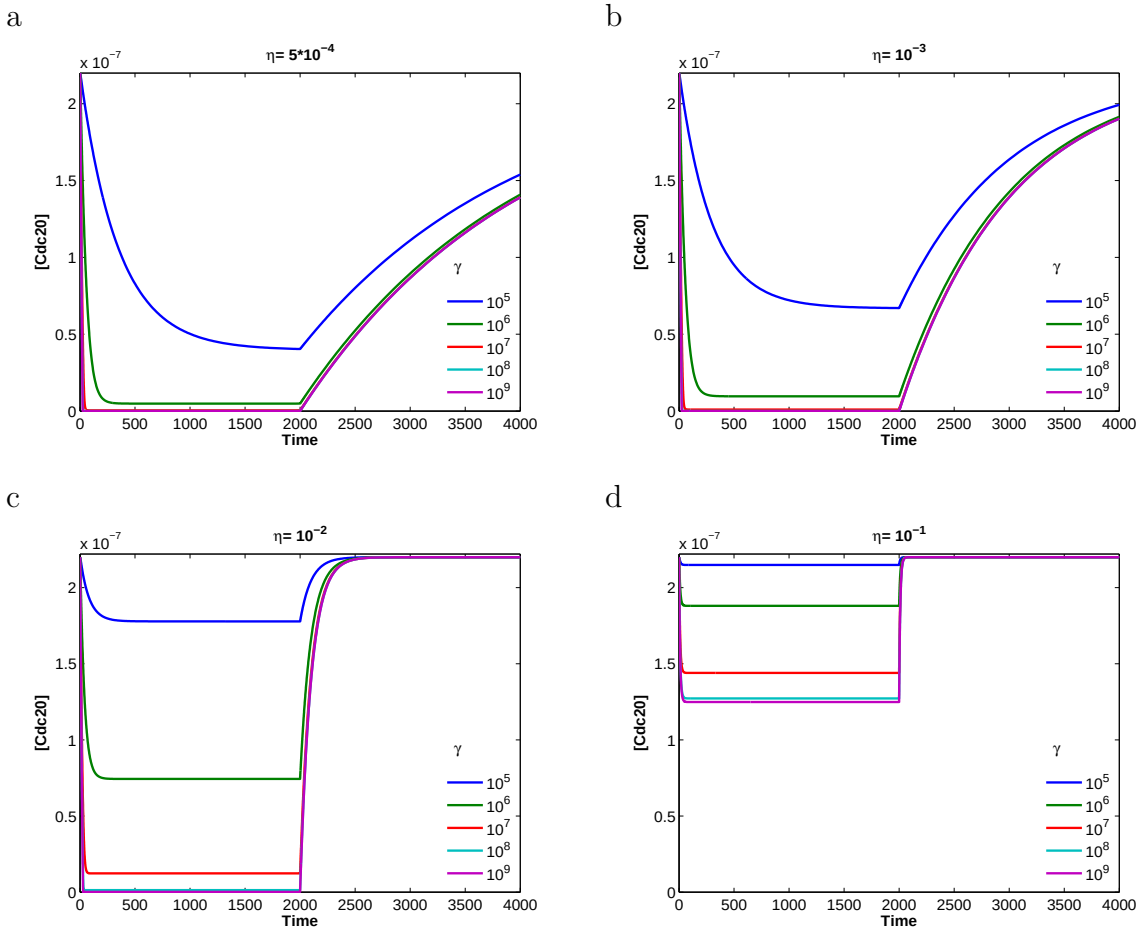

Figure 3.5: The dynamical behavior of the Template model with different values of γ_T and η_T. Figures a, b, c, and d for 8folds increase of free Mad2. Switching of u from 0 to 1 at time 2000 s

3.7 Variations of the Template model

In the Template model, for realistic parameter ranges, Cdc20 inhibition is not as high as anticipated. We therefore modified the model according to recent experimental results.

3.7.1 Amplification Effects

DeAntoni et al. (2005a) hypothesized that in analogy to the reactions in Eqs. (3.6) and (3.7) based on Mad1, Cdc20:C-Mad2 can also be formed by the reactions in Eqs. (3.9) and (3.10) below based on Cdc20. This additional pathway for the production of Cdc20:C-Mad2 results in a signal amplification for the ^{M}SAC since Cdc20:C-Mad2 now is produced not only at the location of Mad1 at the kinetochore but at a larger number of locations everywhere in the cell. To check the effect of this additional pathway, we added two reactions (3.9-3.10) to the Template model (see Figure 3.6 a, ODEs Appendix B B.3):

$$\text{Cdc20:C-Mad2} + \text{O-Mad2} \underset{k_{-4}}{\overset{k_4}{\rightleftharpoons}} \text{Cdc20:C-Mad2:O-Mad2}^* \tag{3.9}$$

$$\text{Cdc20:C-Mad2:O-Mad2}^* + \text{Cdc20} \xrightarrow{k_5} 2\,\text{Cdc20:C-Mad2} \tag{3.10}$$

The Mad2 heterodimer formation at the Mad1 location is considered to be as fast as at Cdc20, so that k_4 and k_5 would be as large as α_T and γ_T, respectively. For k_4 and k_5 both equal to $10^5\text{M}^{-1}\text{s}^{-1}$, $\eta_T = 10^{-3}\text{s}^{-1}$and γ_T in the range between $10^5\text{M}^{-1}\text{s}^{-1}$and $10^9\text{M}^{-1}\text{s}^{-1}$. Our calculations indicate that the switching parameter u has little to no effect on the Cdc20 concentration (Figure 3.7 b). Small $k_4 = k_5 = 10^3\text{M}^{-1}\text{s}^{-1}$have vanishing influence on the model and roughly show the Template model behavior as observed before (Figure 3.7 a). Furthermore, using our fitting procedure for optimal parameters, the values of k_4 and k_5 tend to zero: the amplification is discarded from the reaction scheme.

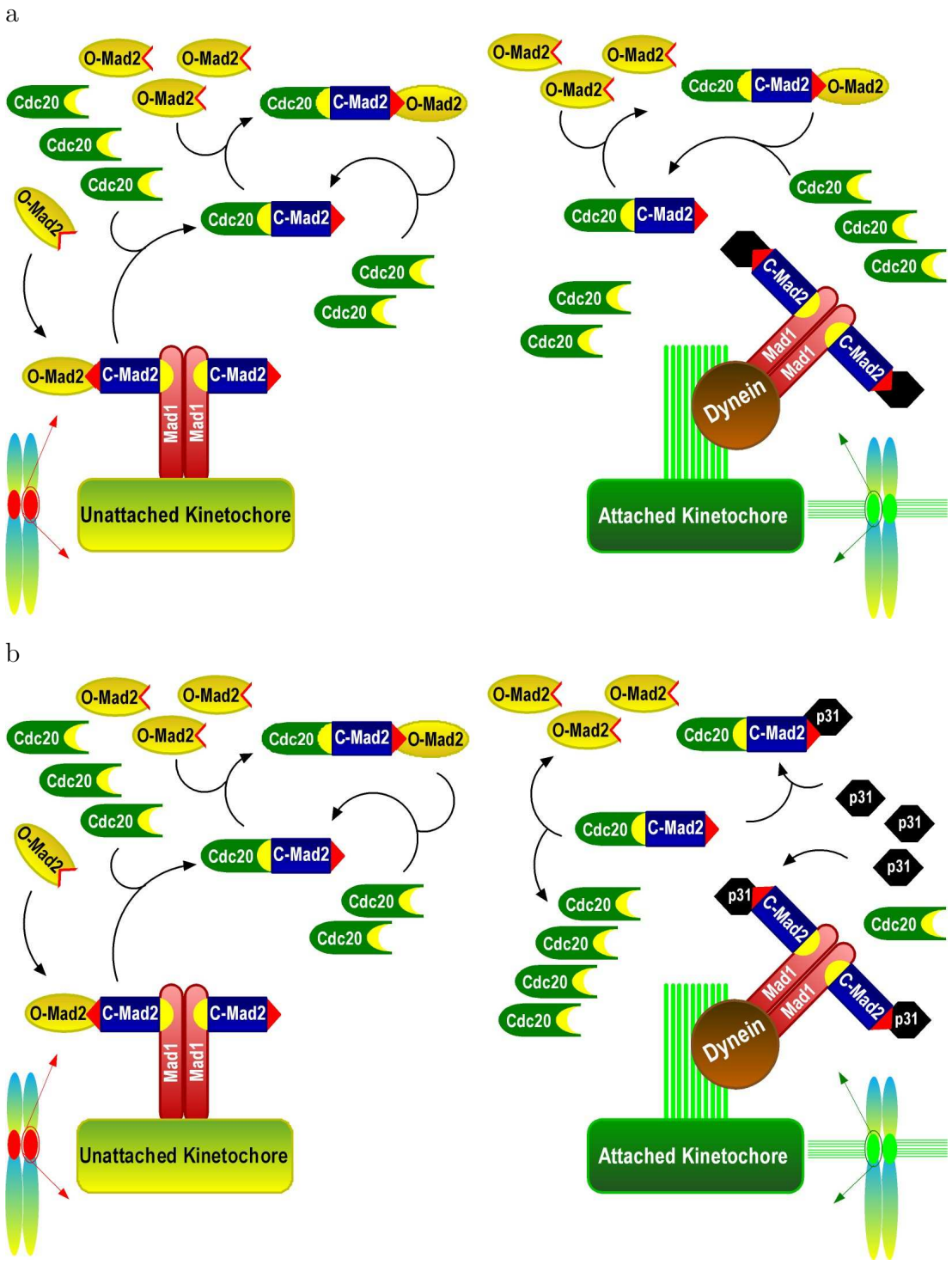

Figure 3.6: Schematic reaction networks and localization: (a) the Template model with amplification, (b) the Template model with amplification controlled by $p31^{comet}$.

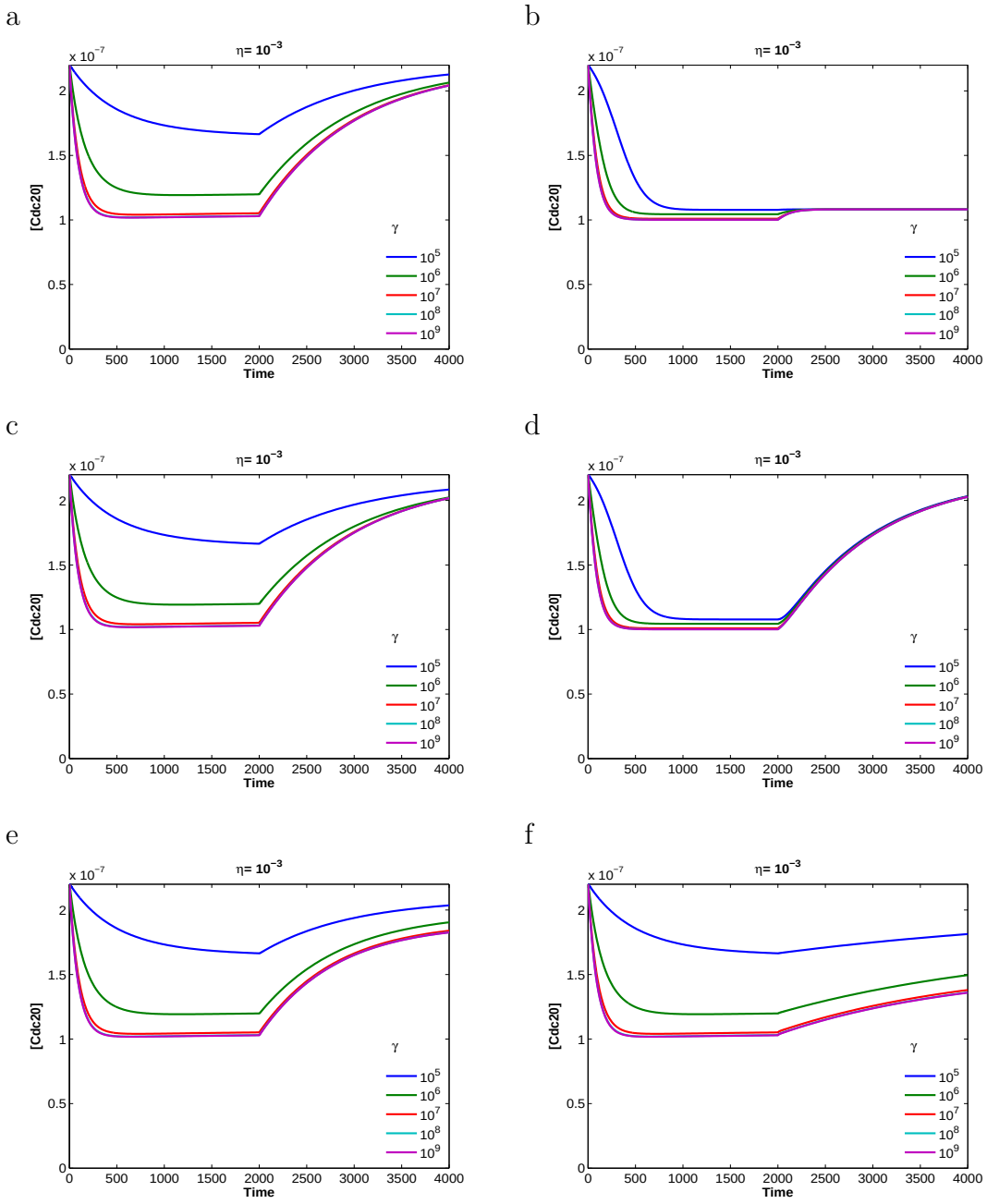

Figure 3.7: The dynamical effects of the different amplification mechanisms in the Template model (time in s) : a and b represent the case, in which the amplification is uncontrolled (Eqs (B.12)-(B.17), Appendix B B.3). c and d: amplification controlled by the switching parameter u (Eqs (B.25)-(B.33), Appendix B B.5). e and f: e and f: controlled amplification, but now with p31$^{\text{comet}}$. Left column (a, c, e): low amplification rate $k_4 = k_5 = 10^3\text{M}^{-1}\text{s}^{-1}$. Right column (b, d, f): high amplification rate $k_4 = k_5 = 10^5\text{M}^{-1}\text{s}^{-1}$. Numerical solution of the differential equations in Appendix B B.3, B.4, and B.5. Color lines represent different values of γ_T.

The additional amplification reactions could contribute to the model behavior, in case the reaction Eq. (3.9) did not take place all the time, but instead would also be controlled by the switching parameter u (k_4 replaced by $k_4.u$). With the same parameter values as in the previous calculation (Figure 3.6 d), we obtained Cdc20 concentrations nearly independent from γ_T: low Cdc20 concentrations were reached now also for small values of γ_T (Figure 3.6 c). However, we have no experimental indication for such an influence of microtubule attachment to kinetochores on k_4.

3.7.2 Inhibition Effects

Another way to vary the Template model is the introduction of the Mad2 ligand p31$^{\text{comet}}$ (formerly CMT2), which is a negative regulator of the spindle checkpoint. It prevents further Mad2 turnover on Mad1 and neutralizes the inhibitory activity of Cdc20-bound Mad2, leading to activation of APC followed by degradation of Securin and Cyclin B (Habu et al., 2002). Its negative effect on the $^{\text{M}}$SAC is based on its competition with O-Mad2 for C-Mad2 binding (Habu et al., 2002; Xia et al., 2004). It forms triple complexes with C-Mad2 and either Mad1 or Cdc20 (Xia et al., 2004). If p31$^{\text{comet}}$ is activated at microtubule attachment to the kinetochores, it might be a cellular factor contributing to the checkpoint switching behavior. Therefore, we introduced an additional reaction 3.11 into the Template model reactions (3.6-3.8) describing the effect of p31$^{\text{comet}}$ (ODEs Appendix B B.4):

$$\text{Mad1:C-Mad2} + \text{p31} \underset{\zeta_T}{\overset{\delta_T.v}{\rightleftharpoons}} \text{Mad1:C-Mad2:p31} \tag{3.11}$$

The activation of p31$^{\text{comet}}$ is taken care of by the introduction of the switching parameter v which is equal to zero until the kinetochores are attached and switches to one afterwards. In fact, the function of the switching parameter u can be totally replaced by p31$^{\text{comet}}$ inhibition, as the p31$^{\text{comet}}$ system with $u = 1$ all the time

shows the same dynamic results as the unmodified Template model (Figure 3.4). Combining both effects (u and v switching) still show the same dynamics.

3.7.3 Amplification plus Inhibition Effects

Including both, amplification and p31$^{\text{comet}}$ inhibition, into the Template model, we obtain the chemical reaction scheme (see Figure 3.6 b), consisting of Eqs. (3.6-3.8), (3.9-3.10), and an additional equation (3.12), (ODEs Appendix B B.5):

$$\text{Cdc20:C-Mad2} + \text{p31} \underset{\sigma_T}{\overset{\xi_T . v}{\rightleftharpoons}} \text{Cdc20:C-Mad2:p31} \tag{3.12}$$

For $u = 1$ before and after attachment (all the time), the model behavior is not influenced before switching ($v = 0$). After switching ($v = 1$), for low $\xi_T = 10^3 \text{M}^{-1}\text{s}^{-1}$, the new additional reaction mechanism is slightly less effective in Cdc20 recovery, whereas for high $\xi_T = 10^5 \text{M}^{-1}\text{s}^{-1}$, Cdc20 cannot recover since it is incorporated into the triple complex with C-Mad2 and p31$^{\text{comet}}$. Combining u and v switching does not change the dynamics.

3.8 Discussion

The mitotic checkpoint proteins Mad1, Mad2 and Cdc20 play an essential role in cell cycle control by contributing to the regulation of the $^{\text{M}}$SAC mechanism (DeAntoni et al., 2005a). Their interactions have been studied experimentally (e.g. (Luo et al., 2004; DeAntoni et al., 2005a; Fang, 2002)) resulting in two alternative models describing their behavior, the “Exchange model” (Luo et al., 2004) and the “Template model” (DeAntoni et al., 2005a). Recently, experimental data questioned the validity of the Exchange model while they supported the Template model (Mapelli et al., 2006; Nezi et al., 2006; Vink et al., 2006). Here, the two models were described by sets of chemical reactions, which were transformed into

Model Parameters

Parameters	References
Species initial concentrations	
[Cdc20]= $2.2 * 10^{-7}$M	(Tang et al., 2001; Fang, 2002; Howell et al., 2000a)
[Mad1]= $0.5 * 10^{-7}$M	(Tang et al., 2001; Fang, 2002; Howell et al., 2000a)
[O-Mad2]= $1.5 * 10^{-7}$M	(Tang et al., 2001; Fang, 2002; Howell et al., 2000a)
[C-Mad2]= $0.1875 * 10^{-7}$M	(Tang et al., 2001; Fang, 2002; Howell et al., 2000a)
[Mad1:C-Mad2]= $0.5 * 10^{-7}$M	(Tang et al., 2001; Fang, 2002; Howell et al., 2000a)
[$p31^{comet}$] = $10 * 10^{-7}$M	(Xia et al., 2004; Mapelli et al., 2006)
Other species are zero	
Template model	
$\alpha_T = 5 * 10^5$ $M^{-1}s^{-1}$	(Vink et al., 2006)
$\beta_T = 0.2$ s^{-1}	(Vink et al., 2006)
$\delta_T = 1.7 * 10^6$ $M^{-1}s^{-1}$	(Vink et al., 2006)
$\zeta_T = 0.037$ s^{-1}	(Vink et al., 2006)
$k_4 = 10^3, 10^5$ $M^{-1}s^{-1}$	This study
$k_{-4} = 0.03$ s^{-1}	This study
$k_5 = 10^3, 10^5$ $M^{-1}s^{-1}$	This study
$\gamma_T = 10^5, 10^6, 10^7, 10^8, 10^9$ $M^{-1}s^{-1}$	This study
$\eta_T = 5 * 10^{-4}, 10^{-3}, 10^{-2}, 10^{-1}s^{-1}$	This study
Exchange model	
$k_1 = 3 * 10^{-5}$ s^{-1}	(Luo et al., 2004)
$k_{-1} = 5.2 * 10^{-6}$ s^{-1}	(Luo et al., 2004)
$\alpha_E = 4 * 10^3$ $M^{-1}s^{-1}$	(Luo et al., 2004)
$k_{-2} = 1.5 * 10^{-2}$ s^{-1}	(Luo et al., 2004)
$k_3 = 2.8 * 10^{-4}$ s^{-1}	(Luo et al., 2004)
$k_{-3} = 23$ $M^{-1}s^{-1}$	(Luo et al., 2004)
$k_E = 10^5, 10^6, 10^7, 10^8, 10^9 M^{-1}s^{-1}$	This study
$\eta_E = 3 * 10^{-5}, 5 * 10^{-4}, 10^{-3}, 10^{-2}s^{-1}$	This study

Table 3.1: Kinetic data. Species initial concentrations and parameters value for models.

sets of nonlinear ordinary differential equations (ODEs). The ODEs quantitatively display the dynamic behavior of the models. Where experimental results were available, parameters were chosen according to these data. The unknown systems parameters were optimized according to the known behavior of the Cdc20 concentration at the metaphase to anaphase transition (Appendix B B.6).

The Exchange model was suggested by Luo et al. (2004) in order to explain their experimental data. This model however had been criticized because it is unable to explain additional experimental data from other groups (Musacchio and Salmon, 2007; Mapelli et al., 2006; Nezi et al., 2006; Vink et al., 2006) and since it assumes that Mad1 competes with Cdc20 for Mad2 binding. We identified an additional weakness of the Exchange model: it is hardly able to show switching kinetics. This property is model inherent since those reactions involving Cdc20 are kinetochore uncontrolled and are not influenced by microtubule attachment. Moreover, the steady state is reached very slowly (about 100 times slower than in the Template model). In addition, when applying experimentally determined parameter values, the Exchange model is not able to sequester Cdc20 sufficiently as would be required for ^{M}SAC regulation. Even a free parameter optimization did not result in a satisfying model switching behavior.

In contrast, the behavior of the Mad2 Template model (DeAntoni et al., 2005a) is in accordance with experimental observations (Fang, 2002; Mapelli et al., 2006; Vink et al., 2006) and shows robust switching behavior. However, the Cdc20 concentration is only reduced down to about half when experimentally determined values are used for the model parameters. This observation is in agreement with Fang (2002), and Luo et al. (2004) in HeLa cells. Complete sequestering of Cdc20 is obtained for higher Mad2 concentrations, as observed by Fang (for a 100fold higher Mad2 concentration). When increasing the free Mad2 concentration 8fold in the Template model, we found complete reduction of Cdc20 concentration. However, there is no experimental indication for such a high Mad2 concentration in HeLa cells. Thus, although showing robust switching behavior when using experimentally determined parameter values, the Template model as listed is unable to result in complete inhibition of Cdc20. This conclusion is in agreement with statements of Fang (2002). Contributions from additional reaction partners

are required for complete Cdc20 sequestering. Such a reaction partner seems to be the checkpoint protein BubR1 which also binds Cdc20 (Fang, 2002; Sudakin et al., 2001; Tang et al., 2001) and cooperates to form the mitotic checkpoint complex MCC (Sudakin et al., 2001).

Mad2 heterodimers can bind to either Mad1 or Cdc20 (DeAntoni et al., 2005a,b). Thus, C-Mad2:Cdc20 complexes can be formed not only at Mad1 kinetochore sites but in the whole cell, amplifying complex formation. To investigate the amplification mechanism, we extended the Template model by the appropriate reactions. When the newly introduced reaction rates are small, these reactions do not contribute to the model behavior. If however the rates are high, there is hardly any Cdc20 recovery after switching since these amplification reactions are not influenced by mitotic progression. Thus, these additional reactions do not improve Template model behavior.

The checkpoint inhibitor $p31^{comet}$ competes with O-Mad2 for C-Mad2 binding, thus preventing the binding of O-Mad2 to C-Mad2 (Mapelli et al., 2006; Habu et al., 2002; Ciliberto et al., 2005). It binds to the surface of C-Mad2 opposite to Mad1 and Cdc20 (Mapelli et al., 2006; Vink et al., 2006), forming triple complexes with these proteins. If $p31^{comet}$ is activated at metaphase to anaphase transition, our model calculations clearly show that $p31^{comet}$ is able to introduce switching behavior into the model and would be even able to replace the function of the switching parameter u: The Template model behavior is very similar when u is removed and $p31^{comet}$ reactions are added to the model. The situation is slightly different in the presence of the amplification reactions. Now, removing u and introducing the $p31^{comet}$ reactions, we found no improved Cdc20 recovery for small reactions rates ξ_T, however, strongly reduced recovery for large ξ_T rates. In order to distinguish between these two cases, additional experimental kinetic data are required for $p31^{comet}$ reactions. In general we observe that $p31^{comet}$ is not sufficient for full ^{M}SAC regulation. This finding is particularly interesting, because it was shown in a very general model that amplification reactions might be necessary to promote the final signal from the last attaching kinetochore for anaphase onset (Doncic et al., 2005; Sear and Howard, 2006). In (Doncic et al., 2005), $p31^{comet}$ is explicitly mentioned as a candidate for this information transmission.

The switching parameter u represents the function of dynein which after microtubule attachment removes the Mad1:C-Mad2 2:2 complex from the kinetochore site. It might also represent potential additional functions which contribute to switching behavior. When both, u and $\mathrm{p31}^{\mathrm{comet}}$, are included in the reaction scheme, the general behavior of the system is not improved over those systems including only u or only $\mathrm{p31}^{\mathrm{comet}}$. We observed an improvement however, when the reaction Eq. (3.9) becomes controlled by u. Now, before attachment, low concentrations for Cdc20 were observed even for low values of γ_T, and after attachment Cdc20 recovers fast independent of γ_T values, showing an considerably improved regulation behavior. However, we have no experimental indication for a mitotic control of reaction Eq. (3.9).

3.9 Conclusion

Taken together we conclude, that the presented Exchange model is not describing checkpoint function. The Template model is clearly superior and shows robust switching behavior. However, applying experimentally determined parameter values to this model, Cdc20 is not sequestered completely. Additional reaction partners would be required for total inhibition of free Cdc20. BubR1 would be a potential candidate for this function. Thus, as a next step (Chapter 4), MCC formation including BubR1 and Cdc20 will be included into the quantitative analysis.

"The best model of a cat is another cat or, better, the cat itself".

Norbert Wiener (1894 - 1964)

"One of the deepest functions of a living organisms is to look ahead... to produce future".

Francois Jacob (1974 -)

Chapter 4

Modeling MCC assembly

Contents

4.1 Summary

BubR1 binds Cdc20 within two seemingly different contexts. In the first context, it forms an isolated complex with Cdc20, whereas in the second it is part of a larger complex of proteins (BubR1, Cdc20, Mad2, Bub3) called "Mitotic Checkpoint Complex", or MCC. We incorporated both contexts in two different models, and found that Cdc20 can be fully sequestered by BubR1 neither in the first nor in the second context. Moreover, it has been postulated that MCC formation can be either Kinetochore-independent (KIM) or Kinetochore-dependent (KDM) (e.g., Musacchio and Salmon, 2007). We found that only the Kinetochore-dependent model can -partially- account for the availability of Cdc20 both before and after the attachment of all chromosomes.

We observed that for the models analyzed, effective MCC formation cannot be combined with complete Cdc20 sequestering. Instead, the MCC might bind and completely block the APC. The ^{M}SAC might function by an MCC:APC complex rearrangement.

4.2 Molecular biological basis of MCC models

Sudakin et al. (2001) analysed and described the MCC in HeLa cells. It contains Mad2, Bub3, BubR1 and Cdc20 in apparently equal stoichiometries. A similar complex was identified in budding (Hardwick et al., 2000) and fission (Millband and Hardwick, 2002) yeasts and in Xenopus (Chung and Chen, 2003). Bub3 associates with BubR1 (Sudakin et al., 2001; Taylor et al., 2004, 1998a). This interaction is constitutive and is required for the localization of BubR1 to the kinetochores during mitosis. In prometaphase, CENP-E activates the kinase activity of BubR1 at unattached kinetochores (Mao et al., 2003, 2005; Chan et al., 1998). It is unclear whether the BubR1 activation is required for ^{M}SAC function (Mao et al., 2003; Chen, 2002b): the kinase activity of BubR1 might not be required in the MCC, however, it might control other aspects of kinetochore signaling or chromosome alignment (Ditchfield et al., 2003; Lampson and Kapoor, 2005)

(reviewed in Musacchio and Salmon (2007)). BubR1 activity is switched off upon microtubule attachment (Mao et al., 2005; Braunstein et al., 2007).

The binding properties of BubR1 are controverse. BubR1 cannot bind Mad2 directly (Fang, 2002). Though it was reported that BubR1 does not form a ternary complex with Mad2 and Cdc20 (Bolanos-Garcia et al., 2005; Davenport et al., 2006), for fission and budding (Burton and Solomon, 2007; King et al., 2007) yeasts such complexes (with Mad3) were found when investigating the highly conserved KEN boxes. Two Cdc20 binding sites were identified on BubR1 (Bolanos-Garcia et al., 2005; Davenport et al., 2006): Binding of the N-terminal region of BubR1 to Cdc20 requires prior binding of Mad2 to Cdc20 (Davenport et al., 2006). The other site (between residues 490 and 560) can bind Cdc20 tightly regardless of Mad2 being bound to Cdc20 (Davenport et al., 2006). Thus, BubR1 can form a ternary complex with Bub3 and Cdc20 which however has no inhibitory activity at the APC (unpublished data (Sudakin et al., 2001)).

During prometaphase, Cdc20 and all ^{M}SAC proteins concentrate at unattached kinetochores (Cleveland et al., 2003; Maiato et al., 2004), like Mad1 (Campbell et al., 2001; Chung and Chen, 2002), Mad2 (Fang et al., 1998a; Lampson and Kapoor, 2005), BubR1 (Morrow et al., 2005; Hoffman et al., 2001), Bub1 (Taylor et al., 1998a; Chen, 2002b), Bub3 (Taylor et al., 1998a; Howell et al., 2004), and Mps1 (Stucke et al., 2004, 2002). Kinetochore localization of Cdc20 and of its binding partners in the MCC is dynamic. Localization of all ^{M}SAC proteins at unattached kinetochores in mitosis provides a catalytic platform and contributes to MCC formation (Kallio et al., 2002a; Howell et al., 2000b; Shah et al., 2004). The MCC is also detectable in normal metaphase-arrested cells in which the ^{M}SAC is inactive. This indicates that MCC formation does not require checkpoint activation (Poddar et al., 2005). Moreover, the MCC is also detectable in checkpoint defective cells (Poddar et al., 2005; Fraschini et al., 2001). A detailed study (Meraldi et al., 2004) proposes that cytosolic Mad2-BubR1 is essential to restrain anaphase onset early in mitosis when kinetochores are still assembling. These arguments support the idea that the MCC (and its subcomplexes) might form in a kinetochore-independent manner (for review see Musacchio and Salmon (2007)). We thus distinguish two dynamical models (see Figure 4.1): a kinetochore

dependent model (KDM), and a kinetochore independent model (KIM). In the following, we define the chemical reaction equations based on empirical results and analyse their properties.

4.3 Mathematical modeling of the MCC

We analyse different models for MCC function considering in particular the role of the attachment status of the kinetochore. For each model, we describe the reaction equations in the usual biochemical notation specifying kinetic constants and assuming mass action rules to derive the differential equations for the concentrations as functions of time. Some of the reactions are independent of the kinetochore attachment status, others are mediated in some way by attachment or non-attachment, respectively. The most prominent equation will be the formation of the MCC complex

$$\text{Cdc20:C-Mad2} + \text{Bub3:BubR1} \underset{\mathrm{k}_{-F}}{\overset{\mathrm{k}_F}{\rightleftharpoons}} \text{MCC}$$

which, in the "kinetochore dependent model" (KDM), proceeds only, when the kinetochore is unattached, whereas in the "kinetochore independent model" (KIM) it proceeds all the time independently of the attachment status. Therefore, in the KDM, we set $\mathrm{k}_F := \mathrm{k}_4 \cdot u$, where u is a switching parameter, which is set to $u = 1$ as long as the kinetochore is unattached and switches to $u = 0$ when it attaches. The backward reaction with kinetic parameter $\mathrm{k}_{-F} := \mathrm{k}_{-4}$ proceeds all the time. In the KIM, on the contrary, we assume no dependency of the forward reaction on the attachment status and set $\mathrm{k}_F := \mathrm{k}_4$. In general, more than one equation will be affected by the kinetochore attachment status, and they will be all regulated by u. We do not consider down or upregulation by a certain percentage, in agreement with experimental findings (Vink et al., 2006; Musacchio and Salmon, 2007). For regulation of reactions proceeding with attached kinetochores only, we use the factor $v = 1 - u$, as is the case in the model with $\mathrm{p31}^{\mathrm{comet}}$ contribution.

Biochemically, the switching parameter u represents the function of dynein, which after microtubule attachment removes the Mad1:C-Mad2 2:2 complex from the

kinetochore site. It might also represent potential additional functions which contribute to switching behavior.

From the reaction equations, ordinary differential equations (ODEs) are derived using mass action kinetics. For a set of given initial concentrations for all reaction partners, the ODEs are integrated until steady state is reached before attachment (phase 1). Then u switches from 1 to 0 and the resulting set of equations is again integrated until steady state is reached (phase 2). For consistency and comparability of all models we use the same initial concentrations (c.f. Table 4.1). The actual values are chosen according to data from the literature. When only a certain range was known, we have used different starting values for our computations, but we did not find qualitatively differing trajectories. The kinetic constants are also taken from literature as far as they are known (Table 5.2). For all other constants (k_2, k_3, k_5, k_7, k_8, see Table 5.2), several computations with values representing the whole physiologically reasonable parameter range are compared. The trajectories are discussed in corresponding figures. They all show a continuous dependence of the parameters used. Criteria for comparison of the ability of the model to show acceptable switching behaviour are the level of MCC depletion and Cdc20 increase and the recovery time after the metaphase to anaphase transition.

4.4 Dynamics of different MCC models

4.4.1 Kinetochore dependent MCC model (KDM)

The Template model (DeAntoni et al., 2005a) for the Cdc20:C-Mad2 complex formation can be regarded as a seeding reaction to MCC assembly. In our recent mathematical description and simulation analysis of the Template model (Chapter 3), we found that for realistic Mad2 concentrations, Cdc20 cannot be sequestered completely in the cell by Mad2 alone. In addition to binding to Mad2, Cdc20 also binds to BubR1 (Bolanos-Garcia et al., 2005; Davenport et al., 2006; Chen, 2002b; Fang, 2002) and it might be this protein which sequesters the remaining part of Cdc20. We therefore added to the reaction equations of the

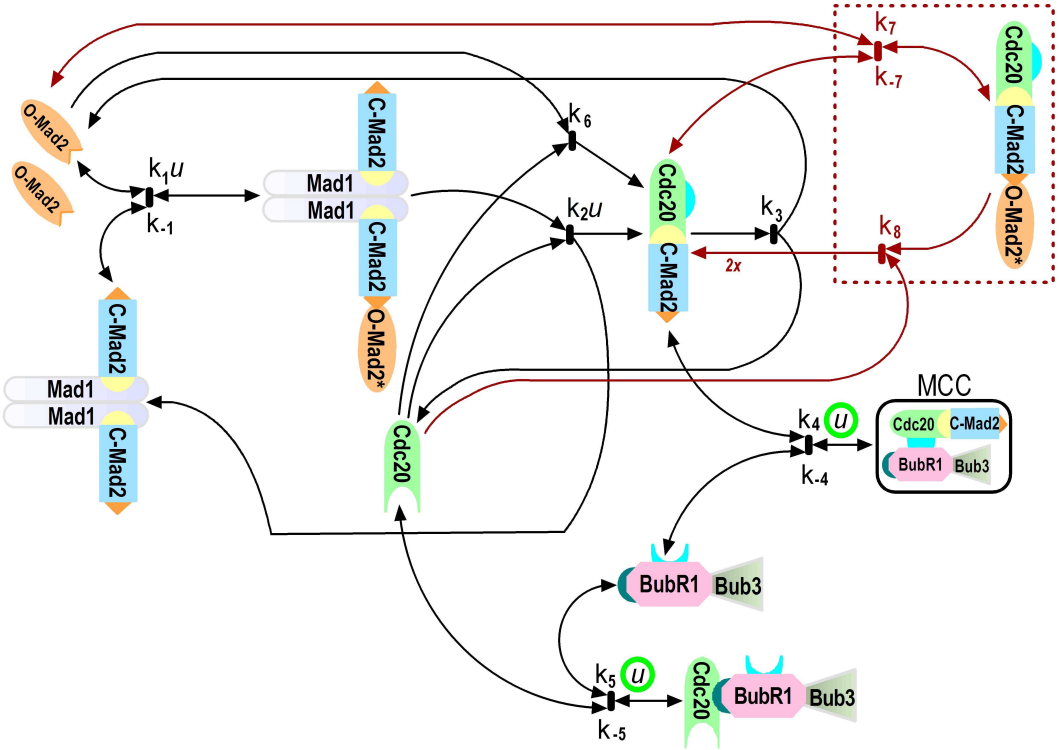

Figure 4.1: Schematic networks of MCC models. Black lines represent the kinetochore dependent (KDM) and the kinetochore independent (KIM) models. The KDM is obtained for u inside the green circles being $= 1$ for phase 1 before kinetochore attachment, and $= 0$ for phase 2 after attachment. In the KIM, in contrast, u inside the green circles is $= 1$ in both phases. The red lines represent the amplification reactions as defined in section 4.4.3. For biochemical details see text.

Template model (Eqs. (4.1)-(4.3), Chapter 3) those reaction equations describing the interaction with BubR1. The reaction scheme is presented in Figure 4.1 and the reaction rules (4.1)-(4.6) are listed below. The BubR1 reaction equations (4.4) for MCC formation and (4.5) for complexation with Bub3 and Cdc20 were deduced from experimental work (Sudakin et al., 2001; Davenport et al., 2006; Fang, 2002). Reaction (4.6) and its low rate were mentioned by Musacchio and Salmon (2007) (see also Fang (2002); Davenport et al. (2006)).

$$\text{Mad1:C-Mad2} + \text{O-Mad2} \underset{\mathrm{k}_{-1}}{\overset{\mathrm{k}_1 \cdot u}{\rightleftharpoons}} \text{Mad1:C-Mad2:O-Mad2}^* \tag{4.1}$$

$$\text{Mad1:C-Mad2:O-Mad2}^* + \text{Cdc20} \xrightarrow{\mathrm{k}_2 \cdot u} \text{Cdc20:C-Mad2} + \text{Mad1:C-Mad2} \tag{4.2}$$

$$\text{Cdc20:C-Mad2} \xrightarrow{\mathrm{k}_3} \text{O-Mad2} + \text{Cdc20} \tag{4.3}$$

$$\text{Cdc20:C-Mad2} + \text{Bub3:BubR1} \underset{\mathrm{k}_{-4}}{\overset{\mathrm{k}_4 \cdot u}{\rightleftharpoons}} \text{MCC} \tag{4.4}$$

$$\text{Cdc20} + \text{Bub3:BubR1} \underset{\mathrm{k}_{-5}}{\overset{\mathrm{k}_5 \cdot u}{\rightleftharpoons}} \text{Bub3:BubR1:Cdc20} \tag{4.5}$$

$$\text{Cdc20} + \text{O-Mad2} \xrightarrow{\mathrm{k}_6} \text{Cdc20:C-Mad2} \tag{4.6}$$

The corresponding differential equations are listed in Appendix A, Eqs. (C.1)-(C.8). The first two reactions (4.1) and (4.2) are kinetochore controlled and therefore the rates are multiplied by the switching parameter u. In the reaction scheme we assume that also the BubR1 forward reactions (4.4) and (4.5) are kinetochore dependent so that also rates k_4 and k_5 are multiplied by u. Most concentrations and rates of this reaction scheme were taken from literature (listed in Table 4.1 and Table 5.2). For k_4 we chose a high rate of 10^7 $\mathrm{M}^{-1}\mathrm{s}^{-1}$ similar to k_1 and k_2 since only for high values of k_4 high amounts of MCC would be formed. Nevertheless, we analysed the consequences of lower values of k_4 (see below). k_5 should be considerably smaller than k_4 and was chosen to be 10^4 $\mathrm{M}^{-1}\mathrm{s}^{-1}$. Below, also the influence of larger values of k_5 was studied. The backward reactions k_{-4} and k_{-5} should be slow and in the range of the experimental values of k_{-1}; we put $\mathrm{k}_{-4} = 0.02$ s^{-1} and $\mathrm{k}_{-5} = 0.2$ s^{-1} (see Table 5.2). For these kinetic data, we calculated the time-dependent values of all species concentrations. Here we

focus our discussion on the dynamics of the Cdc20 and MCC concentrations. In Figure 4.2, the Cdc20 concentration is plotted for three different values of k_3 and five different values of k_2. With increasing values of k_3, we observed faster switching behavior. For $k_3 = 0.01\ s^{-1}$, switching is already considerably fast, consistent with the findings for the Template model. k_2 hardly influenced the Cdc20 concentration when being larger than $10^7\ M^{-1}s^{-1}$. For no parameter value combination of k_2 and k_3 could Cdc20 be sequestered completely. Instead, for low values of k_3 and high values of k_2, Cdc20 concentration was reduced to slightly more than half and other parameter value combinations reduced it even less. The MCC shows fast switching behavior in all cases considered (see Figure 4.2).

In Figure 4.3a, we show the time course of the concentrations of all eight species in the model for the physiologically relevent parameters $k_2 = 10^7 M^{-1}s^{-1}$ and $k_3 = 0.01 s^{-1}$. It is interesting to note that [Bub3:BubR1] does not decay to zero to sequester more Cdc20 into MCC. There is also virtually no Bub3:BubR1:Cdc20 formed. Instead, about 15% of the Bub3:BubR1 concentration remains freely floating in the cell plasma. Another interesting feature is exhibited by the Mad1, Mad2, and Cdc20 dynamics. As there is virtually no Mad1:C-Mad2:O-Mad2* formed, this complex shows its property as short living intermediate in the reactions (4.1) and (4.2), clearly catalysed by Mad1:C-Mad2, staying at constant concentration of $0.5 \cdot 10^{-7}$ M and transforming O-Mad2 plus Cdc20 into Cdc20:C-Mad2. Immediately after switching at 2000 s, the MCC releases at a fast rate Cdc20:C-Mad2, which first increases, but shortly afterwards decays into its components.

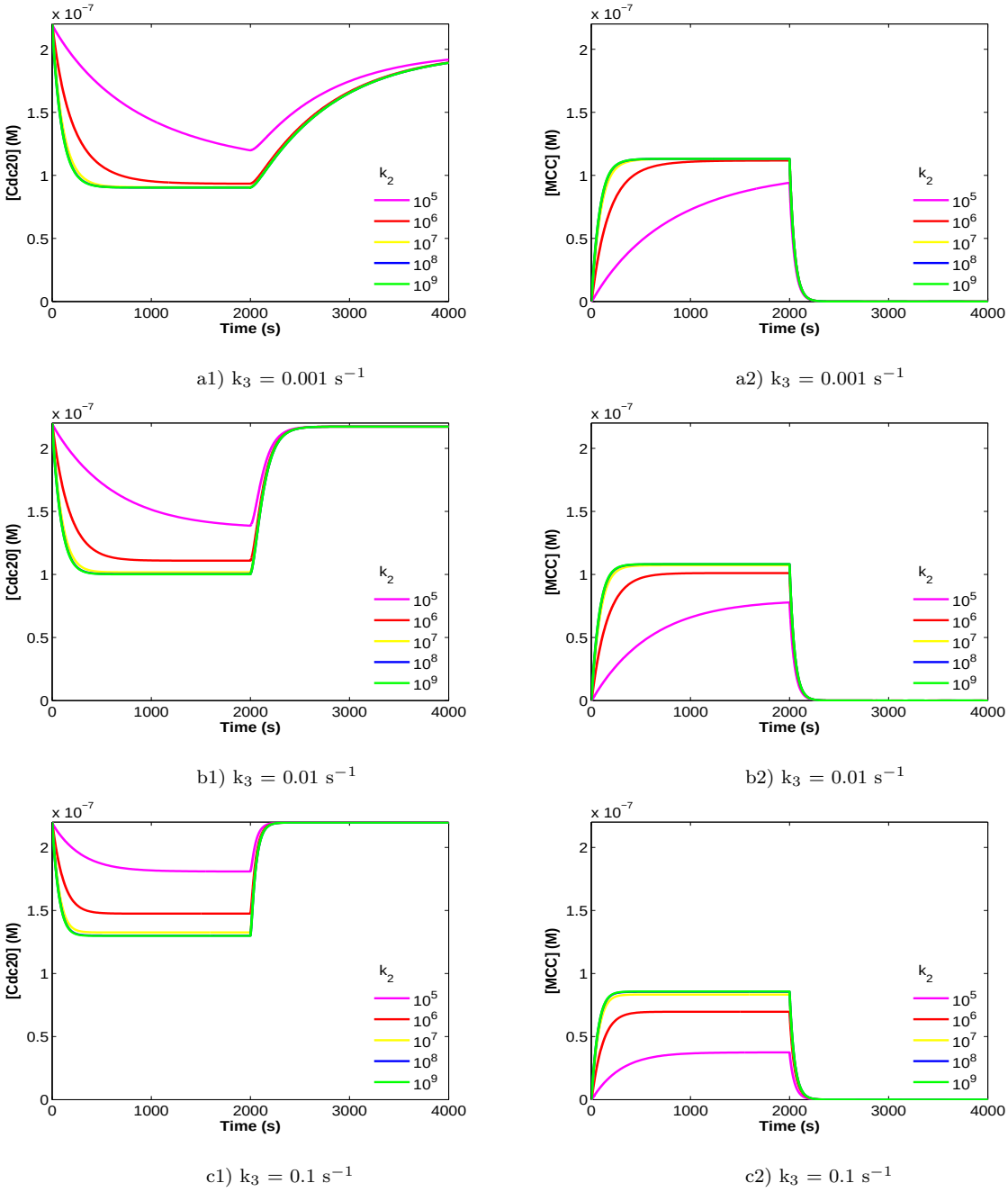

a1) $k_3 = 0.001\ s^{-1}$ a2) $k_3 = 0.001\ s^{-1}$

b1) $k_3 = 0.01\ s^{-1}$ b2) $k_3 = 0.01\ s^{-1}$

c1) $k_3 = 0.1\ s^{-1}$ c2) $k_3 = 0.1\ s^{-1}$

Figure 4.2: Kinetochore dependent MCC model (KDM). For three different k_3-values, the time evolution within phase 1 before attachment (0-2000 s) and within phase 2 after attachment (2000-4000 s) of Cdc20 (a1-c1) and MCC (a2-c2) are shown for five different k_2-values (colored lines). Solutions are nearly independent of k_2 for $k_2 \geq 10^7\ M^{-1}s^{-1}$. Whereas switching behaviour for MCC is satisfactory for any k_3, Cdc20 recovery time becomes short enough only for $k_3 \geq 0.01\ s^{-1}$.

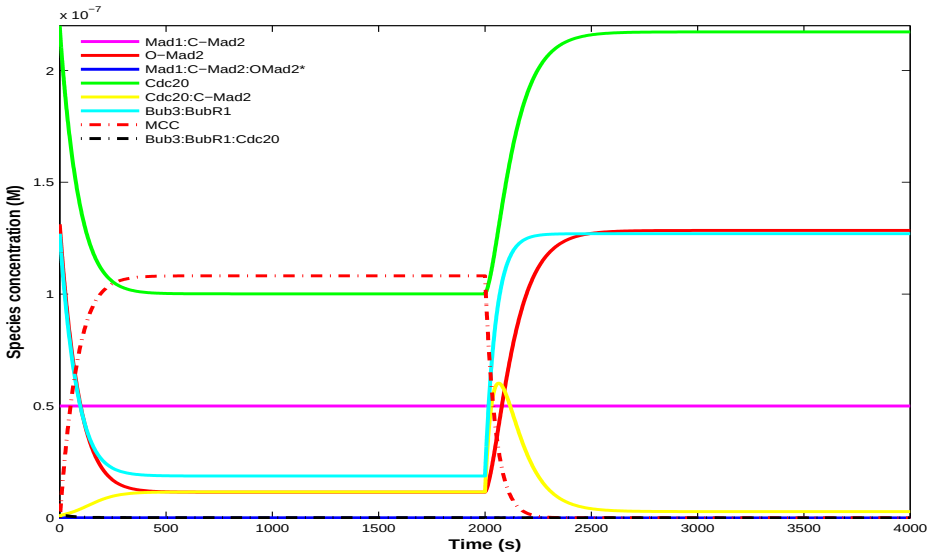

a) Kinetochore dependent model (KDM)

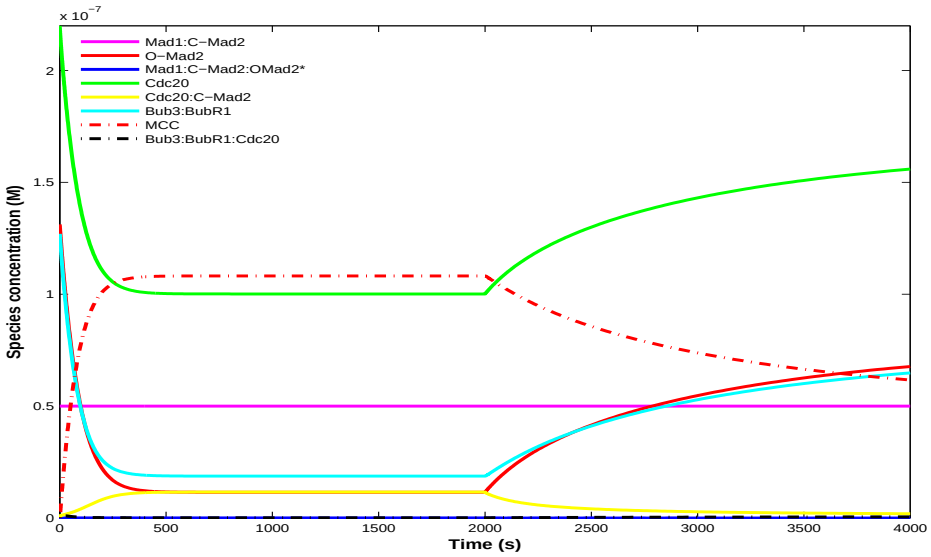

b) Kinetochore independent model (KIM)

Figure 4.3: Species concentrations for KDM (a) and KIM (b). For $k_2 = 10^7 M^{-1}s^{-1}$ and $k_3 = 0.01s^{-1}$, the time evolution of all eight species in the MCC assembly models are shown before (phase 1, $t = 0 - 2000$ s) and after attachment (phase 2, $t = 2000 - 4000$ s). Bub3:BubR1 is noy totally used up to sequester Cdc20. Mad1:C-Mad2 shows its function as a catalyzer for Cdc20:C-Mad2 production. Time evolution is identical in KDM (a) and KIM (b) before $t = 2000$ s, but quantitatively and qualitatively ([Cdc20:C-Mad2]) different after that. Details see text.

4.4.2 Kinetochore independent MCC model (KIM)

The line of biochemical reactions placing MCC formation under the control of the kinetochore are not clear (reviewed by Musacchio and Salmon (2007)). MCC formation might be kinetochore independent (Poddar et al., 2005; Fraschini et al., 2001; Meraldi et al., 2004). We therefore analysed a modified kinetochore independent model in which the reaction equations (4.4) and (4.5) are now replaced by u–independent equations (4.7) and (4.8) (see Figure 4.1):

$$\text{Cdc20:C-Mad2} + \text{Bub3:BubR1} \underset{\mathrm{k}_{-4}}{\overset{\mathrm{k}_4}{\rightleftharpoons}} \text{MCC} \tag{4.7}$$

$$\text{Cdc20} + \text{Bub3:BubR1} \underset{\mathrm{k}_{-5}}{\overset{\mathrm{k}_5}{\rightleftharpoons}} \text{Bub3:BubR1:Cdc20} \tag{4.8}$$

The resulting differential equations are the same as in Appendix A, Eqs. (C.1)-(C.8), except for the kinetic constants $\mathrm{k}_4 \cdot u$ and $\mathrm{k}_5 \cdot u$, which have to be replaced by k_4 and k_5, respectively. Using the same initial concentrations (Table 4.1) and rate values (Table 5.2) as above we calculated the time dependent model behavior. Of course, until kinetochore attachment, both, time dependence and concentrations are unchanged since $u = 1$. After attachment, however, we found very slow switching and Cdc20 and MCC concentration changes only for larger k_3. Even for large k_3, Cdc20 recovery and MCC depletion were not complete (see Figure 4.4). The quantitative failure of this reaction model indicates that the BubR1 reactions are kinetochore controlled.

As already done for the KDM, we show the concentration over time curves for all eight species in the KIM for $\mathrm{k}_2 = 10^7\mathrm{M}^{-1}\mathrm{s}^{-1}$ and $\mathrm{k}_3 = 0.01\mathrm{s}^{-1}$ in Figure 4.3b. The characteristic features of the catalyzing reactions (4.1) and (4.2) involving Mad1 remain the same, but there is a drastic qualitative change in the concentration dynamics of Cdc20:C-Mad2, which decreases immediately after switching, because without kinetochore control it still restores MCC (Eq. 4.7) besides decaying into its components (Eq. 4.3). There is thus not only a quantitative change resulting in a slower dynamics, but also a qualitative change in the time evolution of the trajectory of [Cdc20:C-Mad2].

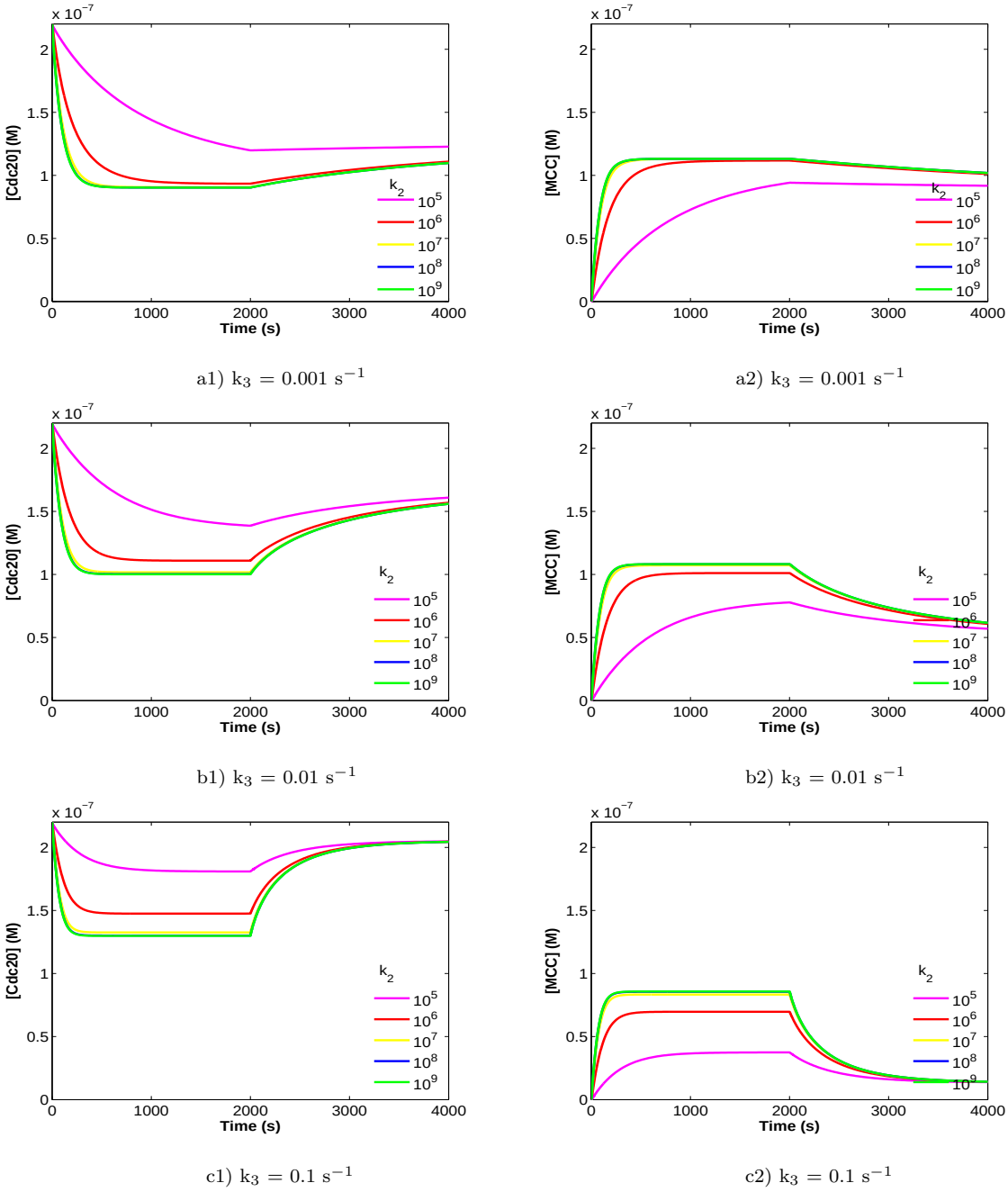

a1) $k_3 = 0.001\ s^{-1}$ a2) $k_3 = 0.001\ s^{-1}$

b1) $k_3 = 0.01\ s^{-1}$ b2) $k_3 = 0.01\ s^{-1}$

c1) $k_3 = 0.1\ s^{-1}$ c2) $k_3 = 0.1\ s^{-1}$

Figure 4.4: Kinetochore independent MCC model (KIM). Same representation as in Figure 4.2. Concentration curves in phase 1 before attachment (0-2000 s) are identical to those in Figure 4.2, whereas in phase 2 after attachment (2000-4000 s) the parameter u (in the green circle in Figure 4.1) is still set to $u = 1$ (no kinetochore control). As a consequence, switching is very slow. Furthermore, Cdc20 recovery and MCC depletion levels are poor.

4.4.3 Amplification effects

DeAntoni et al. (2005a) hypothesized that in analogy to the reactions based on Mad1 (Eqs. (4.1) and (4.2)), Cdc20:C-Mad2 can also be formed by reactions catalyzed by O-Mad2 and Cdc20 in a two step mechanism as described by the two reaction equations (4.9) and (4.10). This additional pathway for the production of Cdc20:C-Mad2 results in a signal amplification for the ^{M}SAC since Cdc20:C-Mad2 now is produced not only at the location of Mad1 at the kinetochore but at a larger number of locations everywhere in the cell. We checked the effect of this assumption by adding two additional reactions to the Template model, but we found no improvement of the Template model behavior (Chapter 3). Also here, we added the two reaction equations (4.9) and (4.10) to the KDM and analysed the influence of the amplification on the model (see Figure 4.1, red arrows).

$$\text{Cdc20:C-Mad2} + \text{O-Mad2} \underset{k_{-7}}{\overset{k_7}{\rightleftharpoons}} \text{Cdc20:C-Mad2:O-Mad2}^* \tag{4.9}$$

$$\text{Cdc20:C-Mad2:O-Mad2}^* + \text{Cdc20} \xrightarrow{k_8} 2\,\text{Cdc20:C-Mad2} \tag{4.10}$$

When calculating the time-dependent Cdc20 and MCC concentrations, we observed hardly any change for small values of k_7 and k_8 (see Figure 4.5, a1-a2) compared to the KDM (Figure 4.2, b1-b2). This result was expected since for small rates, reactions (4.9) and (4.10) do not contribute to the model behavior. When, however, the rates adopt values in the realistic range ($k_7 = k_8 = 10^6$ $M^{-1}s^{-1}$, see Table 5.2), we observed only little Cdc20 recovery after kinetochore attachment (see Figure 4.5, b1-b2). This result is due to both reactions being independent of kinetochore control. The MCC concentration is hardly influenced by these reactions, since they do not contribute to MCC regulation.

It might be speculated that also the amplification reactions might be somehow kinetochore dependent. When multiplying the rates k_7 and k_8 by a switching parameter u (controlled case), we observed the same model behaviour (see Figure 4.5, c1-c2 for fast amplification reaction). as for the KDM without amplification (Figure 4.2, b1-b2). For slow amplification reactions, the concentration curves (figures

not shown) are virtually identical to those in the uncontrolled case (Figure 4.5, a1-a2).

4.4.4 p31$^{\text{comet}}$ contributions

The negative spindle checkpoint regulator p31$^{\text{comet}}$ is a Mad2 ligand. Its negative effect on the $^{\text{M}}$SAC is based on its competition with O-Mad2 for C-Mad2 binding (Habu et al., 2002; Xia et al., 2004; Mapelli et al., 2006; Yu, 2006). It forms triple complexes with C-Mad2 and either Mad1 or Cdc20 (Xia et al., 2004; Vink et al., 2006; Mapelli et al., 2006). In our analysis of the Template model (Chapter 3), we added a reaction describing the effect of p31$^{\text{comet}}$. We could show that, when p31$^{\text{comet}}$ is activated at microtubule attachment to the kinetochores, it can function as a cellular factor contributing to the checkpoint switching behavior: p31$^{\text{comet}}$ function can replace the switching parameter u. Here, we introduced the same p31$^{\text{comet}}$ reactions (4.17) and (4.18) to the KDM:

$$\text{Mad1:C-Mad2} + \text{O-Mad2} \underset{\text{k}_{-1}}{\overset{\text{k}_1}{\rightleftharpoons}} \text{Mad1:C-Mad2:O-Mad2}^* \tag{4.11}$$

$$\text{Mad1:C-Mad2:O-Mad2}^* + \text{Cdc20} \xrightarrow{\text{k}_2} \text{Cdc20:C-Mad2} + \text{Mad1:C-Mad2} \tag{4.12}$$

$$\text{Cdc20:C-Mad2} \xrightarrow{\text{k}_3} \text{O-Mad2} + \text{Cdc20} \tag{4.13}$$

$$\text{Cdc20:C-Mad2} + \text{Bub3:BubR1} \underset{\text{k}_{-4}}{\overset{\text{k}_4 \cdot u}{\rightleftharpoons}} \text{MCC} \tag{4.14}$$

$$\text{Cdc20} + \text{Bub3:BubR1} \underset{\text{k}_{-5}}{\overset{\text{k}_5 \cdot u}{\rightleftharpoons}} \text{Bub3:BubR1:Cdc20} \tag{4.15}$$

$$\text{Cdc20} + \text{O-Mad2} \xrightarrow{\text{k}_6} \text{Cdc20:C-Mad2} \tag{4.16}$$

$$\text{Mad1:C-Mad2} + \text{p31} \underset{\text{k}_{-7p}}{\overset{\text{k}_{7p} \cdot v}{\rightleftharpoons}} \text{Mad1:C-Mad2:p31} \tag{4.17}$$

$$\text{Cdc20:C-Mad2} + \text{p31} \underset{\text{k}_{-8p}}{\overset{\text{k}_{8p} \cdot v}{\rightleftharpoons}} \text{Cdc20:C-Mad2:p31} \tag{4.18}$$

This corresponds to the differential equations Eqs. (C.18)-(C.28) in Appendix C, where $v = 1 - u$. Reaction equations (4.11) and (4.12) are now kinetochore uncontrolled (no multiplication of the rates by u). However, MCC formation (4.14)

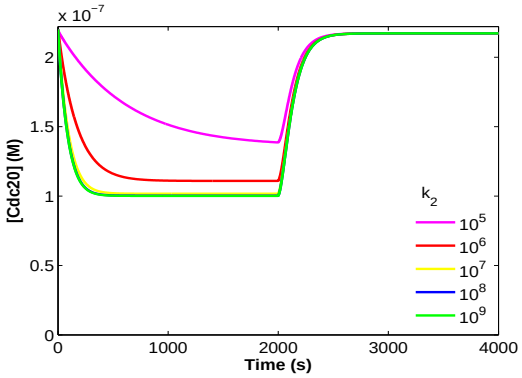

a1) slow ($k_7 = k_8 = 10^4$ $M^{-1}s^{-1}$)

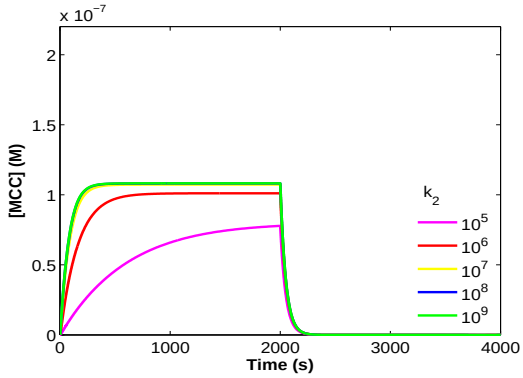

a2) slow ($k_7 = k_8 = 10^4$ $M^{-1}s^{-1}$)

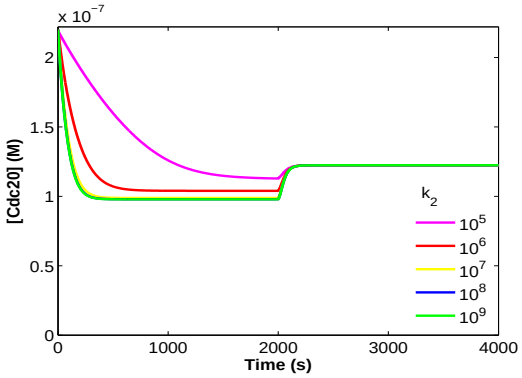

b1) fast ($k_7 = k_8 = 10^6$ $M^{-1}s^{-1}$)

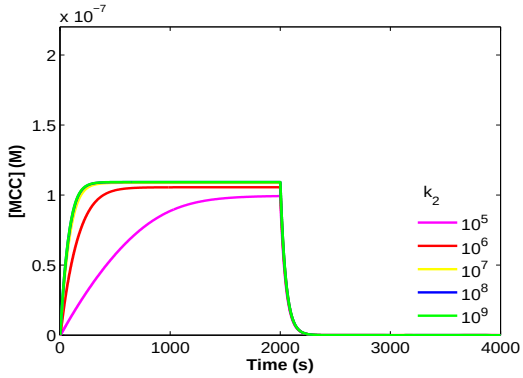

b2) fast ($k_7 = k_8 = 10^6$ $M^{-1}s^{-1}$)

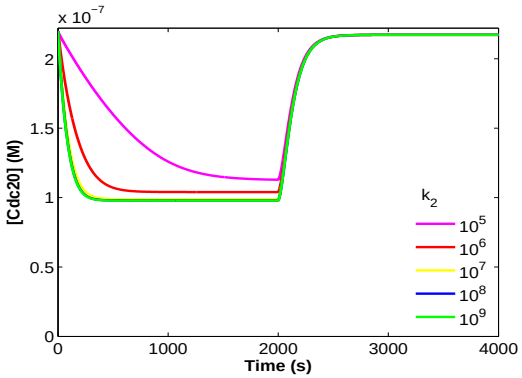

c1) fast ($k_7 = k_8 = 10^6$ $M^{-1}s^{-1}$)

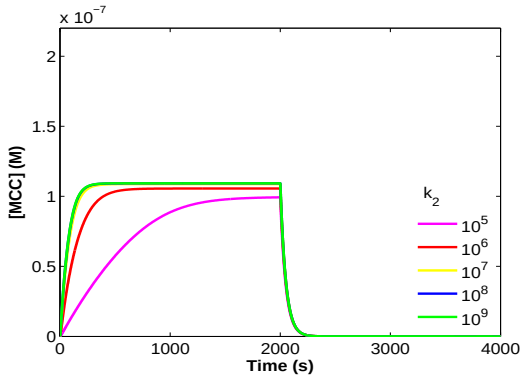

c2) fast ($k_7 = k_8 = 10^6$ $M^{-1}s^{-1}$)

Figure 4.5: Amplification effects. Here, $k_3 = 0.01$. For slow (a1, a2) and fast (b1, b2, c1, c2) amplification reaction rates, the concentration curves for Cdc20 and MCC show fast switching behaviour in the uncontrolled (a1/2-b1/2) as well as in the controlled (c1-c2) case, where rates k_7 and k_8 are multiplied by u. Only for fast ($k_7 = k_8 = 10^6$ $M^{-1}s^{-1}$) amplification reaction rates in the uncontrolled case, Cdc20 does not recover to the maximal level (b1).

and the BubR1 reaction (4.15) are not linked to $p31^{comet}$ function, so that these reactions remain kinetochore controlled with rates multiplied by the switching parameter u. Thus, the reaction scheme (Eqs. (4.11) - (4.18)) remains kinetochore dependent. We studied the influence of $p31^{comet}$ on the behavior of this model and observed, as for the Template model (Chapter 3), that u in reactions (4.1) and (4.2) can be replaced by $p31^{comet}$ function without changing the behavior of Cdc20 and MCC (data not shown). In this respect, the switching parameter u additionally represents $p31^{comet}$ function and further potentially unidentified reactions by additional proteins. An example could be UbcH10 (Townsley et al., 1997), which plays a role in checkpoint inactivation (Reddy et al., 2007). Also other effects like protein activation, inhibition, or degradation might contribute to u.

When keeping the original KDM (with reactions (4.1) and (4.2) controlled by u, instead of uncontrolled (4.11) and (4.12)) and including the $p31^{comet}$ contribution (Eqs. (4.17) and (4.18)), the system behaviour virtually does not change (data not shown).

4.4.5 Maximum sequestering of Cdc20

For realistic parameter values, Cdc20 cannot be totally sequestered in the MCC models analysed. As shown in *in vitro* assays (Fang, 2002), complete Cdc20 binding is obtained when the Mad2 concentration is increased to at least eight-fold beyond experimentally measured physiological values. Figure 4.6 shows that indeed for eight-fold higher Mad2 concentrations, the Cdc20 concentration decreased down to zero for low values of k_3 and high values of k_2 in our simulation of the KDM, while the MCC concentration slightly increased independently of k_3. The MCC concentration increased since there is more Cdc20:Mad2 available. The concentration increase is limited due to limitations in the BubR1:Bub3 concentration.

In addition to Cdc20 reduction to zero due to high Mad2 values, Cdc20 can also be strongly reduced for high values of k_5. In this case, most of BubR1:Bub3 binds Cdc20 and removes it from the cell plasma. Figure 4.7 displays the low

Cdc20 concentrations for low values of k_3 and high values of k_2 as well as the fast switching behavior of the model. However, most of BubR1:Bub3 is used–up for this reaction so that hardly any MCC can form (see Figure 4.7, a2, for the lowest value of k_3). For higher k_3, there is virtually no MCC assembled. Thus, for high values of k_5, strong Cdc20 sequestering is combined with MCC depletion which would leave the APC uncontrolled. On the other hand, maximum MCC concentration was obtained for low values k_5: in this case, most BubR1:Bub3 contributes to MCC formation so that hardly any BubR1:Bub3:Cdc20 can form (data not shown).

Thus, for the assumed concentrations of [Bub3:BubR1] = $1.5 \cdot 10^{-7}$M and [Cdc20] = $2.2 \cdot 10^{-7}$M (Table 4.1), MCC cannot sequester Cdc20 totally. In addition, the formation of Bub3:BubR1:Cdc20 (Eq. 4.5) and Cdc20:C-Mad2 by the two step catalysis (Eq. 4.1 and 4.2) and the direct reaction (Eq. 4.6) are not well suited to sequester a considerable amount of Cdc20, as Figure 4.3a showed. We therefore studied the effect of the initial Bub3:BubR1 concentration on the system by increasing it 8-fold to $10.4 \cdot 10^{-7}$ M. The result is shown in Figure 4.8. Comparing it to Figure 4.2 with [Bub3:BubR1] = $1.3 \cdot 10^{-7}$ M, we see a slightly better degree of Cdc20 sequestering to about 45% of the initial concentration for all values of k_3 and $k_2 \geq 10^7$. In these cases, also [MCC] attains it maximal level of about $1.3 \cdot 10^{-7}$ M. The corresponding values in Figure 4.2 are depentent on k_3. Also, the switching behaviour for both Bub3:BubR1 concentrations is comparable. Altogether, we conclude that the Bub3:BubR1 initial concentration has no major influence on Cdc20 sequestration.

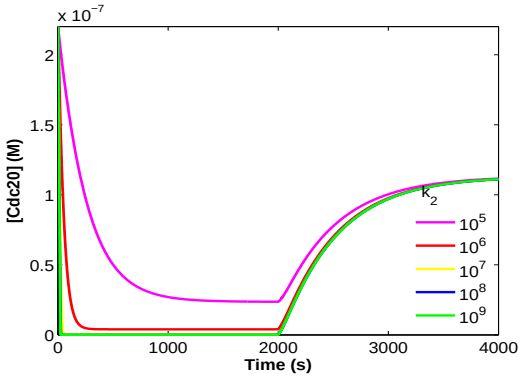

a1) $k_3 = 0.001\ s^{-1}$

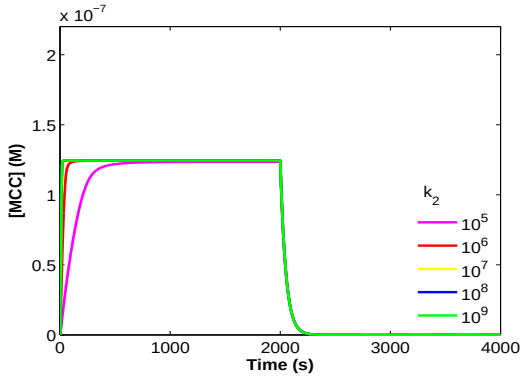

a2) $k_3 = 0.001\ s^{-1}$

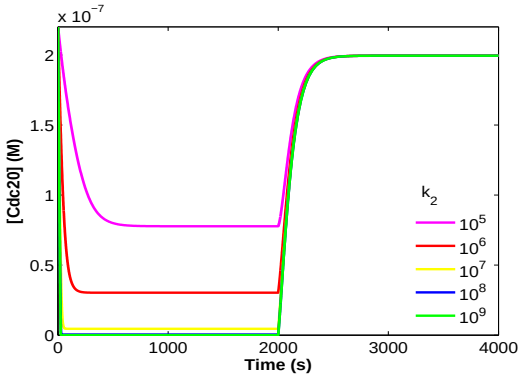

b1) $k_3 = 0.01\ s^{-1}$

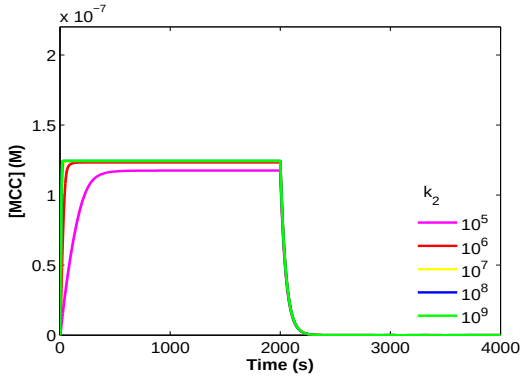

b2) $k_3 = 0.01\ s^{-1}$

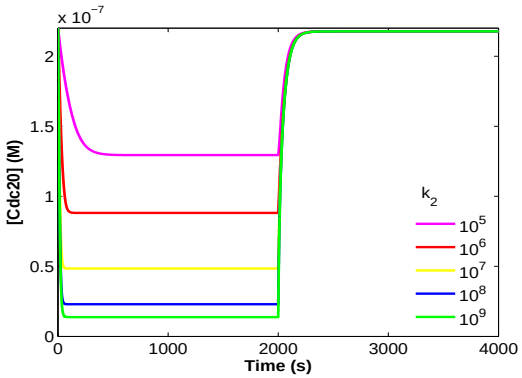

c1) $k_3 = 0.1\ s^{-1}$

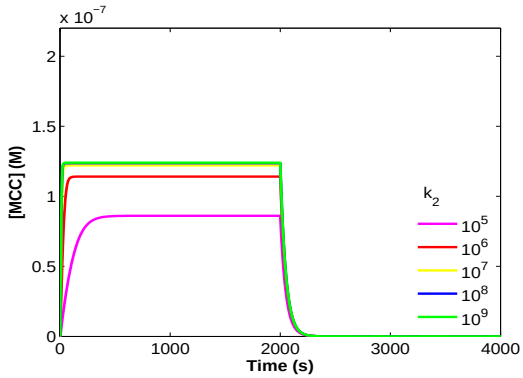

c2) $k_3 = 0.1\ s^{-1}$

Figure 4.6: Maximal Cdc20 sequestering through increase of free Mad2. The dynamical behavior of the KDM showing the time evolution of [Cdc20] (a1-c1) and [MCC] (a2-c2) for the same values of k_2 and k_3 as in Figure 4.2. In contrast, here the Mad2 initial level is 8-fold increased. Cdc20 concentration decreases to zero for low k_3 and high k_2, while the MCC concentration increases slightly independent of k_3.

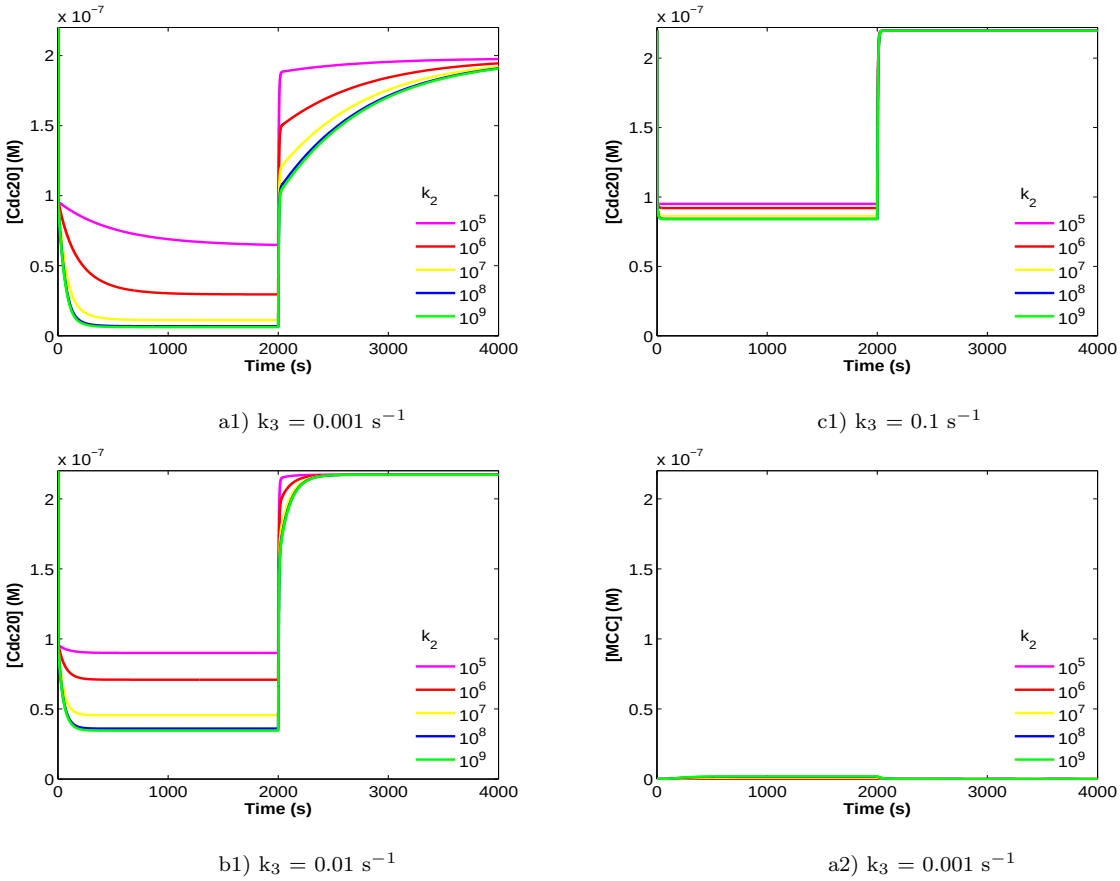

a1) $k_3 = 0.001\ s^{-1}$

c1) $k_3 = 0.1\ s^{-1}$

b1) $k_3 = 0.01\ s^{-1}$

a2) $k_3 = 0.001\ s^{-1}$

Figure 4.7: Maximal Cdc20 sequestering through increased BubR1 rates. The dynamical behavior of the KDM for $k_5 = 10^8\ M^{-1}s^{-1}$showing low [Cdc20] for low k_3 and high k_2 (a1-c1). Obviously, most of BubR1:Bub3 binds Cdc20, but hardly any MCC can form (a2, for $k_3 = 0.001\ s^{-1}$). On the other hand, good switching behaviour for Cdc20 is correlated to a low sequestering degree.

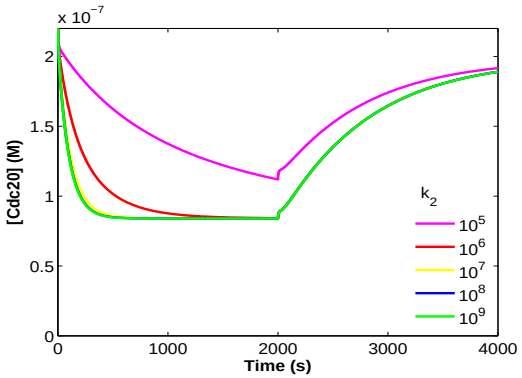

a1) $k_3 = 0.001\ s^{-1}$

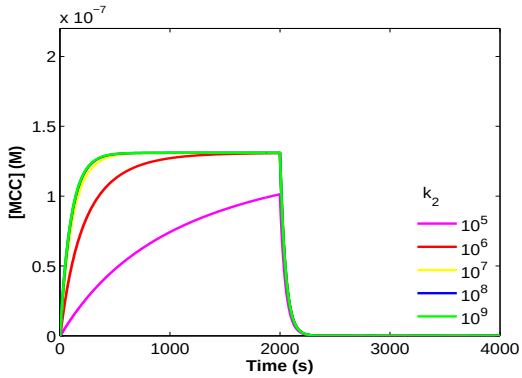

a2) $k_3 = 0.001\ s^{-1}$

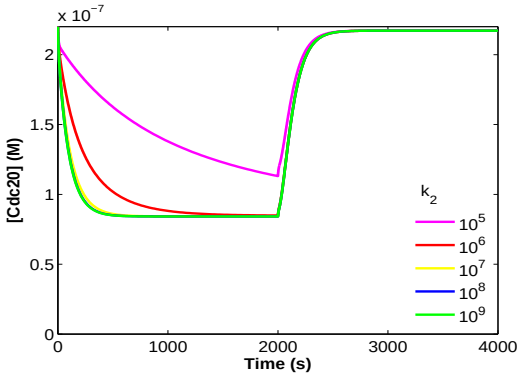

b1) $k_3 = 0.01\ s^{-1}$

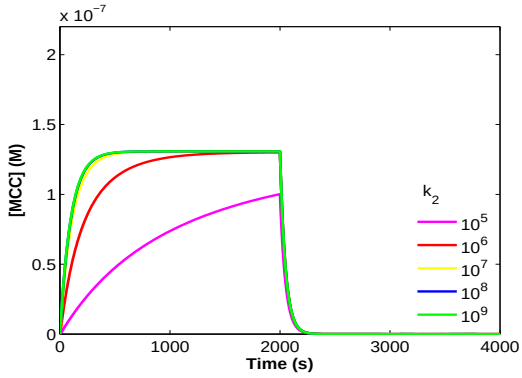

b2) $k_3 = 0.01\ s^{-1}$

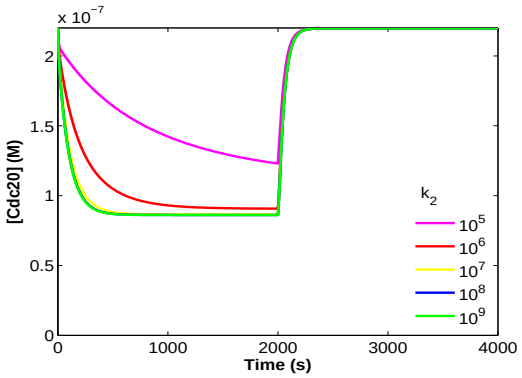

c1) $k_3 = 0.1\ s^{-1}$

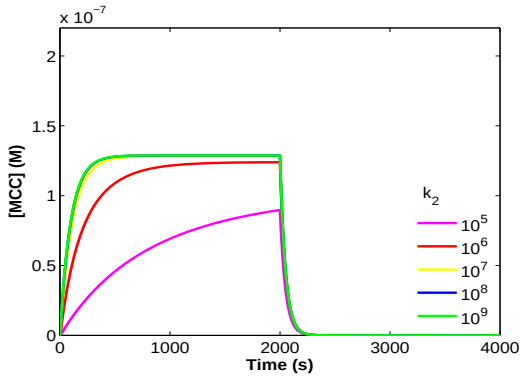

c2) $k_3 = 0.1\ s^{-1}$

Figure 4.8: KDM with 8-fold increased BubR1:Bub3 initial concentration. Same representation as in Figure 4.2. The comparison shows that BubR1:Bub3 initial concentration has no major influence on Cdc20 sequestration.

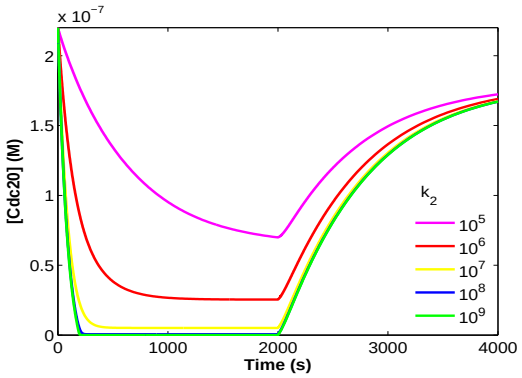

a1) $k_3 = 0.001\ s^{-1}$

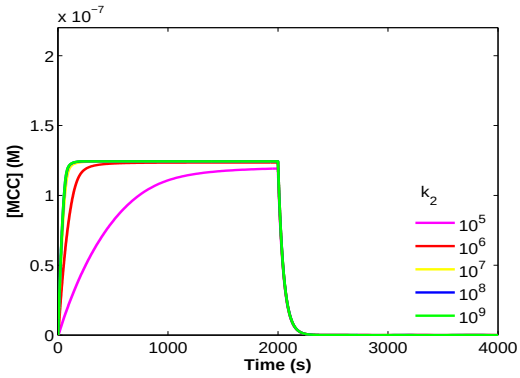

a2) $k_3 = 0.001\ s^{-1}$

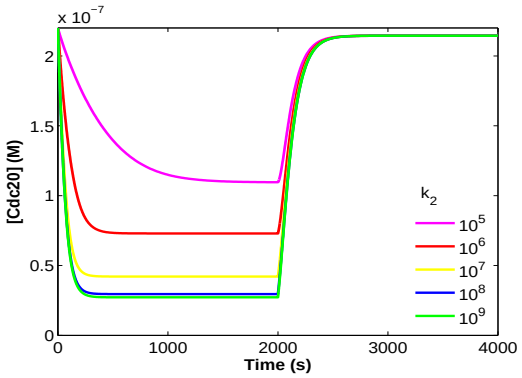

b1) $k_3 = 0.01\ s^{-1}$

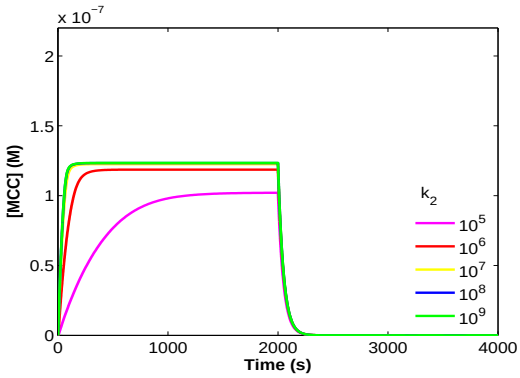

b2) $k_3 = 0.01\ s^{-1}$

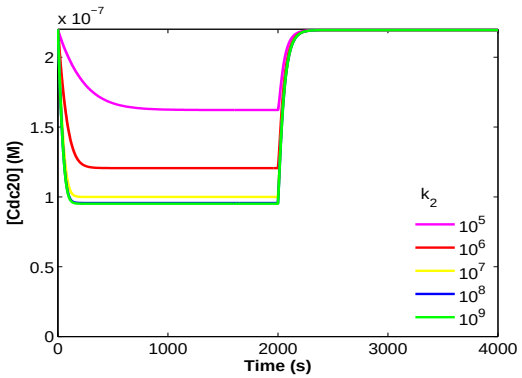

c1) $k_3 = 0.1\ s^{-1}$

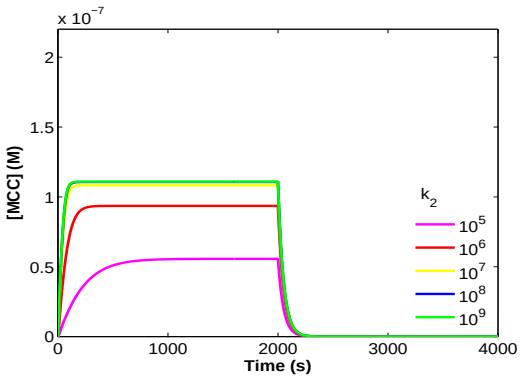

c2) $k_3 = 0.1\ s^{-1}$

Figure 4.9: KDM with 2-fold increased Free Mad2 initial concentration. Cdc20 got maximum sequestering only for small k_3 and very high k_2.

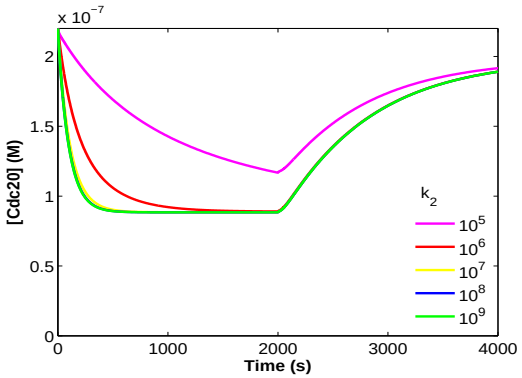

a1) $k_3 = 0.001\ s^{-1}$

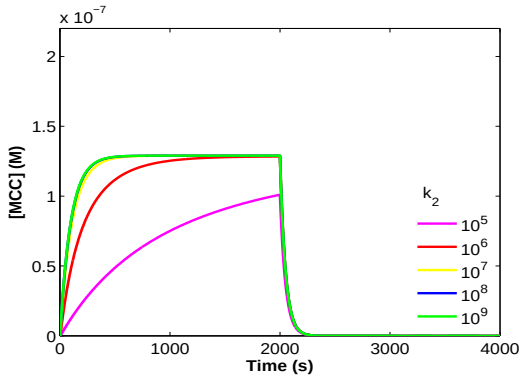

a2) $k_3 = 0.001\ s^{-1}$

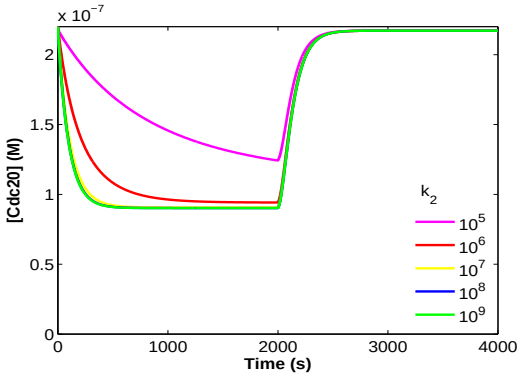

b1) $k_3 = 0.01\ s^{-1}$

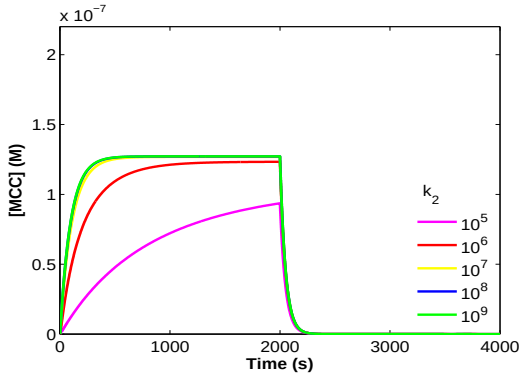

b2) $k_3 = 0.01\ s^{-1}$

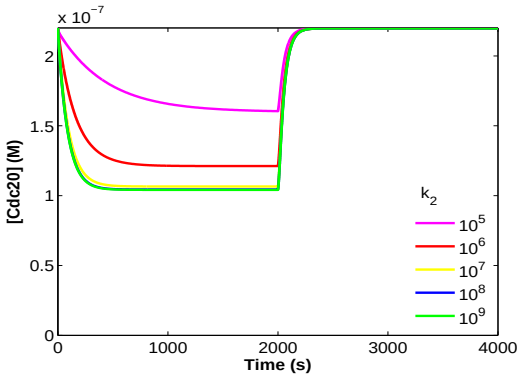

c1) $k_3 = 0.1\ s^{-1}$

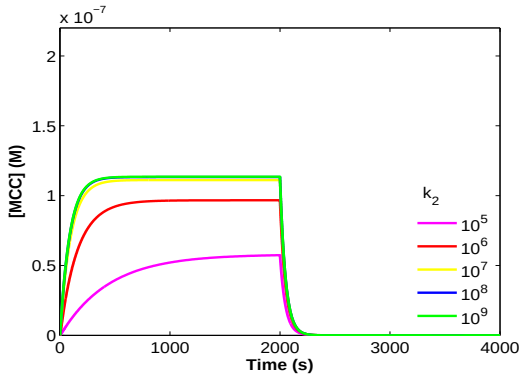

c2) $k_3 = 0.1\ s^{-1}$

Figure 4.10: KDM with 2-fold increased Bub3:BubR1 initial concentration. Same representation as in Figure 4.2. The comparison shows that BubR1:Bub3 initial concentration has no major influence on Cdc20 sequestration.

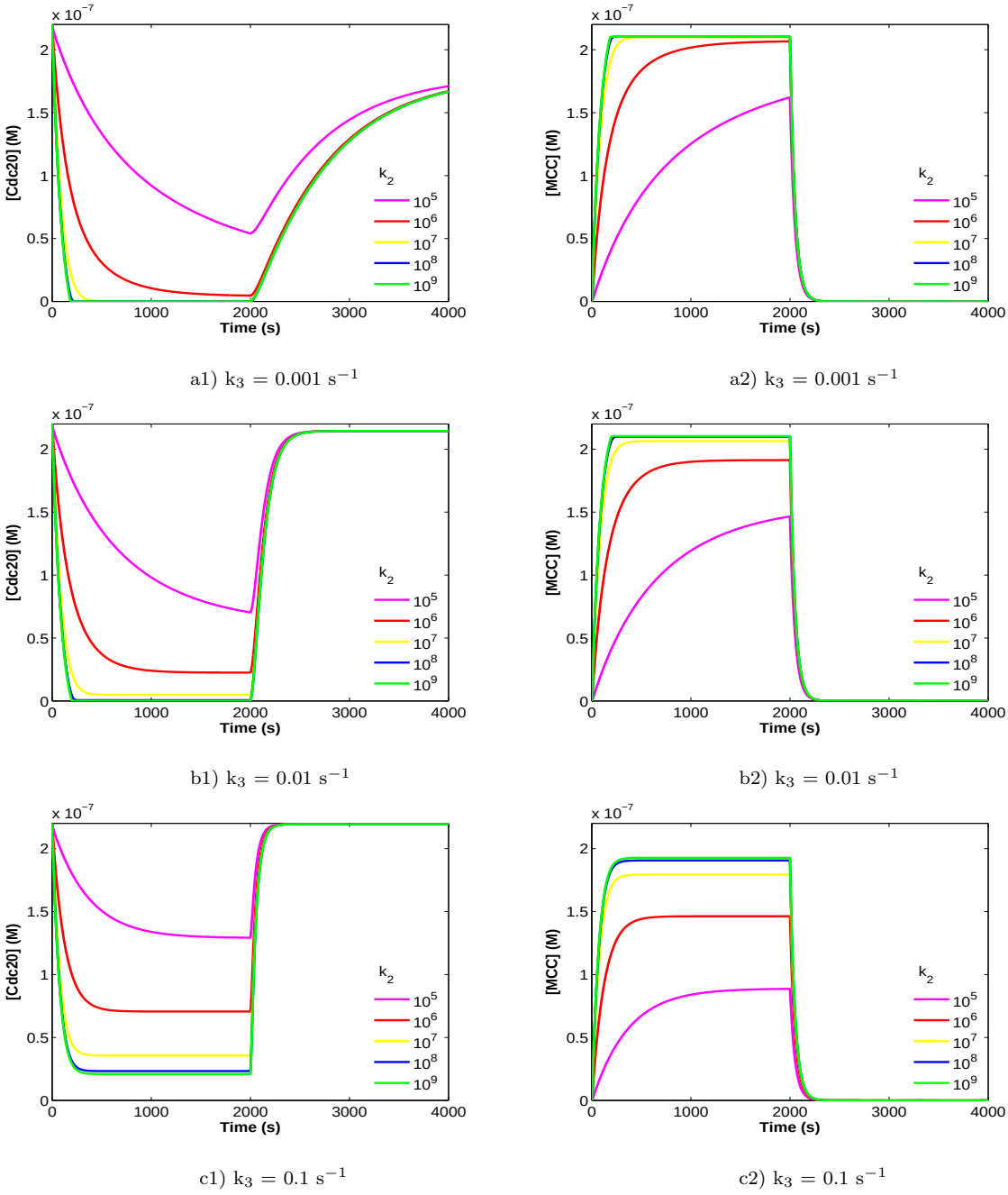

a1) $k_3 = 0.001\ s^{-1}$ a2) $k_3 = 0.001\ s^{-1}$

b1) $k_3 = 0.01\ s^{-1}$ b2) $k_3 = 0.01\ s^{-1}$

c1) $k_3 = 0.1\ s^{-1}$ c2) $k_3 = 0.1\ s^{-1}$

Figure 4.11: KDM with 2-fold increased of both free Mad2 as well as Bub3:BubR1 initial concentration. This demonstrates that Cdc20 can be sequestered for very high k_2. Additionally, only the case in which MCC amount can be get about doubling.

4.5 Discussion and Conclusions

Building on our investigation (Chapter 3) of different models for Cdc20:Mad2 complex formation, we have extended the mathematical description of the Template model by those reaction equations, which describe Cdc20 sequestration. The major role is played by Bub3:BubR1 and the MCC, which, in turn, blocks the APC. We analysed MCC formation, distinguishing a "kinetochore dependent model" (KDM) and a "kinetochore independent model" (KIM). The latter failed to describe correct metaphase to anaphase switching. Considering the KDM under realistic conditions, Cdc20 is not sequestered completely but instead remains in the cell plasma to a considerable amount. Complete Cdc20 binding is either attained for unrealistically high concentrations of Mad2 or for high rate values of BubR1:Bub3:Cdc20 formation; the latter, however, sacrifying MCC formation and thus APC control. The behaviour of the KDM is virtually independent of the Bub3:BubR1 initial concentration. Amplification effects or a detailed desciption of $p31^{comet}$ contribution did not improve the situation. These results indicate that, on the basis of the reactions considered here, the ^{M}SAC regulation does not function through Cdc20 sequestration.

Extending previous work (Sear and Howard, 2006; Doncic et al., 2005) based on partial differential equations, Doncic et al. (2006) showed in an analysis based on ordinary differential equations that ^{M}SAC can act through Cdc20 sequestration. Investigating statistical error propagation in two models describing abstract kinetochore mediated inhibition mechanisms, they exclude that Cdc20 is inhibited solely by protein degradation. However, both mechanisms, sequestration and degradation, can act in parallel showing almost linear behaviour in combination. Their model includes only two species, Cdc20 and an abstract signalling complex m which could be Mad2 or another sequestering molecule. This comes very close to our analysis (Chapter 3) of the Template model, where we found complete sequestering of Cdc20 as confirmed by *in vitro* assays (Fang, 2002), but only for unphysiological parameter sets. The same holds true for this investigation (Figures 4.6, c1, d1, and 4.7, a1, b1).

Which complexes Bub3:BubR1 is able to form, is a crucial question for MCC formation. It is a general problem of simulation studies to identify all reaction schemes and to incorporate them with the correct reaction kinetics. In general, our study can help to falsify assumptions, but can hardly proof the correctness of a pathway (Popper, 1935). In our analysis, we have found that the KIM is very unlikely to describe MCC assembly, but that the KDM could be a basis for further pathway design.

In our model, we analysed the influence of Cdc20 sequestration on ^{M}SAC operation (Musacchio and Salmon, 2007). In how far partial inhibition of the APC by the ^{M}SAC is tolerable by cell cycle control, is currently unclear. As the basic reactions, described here and previously (Chapter 3), do not lead to complete Cdc20 sequestration, we speculate that the MCC binds and completely blocks the APC. APC activation might then be a consequence of a MCC:APC complex modification or rearrangement. To investigate the further reaction scheme for checkpoint function, we have integrated the "kinetochore dependent model" (KDM) investigated here into a model describing APC inhibition and APC^{Cdc20} formation after metaphase to anaphase transition, which should be the basis of more complex investigations. The "tightness" of the APC control might be a topic of these future studies.

Table 4.1: Initial Concentrations for Integration

Species	**Initial Concentration**	**Comments and References**
[Cdc20]	$2.2 * 10^{-7}$M	Fang (2002); Howell et al. (2000b); Tang et al. (2001)
[O-Mad2]	$1.5 * 10^{-7}$M	Fang (2002); Howell et al. (2000b); Tang et al. (2001)
[Mad1:C-Mad2]	$0.5 * 10^{-7}$M	Luo et al. (2004); Fang (2002); Howell et al. (2000b)
[Bub3:BubR1]	$1.3 * 10^{-7}$M	Fang (2002); Tang et al. (2001)
[$p31^{comet}$]	$1 * 10^{-6}$M	Xia et al. (2004); Mapelli et al. (2006)

Initial Concentrations of other species are zero.

Table 4.2: Kinetic Parameters

Parameter	**Value or Range**	**Comments and References**
k_1	$2 * 10^5$ $M^{-1}s^{-1}$	Vink et al. (2006)
k_{-1}	0.2 s^{-1}	Vink et al. (2006)
k_2	$10^5, 10^6, 10^7, 10^8, 10^9$ $M^{-1}s^{-1}$	Chapter 3
k_3	$10^{-3}, 10^{-2}, 10^{-1}s^{-1}$	Chapter 3
k_4	10^7 $M^{-1}s^{-1}$	This study
k_{-4}	0.02 s^{-1}	This study
k_5	$10^4, 10^8$ $M^{-1}s^{-1}$	This study
k_{-5}	0.2 s^{-1}	This study
k_6	10^3 $M^{-1}s^{-1}$	Musacchio and Salmon (2007)
k_7	$10^4{}_{(\text{slow})}, 10^6{}_{(\text{fast})}$ $M^{-1}s^{-1}$	This study
k_{-7}	0.2 s^{-1}	This study
k_8	$10^4{}_{(\text{slow})}, 10^6{}_{(\text{fast})}$ $M^{-1}s^{-1}$	This study
k_{7p}	$1.7 * 10^6$ $M^{-1}s^{-1}$	Vink et al. (2006)
k_{-7p}	0.037 s^{-1}	Vink et al. (2006)
k_{8p}	10^5 $M^{-1}s^{-1}$	This study
k_{-8p}	0.3 s^{-1}	This study

"There is no way in which a simple substance could begin in the course of nature, since it cannot be formed by means of compounding". Gottfried Leibniz (1646 - 1716)

"In mathematics you don't understand things. You just get used to them". Johann von Neumann (1903 - 1957)

Chapter 5

Modeling APC Control

Contents

5.1 Summary

We have constructed and validated for the human ^{M}SAC mechanism an *in silico* dynamical model, integrating 11 proteins and complexes. The model incorporates the perspectives of three central control pathways, namely Mad1/Mad2 induced Cdc20 sequestering based on the Template Model (Chapter 3), MCC formation (Chapter 4), and APC inhibition. Originating from the biochemical reactions for the underlying molecular processes, non-linear ordinary differential equations for the concentrations of 11 proteins and complexes of the ^{M}SAC are derived. Most of the kinetic constants are taken from literature, the remaining four unknown parameters are derived by an evolutionary optimization procedure for an objective function describing the dynamics of the APC:Cdc20 complex. MCC:APC dissociation is described by two alternatives, namely the "Dissociation" and the "Convey" model variants. The attachment of the kinetochore to microtubuli is simulated by a switching parameter silencing those reactions which are stopped by the attachment. For both, the Dissociation and the Convey variants, we compare two different scenarios concerning the microtubule attachment dependent control of the dissociation reaction. Our model is validated by simulation of ten perturbation experiments. Only in the controlled case, our models show ^{M}SAC behaviour at meta- to anaphase transition in agreement with experimental observations. Our simulations revealed that for ^{M}SAC activation, Cdc20 is not fully sequestered; instead APC is inhibited by MCC binding.

5.2 Biochemical background

Our model incorporates three ^{M}SAC -related mechanisms: the Template Model, the (kinetochore dependent) MCC formation, and the APC inhibition. Their biochemical details will be explained in the following.

5.2.1 Mad2 Template Model

DeAntoni et al. (2005a) proposed the "Template Model" explaining the mechanism of Mad2 recruitment to the kinetochore during checkpoint activation and subsequent transfer to sequester Cdc20. Recent work by Vink et al. (2006) and Mapelli et al. (2006) provide additional support for the Template Model. Moreover, this model has been confirmed by Nezi et al. (2006), and is entirely consistent with recent Fluorescence Recovery After Photobleaching (FRAP) data (Vink et al., 2006). The Template Model (DeAntoni et al., 2005a) is superior and more solid than the Exchange Model (Luo et al., 2004), which we confirmed in a recent *in silico* study (for comparison and details see Chapter 3).

The Mad2 Template Model is described by the reaction equations Eqs. (5.1)-(5.3) (see chemical reaction scheme, below). It is assumed that Mad1 and C-Mad2 form a stable core complex Mad1:C-Mad2 at unattached kinetochores (DeAntoni et al., 2005a). In our nonlinear ordinary differential equations (ODEs) model, we assume that this process has already been completed. Therefore, there is no free Mad1. Equation (5.1) describes how the Mad1:C-Mad2 core complex binds additional molecules of O-Mad2 through formation of conformational heterodimers between the C- Mad2 subunit of the Mad1:C-Mad2 complex and O-Mad2. Upon Mad1:C-Mad2 binding, O-Mad2 adopts an intermediate conformation (O-Mad2*), which can quickly and efficiently bind Cdc20 and switch to the C-conformation. This process is documented by Eq. (5.2): Cdc20 binding to the complex Mad1:C-Mad2:O-Mad2* leads to the conversion of O-Mad2* to C-Mad2 forming together with Cdc20 the complex Cdc20:C-Mad2; Cdc20:C-Mad2 is assumed then to dissociate off Mad1:C-Mad2 (Fang, 2002). Finally, we assume that the Cdc20:C-Mad2 complex can dissociate into Cdc20 and O-Mad2 (Eq. (5.3)).

5.2.2 MCC Assembly

Equations (5.4) and (5.5) describe the formation of the MCC, which contains Mad2, Bub3, BubR1 and Cdc20 in apparently equal stoichiometries (Sudakin et al., 2001; Hardwick et al., 2000; Millband and Hardwick, 2002; Chung and Chen,

2003). Bub3 associates quite stably with BubR1 (Sudakin et al., 2001; Taylor et al., 2004, 1998a). This interaction is constitutive and is required for the localization of BubR1 to the kinetochores during mitosis. Like for the Mad1:C-Mad2 complex, we do not model the dynamics of the formation of the BubR1:Bub3 complex. BubR1 cannot bind Mad2 directly (Fang, 2002). Moreover, BubR1 does not form a ternary complex with Mad2 and Cdc20. Two Cdc20 binding sites were identified on BubR1 (Bolanos-Garcia et al., 2005; Davenport et al., 2006). Binding of the N-terminal region of BubR1 to Cdc20 requires prior binding of Mad2 to Cdc20 (Davenport et al., 2006). Consistently, the Bub3:BubR1 complex can bind to Cdc20:C-Mad2 in order to form the MCC (Eq. (5.4), rate constants k_4 and k_{-4}). The other site of BubR1 (between residues 490 and 560) can bind Cdc20 tightly regardless of Mad2 being bound to Cdc20 (Davenport et al., 2006). Thus, BubR1 can form a ternary complex with Bub3 and Cdc20 (Eq. (5.5)) which however has no inhibitory activity at the APC (unpublished data (Sudakin et al., 2001)). Equation (5.6) and its low rate were mentioned Musacchio and Salmon (2007) (details are discussed in Chapter 4).

5.2.3 APC Inhibition

The MCC is considered to be essential for ^{M}SAC function, because it binds and inhibits the APC (see Chapter 2) However, MCC inhibits only the mitotic, and not the interphase APC (Pinsky and Biggins, 2005). The interaction between APC and MCC is quite labile in the absence of unattached kinetochores (Sudakin et al., 2001). How the MCC inhibits APC activity is poorly understood (Musacchio and Salmon, 2007). The MCC might bind to the APC as a pseudosubstrate due to a KEN-box motif in BubR1 (Fang, 2002; Morrow et al., 2005; Burton and Solomon, 2007; King et al., 2007). This indicates that the MCC needs to disassemble from the APC at metaphase to elicit anaphase (Morrow et al., 2005; Fang, 2002). Bub1 and Aurora-B kinase contribute directly to the formation of a complex of the MCC with the APC (Morrow et al., 2005) (represented by k_7 in Eq. (5.7)). Unattached kinetochores might sensitize the APC for inhibition by the MCC (Sudakin et al., 2001; Chan et al., 2005; Doncic et al., 2005; Sear and Howard, 2006) (represented

by u in Eq. (5.7), see below). In addition to kinetochore attachment, tension is important for ^{M}SAC inactivation (Nicklas et al., 1995; Nicklas, 1997): if both sister kinetochores attach to microtubules from the same pole, not enough tension is generated and microtubules kinetochore attachment is destabilized to correct the problem (Musacchio and Salmon, 2007). This destabilization depends on Aurora-B kinase (Hauf et al., 2003; Pinsky and Biggins, 2005; Tanaka et al., 2002; Lampson et al., 2004). Again, these effects are subsumed by the switching parameter u. For complex dissociation we consider two model variants:

In the "Dissociation variant", we assume that MCC binds to APC and that this binding is reversible (Eq. (5.7)). Free Cdc20 has to bind reversibly to APC (Eq. (6.7^{a})), effectively competing with MCC.

In the "Convey variant", we do not assume that the APC:MCC complex simply dissociates into APC and MCC, but that the MCC complex falls apart so that the Cdc20 contained in the MCC complex can bind to the APC (Eq. (6.7^{b})).

5.2.4 Control by Attachment

Several reactions in the reaction scheme are controlled by the attachment of microtubules to the kinetochore which is realized by the factor u present in several reaction equations (Chapter 3). Factor u represents the function of proteins like $p31^{comet}$, UbcH10, and Dynein (and its activator Spindly (Griffis et al., 2007)). $p31^{comet}$ prevents further Mad2 turnover on Mad1 and neutralizes the inhibitory activity of Cdc20-bound Mad2 (Habu et al., 2002; Xia et al., 2004; Mapelli et al., 2006; Yang et al., 2007). Catalytically active UbcH10 can promote the release of checkpoint proteins from APC (Reddy et al., 2007). Dynein (Howell et al., 2001) removes the Mad1:C-Mad2 2:2 complex from the kinetochore site after microtubule attachment. Thus, $p31^{comet}$, UbcH10, and Dynein work in concert during checkpoint inactivation.

Also the MCC:APC complex dissociation might be attachment controlled. We therefore introduced the factor u′ in Eq. (6.7^{a}) and Eq. (6.7^{b}), allowing us to compare the uncontrolled (u′= 1) with the controlled (u′= 0 before and u′= 1

after attachment) case. The switching parameter u′ might represent the protein function of Usp44, which deubiquitinates the APC co-activator Cdc20 both *in vitro* and *in vivo*, and thereby directly counteracts the APC-driven disassembly of Mad2:Cdc20 complexes (Stegmeier et al., 2007; Diaz-Martinez and Yu, 2007).

5.2.5 Chemical Reaction Scheme

In our model of the ^{M}SAC mechanism, 9 biochemical reaction equations describe the dynamics of the following 11 species: Mad1:C-Mad2, O-Mad2, Mad1:C-Mad2:O-Mad2*, Cdc20, Cdc20:C-Mad2, Bub3:BubR1, MCC, Bub3:BubR1:Cdc20, APC, MCC:APC, and APC:Cdc20. Because the dissociation of the MCC:APC complex is not known in detail, we introduce two variants for the reaction equation for MCC:APC dissociation.

The Dissociation variant is defined by the following reaction rules (Figure 5.1, red lines):

$$\text{Mad1:C-Mad2} + \text{O-Mad2} \underset{k_{-1}}{\overset{k_1.u}{\rightleftharpoons}} \text{Mad1:C-Mad2:O-Mad2}^* \tag{5.1}$$

$$\text{Mad1:C-Mad2:O-Mad2}^* + \text{Cdc20} \xrightarrow{k_2.u} \text{Cdc20:C-Mad2} + \text{Mad1:C-Mad2} \tag{5.2}$$

$$\text{Cdc20:C-Mad2} \xrightarrow{k_3} \text{O-Mad2} + \text{Cdc20} \tag{5.3}$$

$$\text{Cdc20:C-Mad2} + \text{Bub3:BubR1} \underset{k_{-4}}{\overset{k_4.u}{\rightleftharpoons}} \text{MCC} \tag{5.4}$$

$$\text{Cdc20} + \text{Bub3:BubR1} \underset{k_{-5}}{\overset{k_5.u}{\rightleftharpoons}} \text{Bub3:BubR1:Cdc20} \tag{5.5}$$

$$\text{Cdc20} + \text{O-Mad2} \xrightarrow{k_6} \text{Cdc20:C-Mad2} \tag{5.6}$$

$$\text{MCC} + \text{APC} \xrightarrow{k_7.u} \text{MCC:APC} \tag{5.7}$$

$$\text{MCC:APC} \xrightarrow{k_{-7}.u'} \text{APC} + \text{MCC} \tag{6.7^{a}}$$

$$\text{APC} + \text{Cdc20} \underset{k_{-8}}{\overset{k_8}{\rightleftharpoons}} \text{APC:Cdc20} \tag{5.8}$$

The reaction rules defining the second variant, the Convey variant, are different from this set by replacing the back reaction Eq. (6.7[a]) by Eq. (6.7[b]) (see Figure 5.1, green lines):

$$\text{MCC:APC} \xrightarrow{\text{k}_{-7}.\text{u}'} \text{APC:Cdc20} + \text{O-Mad2} + \text{Bub3:BubR1} \qquad (6.7^{\text{b}})$$

Both variants are controlled by the switching parameters u and u′. They represent a signal generated by the unattached and attached kinetochores, respectively. If the kinetochore is unattached, we set u = 1, otherwise u= 0. For instance, formation of Mad1:C-Mad2:O-Mad2* (Eq. 5.1) can only take place as long as the kinetochores are unattached (DeAntoni et al., 2005a).

The switching parameter u′ represents an additional hypothetical control, whose biochemical realization is described above. For each of the two resolution pathways, we therefore considered two scenarios: In the first, we assume that this control does not exist by setting u′= 1. In the second, we assume that there is a control by setting u′= $1 - u$. This is summarized in Table 5.1:

Model Variants

Scenario	Model variants	Reaction rules	Control of MCC:APC dissociation
Uncontrolled	Dissociation	Eqs. (5.1)-(5.7), (6.7[a]), (5.8)	u′= 1
Controlled	Dissociation	Eqs. (5.1)-(5.7), (6.7[a]), (5.8)	u′= 1−u
Uncontrolled	Convey	Eqs. (5.1)-(5.7), (6.7[b]), (5.8)	u′= 1
Controlled	Convey	Eqs. (5.1)-(5.7), (6.7[b]), (5.8)	u′= 1−u

Table 5.1: Model Variants, related equations, control status of MCC:APC dissociation.

5.2.6 Mathematical Treatment and Simulation

By applying general principles of mass-action kinetics, we converted the reaction rules into sets of time dependent nonlinear ordinary differential equations (ODEs) for the Dissociation variant (Appendix D, Eqs. (D.1)-(D.11)) and for the Convey variant (Appendix D, Eqs. (D.12)-(D.22)).

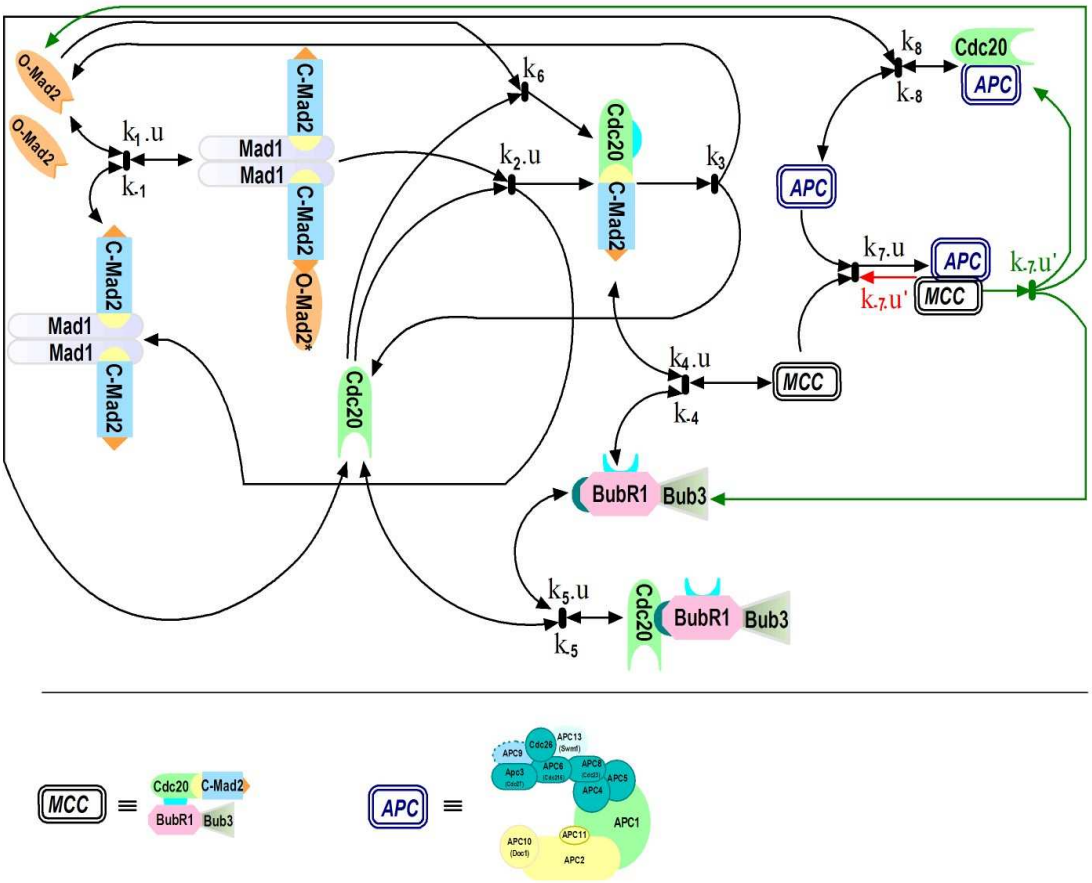

Figure 5.1: Schematic network of the ^{M}SAC model. The arrows describe the interactions between the proteins and complexes. Red lines represent the "Dissociation variant", green lines represents the "Convey variant", while the black arrows are common to both. The switching parameter u models the effect of the attachment. We set u= 1 for the unattached case and u= 0 for the attached case. We set u′= 1 for the uncontrolled scenario and u′= $1 - u$ for the controlled scenario(see Table 5.1).

For the rate constants k_i, we selected experimentally determined values, if available (Table 5.2). In the other cases, we selected representative values exemplifying their whole physiologically possible range. We also fitted unspecified parameters by minimizing an APC:Cdc20 concentration dependent objective functional (Appendix D, D.3), taking into account the range of parameter values from experiments (Fang, 2002; Howell et al., 2000a; Tang et al., 2001; Vink et al., 2006; Musacchio and Salmon, 2007).

In a typical simulation, we initialized all reaction partners according to Table 5.2 and numerically integrated the ODEs until steady state was reached using u= 1 (denoting unattached kinetochores). Then we set u= 0 (kinetochores attached) and continued integrating the ODEs until we again reached a steady state.

The minimum concentration of APC:Cdc20 before attachment and the speed of recovery after attachment (recovery time) are criteria for ^{M}SAC function and were analyzed to compare the models. Deduced from the biochemical data (see above), the APC:Cdc20 concentration must be low before and the recovery must be fast after attachment.

5.3 Results

We developed a theoretical model of the human biochemical mitotic checkpoint at meta- to anaphase transition. As described in the literature, many proteins contribute to checkpoint function. The key players and their interactions are captured by the reaction equations introduced in the previous section. We transformed these equations into ODEs and selected specific values for the initial concentrations and rate constants from the literature and our previous publications (summarized by Table 5.2). For only four values we could not identify specific data in the literature. We obtained these values by optimizing the properties of the model according to the APC:Cdc20 level: this complex level should be low in metaphase and high in anaphase; furthermore, the switching should be fast (see Appendix D for details). We found good behavior of the model network for the values $k_7 = 10^8 M^{-1}s^{-1}$, $k_{-7} = 0.08s^{-1}$, $k_8 = 5 * 10^6 M^{-1}s^{-1}$, and $k_{-8} = 0.08s^{-1}$.

Model parameters

Parameters	Comments and References
Species initial concentration	
[Cdc20]= $2.2 * 10^{-7}$M	(Fang, 2002; Howell et al., 2000a; Tang et al., 2001)
$[Mad2]_{total}$= $2 * 10^{-7}$M	(Fang, 2002; Howell et al., 2000a; Tang et al., 2001)
[BubR1:Bub3]= $1.3 * 10^{-7}$M	(Fang, 2002; Tang et al., 2001)
[APC]= $0.9 * 10^{-7}$M	(Stegmeier et al., 2007)
Other species are zero	
Species concentration ratios	
25% of $[Mad2]_{total}$ associated with Mad1, [Mad1:C-Mad2]=25%$[Mad2]_{total}$	(Luo et al., 2004; Fang, 2002)
[O-Mad2]= 75%$[Mad2]_{total}$	
Model - Parameters	
$k_1 = 2 * 10^5$ $M^{-1}s^{-1}$	(Vink et al., 2006)
$k_{-1} = 2 * 10^{-1}$ s^{-1}	(Vink et al., 2006)
$k_2 = 10^8 M^{-1}s^{-1}$	Chapter 3
$k_3 = 1 * 10^{-2}s^{-1}$	Chapter 3
$k_4 = 10^7$ $M^{-1}s^{-1}$	Chapter 3
$k_{-4} = 2 * 10^{-2}$ s^{-1}	Chapter 3
$k_5 = 10^4$ $M^{-1}s^{-1}$	Chapter 3
$k_{-5} = 2 * 10^{-1}$ s^{-1}	Chapter 3
$k_6 = 10^3$ $M^{-1}s^{-1}$	(Musacchio and Salmon, 2007)
$k_7 = 10^8$ $M^{-1}s^{-1}$	This study
$k_{-7} = 8 * 10^{-2}$ s^{-1}	This study
$k_8 = 5 * 10^6$ $M^{-1}s^{-1}$	This study
$k_{-8} = 8 * 10^{-2}$ s^{-1}	This study

Table 5.2: Model parameters: Initial concentration and rate constants.

5.3.1 ^{M}SAC Model Behavior

We analyzed the dynamics of the model integrating 11 proteins and complexes of the ^{M}SAC . The literature does not provide a clear view, yet, about how the MCC:APC complex dissociates resulting in APC activation. Therefore, we introduced two alternative reaction pathways: In the first variant, we assume that the MCC:APC complex dissociate into MCC and APC (reaction Eq. (6.7^{a})), subsequently allowing the MCC to disassemble into its parts according to reaction Eq. (5.4) (Dissociation variant). In the second variant, the MCC component Cdc20 may stay in the complex with APC and only the further MCC complex members dissociate according to reaction Eq. (6.7^{b})(Convey variant).

Figure 5.2 displays the APC:Cdc20 concentrations over time. For both, Dissociation and Convey variant, we have selected the time range such that each concentration can reach steady state. For all calculations, the concentrations and rates of Table 5.2 were chosen including those for k_7, k_8, and k_{-8}. We varied the rate of k_{-7} (dissociation of MCC:APC) between 0.0008 and 0.08, because k_{-7} is unknown and crucial for model behavior. For both model variants, we distinguished 2 scenarios: in one scenario reaction Eq. (6.7^{a}) (or Eq. (6.7^{b})) of the checkpoint is valid all the time ("uncontrolled"), while in the other case this reaction is silenced until it is activated by microtubule attachment to the kinetochore ("controlled"). This property of the controlled case is realized by introducing the factor u′for reaction Eq. (6.7^{a}) and Eq. (6.7^{b}).

In the uncontrolled case, our model cannot explain the checkpoint behavior, independently of which pathway is chosen (Figure 5.2 A-B). For the Dissociation variant, the APC:Cdc20 concentration is low for low values of k_{-7}, however, in this case the switching recovery is unrealistically slow. On the other hand, for fast switching, k_{-7} must be high resulting in an increased APC:Cdc20 concentration before attachment (Figure 5.2 A-B). This behavior is even worse for the Convey variant in the uncontrolled case (Figure 5.2 B). For low values of k_{-7}, both pathways behave rather similarly; for higher values of k_{-7} the Convey variant is even less satisfying compared to the Dissociation variant.

The Dissociation variant **The Convey variant**

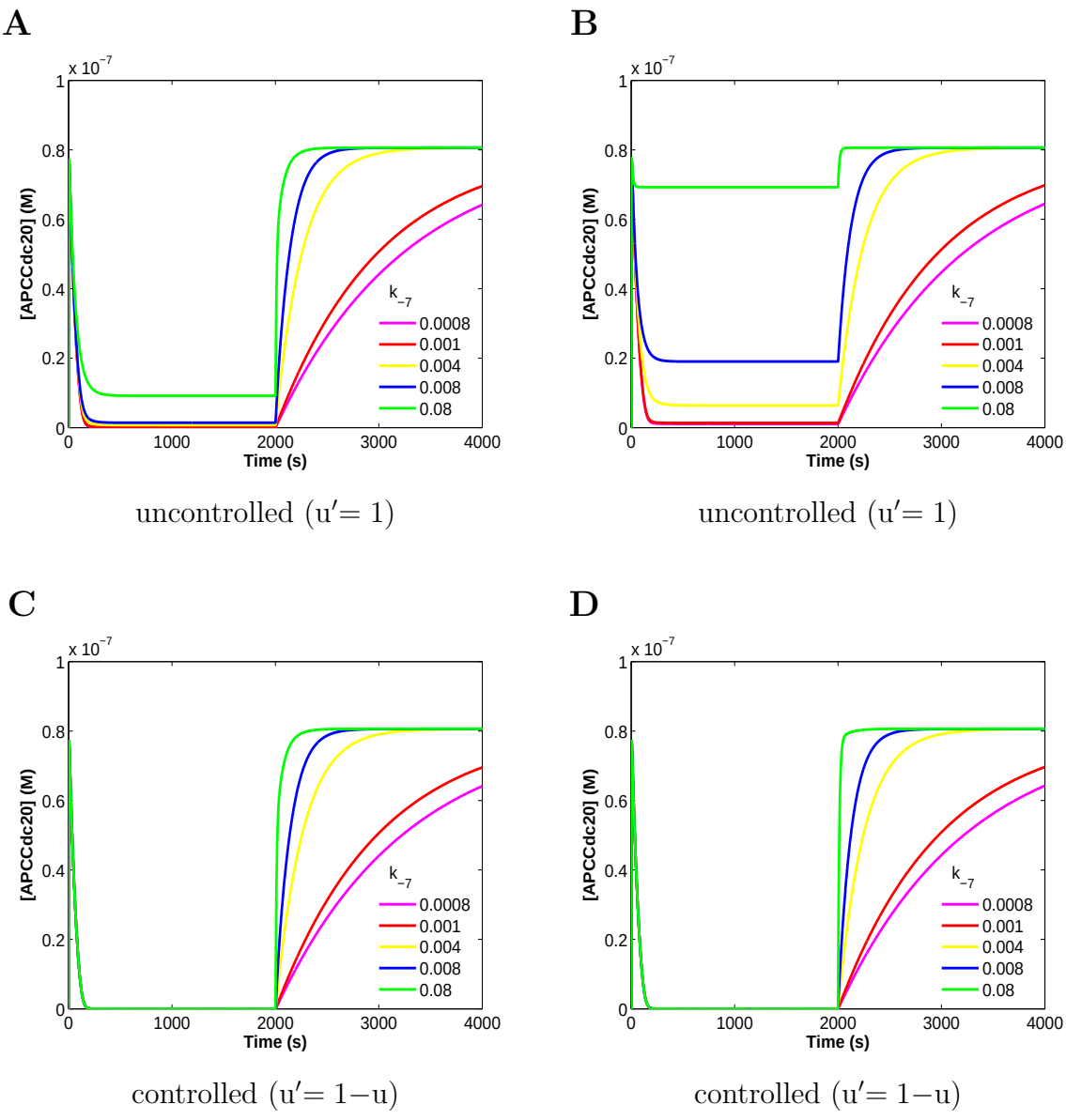

uncontrolled ($u' = 1$) uncontrolled ($u' = 1$)

controlled ($u' = 1-u$) controlled ($u' = 1-u$)

Figure 5.2: Dynamical behavior of APC:Cdc20 concentration versus time for the Dissociation variant (A, C) and the Convey variant (B, D) each in the uncontrolled (A, B) and the controlled (C, D) case. Calculation results are presented for different values of the rate k_7 in $[s^{-1}]$, as indicated. The APC:Cdc20 concentration should be close to zero before attachment and should rise quickly after attachment. Spindle attachment occurs at t=2000s (switching parameter u from 1 to 0). Parameters setting according to Table 5.1 and Table 5.2.

In the controlled case, we introduced the factor u′(see above) regulating reaction Eq. (6.7[a]) and Eq. (6.7[b]), and re-calculated the model. Both pathways fully inhibit APC:Cdc20 before attachment and both show very fast switching recovery for high k_{-7} values (Figure 5.2 C-D). Thus, a distinction between the two pathways in the controlled case is not possible based on our theoretical results. We observed that the controlled Convey variant is slightly faster (by about 5 mins) in switching compared to the controlled Dissociation variant. This makes the Convey variant slightly superior, however, we think that this difference is too small for a clear preference between the two pathways. Experimental measurements have to distinguish between these cases. Such experiments are in progress in our laboratory.

In addition to the APC:Cdc20 concentration values, we also analyzed the time-dependent concentrations of all reaction components. We observed differences between the two pathways in the controlled case for sub-complexes like Cdc20:C-Mad2 and MCC (Figures 5.4 5.5).

In our simulations, the MCC completely sequesters the APC so that no free APC is available until the microtubules are attached. Thus, Cdc20 has a dual function: until kinetochore attachment, Cdc20 contributes to MCC formation and thus APC inhibition, while after attachment Cdc20 acts as the APC activator. The effect of the switching parameter u is presented in Figure 5.3, where u varied between 1 and 0 for 101 time instead of two values 1 and 0.

The Dissociation variant | **The Convey variant**

A

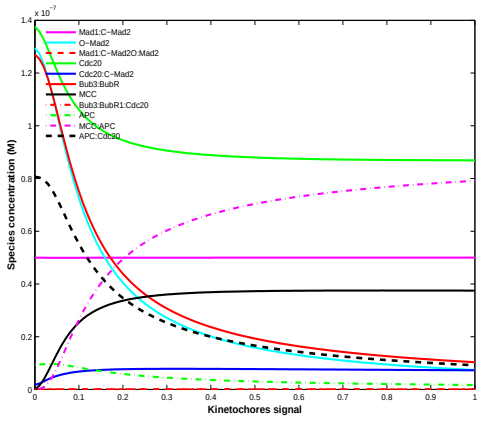

uncontrolled (u′= 1)

B

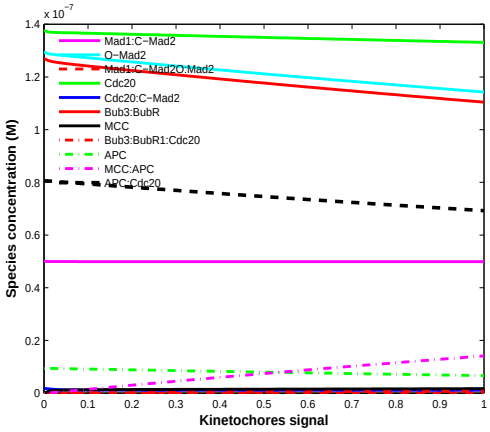

uncontrolled (u′= 1)

C

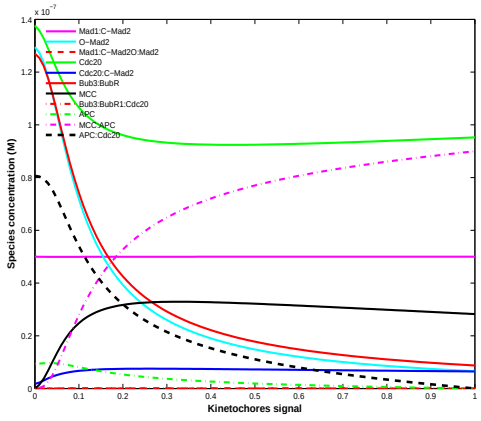

controlled (u′= 1−u)

D

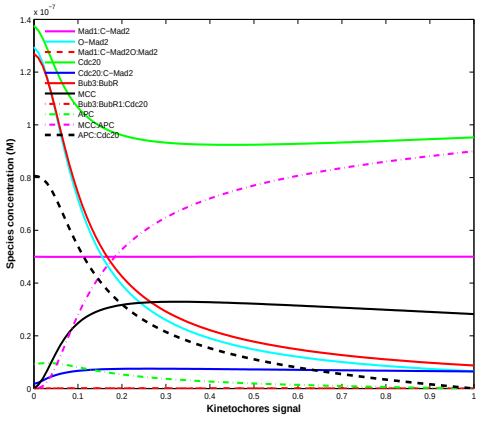

controlled (u′= 1−u)

Figure 5.3: Kinetochore switching signal (u and u′) on Models Simulation. The signal has taken for 101 increments between 0 and 1. Figures A and B for the controlled case. Figures C and D for the uncontrolled case.

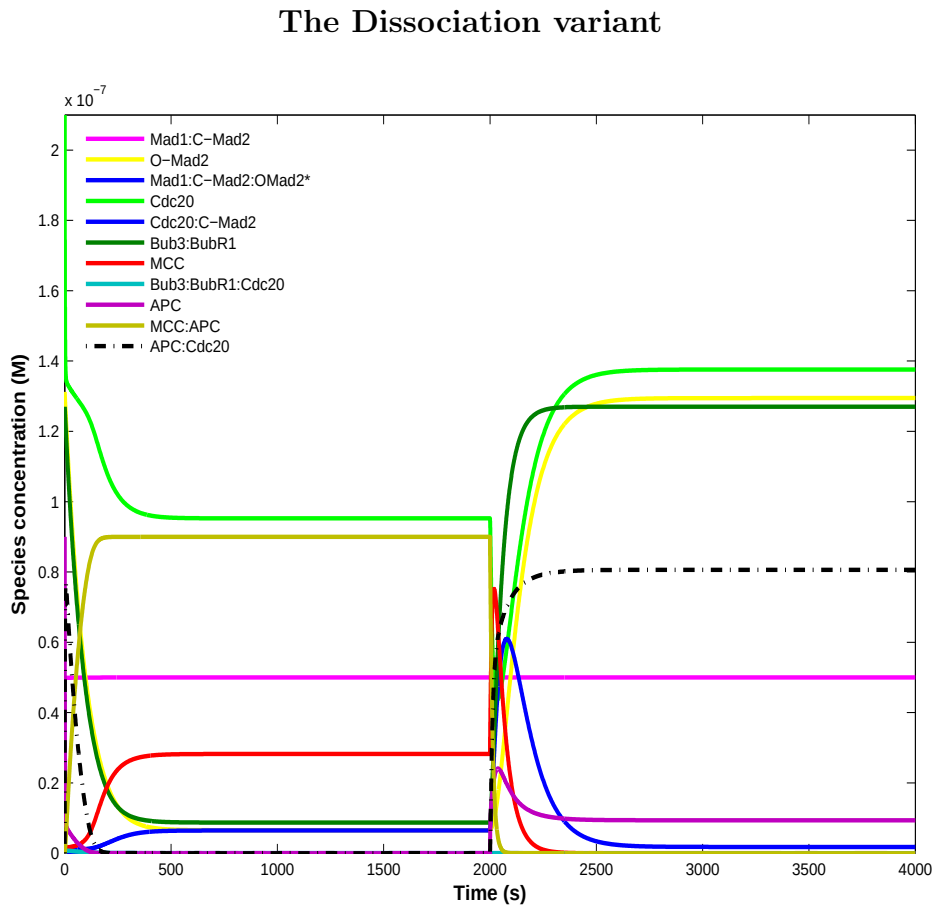

Figure 5.4: Species concentration over time for the controlled Dissociation (wild type). Spindle attachment occurs at t = 2000s (switching parameter u from 1 to 0 and u′from 0 to 1). Parameters setting according to Table 5.2.

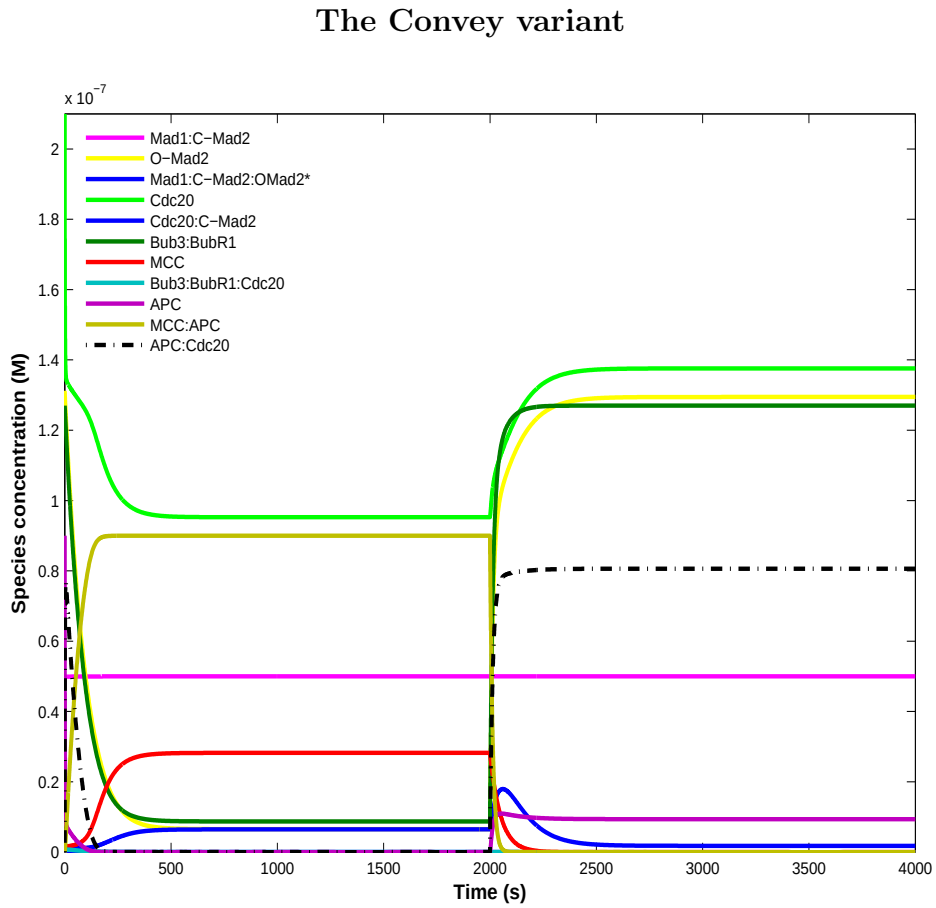

Figure 5.5: Species concentration over time for the controlled Convey variants (wild type). Spindle attachment occurs at t = 2000s (switching parameter u from 1 to 0 and u′from 0 to 1). Parameters setting according to Table 5.2.

5.3.2 Model Validation by Mutation Experiments

In order to validate our model, we tested different mutations (deletion and over-expression) of the proteins and complexes involved, measured in different organisms (Table 5.3).

Recent experimental studies report that deletion in different organisms of any of Mad2 (Nezi et al., 2006; Dobles et al., 2000; Michel et al., 2001; Fang et al., 1998b),Mad1 (Kienitz et al., 2005; Lee and Spencer, 2004; Iwanaga et al., 2007; Hardwick and Murray, 1995; Chen et al., 1999b), Bub3 (Kalitsis et al., 2000; Taylor et al., 1998b), BubR1 (Davenport et al., 2006; Wang et al., 2004b; Schmidt and Medema, 2006; Hanks et al., 2004), Cdc20 (Zhang and Lees, 2001b), Bub1 (Basu et al., 1999; Taylor et al., 1998b), or Aurora B (Kallio et al., 2002b; Biggins and Murray, 2001; Cheeseman et al., 2002) resulted in ^{M}SAC defects like premature sister-chromatid separation, no mitotic arrest, reduced partner binding, increase of polyploidy, or death. Experimental details and our model predictions are in qualitative agreement as summarized in Table 5.3: For example, over-expression of Mad2 (He et al., 1997; DeAntoni et al., 2005a) activates the ^{M}SAC resulting in mitotic arrest, while over-expression of Cdc20 (Hwang et al., 1998) allows cells to exit from mitosis, however with a depolymerized spindle or damaged DNA. Deletion of any of the APC subunits Cdc26, Apc9, Cdc6 or Doc1 disrupts complex association (Passmore, 2004b; Boronat and Campbell, 2007) with no anaphase initiation. We observed that deletions and/or over-expression of proteins, realized experimentally or in our model, change checkpoint function in the same way.

For the essential checkpoint proteins, Mad2 and Cdc20, we present the mutation effect on our model in detail in Figure 5.6 for the Convey variant. The effect is basically the same for the Dissociation variant (Figure 5.7). For Mad2 or Cdc20 deletion, the concentrations of all model components are rather stable, that is, they are almost not affected by microtubule attachment. However, in the case of Mad2 deletion, the APC:Cdc20 concentration is high (Figure 5.6 A) while for Cdc20 deletion this concentration is zero by definition (Figure 5.6 C). In the case of Mad2 or Cdc20 over-expression, many component concentrations were affected. In particular, for Mad2 over-expression the APC:Cdc20 concentration

remains low before and significantly lower than in the wild type after attachment, explaining mitotic arrest and the delay of exit from mitosis (Figure 5.6 B). In contrast, for Cdc20 over-expression, the APC:Cdc20 concentration is high before and after attachment (Figure 5.6 D) resulting in total checkpoint failure. Thus, our ^{M}SAC model is able to explain the presented mutation phenotypes (Table 5.3, Figures 5.6 5.7 5.9 5.8).

Model Validation

No.	**Species**	**Organisms**	**Exp.**	**Experimental effects**	**Effects in our models**
1.	Mad2	H. s.	D	-Impaired ^{M}SAC (Nezi et al., 2006)	^{M}SAC fails to arrest
	Mad2	M.	D	-Unable to arrest (Dobles et al., 2000)	& no Cdc20 Sequestering
	Mad2	H. s.& M.	D	-Defective ^{M}SAC (Michel et al., 2001)	[APC:Cdc20] very high
	Mad2	H. s.	D	-Unable to bind Cdc20 or Mad1 (Fang et al., 1998b)	
				More refs. (Chen et al., 1999c; DeAntoni et al., 2005b	
				Luo et al., 2000b; Zhang and Lees, 2001a)	
2.	Mad2	H. s.	O	-Activates the ^{M}SAC (DeAntoni et al., 2005a)	Activates the ^{M}SAC
	Mad2	S.p.	O	-Blocks mitosis (He et al., 1997)	& full Cdc20 sequestering
					[APC:Cdc20] very low
3.	Mad1	H. s.	D	-^{M}SAC inactivation	^{M}SAC fails to arrest
				and aneuploidy (Kienitz et al., 2005)	& no Cdc20 sequestering
	Mad1	S.p.	D	-Cell death (Lee and Spencer, 2004).	[APC:Cdc20] very high
				More refs. (Iwanaga et al., 2007	
				Chen et al., 1999b; Hardwick and Murray, 1995).	
4.	BubR1	H. s.	D	-Reduced ^{M}SAC function, reduce ^{M}SAC binding to	^{M}SAC fails to arrest
				Cdc20:C-Mad2 (Davenport et al., 2006)	[APC:Cdc20] very high
		M.	D	Increase polyploidy (Wang et al., 2004b)	
				More refs.(Schmidt and Medema, 2006	
				Hanks et al., 2004)	
5.	Bub3	M.	D	-Fail to arrest (Kalitsis et al., 2000	^{M}SAC fails to arrest
				Taylor et al., 1998b)	[APC:Cdc20] very high
					(P.S. same as BubR1)

Model Validation (continued)

No.	**Species**	**Organisms**	**Exp.**	**Experimental effects**	**Effects in our models**
6.	Cdc20	S.c.	O	-Allows cells with a depolymerized spindle or damaged DNA to leave mitosis (Hwang et al., 1998). -Impairment ^{M}SAC and aneuploidization in oral cancer (Mondal et al., 2007b)	^{M}SAC fails to arrest [APC:Cdc20] very high
7.	Cdc20	H. s.	D	-Reduce binding to Mad2 and selective disruption from Mad2 (Zhang and Lees, 2001b).	Mitosis blocks [APC:Cdc20] very low
		S.p.	D	-Arrest in metaphase (Shirayama et al., 1999).	
8.	Bub1	Drosophila	Inh.	-Chromosome missegregation (Basu et al., 1999)	^{M}SAC fails to arrest
		H. s.	Inh.	-Disrupt Bub3 localization, disrupt of Bub3 binding to BubR1 (Taylor et al., 1998b)	[APC:Cdc20] very high
9.	Aurora B	Xenopus	Inh.	-Override the ^{M}SAC function, Perturbs MTs Dynamics (Kallio et al., 2002b)	^{M}SAC fails to arrest [APC:Cdc20] very high
		S.c.	Inh.	-Unregulated MTs, ^{M}SAC fails to arrest (Biggins and Murray, 2001; Cheeseman et al., 2002).	(P.S. same as Bub1)
10.	APC units cdc26, apc9 cdc6, Doc1	S.p.	D	-Disrupt complex association (Passmore, 2004b; Boronat and Campbell, 2007) More refs.(Chang et al., 2001)	Activates the ^{M}SAC [APC:Cdc20] very low

Table 5.3: Mutation Experiments; D for deletion or knockdown experiments, O for over-expression experiments, and Inh. for inhibition; S.c., Saccharomyces cerevisiae; S.p., Schizosaccharomyces pombe; H. s., Homo sapiens(Human); and M., Murine

5.4 Discussion

Although our model is able to explain checkpoint function, this explanation does not contain details regarding the bio-molecular nature of the switching signal represented by the abstract factor u in our model. For a general explanation of mitosis it is desirable to replace the abstract factor u by chemical reactions of species like $p31^{comet}$, Dynein, Usp44, and/or UbcH10. These species play a role in the signaling of the attachment to the ^{M}SAC control network we modeled here. When further biochemical details become available, we will replace u by a network model encompassing these species. Other additional proteins and complexes are involved in ^{M}SAC function implicitly. These species grant localization of outer kinetochore proteins as well as checkpoint proteins, which do not appear in our model explicitly. Examples are Bub1 (responsible for Bub3 and BubR1 localization (Taylor et al., 1998a; Chen, 2002b; Larsen et al., 2007)) and Mps1, an essential component of the ^{M}SAC (Hardwick et al., 1996; Stucke et al., 2002; Palframan et al., 2006; Abrieu et al., 2001; Millband and Hardwick, 2002) required for kinetochore localization of Mad1 and Mad2 (Vigneron et al., 2004; Liu et al., 2003; Stucke et al., 2004; Hoffman et al., 2001; Fisk et al., 2004; Fisk and Winey, 2004, 2001; Tang et al., 2004). Considering these additional proteins and their spatial localization would be an important next step towards a systems level model of mitosis.

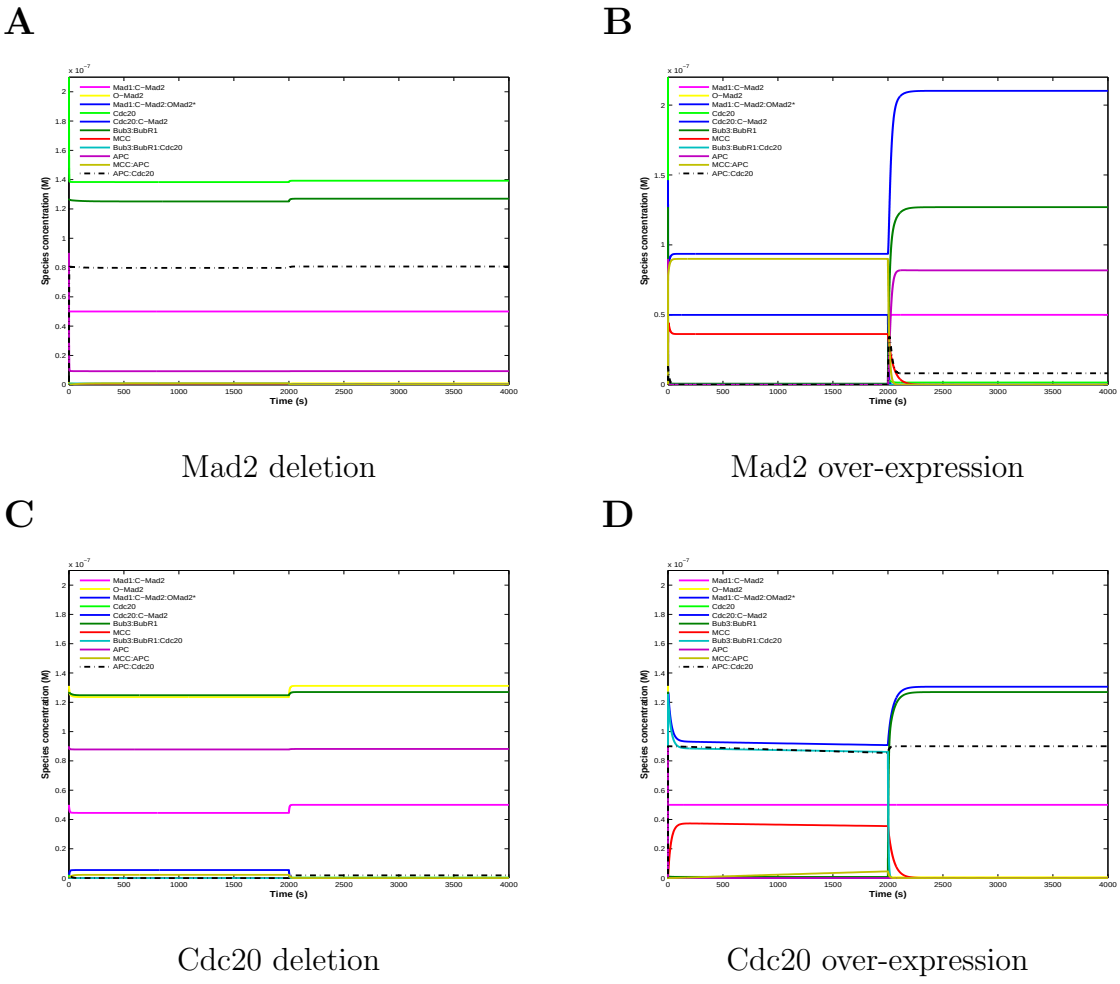

Mad2 deletion

Mad2 over-expression

Cdc20 deletion

Cdc20 over-expression

Figure 5.6: Simulation of Mad2 and Cdc20 mutations for the controlled Convey variant. For deletion we set the respective initial concentration 100 times lower, and for over-expression 1000 times higher. Further setting as in Figure5.4

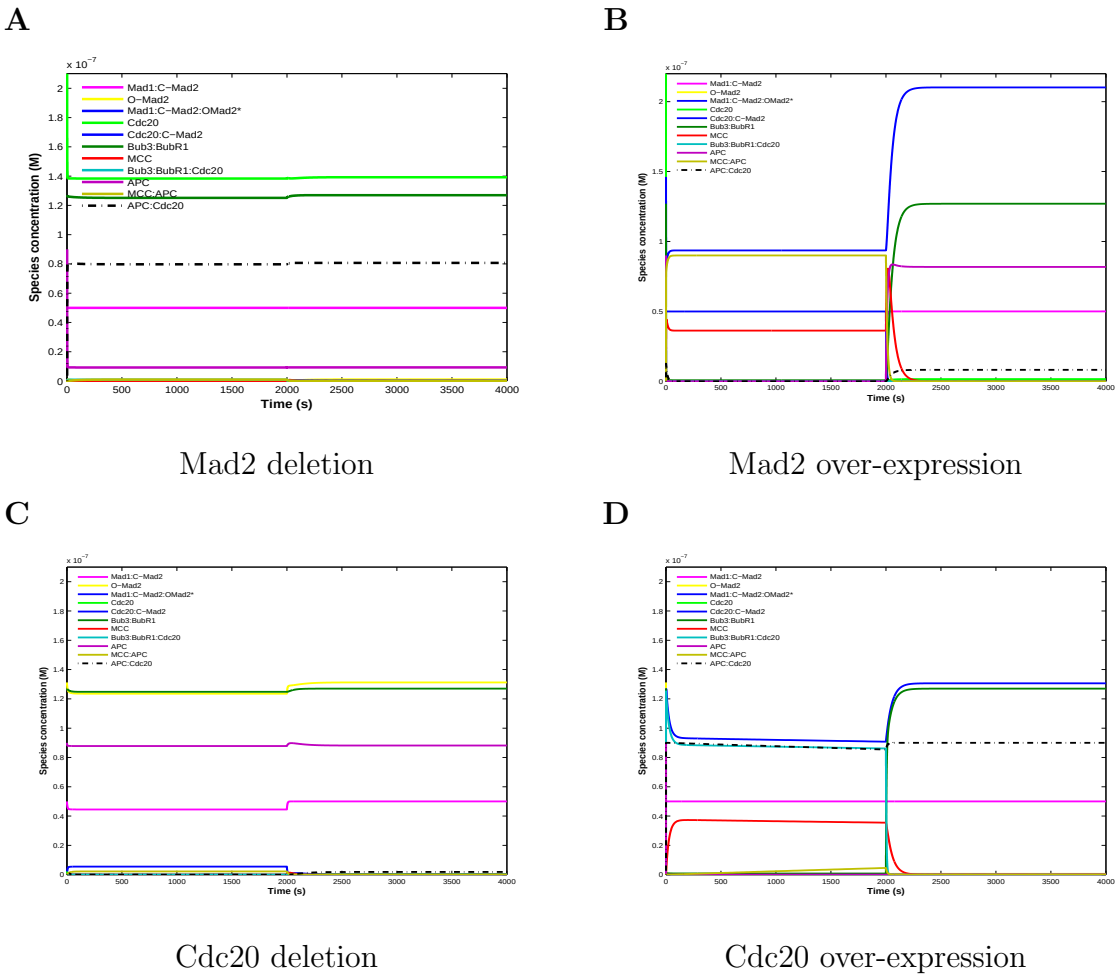

Mad2 deletion

Mad2 over-expression

Cdc20 deletion

Cdc20 over-expression

Figure 5.7: Simulation of Mad2 and Cdc20 mutations for the controlled Dissociation variant. For deletion we set the respective initial concentration 100 times lower, and for over-expression 10000 times higher. Note that Bub3 deletion has same effect as BubR1 (data not shown), and Bub1 has the same effect as aurora B (data not shown). Further setting as in Figure 5.2.

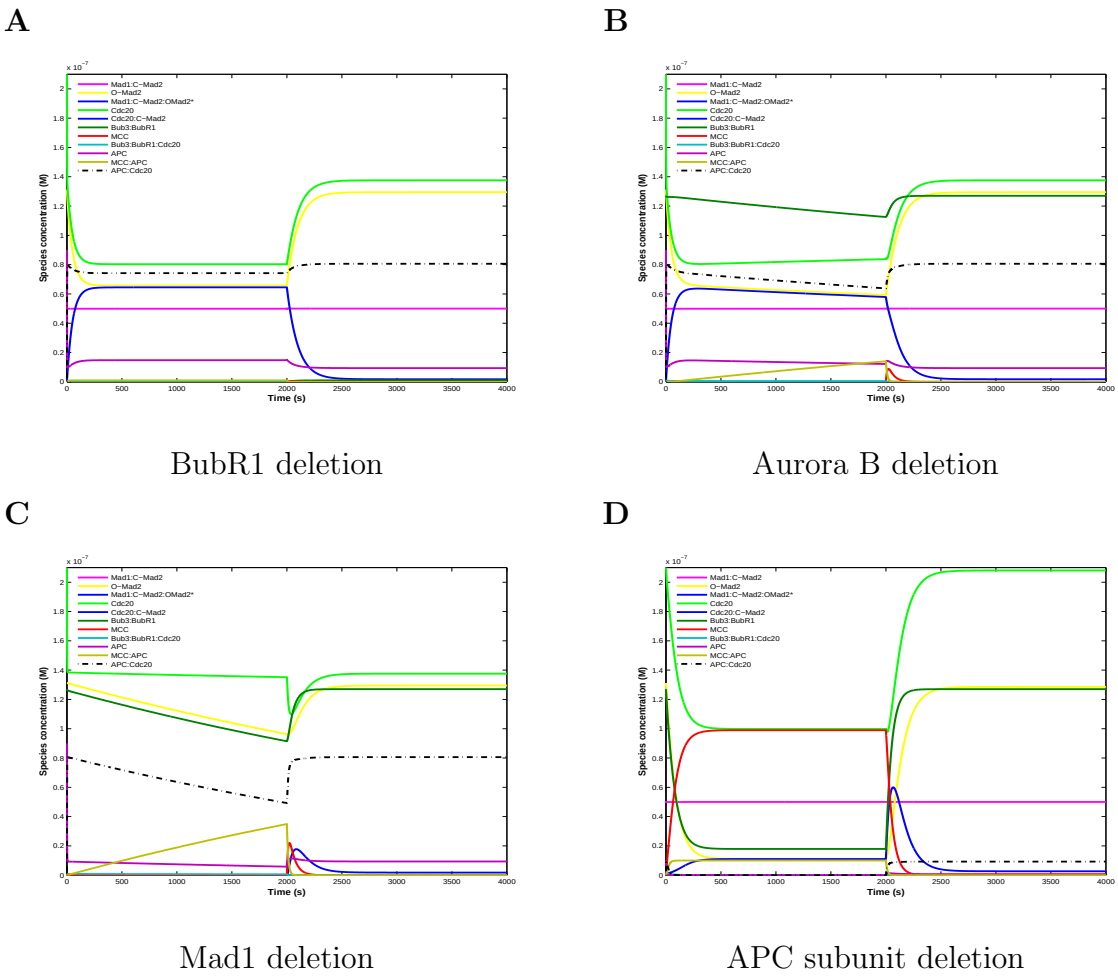

BubR1 deletion

Aurora B deletion

Mad1 deletion

APC subunit deletion

Figure 5.8: Simulation of BubR1, Aurora B, Mad1, and APC (subunits) for the controlled Dissociation variant. For deletion we set the respective initial concentration 100 times lower. Further setting as in Figure 5.2.

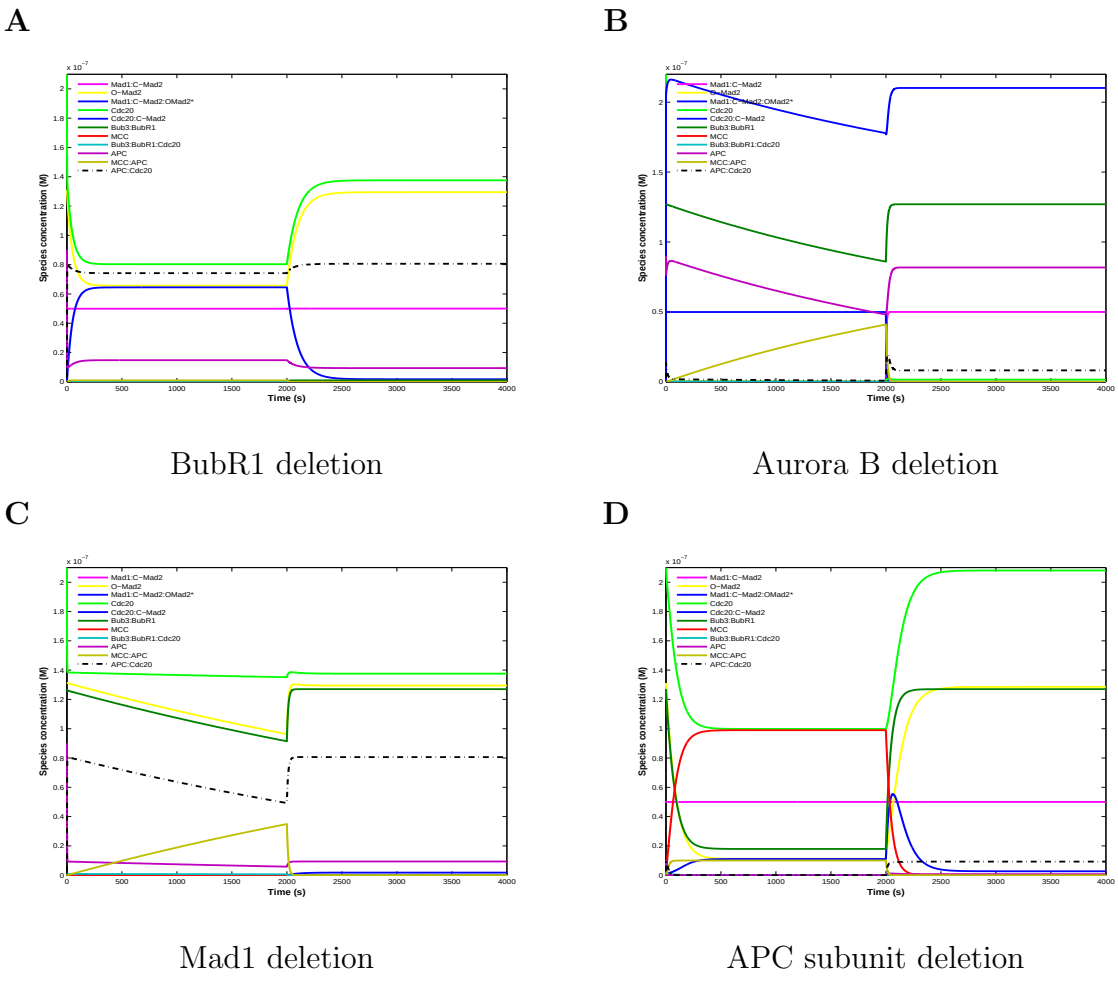

BubR1 deletion

Aurora B deletion

Mad1 deletion

APC subunit deletion

Figure 5.9: Simulation of BubR1, Aurora B, Mad1, and APC (subunits) for the controlled Convey variant. For deletion we set the respective initial concentration 100 times lower. Further setting as in Figure 5.2.

"If I feel unhappy, I do mathematics to become happy.
If I am happy, I do mathematics to keep happy.".
Alfred Rényi (1921 - 1970).

"A Mathematician is someone who can take a cup of coffee and turn it into a theory". Paul Erdös (1913 - 1996)

Chapter 6

Robustness and Stochasticity Effect

Contents

6.1 Summary

Intrinsic fluctuations due to the stochastic nature of biochemical reactions can have large effects on the response of biochemical networks. In this chapter, we view results from stochastic differential equations to capture noise and fluctuations effects. We have developed a "qualitative" model based on 14 proteins and complexes to describe concentration dynamics by nonlinear ordinary differential equations in three compartments coupled by diffusion. One kinetochore in each compartment determines the attachment status to the spindle pole. Here, we focus on the role of noise in the segregation surveillance process. The deterministic differential equations are enriched by a stochastic term adding white noise of different amplitudes. Obviously, for the known physiological parameter ranges, noise does not disturb the checkpoint function. On the other hand, there is a connection between diffusion and noise, that could become important when considering a larger number of chromosomes.

6.2 Introduction

Several deterministic models have been presented for the mitosis control during the past few months (Ibrahim et al., 2008a,b; Toth et al., 2007). When studying the behavior of these deterministic models, it has become clear that, with the given parameter values, the deterministic models, and in more general cell cycle models, are not capable of reproducing the experimentally observed irregular behavior *in vitro* in response to noise (Steuer, 2004).

Although most cellular processes proceed in a spatially and temporally ordered fashion, not all noise is rejected (Rao et al., 2002). Moreover, it has become clear that the role of intrinsic noise in cellular functions may be complex and cannot always be treated as a small perturbation to the deterministic behavior (Steuer et al., 2003). Different studies have explored the influence of molecular fluctuations on complex processes and cases have been found where noise seems to be essential for the required biological function (Steuer, 2004). In addition, this type of

modeling is becoming increasingly important in the field of systems biology, e.g. for modeling the cell cycle and gene regulation (Steuer, 2004; Battogtokh and Tyson, 2004; Chen et al., 2005; Steuer et al., 2003; Kaern et al., 2005; Kepler and Elston, 2001). Cell cycle control is subject to fluctuations from different sources (Battogtokh and Tyson, 2004; Steuer, 2004) in a natural environment.

In this chapter, we focus on the investigation of the role of noise in a qualitative deterministic model as it studied and mentioned in (Ibrahim et al., 2007; Lenser et al., 2007). Here, we make use of stochastic differential equations (SDEs) to simulate in particular the implications of molecular fluctuations on the Mitotic Spindle Assembly Checkpoint (^{M}SAC). Regarding the concentrations of [APC:Cdc20] and [MCC:APC] as measurements for the switch triggering exit from metaphase to anaphase, we model the dynamics of these concentrations in dependency of attachment states of the involved kinetochores by a deterministic description of a network of 14 proteins and protein complexes which regulate the dynamics of [APC:Cdc20] and [MCC:APC]. Only when the last kinetochore attaches, the APC:Cdc20 complex is allowed to form and thus starts a signalling cascade leading to onset of anaphase. Adding white noise to the deterministic equations allows the investigation of fluctuation effects.

6.3 The Model and its Simulation

In our model, we consider 14 proteins and protein complexes, called species here, namely Mad2, Mad1, BubR1, Bub3, Mad2*, Mad1*, BubR1*, BubR1:Bub3, APC, Cdc20, MCC, MCC:APC, Cdc20:Mad2, and APC:Cdc20. A detailed quantitative bio-molecular description of the reactions involved can be found in (Ibrahim et al., 2008a). In an illustration(Figure6.1), we show the proteins, indicating also their localization in the reaction process. Here, we summarize the reaction equations. Three activation reactions are mediated by the kinetochore:

$$\text{Mad2} \underset{\text{k}_{-1}}{\overset{\alpha}{\rightleftharpoons}} \text{Mad2}^* \tag{6.1}$$

$$\text{Mad1} \underset{\text{k}_{-2}}{\overset{\beta}{\rightleftharpoons}} \text{Mad1}^* \tag{6.2}$$

$$\text{BubR1} \underset{\text{k}_{-3}}{\overset{\gamma}{\rightleftharpoons}} \text{BubR1}^* \tag{6.3}$$

The forward reactions with kinetic constants α, β, and γ (Table 6.1) in the unattached state stop when the kinetochore attaches. Therefore, in the attached state, we put $\alpha = \beta = \gamma = 0$. Therefore, Mad2*, Mad1*, and BubR1* are not any longer produced by activation at the respective kinetochore, but they are still supplied by diffusion from other compartments with unattached kinetochores. The backward reactions as well as all other reaction equations are not influenced by the attachment status of the kinetochore:

$$\text{BubR1} + \text{Bub3} \underset{\text{k}_{-4}}{\overset{\text{k}_4}{\rightleftharpoons}} \text{BubR1:Bub3} \tag{6.4}$$

$$\text{Mad2} + \text{BubR1:Bub3} + \text{Cdc20} \underset{\text{k}_{-5}}{\overset{\text{k}_5}{\rightleftharpoons}} \text{MCC} \tag{6.5}$$

$$\text{MCC} + \text{APC} \underset{\text{k}_{-6}}{\overset{\text{k}_6}{\rightleftharpoons}} \mathit{MCC} : \mathit{APC} \tag{6.6}$$

$$\text{Mad2}^* + \text{Mad1}^* + \text{Cdc20} \xrightarrow{k_7} \text{Cdc20:Mad2} + \text{Mad1} \tag{6.7}$$

$$\text{Cdc20:Mad2} \xrightarrow{k_8} \text{Cdc20} + \text{Mad2} \tag{6.8}$$

$$\text{MCC:APC} \xrightarrow[\substack{\perp \\ \text{BubR1}^* \\ \text{Cdc20:Mad2}}]{\text{Inhibitors}} \text{APC:Cdc20} + \text{BubR1:Bub3} + \text{Mad2} \tag{6.9}$$

$$\text{APC:Cdc20} \underset{\text{k}_{-9}}{\overset{\text{k}_9}{\rightleftharpoons}} \text{APC} + \text{Cdc20} \tag{6.10}$$

$$\text{Cdc20:Mad2} + \text{BubR1:Bub3} \xrightarrow{\text{k}_{10}} \text{MCC} \tag{6.11}$$

The reaction equations define ordinary differential equations for the concentrations of the respective molecules. Mass action kinetics is assumed for reaction rules (6.1)-(6.8) and (6.10)-(6.11). Not much is known about MCC:APC dissociation

(6.9), so we have used a mixed inhibition function of Michaelis-Menten type:

$$f_{Inh}(S,I) = \frac{\mathrm{V} * S}{k_m * (1 + \frac{I}{k_{is}}) + S * (1 + \frac{I}{k_{ic}})}$$

where $S \equiv$ [MCC:APC] is the substrate , $I \equiv$ [BubR1*] + [Cdc20:Mad2] is the inhibitor concentration, V is the forward maximum velocity, k_m is the forward Michaelis-Menten constant, k_{is} is the specific (competitive) inhibition constant, and k_{ic} is the catalytic (noncompetitive) inhibition constant.
Here, we give examples for two of the 14 ordinary differential equations, namely for the concentration of the complexes MCC:APC and APC:Cdc20 :

$$\frac{\mathrm{d[MCC:APC]}}{\mathrm{dt}} = \mathrm{k}_6[\mathrm{MCC}][\mathrm{APC}] - \mathrm{k}_{-6}[\mathrm{MCC:APC}] - f_{Inh}(S,I) \quad (6.12)$$

$$\frac{\mathrm{d[APC:Cdc20]}}{\mathrm{dt}} = f_{Inh}(S,I) - \mathrm{k}_{10}[\mathrm{APC:Cdc20}] + \mathrm{k}_{-10}[\mathrm{APC}][\mathrm{Cdc20}] \quad (6.13)$$

The equations described so far show the evolution in time of the concentrations of the 14 species near one kinetochore. To concentrate on the main effects, we consider three compartments X, Y, and Z in a linear spatial arrangement, so that molecules can only diffuse between X and Y, and between Y and Z. Each compartment contains one kinetochore, which can be attached or not attached to the spindle. As mentioned before, the attachment of the spindle within a specific compartment is represented as a change of parameters α, β, and γ in that compartment according to the values in Table 6.1 (unattached) and the value 0 (attached).

Instead of introducing spatial variables, we use Fick's first law to describe diffusion between compartments. In our simulation with discretized time, diffusion is then discribed by a characteristic constant $\Omega = \frac{D}{l^2}$ (Paliwal et al., 2004; Thorwarth et al., 2005) that multiplies the concentration differences. We obtain for a species i and reaction terms $R_{i,A}$ in compartment A the following equations:

$$d[i]_X/dt = \Omega([i]_Y - [i]_X) + R_{i,X} \quad (6.14)$$

$$d[i]_Y/dt = \Omega([i]_X - 2[i]_Y + [i]_Z) + R_{i,Y} \quad (6.15)$$

$$d[i]_Z/dt = \Omega([i]_Y - [i]_Z) + R_{i,Z} \quad (6.16)$$

Because many biological details are yet unknown, we set $\Omega = 1s^{-1}$, assuming a diffusion constant of $D = 0.01\mu m^2 s^{-1}$ and a distance of $l = 10\mu m$ between compartments for all substances. This estimate is based on the known diffusion constants.

In these equations, subscripts X, Y, and Z denote the concentrations of the specific species in the respective compartment. Hence, the complete system consists of 42 concentration functions of time as solution of a system of 42 ordinary differential equations. Note, that attachment states of the three compartments are additional parameters. Beginning with initial concentrations taken from literature (e.g. (Chen et al., 2004)), the equations are integrated with all attachment parameters in the state "unattached" (symbolized by UUU) until equilibrium is reached. Then, attachment parameter of compartment X is turned on (UUA), and the three activation reactions (6.1)-(6.3) in X are set to zero. After equilibrium is reached again, attachment in compartment Y is turned on (UAA) until equlibrium is reached. Finally, all three kinetochores are attached (AAA). These symbols are also used in Figures 6.2–6.4, where they designate the end of the simulation time of the respective phase.

For integration, those kinetic constants, which are documented in the literature, are used directly, whereas for all other constants physiologically reasonable values are substituted. This is done for many choices, and performance of the model is optimized according to an objective function measuring the concentration of APC:Cdc20, which should be 0 for the first three phases UUU, UUA, UAA, and should rise to a maximal value in phase AAA within a time scale of about 3 to 5 minutes. The optimization details can be found in (Ibrahim et al., 2008a). As a result, the values in Table 6.1 were found as optimal values for the kinetic parameters. They are also used in our perturbation model here.

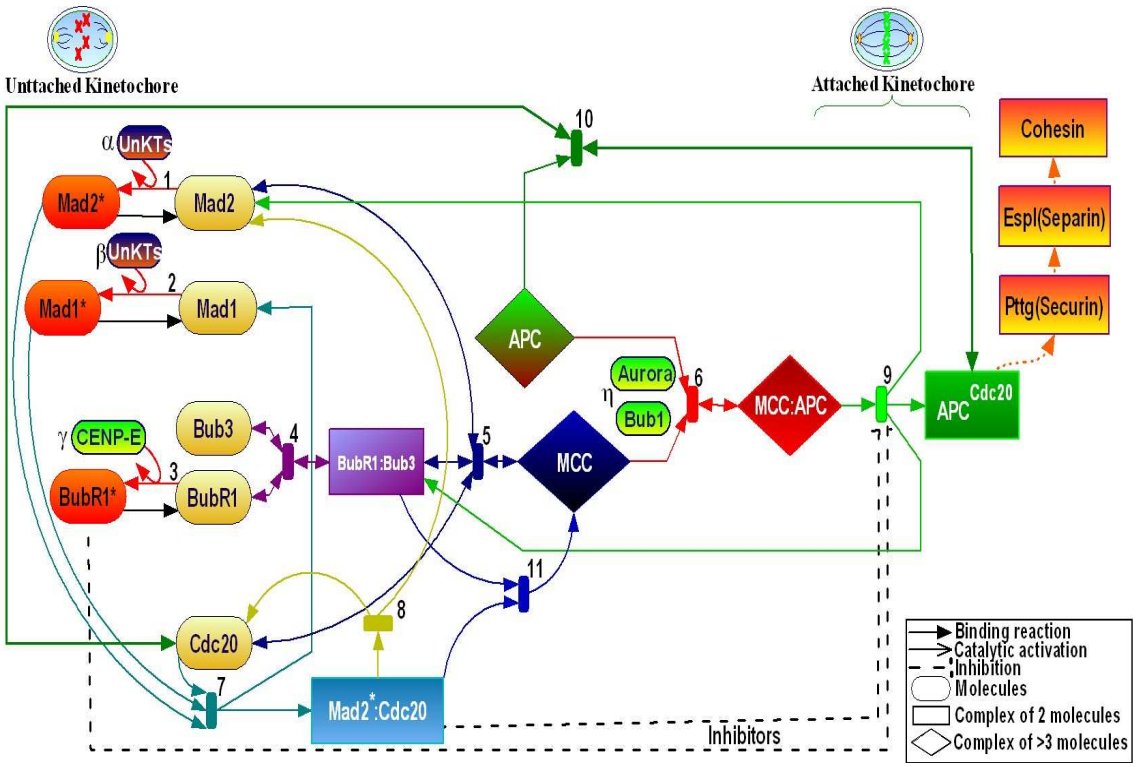

Figure 6.1: Reaction network for one compartment. The activation reactions with parameters α, β, and γ continue, as long as the kinetochore is unattached (left). When the respective kinetochore attaches, α, β, and γ are set to 0. A network of reactions leads to the formation of the MCC:APC complex (middle). These reactions continue as long as there is at least one unattached kinetochore. This is the consequence of the diffusion in the system, because the respective kinetochore does not any longer supply activated Mad1*, Mad2*, and BubR1*. When the last kinetochore attaches, the APC:Cdc20 complex begins to form and leads to a cascade of reactions cutting cohesin in the end and initiating anaphase (right).

Kinetic parameters

α	= 4.82	k_{-1}	= 0.00752	k_7	= 10.0		
β	= 9.92	k_{-2}	= 0.00100	k_8	= 0.00235		
γ	= 6.08	k_{-3}	= 9.83	k_9	= 0.00271	k_{-9}	= 10.0
k_4	= 0.412	k_{-4}	= 3.44	k_{10}	= 10.0		
k_5	= 0.00100	k_{-5}	= 0.00100	V	= 0.0197	k_{ic}	= 6.84
k_6	= 10.0	k_{-6}	= 0.00100	k_m	= 9.21	k_{is}	= 0.00100

Table 6.1: Kinetic parameters used for simulation: reaction rates for mass action and Michaelis-Menten kinetics.

As we do not have any special information about the origin of fluctuations in the cell cycle (Steuer, 2004; Battogtokh and Tyson, 2004), we assume random extrinsic fluctuations, mathematically described by white noise (Rao et al., 2002; Gillespie, 2002; Battogtokh and Tyson, 2004). For each species i in compartment j, the stochastic Langevin-type equation has the following form:

$$\frac{d[i]_j}{dt} = C(i)_j + W_i(t)\sqrt{2 \cdot N_i \cdot [i]_j}$$

where $C(i)_j$ is the original right-hand side of the deterministic equation and $W_i(t)$ is the (multiplicative) Gaussian white noise for species i with zero mean and unit variance

$$\langle W_i(t) \rangle = 0, \qquad \langle W_i(t) W_i(t') \rangle = \delta(t - t').$$

$N = N_i$ denotes the noise amplitude parameter, which, for simplicity, is the same for all species.

We computed the concentration functions for several values of N. Here, we show the results for $N = 10^{-8}$ (almost no noise) and $N = 10^{-5}$. We used $\Omega = 1$ as in the deterministic simulation, but in addition, to simulate the influence of diffusion on the system, we used $\Omega = 0.01$ and $\Omega = 0.005$.

The simulations were performed using standard numerical techniques for stochas-

tic differential equations (including the strong implicit 1.5 order Runge-Kutta method (Kloeden and Platen, 1999a), and the explicit Runge-Kutta method of order 1.5 (Kloeden and Platen, 1999a)). We implemented our code in (MATLAB , Matrix Labrotory).

6.4 Results

In Figure 6.2, the concentration curves for APC:Cdc20 and MCC:APC complexes are shown for a time period of about 12 minutes. The noise amplitude is $N = 10^{-8}$. In all simulations, steady state conditions (regarding noise, this means constant average of concentration) are reached within less than 3 minutes in all 3 phases (UUU, UUA, UAA) with at least one unattached kinetochore. For $\Omega = 1$ (top), there are no visible differences between the concentration curves for compartments X, Y, and Z (data not shown). Diffusion is obviously fast enough to level out the small differences induced by noise. In addition, after steady state is reached in phase UUU, the concentrations remain at that level during phases UUA and UAA. The graphs are almost identical to the concentration curves in the deterministic simulation without noise ((Lenser et al., 2007)). For $\Omega = 0.01$ (middle), first differences appear in phases UUA and UAA as compared to UUU: the equilibrium value is rising. Also in phase AAA, the onset of APC:Cdc20 increase and MCC:APC decrease is much faster. Also, concentration dynamics differences between compartments X, Y, and Z become visible (data not shown). For $\Omega = 0.005$ (bottom), these effects become even more pronounced.

In Figure 6.3, showing the same concentration functions in the same ordering of Ω, the noise level is much higher at $N = 10^{-5}$. Whereas for $\Omega = 1$ the overall shapes of the curves still resemble the curves for low noise level, there is a large overshoot of [MCC:APC] ($\Omega = 0.01$) in phase UUU, and, for $\Omega = 0.005$, [MCC:APC] decays very rapidly already in phase UAA. It is also questionable, whether the concentration reached is enough to prevent exit from metaphase to anaphase. These effects increase for even higher $N-$values and disrupt mitotic control. To give an impression of the different behaviour in the three compartments, we have

included Figure 6.4 which shows the respective dynamics in these compartments for $N = 10^{-5}$ and $\Omega = 0.005$.

6.5 Discussion and Conclusion

The proper segregation of sister chromatids at onset of anaphase is surveyed by the mitotic spindle assembly checkpoint. The concentration dynamics of the complexes APC:Cdc20 and MCC:APC determine exit from metaphase to anaphase. Our model, describing concentration dynamics by ordinary differential equations, is based on 14 proteins and complexes, which determine increase or decrease of the two key complexes near a kinetochore, dependent on its attachment status. To investigate the interaction of concentrations near different kinetochores, we have coupled three compartments by diffusion. As for many reaction constants only ranges, but no exact values, are known, we optimized a particular objective function based on the expected dynamics of APC:Cdc20 concentration in (Ibrahim et al., 2008a), where the details of this procedure can be found. The result was a set of concentration parameters and initial values, allowing the simulation of the deterministic model showing a correct behaviour of the spindle checkpoint and also reproducing over-expression and deletion effects (Ibrahim et al., 2008a). The model is based on mass action laws for all reactions except one (6.9), which is described by a mixed Michaelis-Menten kinetic. This may be an oversimplification, because non-linear effects may be involved. On the other hand, this argument applies to almost all reactions considered here. It is even questionable, how diffusion can be described correctly, as ongoing research shows that certain signalling molecules seem to travel along one dimensional fibres. So, the formulation of the reaction equations might be only a first step. However, for example the mixed Michaelis-Menten kinetic, we used here, has several parameters which were optimized and could in this way provide a description which is close to the actual reaction.

As in natural processes noise is a never neglectable ingredient, we have addressed here the question, whether noise has a destructive influence, or, as in Steuer (2004), is even essential for the correct function. We therefore take the same description

by differential concentration equations for the single compartments and also the same geometric arrangement of three compartments as in (Lenser et al., 2007). But here, the deterministic differential equations are enriched by a stochastical term adding white noise of different amplitudes.

We could show that the spindle checkpoint dynamics as described by our model is stable with respect to extrinsic white noise to a rather large extend. Only for a noise amplitude larger than $N = 10^{-4}$, the function of the checkpoint is disrupted. The influence of noise, on the other hand, is dependent on the diffusion coefficient. Whereas diffusion in the known physiological parameter ranges is fast enough to level out concentration differences in the distinct compartments, noise is able to build up considerably different dynamics near different kinetochores when the diffusion constant is decreased. This effect could become important when considering more chromosomes, which is necessary to simulate human checkpoint behaviour.

We did not find indications that noise is essential for the checkpoint function, in contrast to the effects of noise in the cell cycle as a whole, where noise seems to prevent dynamics from getting stuck in singular points (Steuer, 2004). Our results suggest that a fast diffusion, as in the physiologically relevant parameter ranges, helps to stabilize the system and to prevent noise to disrupt the checkpoint function. Along these lines it will be interesting to investigate the system using methods developed in (Levine and Hwa, 2007). They show, using a master equation approach, that in certain metabolic networks noise is not propagated, but has only local influence. These findings coincide with ours on a global level. On the other hand, we did not yet investigate the influence of a single perturbation on the system, e.g. by a concentration impulse response, as they suggest. But this will be a challenging task for us for the future.

In the model presented here, a linear arrangement of three compartments was used. This is only a first approximation to a more complex model for 46 chromosomes, arranged in a two dimensional mitotic equatorial plate, where each inner kinetochore has six neighbors – for mathematical symmetry. The outside kinetochores in this geometry have also connection to an outer region without any kinetochores, which is also connected to all kinetochores via the third dimension. Presently, we

are modeling this situation, which is much more involved. There are still debates about the exact ranges of diffusion coefficients, and also the dimensionality is in question. There are hints for one dimensional diffusion in certain cases, possibly enabled by diffusion along fibres. In further investigations, we will therefore use different diffusion constants for distinct reactants and also try to simulate different dimensionalities. A further goal is also the investigation of the influence of the geometry (e.g. in the mitotic equatorial plate) on the checkpoint dynamics using partial differential equations. Here, the localization of the reactions and reactants to the kinetochore, on the one hand side, or to the 'nucleosol', on the other hand side, may play an important role.

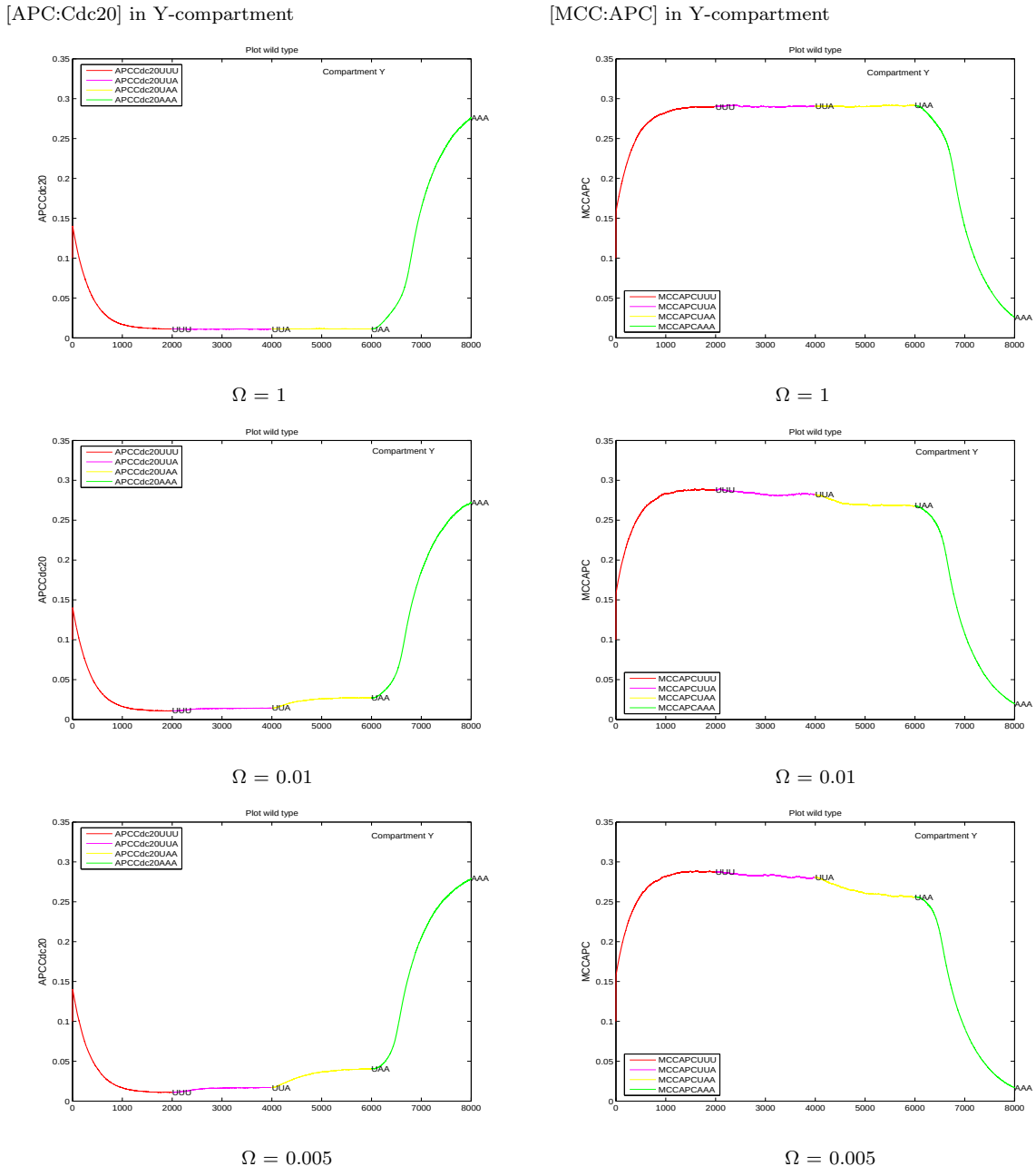

Figure 6.2: Concentration of APC:Cdc20 (left) and MCC:APC (right) as a function of time (8000 iterations corresponding to 12 min) in the middle compartment Y at noise amplitude $N = 10^{-8}$. The first part (orange, from time 0 to 'UUU') of the curves describes the phase with three kinetochores Unattached (UUU); the second part (red, 'UUU'-'UUA'), the phase with two kinetochores Unattached and one Attached (UUA); etc. (cf. insert). With decreasing diffusion coefficient Ω (cf. text), the concentration differences within the 3 phases UUU, UUA, UAA, increase more and more. Steady state is reached after at most 3 min. When all kinetochores are attached (green curve 'UAA'-'AAA', phase AAA), APC:Cdc20 rises immediately and MCC:APC decays.

[APC:Cdc20] in Y-compartment

[MCC:APC] in Y-compartment

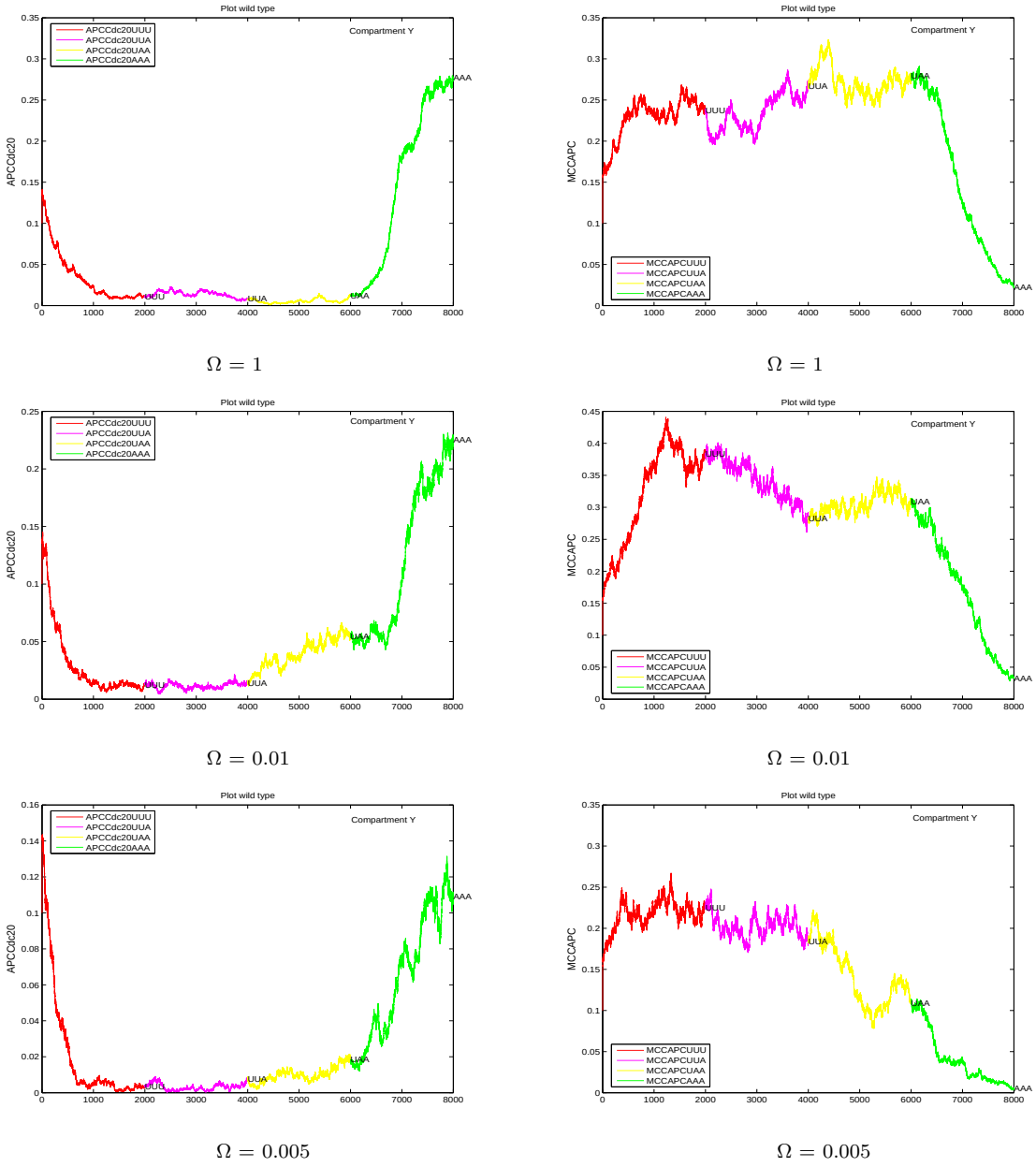

$\Omega = 1$ $\Omega = 1$

$\Omega = 0.01$ $\Omega = 0.01$

$\Omega = 0.005$ $\Omega = 0.005$

Figure 6.3: Concentration of APC:Cdc20 (left) and MCC:APC (right) as a function of time (8000 iterations corresponding to 12 min) in the middle compartment Y at noise amplitude $N = 10^{-5}$. With decreasing diffusion coefficient Ω, dynamics in the phases with one kinetochore unattached (UAA) become more and more distinct, and in some cases a steady state equilibrium is not reached any more within phase simulation time (3 min).

[APC:Cdc20] in compartments X,Y,Z

[MCC:APC] in compartments X,Y,Z

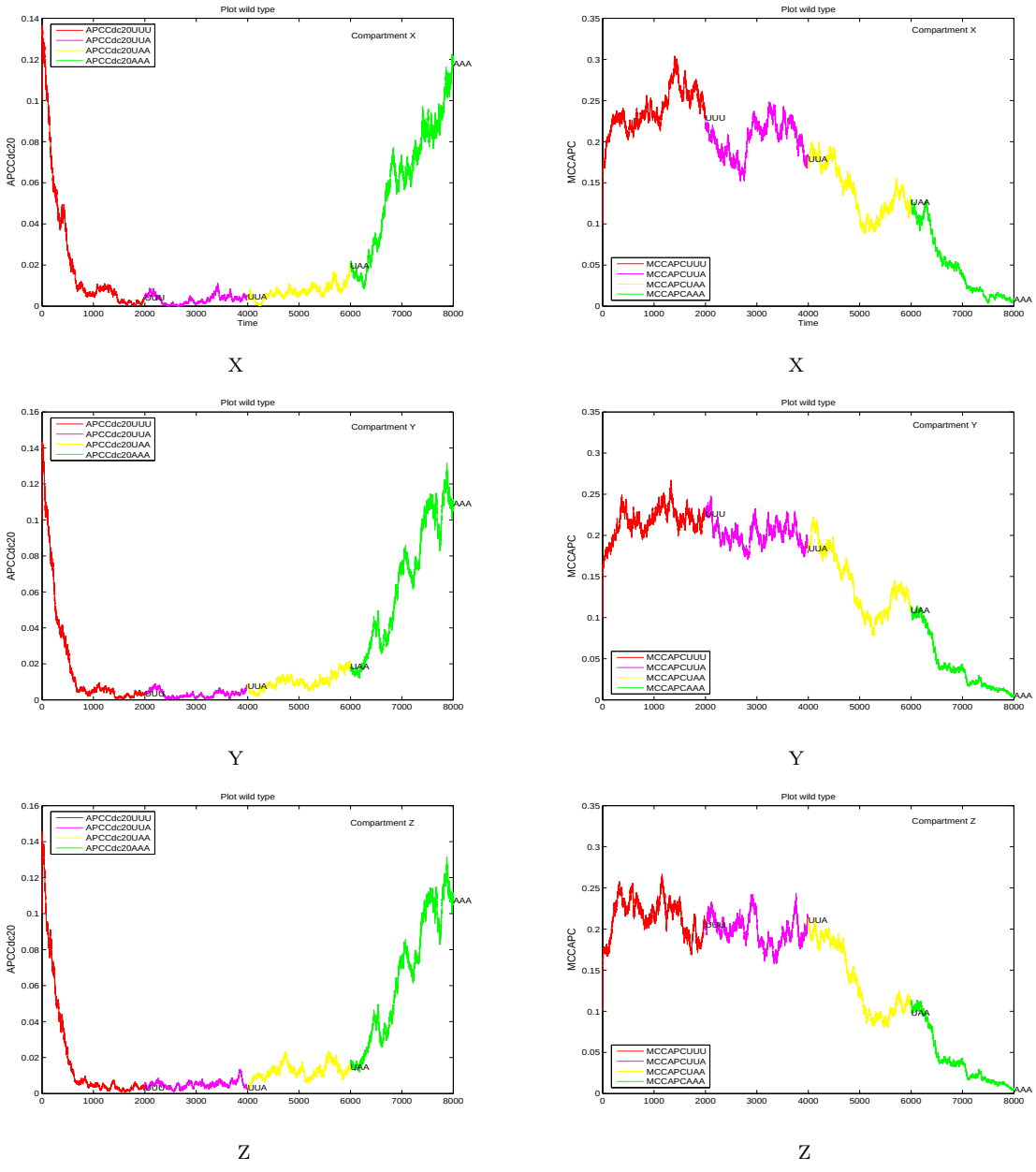

X

X

Y

Y

Z

Z

Figure 6.4: Concentration of APC:Cdc20 (left) and MCC:APC (right) in the three compartments X,Y,Z, at a noise amplitude of $N = 10^{-5}$ for diffusion coefficient $\Omega = 0.005$. For these parameters, strong differences in the [APC:Cdc20] and [MCC:APC] dynamics in the different compartments become visible.

Mitosis Consolidation

"Imagination is more important than knowledge...".

Albert Einstein (1879 - 1955)

"To create a good philosophy you should renounce metaphysics but be a good mathematician".

Bertrand Russell (1772 - 1970)

Chapter 7

Integrative Model of Mitosis Transition Control Mechanisms

Contents

7.1 Summary

Two forms of the Anaphase Promoting Complex (APC), bound to Cdc20 or Cdh1, regulate mitosis transition. During the metaphase-to-anaphase transition, APC:Cdc20 mediates the ubiquitination and degradation of Securin protein, leading to the activation of Separase, dissolution of the Cohesin complex, and chromatid separation. In addition, APC:Cdc20 mediates the first phase of Cyclin B proteolysis. During anaphase and transition to telophase, APC:Cdh1 is turned on and completely ubiquitinates Cyclin B, thus inactivating the CyclinB:Cdk1 mitotic kinase and triggering the exit from mitosis to cytokinesis.

Herein, we incorporated an adapted Exit From Mitosis (EFM) model that involves the activity of APC:Cdh1 and build an integrative model that also involves the activity of APC:Ccd20. Hence, we addressed simultaneously the functioning of both transition control mechanisms, ^{M}SAC and EFM (see Figure 7.1). This new model consists of 19 species and 15 reactions. It is validated by simulation of mutation experiments. The model is described by non-linear ordinary differential equations. The values of the kinetic parameters are derived from literature and the remaining values of parameters are obtained with parameter optimization. The parameter optimization will be performed with three optimization techniques, two evolutionary and one deterministic technique; namely Covariance Matrix Adaptation Evolutionary Strategy (CMA-ES), Differential Evolution (DE), and the Hooke-Jeeves (HJ) algorithm, respectively.

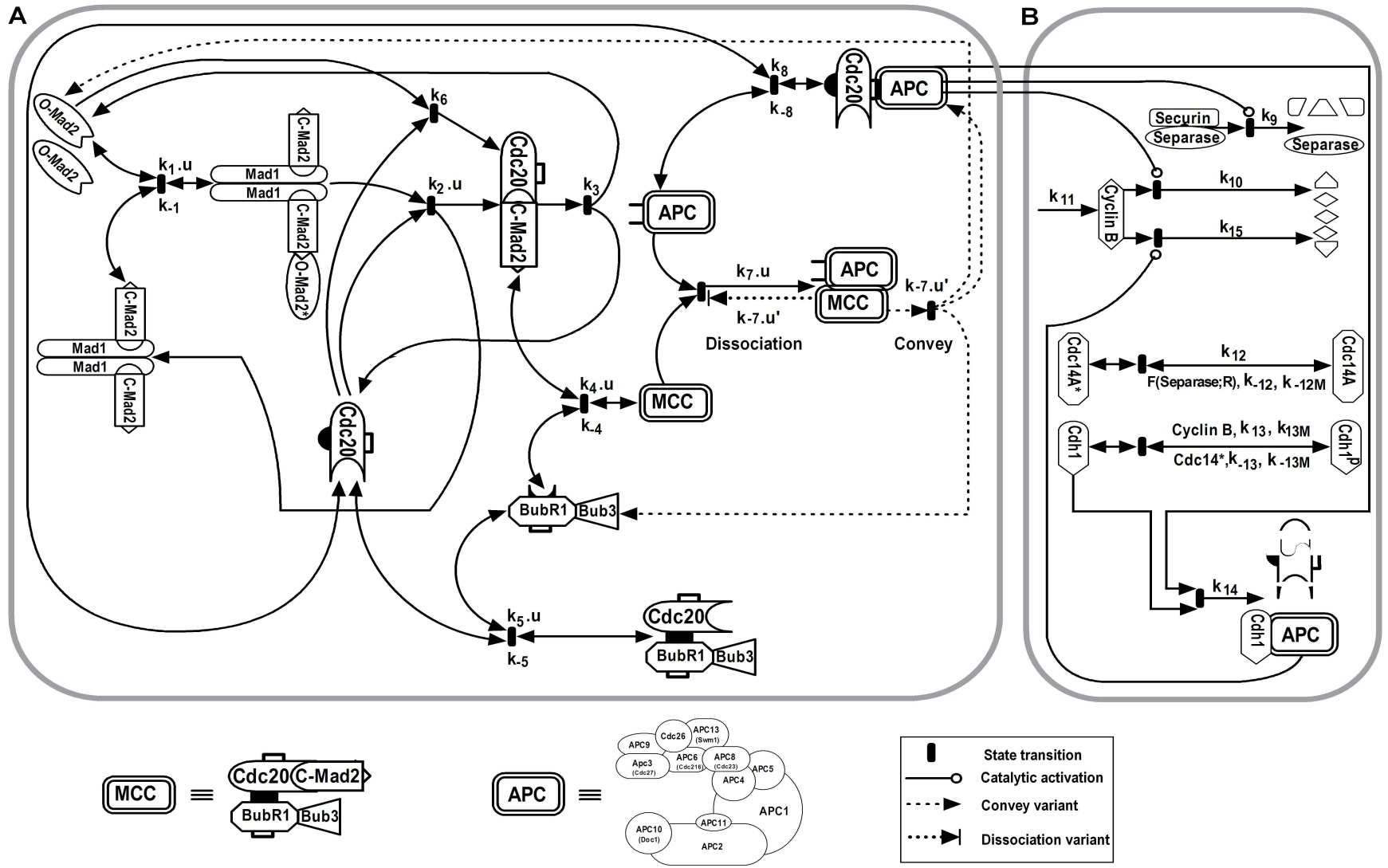

Figure 7.1: Schematic networks of an integrative model of mitosis transition control mechanisms. Module A represents the ^{M}SAC mechanism (Chapter 5), in which APC activation by Cdc20 is the output. Module B represents the EFM mechanism, in which APC functions by both Cdc20 and Cdh1 are analyzed (for details see text).

7.2 Biochemical Background of the Integrative Model

The integrative model includes two sub-models; ^{M}SAC and EFM model. ^{M}SAC model is described as mass-action kinetics (reaction Eqs.(7.1)-(7.8)) in two model variants (see Chapter 5), the "Dissociation"(Eq. (7.D)) and the "Convey"(Eq. (7.C)) model. The output signal of ^{M}SAC model (Anaphase initiation) is the activation of APC by its first mitotic co-activator Cdc20 in APC:Cdc20 complex form. The APC:Cdc20 complex has two main functions. One is to activate Separase by ubiquitylating of Securin (Eq.(7.9)). The other function is to proteolysis the first phase of Cyclin B (Eq.(7.10)) that occurs when cellular levels of the Cyclin B are high. Here Cyclin B activity refers to Cdk1:Cyclin B complex. However, APC:Cdc20 is unable to reduce Cyclin B activity to a level low enough to complete exit from mitosis (Yeong et al., 2000). These two reactions of APC functions are important to connect the ^{M}SAC model with the EFM model. Both reactions are based on empirical data (e.g, Morgan, 1999; King et al., 1996; Alexandru et al., 1999; Nasmyth et al., 2000; Uhlmann et al., 1999).

The EFM model is described by reaction Eqs.(7.11)-(7.15). Three of these reactions are taken from the model proposed by Toth et al. (2007) for budding yeast which is used as a basis for our Human EFM model. Reaction equation (7.11) describes the constant production of Cyclin B. Reaction equation (7.12) describes the regulation of a phosphatase, called Cdc14 (human homology hCdc14A, we will use Cdc14A for simplicity now on). The inactivation of Cdc14A is considered to be mass-action kinetics, while the activation as Michael-Menten kinetics. The activation of Cdc14 is better understood in Yeast, through two networks (Toth et al., 2007) called FEAR (Cdc Fourteen Early Anaphase Release) (Stegmeier et al., 2002; Sullivan and Uhlmann, 2003) and MEN (Mitotic Exit Network) (Jaspersen et al., 1998; Lee et al., 2001; Stegmeier and Amon, 2004). The FEAR network is assumed to be less essential than MEN because mutants in FEAR pathway show only a delay in activation of Cdc14 while mutants of MEN block at telophase (Stegmeier et al., 2002). In spite of this assumption, Separase plays an essential role in

Cdc14 activation which is also a component of FEAR pathway (Queralt et al., 2006; Sullivan and Uhlmann, 2003). Because of this function and the lack of knowledge for Human Cdc14A regulation, we propose a Michaelis-Menten kinetic function based on a rate limiting function of Separase as well as both parametric FEAR and MEN pathways (reaction Eq.(7.12)). Moreover, we think such a function can mathematically be consistent with the empirical data as we will see in the model validation section. Active Cdc14A (Cdc14A* nomenclature will be used from now on) dephosphorylates (and thereby activates) the second APC co-activator, Cdh1 (a human homology is hCdh1, Cdh1 will be used from now on) (Eq.(7.13)) (Bembenek and Yu, 2001b). We refer to phosphorylated Cdh1 by ($\mathrm{Cdh1^P}$). For both phosphorylation and the dephosphorylation Michaelis-Menten kinetics are used (Toth et al., 2007). The conversion between both APC's activators, Cdc20 and Cdh1 is an uncatalyzed reaction and therefore described with mass-action kinetics (Eq.(7.14)), this reaction models the exchange of Cdc20 by Cdh1 and Cdc20 degradation in single reaction. Subsequently, APC:Cdh1 promotes completion of Cyclin B destruction (Eq.7.15) (Prinz et al., 1998).

$$\text{Mad1:C-Mad2} + \text{O-Mad2} \underset{\mathrm{k_{-1}}}{\overset{\mathrm{k_1.u}}{\rightleftharpoons}} \text{Mad1:C-Mad2:O-Mad2}^* \tag{7.1}$$

$$\text{Mad1:C-Mad2:O-Mad2}^* + \text{Cdc20} \xrightarrow{\mathrm{k_2.u}} \text{Cdc20:C-Mad2} + \text{Mad1:C-Mad2} \tag{7.2}$$

$$\text{Cdc20:C-Mad2} \xrightarrow{\mathrm{k_3}} \text{O-Mad2} + \text{Cdc20} \tag{7.3}$$

$$\text{Cdc20:C-Mad2} + \text{Bub3:BubR1} \underset{\mathrm{k_{-4}}}{\overset{\mathrm{k_4.u}}{\rightleftharpoons}} \text{MCC} \tag{7.4}$$

$$\text{Cdc20} + \text{Bub3:BubR1} \underset{\mathrm{k_{-5}}}{\overset{\mathrm{k_5.u}}{\rightleftharpoons}} \text{Bub3:BubR1:Cdc20} \tag{7.5}$$

$$\text{Cdc20} + \text{O-Mad2} \xrightarrow{\mathrm{k_6}} \text{Cdc20:C-Mad2} \tag{7.6}$$

$$\text{MCC} + \text{APC} \xrightarrow{\mathrm{k_7.u}} \text{MCC:APC} \tag{7.7}$$

$$\text{MCC:APC} \xrightarrow{\mathrm{k_{-7}.u'}} \text{APC} + \text{MCC} \tag{7.D}$$

$$\text{MCC:APC} \xrightarrow{\mathrm{k_{-7}.u'}} \text{APC:Cdc20} + \text{O-Mad2} + \text{Bub3:BubR1} \tag{7.C}$$

$$\text{APC} + \text{Cdc20} \underset{\mathrm{k_{-8}}}{\overset{\mathrm{k_8}}{\rightleftharpoons}} \text{APC:Cdc20} \tag{7.8}$$

$$\text{Separse:Securin} \xrightarrow{\text{APC:Cdc20, } k_9} \text{Separase} + \text{waste} \tag{7.9}$$

$$\text{Cyclin B} \xrightarrow{\text{APC:Cdc20, } k_{10}} \text{waste} \tag{7.10}$$

$$\xrightarrow{k_{11}} \text{Cyclin B} \tag{7.11}$$

$$\text{Cdc14A} \underset{\text{f(Separase;R), } k_{-12}, k_{-12M}}{\overset{k_{12}}{\rightleftharpoons}} \text{Cdc14A}^* \tag{7.12}$$

$$\text{Cdh1}^{\text{P}} \underset{\text{Cyclin B, } k_{-13}, k_{-13M}}{\overset{\text{Cdc14A*, } k_{13}, k_{13M}}{\rightleftharpoons}} \text{Cdh1} \tag{7.13}$$

$$\text{APC:Cdc20} + \text{Cdh1} \xrightarrow{k_{14}} \text{APC:Cdh1} + \text{waste} \tag{7.14}$$

$$\text{Cyclin B} \xrightarrow{\text{APC:Cdh1, } k_{15}} \text{waste} \tag{7.15}$$

7.3 Simulation

By applying general principles of mass-action as well as Michaelis-Menten kinetics, we convert the reaction rules (Eqs.(7.1)-(7.15)) into sets of nonlinear Ordinary Differential Equations (ODEs) for the Dissociation variant (Appendix E , Eqs. (E.1)-(E.19)) and similarly for the Convey variant (Appendix E , Eqs. (E.20)-(E.38)). Starting from initial concentrations for all reactions taken from literature listed in Table 5.2, Cdh1^{P} is assumed to be equal to the initial concentration of Cdc20. In this manner there will be enough Cdh1 to convert all the APC:Cdc20 into APC:Cdh1.

The initial concentrations of Cdc14A and Separase:Securin are set equal to the initial Cyclin B concentration (200nM, Moore et al. (2003)).

The product of APC:Cdc20 subjected to high initial concentration of both APC and Cdc20 for the first few seconds should be avoided. During the first time steps APC may be activated and will cause undesirable model behavior. This is prevented by cutting the first step into two sub-steps. During the first 120 sec APC:Cdc20 reaction is slower 1000folds as for the relation to prophase. Afterwards $^{\text{M}}$SAC is

completely active and APC cannot be activated by Cdc20 anymore. The initial concentration for the succeeding steps will be equal to the final concentrations of the previous step. The ODEs are integrated until steady state is reached before attachment (using u = 1, time is about 25 mins: Prometaphase and Metaphase). After switching u to 0 (about 50 mins: Anaphase and Telophase), the equations are again integrated until steady state is reached. The minimum concentration of APC:Cdc20, APC:Chd1, Cyclin B, Cdc14A*, and Securin before attachment and the recovery after attachment are criteria for fitness function as explained in the following section.

7.3.1 Optimization

This objective function $f(P)$ compares the model behavior with current parameters to prescribed model behavior. It assigns a quality (i.e., a positive real number) to a given set of parameters P=(k_n, n=1,...,12). In our case, the parameters are the reaction constants. In order to fit the parameters with respect to the observed qualitative function of the ^{M}SAC and EFM control mechanisms, 5 model outputs will be used: APC:Cdc20, APC:Cdh1, Cyclin B, Cdc14A* and Securin. APC:Cdc20, APC:Cdh1 and Cdc14A* have switch-like behavior. APC:Cdc20 reaches its maximum concentration of 90 nM in the first simulation phase (t< 25 mins), and APC:Cdh1 (t>25 mins) reaches the same concentration in the second simulation phase. Cdc14A* can reach the maximum concentration (200 nM) only after 25 mins. Cyclin B and Securin have a similar behavior (Hagting et al., 2002), which is high in the fist simulation phase, and once APC:Cdc20 appears they will degrade. We used a general form of the following fitness function:

$$f(P) = \sum_{j=1}^{5} \{W_0([x_j]_0 - A_{0,j})^2 + \sum_{i=1}^{6} W_i([x_j]_i - A_{i,j})^2\} \tag{7.16}$$

$j \in$ { APC:Cdc20, APC:Cdh1, Cyclin B, Cdc14A*, Securin}

i has seven time points. $i = 0$ refers to the steady state of the simulation where kinetochore is unattached (u= 1). $i = 1, ..., 6$ are six different time points after

attachment (silence ^{M}SAC and EFM).

More specifically, the comparisons of the measurement occur at 25%, 50%, 60%, 70%, 80% and 100% of the simulated time after attachment. $A_{i,j}$ is a matrix in which each row is related to time point i, each column is related to species element j (Table 7.1). Each element of the matrix $A_{i,j}$ is fixed number between 0 and related species maximum. W is the weight constants vector: $W = [100, 200, 250, 350, 300, 150]$, which focuses on some term more and by which gives the best result.

Fitness function constant values

i	Time	$A_{i,[\text{APC:Cdc20}]}$	$A_{i,[\text{APC:Cdh1}]}$	$A_{i,[\text{Cyclin B}]}$	$A_{i,[\text{Cdc14A*}]}$	$A_{i,[\text{securin:Separase}]}$
0	100%F	0	0	$1.0[\ ]_{IC}$	0	$1.0[\ ]_{IC}$
1	25%S	$0.9[\ ]_{IC}$	$0.1[\ ]_{IC}$	$0.75[\ ]_{IC}$	$0.3[\ ]_{IC}$	$0.75[\ ]_{IC}$
2	50%S	$0.8[\ ]_{IC}$	$0.2[\ ]_{IC}$	$0.5[\ ]_{IC}$	$0.4[\ ]_{IC}$	$0.5[\ ]_{IC}$
3	60%S	$0.5[\ ]_{IC}$	$0.5[\ ]_{IC}$	$0.35[\ ]_{IC}$	$0.5[\ ]_{IC}$	$0.35[\ ]_{IC}$
4	70%S	$0.3[\ ]_{IC}$	$0.7[\ ]_{IC}$	$0.15[\ ]_{IC}$	$0.6[\ ]_{IC}$	$0.15[\ ]_{IC}$
5	80%S	$0.1[\ ]_{IC}$	$0.9[\ ]_{IC}$	$0.05[\ ]_{IC}$	$0.75[\ ]_{IC}$	$0.05[\ ]_{IC}$
6	100%S	0	$1.0[\ ]_{IC}$	0	$1.0[\ ]_{IC}$	0

Table 7.1: Fitness function constant values, F refers to the first phase and S refers to the second simulation phase. $[\ ]_{IC}$ represents the initial concentration for a related species j. $A_{i,j}$ refers to the comparisons of the measurements.

.

Parameter optimization was performed for the Dissociation variant of the integrative model using three optimization techniques: CMA-ES (Hansen and Kern, 2004), DE (Storn and Price, 1997) and HJ (Hooke and Jeeves, 1961). All optimization techniques were used with the same objective function. Because of the wide parameters range (e.g. 10^{-12} and 10^{12}), we used an exponential scaling, by which parameter estimation can be efficiently and more accurately performed (Rohn et al., 2008). The optimization algorithms in the unscaled case allow parameters P (vector) in the range between 10^{-n} and 10^{n}, where n is any real number, the scaled case considers parameters P between 0 and 1. The changed parameters $\bar{P}$

were inserted and evaluated. The relationship between P and $\bar{P}$ is

$$\bar{P} = a \cdot 10^{b+c \cdot P} \tag{7.17}$$

where e.g., $a = 1$, $b = -12$ and $c = 24$ resulting in $10^{-12} \leq \bar{P} \leq 10^{12}$. As a result of this scaling, search steps are larger for high parameter values and smaller for low values, independently of the optimization procedure. This allows a optimization procedure to investigate small parameter values with high resolution and large parameter values with low resolution without having to internally adapt the search step-size.

We ran the three optimization techniques 90 times in total and picked the best fitness and model behavior. Parameter optimization with CMA-ES as well as HJ were much faster than optimization with DE. Optimization showed that good parameter sets could be found within the parameter ranges (Table 7.2), in which HJ was a bit better than CMA-ES as well as DE. These local minima varied slightly. All parameters value lie within realistic range (see for example, Chapter 5).

Integrative model parameters

Parameters	Comments and References
$k_1 = 2 * 10^5$ $M^{-1}s^{-1}$	Chapter 5
$k_{-1} = 2 * 10^{-1}$ s^{-1}	Chapter 5
$k_2 = 10^8 M^{-1}s^{-1}$	Chapter 5
$k_3 = 1 * 10^{-2}s^{-1}$	Chapter 5
$k_4 = 10^7$ $M^{-1}s^{-1}$	Chapter 5
$k_{-4} = 2 * 10^{-2}$ s^{-1}	Chapter 5
$k_5 = 10^4$ $M^{-1}s^{-1}$	Chapter 5
$k_{-5} = 2 * 10^{-1}$ s^{-1}	Chapter 5
$k_6 = 10^3$ $M^{-1}s^{-1}$	Chapter 5
$k_7 = 10^8$ $M^{-1}s^{-1}$	Chapter 5
$k_{-7} = 8 * 10^{-2}$ s^{-1}	Chapter 5
$k_8 = 5 * 10^6$ $M^{-1}s^{-1}$	Chapter 5
$k_{-8} = 8 * 10^{-2}$ s^{-1}	Chapter 5
$\mathbf{k_9} = 1.55{*}10^4$ $M^{-1}s^{-1}$	**This study**
$\mathbf{k_{10}} = 1.6{*}10^4$ $M^{-1}s^{-1}$	**This study**
$\mathbf{k_{11}} = 1.16{*}10^{-12}$ Ms^{-1}	**This study**
$\mathbf{k_{12}} = 1.53{*}10^3$ s^{-1}	**This study**
$\mathbf{k_{13}} = 4{*}10^4$ s^{-1}	**This study**
$k_{14} = 1.47{*}10^9$ $M^{-1}s^{-1}$	**This study**
$\mathbf{k_{15}} = 1.4{*}10^5$ $M^{-1}s^{-1}$	**This study**
$\mathbf{k_{-12}} = 5.4{*}10^3$ s^{-1}	**This study**
$\mathbf{k_{-13}} = 2.78{*}10^9$ s^{-1}	**This study**
$\mathbf{k_{13M}} = 3.3{*}10^{-8}$ M	**This study**
$\mathbf{k_{-12M}} = 4.56{*}10^{-7}$ M	**This study**
$\mathbf{k_{-13M}} = 10^4$ M	**This study**

Table 7.2: Model parameters: rate constants of mass-action and Michaelis-Menten kinetics. Last 12 parameters in bold line ($\mathbf{k_9}$-to-$\mathbf{k_{-13M}}$) are the result from optimization techniques.

7.3.2 Model Behavior

We analyzed the dynamics of the integrative model of ^{M}SAC and EFM mechanisms.

Figure 7.2 displays concentrations of the key players over time. For the Dissociation variant, we have selected the time range such that each concentration can reach steady state. For all species dynamic of both Dissociation as well as Convey variant see Figure 7.3. For all integrations, the concentrations and rates of Table 7.2 were chosen including those 12 parameters that were optimized. Before attachment (25 mins), four of these key players (APC:Cdc20, APC:Cdh1; Cdh1, Cdc14A*) are very low, while only, Cyclin B, Securin, and Cdc14A have high concentration. Once attachment takes place, things are changed (after 25 mins). In general, Cdc14A*, Separase, become high gradually over time. Cyclin B and Securin are degrading gradually once ^{M}SAC deactivates. APC:Cdc20 activates fast, degradates Securin and the first phase of Cyclin B to be ended with very low concentration at 30mins of its activation. Meanwhile, once Cdh1 is available, APC:Cdh1 will be formed and increase fast. APC:Cdh1 make full degradation of Cyclin B as well as Cdc20.

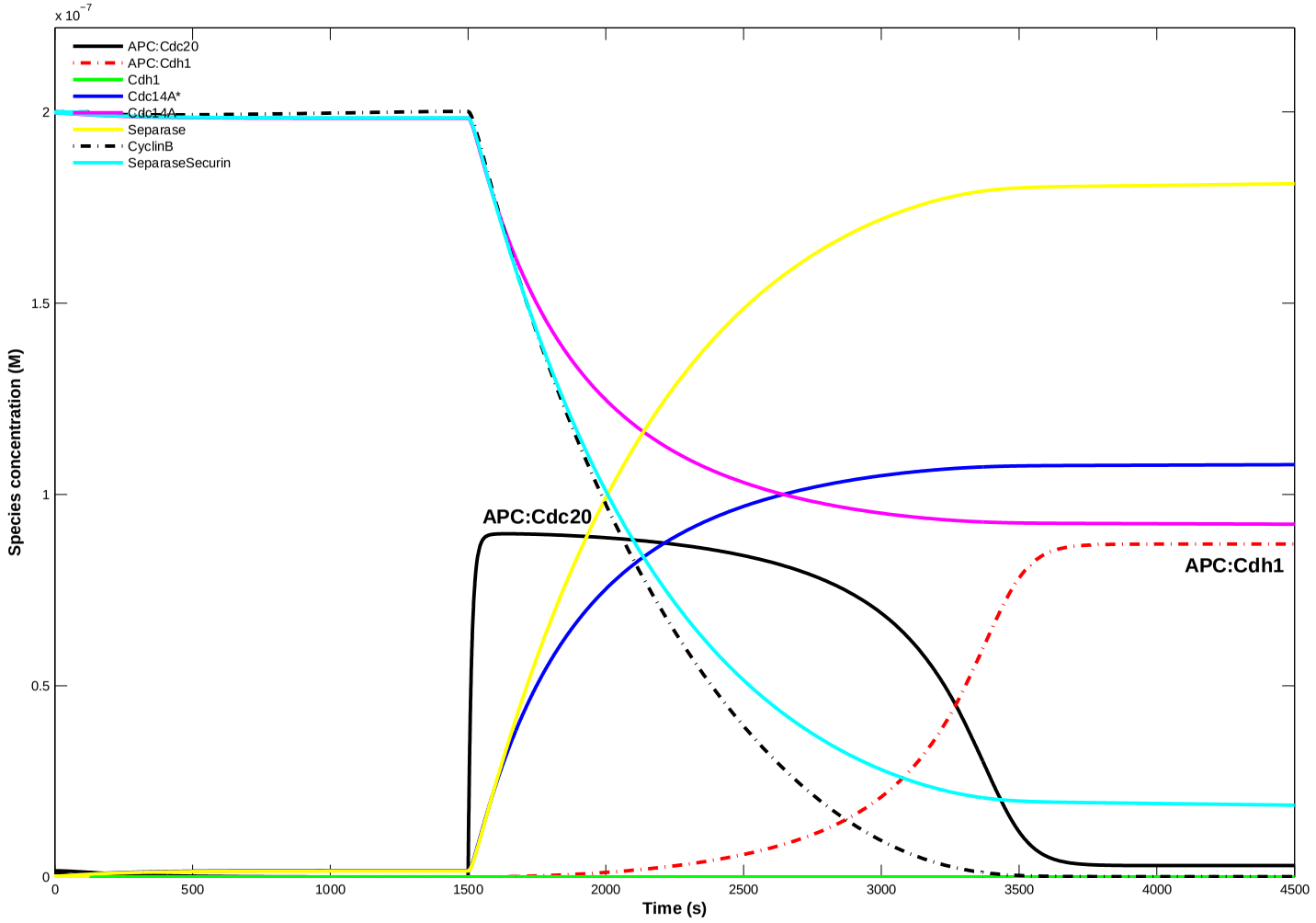

Figure 7.2: Key species concentration over time for the Dissociation. Spindle attachment occurs at t = 1500 sec (switching parameter u from 1 to 0 and u′ from 0 to 1). Parameters are setting according to Table 7.2.

7.4 Model Validation

The optimized parameter set and initial concentration results in the expected model behavior. Yet, when an initial concentration or a kinetic parameter value is changed the model behavior might change as well accordingly. In order to validate our model, we tested different mutations (deletion and over-expression) of the proteins and complexes involved, measured in different organisms. Model validation will be performed for a number of species elements. That are either part of the ^{M}SAC or the EFM mechanisms. Numerous empirical data have been reported for mutation experiments (see Chapter 5.3.2). Our integrative model is able to explain different mutation phenotypes. We will discuss, some mutations of essential proteins in details, namely the APC's activators, Cdc20 and Cdh1. We also discuss the effect of FEAR and MEN parameter.

Cdc20 deletion might cause checkpoint failure (e.g. reduce the binding of C-Mad2 to Cdc20, cells leave mitosis and oral cancer, see for example, Hwang et al., 1998; Mondal et al., 2007b). In different organisms Cdh1 deletion can cause delay of Cyclin B degradation as well as EFM delay but does not block mitosis (Sudo et al., 2001; Sigrist and Lehner, 1997; Kitamura et al., 1998; Yamaguchi et al., 1997; Schwab et al., 1997). With respect to over-expression, Cdc20 over-expression cause failure in ^{M}SAC function and arrests in metaphase (Zhang and Lees, 2001b; Shirayama et al., 1999). Cdh1 over-expression data is not available yet.

For Cdc20 deletion in our model, the concentrations of the model components are rather stable, that is, they are almost not affected by microtubule attachment. However, in the case of Cdh1 (inactive form) deletion (100folds), the APC:Cdc20 concentration stays high and no APC:Cdh1 is presented (Figure 7.5 B) which means Cyclin B inhibition failure, while for Cdc20 deletion (100folds) these concentrations are approximately zero (Figure 7.5 A). In the case of Cdh1 or Cdc20 over-expression, many component concentrations were affected. In particular, for Cdh1 over-expression (100folds) the APC:Cdc20 concentration remains low before attachment and switches to high after attachment rather short time, which affect Securin degradation (Figure 7.6 B). For Cdc20 over-expression (10000folds, less

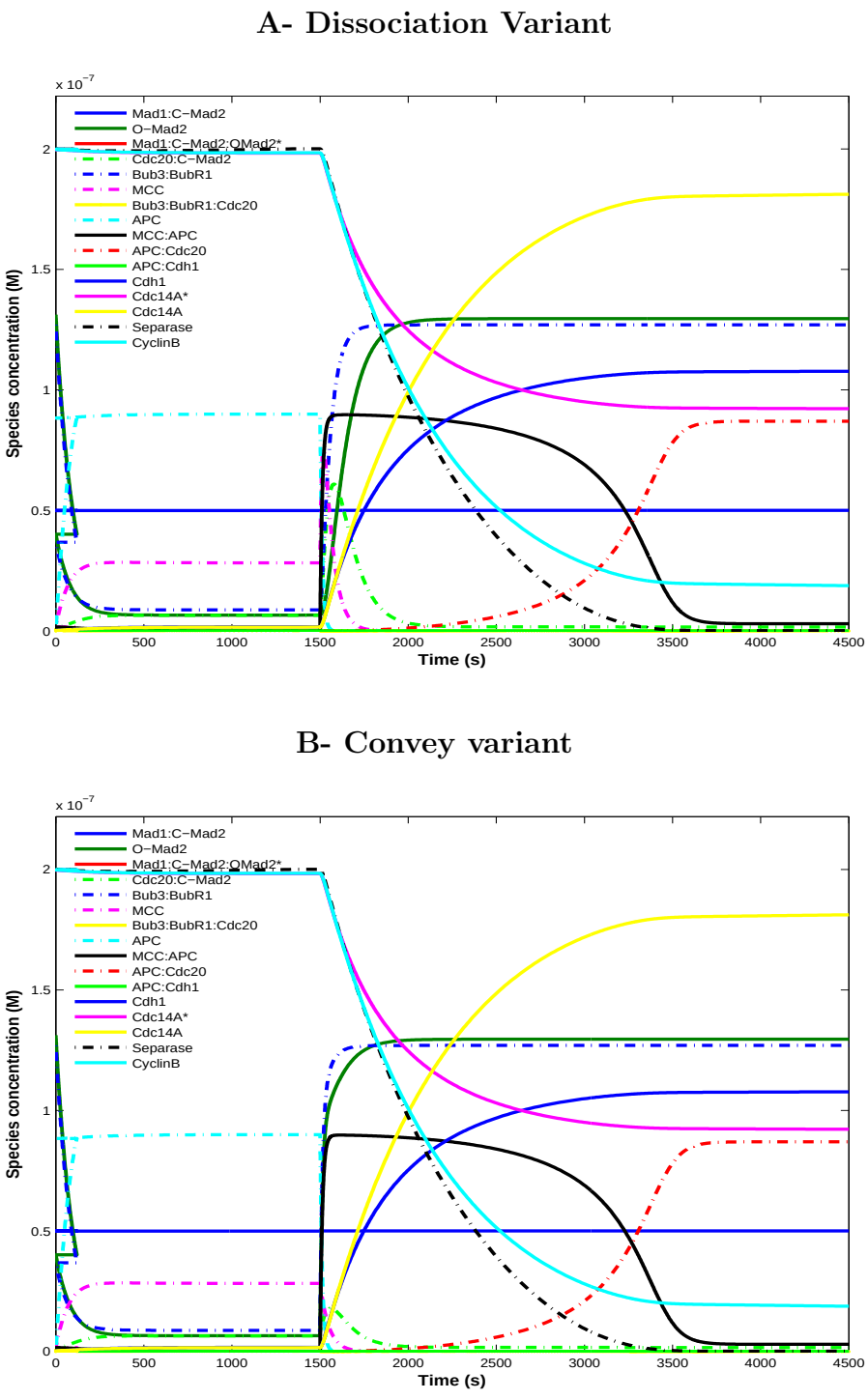

Figure 7.3: Species concentration over time for the both Dissociation and Convey variant (wild type). Spindle attachment occurs at t = 1500s, then ^{M}SAC becomes silent and EFM triggers. Parameters are setting according to Table 7.2. Both variants are equally suitable, by which the Convey variant is slightly faster).

has no qualitative effect), the APC:Cdc20 concentration is relatively high before attachment (Figure 7.6 A) resulting in checkpoint failure.

Mutants in FEAR pathway show only delay in activation of Cdc14 while mutants in MEN block at telophase (Stegmeier et al., 2002). The FEAR pathway is still essential (Queralt et al., 2006; Sullivan and Uhlmann, 2003), but maybe its full mechanism is not yet known. In human, most FEAR as well as MEN candidates are not yet identified. Therefore, we discuss the effect of both FEAR and MEN pathways qualitatively as a function of separase with an additional parameter R (see reaction Eq.(7.12)), which is defined mathematically as follows:

$$f(\text{Separase;R}) = [\text{Separase}] * \text{R} \tag{7.18}$$

where R defined as:

$$\text{R} = \text{MEN} * (\frac{1 + \text{FEAR}}{2 + \text{FEAR}}). \tag{7.19}$$

Note that R is set to be the Michaelis-Menten constant k_{-12} (see Table 7.2). The dependence of R on the FEAR pathway can be seen in Figure 7.4.

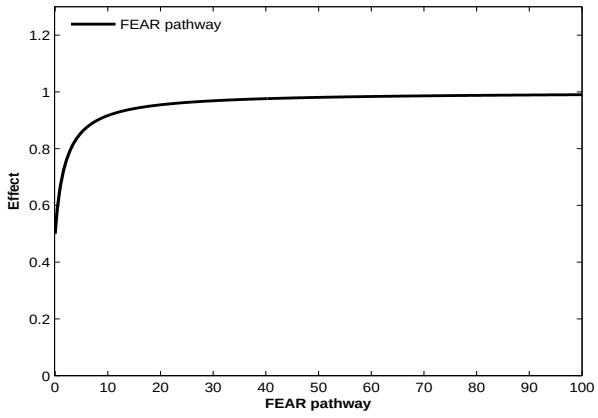

Figure 7.4: FEAR pathway effect on the parameter R. FEAR effect is between 0 and 1 which has only very limited impact on R. In contrast MEN effect is linear as defined in Eq.7.19.

When we reduce the parameter R by inhibiting FEAR pathway, we found very similar behavior to the wild type (see Figure 7.7 B), while when inhibiting the effect of MEN (only reduced 10 order of magnitude), we got mitosis block (see Figure 7.7 B). For quantitative effect of FEAR and MEN, more experimental data is required. These can be easily integrated into our model.

7.5 Concluding Remarks

We have consolidated and validated an *in silico* dynamical model based on a biomolecular reaction network (Figure 7.1). The model consists of 19 species, 15 reactions and 27 parameters. Twelve parameters are unknown and have been fitted using two evolutionary and one deterministic optimization techniques; namely CMA-ES, DE, and HJ algorithm, respectively. Despite the model complexity, the network still does not contain all the biochemical interactions (e.g. FEAR and MEN details). The reason is that most of these reactions are not yet identified in Human. However, it can be easily integrated into our model.

The most important features are to show the interaction and dynamics of each species over time (Figure 7.3). In particular, to capture APC functions which were not computed in Chapter 5. APC:Cdc20 function is the activation of Separase and dissolution of the Cohesin complex, and chromatid separation. Another function is to degrade the first phase of mitotic Cyclin (Cyclin B:Cdk1). APC:Cdh1 function is to fully degrade the mitotic cyclin. Our integrative model of mitosis transition control mechanisms reproduces in detail the behavior of wild-type and mutant.

A- Cdc20 deletion

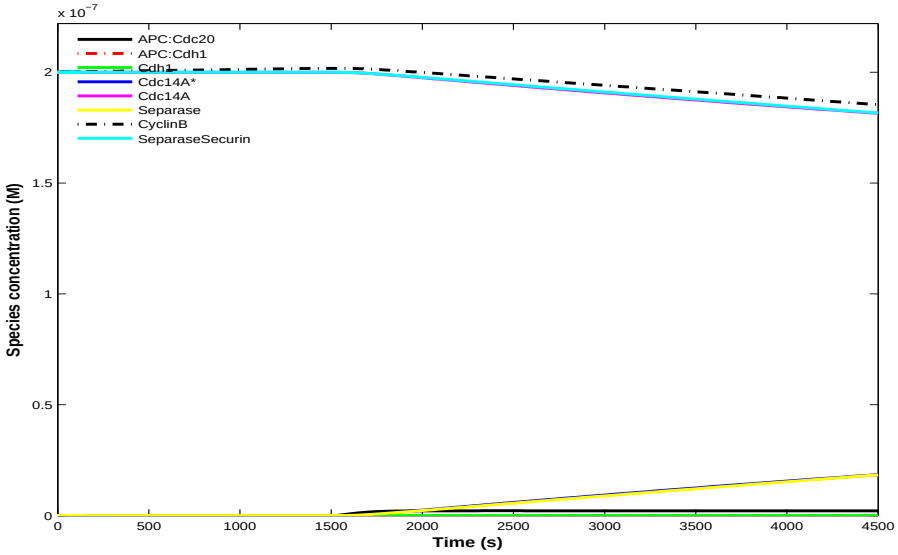

B- Cdh1 deletion

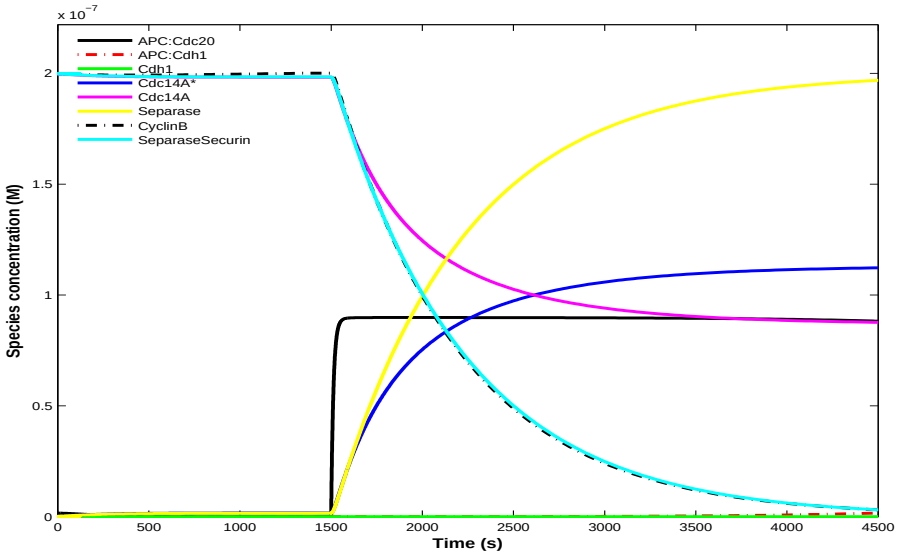

Figure 7.5: Simulation of Cdc20 and Cdh1 mutations. For deletion we set the respective initial concentration 100 times lower.

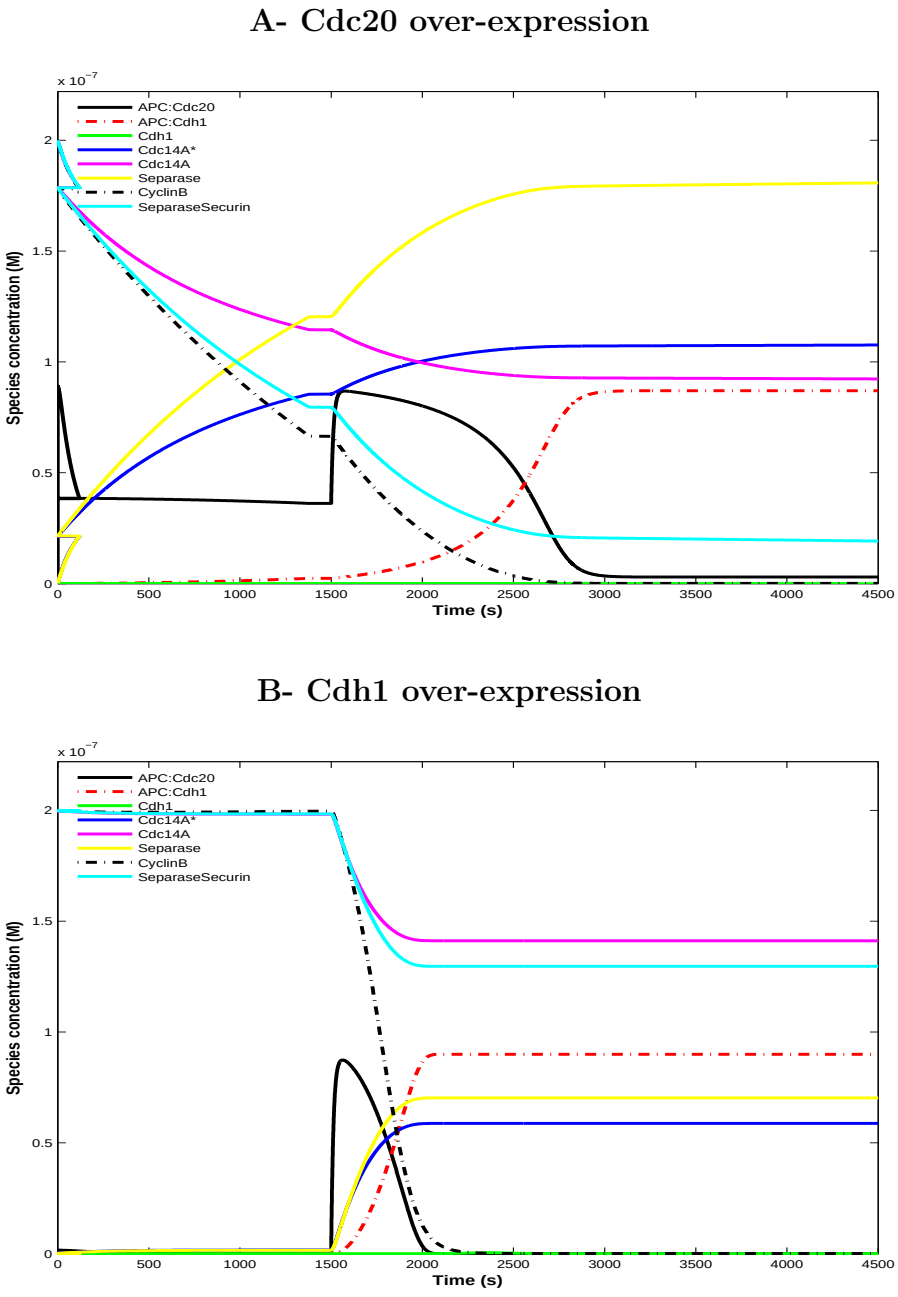

Figure 7.6: Simulation of Cdc20 and Cdh1 mutations. For for over-expression 10000 times higher of Cdc20 while only 100 times higher Cdh1.

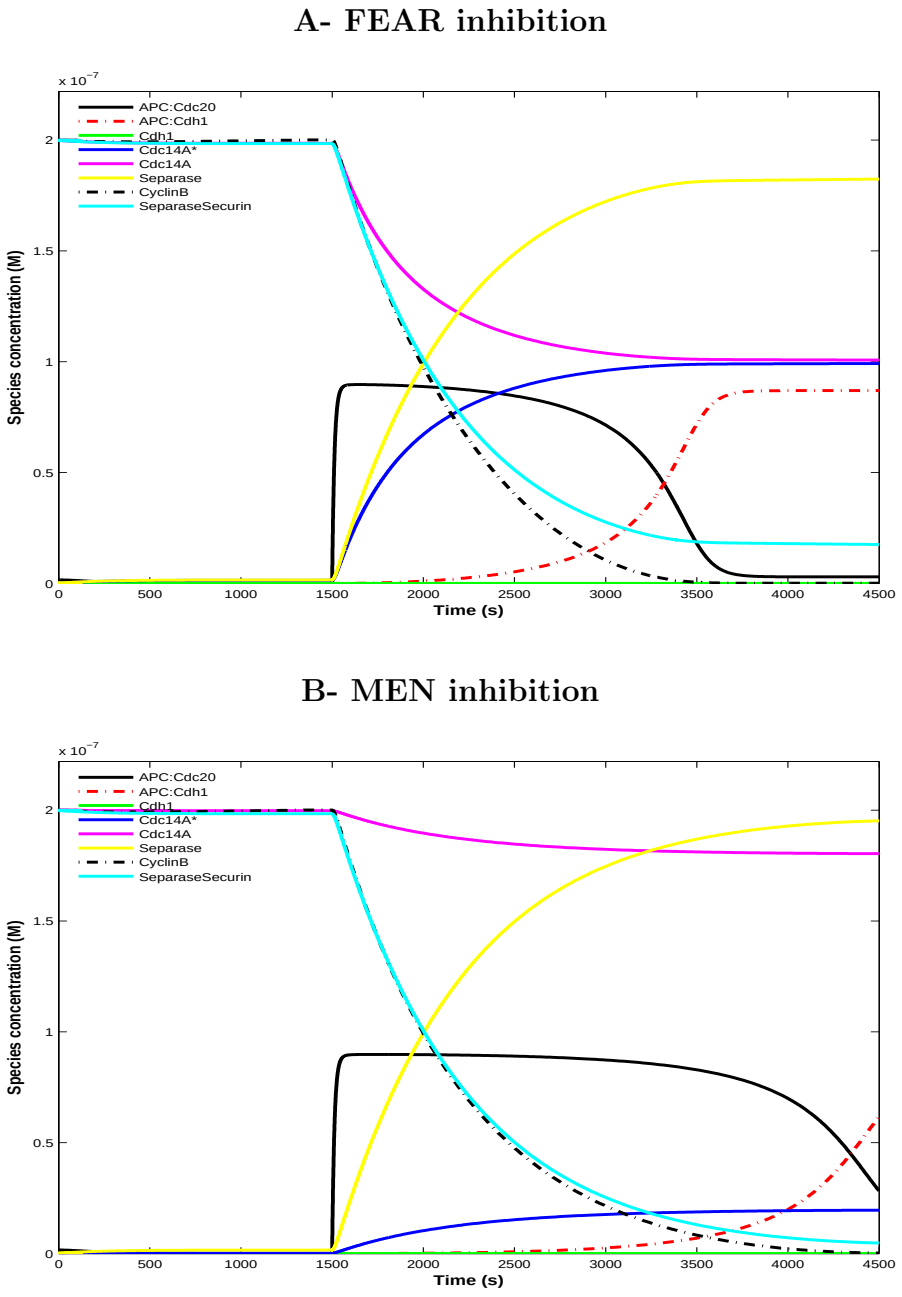

Figure 7.7: Simulation of FEAR or MEN pathway inhibition. Parameter R is reduces 10 order of magnitude for MEN inhibition and 0.1 for FEAR according to Section 7.4

7. INTEGRATIVE MODEL OF MITOSIS TRANSITION CONTROL MECHANISMS

"Every object that biology studies is a system of systems."

Francois Jacob (1974)

"How everything is connected to everything else and what it means for science, business and everyday life".

Albert-László Barabási (2002)

Chapter 8

Conclusion

Mitosis progression is a tightly regulated process. Eukaryotic cells, indeed, have evolved surveillance transition control mechanisms regulating the transition from any given stage of cell division to the next one. The so called '**M**itotic-**S**pindle-**A**ssembly-**C**heckpoint (^{M}SAC)' and '**E**xit-**F**rom-**M**itosis (EFM)' are examples of such mechanisms. ^{M}SAC prevents a dividing cell's progression into anaphase until all chromosomes are properly attached to the mitotic spindle, whereas EFM guarantees that each of the two daughter nuclei receives a single copy of each chromosome. In principle, ^{M}SAC controls the activity of a complex of proteins called "Anaphase Promoting Complex", or APC, during the transition from metaphase to anaphase, when chromosomes are not yet attached. APC becomes inactive after all chromosomes are attached. APC interacts with its co-activator, a protein called "Cell Division Cycle", or Cdc20. The function of the ensuing complex 'APC:Cdc20' is twofold. First, it activates a protein called 'Separase', involved in breaking-up the so called 'Cohesion ring'; this leads to the separation of the sister chromatids. Second, APC:Cdc20 is involved in the partial degradation of 'Cyclin B', a mitotic cyclin. Mitosis then progresses and becomes the subject of the second transition control mechanism, EFM. Generally speaking, EFM guarantees a full degradation of Cyclin B via the activity of a complex called 'APC:Cdh1', formed by APC and its second co-activator, a protein called Cdh1. After the full degradation of Cyclin B, the process of cell division

progresses into cytokinesis. Both ᴹSAC and EFM have complex dynamics and involve numerous interacting elements. This is probably the reason why their functional and topological structures remain still poorly understood. At present, for example, no model provides a satisfactory account of how ᴹSAC actually works. In contrast, there are several models -all them based on data from yeast- describing how EFM works. Still, these two mechanisms have not yet been incorporated into a single model. We aimed to contribute towards an integrative model addressing both ᴹSAC and EFM in human cells.

To this end, we built-up a series of dynamic models based on empirical data, and tested their ensuing predictions on the functioning of both ᴹSAC and EFM. Our *in-silico* approach suggests that cells are unable to completely sequester 'Cdc20', thereby preventing the formation of the complex 'APC:Cdc20'. It also suggests that it is an interaction between APC and another regulatory element of mitosis, MCC, that explains APC's lack of activity of during metaphase, necessary for the progression of the ongoing process (see Chapters 5 and 4). Moreover, previous modeling approaches to ᴹSAC , captured by the so called "Template" and "Exchange" models, had led to somehow contradictory views on its underlying regulation. Intriguingly, our simulations gave partial support to only one of such models (see Chapter 3). Finally, we simultaneously addressed the functioning of both transition control mechanisms, ᴹSAC and EFM, by incorporating an adapted EFM model involving the activity of 'APC:Cdh1' into an integrative model that also involves the activity of 'APC:Ccd20' (see Chapter 7). Our results also stress important, additional questions. Answering these questions, however, demands understanding how the mechanisms controlling mitosis work in three dimensions. This requires, in turn, developing specific and suitable tools. We currently develop a software tool called "Mitosis Arena", in order to test network models of mitosis embedded in a three-dimensional (3-D) framework. "Mitosis Arena" will be available to the scientific community so that alternative models could easily be studied within a dynamical 3-D environment. It has been designed in accordance with standard languages, and would eventually be combined with other Systems Biology software tools.

Molecular biology has progressed extraordinarily by rapidly producing huge amounts of empirical data. Yet, what is frequently missing in molecular approaches to biology is a robust account of the structure and dynamics of the -typically complex- networks serving the various cellular functions being studied. The emergent interdisciplinary field of "Systems Biology" studies cells as networks of interacting molecules using an integrative approach to theory. It deals with modeling and simulation, and involves concepts from mathematics, computer science, physics, biochemistry, and engineering. Typically, in such studies models are used to highlight principles, design experiments, or to act in a predictive mode to specifically modify cellular behavior. Mitosis is an exceedingly complex process, and molecular biologists typically characterize the activity, aggregation and interactions of tens of cellular elements involved in mitosis, although the relation between such interacting elements and their respective environment remains still elusive. Predictions, therefore, are not straightforward. There is a need for a system-level understating of the regulatory mechanisms involved in mitosis. This might be of major relevance for medical research, and for a better understating of other cellular processes, as well. We refer to the present work as to a "Systems Biology of Mitosis", with emphasis on human cells, simply because we benefited from modeling and simulation approaches embedded in a cross-disciplinary framework, in order to contribute to a deeper understanding of mitotic regulatory mechanisms. Eventually, our "Dissociation" and "Convey" model variants would prove fruitful in designing further laboratory experiments.

"Every new body of discovery is mathematical in form because there is no other guidance we can have".

Charles Darwin (1809-1882)

"No great discovery was ever made without a bold guess".

Isaac Newton (1642-1727)

Appendix A

Modeling and Simulation for Systems Biology

A.1 Prologue

"Today we increasingly recognize that nothing happens in isolation. Most events and phenomena are connected, caused by, and interacting with a huge number of other pieces of a complex universal puzzle. We have come to see that we live in a small world, where everything is linked to everything else. We are witnessing a revolution in the making as scientists from all different disciplines discover that complexity has a strict architecture. We have come to grasp the importance of networks" (Barabási, 2002).

Biological regulatory mechanisms, including mitosis, are inherently complex and highly cross linked (as seen in Chapter 2). They cannot be understood from reflections on the individual components (proteins, complexes etc) alone, but should be understood through considerations involving all components at the same time. Thus, mathematical network models formalism is used. It is a fundamental and quantitative way to understand and analyze complex systems and phenomena, complement to theory and experiments, and often integrate them,

Models Classifications	
Quantitative	Qualitative
Deterministic	Stochastic (Probabilistic)
Geometrical	Physical
Static	Dynamic
Descriptive	Normative
Linear	Non-Linear
low dimension	space
⋮	⋮

Table A.1: Several model classifications in science and engineering

synthesize control, verify hypotheses, improve design, and prediction. It becomes widespread in biology and medicine.

In a more general overview, models are either stochastic, deterministic or mixed approaches. Many model classifications can be found in the literature where they might differ for each field of research (e.g. Table A.1). It is rather difficult to do such classifications for systems biology. For instance, biological systems are not binary entities, in which something is either on or off; they could be stochastic, subject to nonlinear behavior. Nevertheless, in this chapter we will try to give an overview classifications of modeling for systems biology, taking into account aim(s) and ability(ies) of a model; namely, "Network (descriptive) models", "Algebraic (discrete dynamical) models ", "Time dynamical models", and "Space dynamical models".

Before starting our classification, you can have an outlook on the process of building a model (Figure A.1). Moreover, we are going to review, in particular, for non modelers, some colligated concepts that you might need to follow this chapter.

System: is a set of interacting or interdependent entities working together towards some kind of process. All systems have inputs, outputs, and feedback, and maintain a basic level of equilibrium. For example, in the human body the heart functions to support the circulatory system, which is vital to the survival of

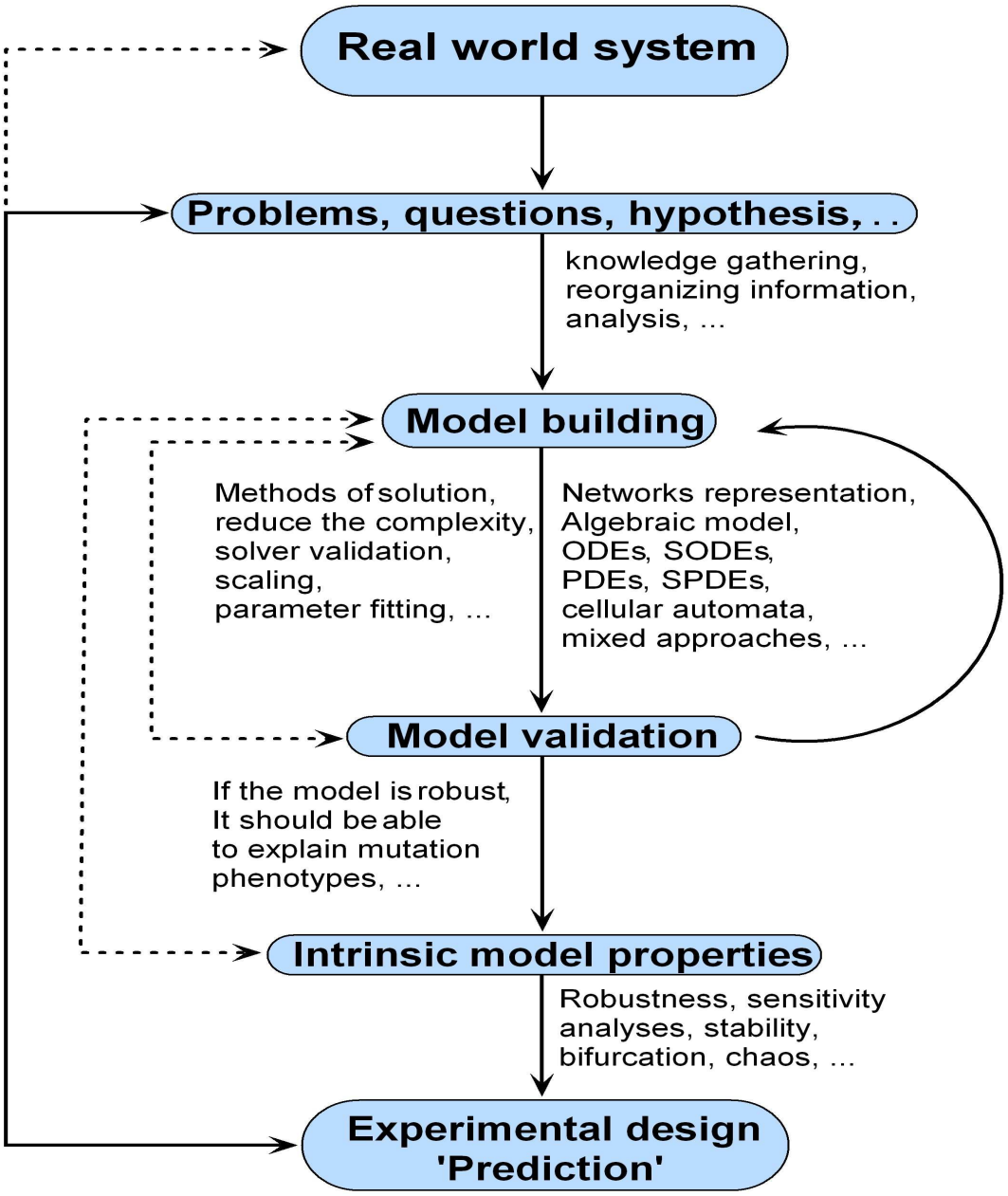

Figure A.1: Models build and use. Starting from the real world system. Gathering knowledge, make hypothesis, then build a model using a suitable modeling approach. The model should capture the expected behavior and in agreement with experimental findings. Validation like mutation experiments will explain the solidity of the model. Intrinsic properties can lead to deeper understanding (e.g. robustness, sensitivity of parameters, bifurcation analyzes). Ended with possible prediction and experimental design. Solid lines refers to usual interactions, while dash lines refers to possible interactions.

the entire body. Scientists have examined and classified many types of systems, following some examples:

- Isolated System - a system that has no interactions beyond its boundary layer. Many controlled laboratory experiments are this type of system.
- Closed System - is a system that transfers energy, but not matter, across its boundary to the surrounding environment. Our planet is often viewed as a closed system, also mechanical systems are closed systems.
- Open System - is a system that transfers both matter and energy can cross its boundary to the surrounding environment. People are open systems in that they must interact with their environment in order to take in food, water, and obtain shelter.
- Control System - a system that can be intelligently manipulated by an external action.

Model: is a simplified description or representation of a system that may be used to predict or explain the behavior of the system.

Ordinary Differential Equation (frequently called ODE): a differential equations[1](DE) that involves only *one* independent variable is called ordinary differential equation.

An ODE of order n is an equation[2] of the form $F(t, y, y', ..., y^{[n]}, \mathrm{P}) = 0$, where t is the time, y is an independent variable, and P is vector of phenomenological parameters. ODEs may have initial conditions[3] or boundary conditions[4].

[1]**Differential Equation (frequently called DE):** is an equation that involves the derivatives of a function as well as the function itself.

[2]**Equation(s):** describe the relations between the dependent and independent variables. An equal sign "=" is required in every equation.

[3]**Initial Condition:** Constrains that are specified at the initial point, generally time point, are called initial conditions. Problems with specified initial conditions are called initial value problems (IVPs).

[4]**Boundary Condition:** Constrains that are specified at the boundary points, generally space points, are called boundary conditions. Problems with specified boundary conditions are called boundary value problems (BVPs).

Moreover, ODEs have properties like order[1] and degree[2] and could be linear[3] or homogeneous[4].

Partial Differential Equation (frequently called PDE): a DE that involves *two* or *more* independent variables is called partial differential equations. An widespread example for systems biology is the Reaction-Diffusion systems:

$$\frac{\partial[C_i]}{\partial t} = \underbrace{\mathrm{D}_i \nabla^2[C_i]}_{\text{Diffusion}} + \underbrace{R_i(\{[C_j]\}, \mathrm{P})}_{\text{Reaction}}$$

The first term on the right hand side represent the diffusion and the second one represent the biochemical reactions. Where $[C_i]$ refers to the concentration of species, ∇ is the spatial gradient. D_i denotes to the constant diffusion coefficients for species, $i = 1, ..., n$, t adverts the time, and P refers to phenomenological parameters.

Stochastic Differential Equation (frequently called SDE): is a DE in which one or more of the terms is a stochastic process, thus resulting in a solution which is itself a stochastic process. Typically, SDEs incorporate white noise (see example below) which can be thought of as the derivative of Brownian motion (or the Wiener Process); however, it should be mentioned that other types of random fluctuations are possible. We should emphasize, that SDEs can be ordinary (see following example) or partial, which is hard to handel numerically.

[1] **Order**: The order of a differential equation is the highest power of derivative which occurs in the equation, e.g., Newton's second law produces a 2^{nd} order differential equation because the acceleration is the second derivative of the position.

[2] **Degree**: The degree of a differential equation is the power of the highest derivative term.

[3] **Linearity**: A differential equation is said to be linear if each term in the equation has only one order of derivative, e.g., no term has both y and the derivative of y with respect to time. Also, no derivative is raised to a power.

[4] **Homogeneousity**: A differential equation is said to be homogeneous if there is no isolated constant term in the equation, e.g., each term in a differential equation for y has y or some derivative of y in each term.

For each species i, the stochastic Langevin-type equation (a well known example type of SDEs) has the following form:

$$\frac{\mathrm{d}[C_i]}{\mathrm{dt}} = \mathrm{RH}(\{[C_j]\}, \mathrm{P}) + W_i(t)\sqrt{2 \cdot N_i \cdot [C_i]}$$

where RH is the original right-hand side of the deterministic equation and $W_i(t)$ is the (multiplicative) Gaussian white noise for species i with zero mean and unit variance

$$\langle W_i(t) \rangle = 0, \qquad \langle W_i(t) W_i(t') \rangle = \delta(t - t').$$

$N = N_i$ denotes the noise amplitude parameter, which, for simplicity, is the same for all species. P refers to a vector of phenomenological parameters.

A.2 Network Models

Network models are crucial for shaping our understanding of complex networks and help to explain the origin of observed network characteristics. Rapid advances in biological network indicate that cellular networks are governed by universal laws and offer a new conceptual framework that could potentially revolutionize our view of biology and disease pathologies in the twenty-first century (Barabási and Oltvai, 2004). Network models have become common in a wide range of disciplines. In particular, systems biology has focused attention on the need to study biological systems from a "top-down" point of view rather than from a reductionist "bottom-up" point of view. Thus, networks have to be studied. Recent revolutionary technological advances have made it possible to study the molecular networks that make up the complex intracellular biochemistry of organisms, including *gene regulatory networks*, *signal transduction networks*, and *metabolic networks*. The availability of system-level data for these networks makes it possible to represent complex biochemical reaction networks through mathematical network models.

Gene Regulatory Networks. (also called a GRN or genetic regulatory network). Genes are stretches of DNA that, once activated, are transcribed into mRNA. The mRNA fragments then are translated into proteins that carry out the cellular processes. The activation of genes depends on the binding of specific proteins called transcription factors to the promoter region of a gene. Within gene regulatory networks, the nodes represent genes, and the links specify how a gene activates or inactivates other genes. Gene regulatory networks are modeled using a variety of different techniques. See review by de Jong (2002) for an overview.

Signal Transduction Networks. Cells detect external signals by receptor proteins permeating the cell membrane. The signal is then propagated through a phosphorylation cascade inside the cell and finally reaches the nucleus where a change in transcription constitutes the response to the extracellular signal. In such networks, the nodes represent proteins and compounds that are involved in signal detection, propagation, and processing. The links can detail biochemical reactions or on a more abstract level functional and causal relationships between

the nodes. A review on the reconstruction and analysis of signal transduction networks is provided by Papin et al. (2005).

Metabolic Networks. The uptake and utilization of nutrients within the cell is detailed in metabolic networks. Nutrients enter the cell and are consecutively transformed into different metabolites by enzymes. These processes can be modeled in networks where the nodes represent the metabolites and the links the enzymatic reactions. An overview on modeling and analyzing metabolic networks is given in (Heinrich and Schuster, 1996).

Beside these intracellular networks, many more biological networks exist. Considering a slightly larger scale, cells communicate with each other in intercellular networks as the endocrine network and the immune network. On an even larger scale, the species within an ecosystem form foodwebs, a special network describing which species depend on which others as their food source. And finally, on a more abstract level, the evolutionary lineage of species can be depicted in phylogenetic trees and networks (reviewed by Centler (2008)). In this studies, we use biochemical network (signal transduction networks) as a base of our models.

A.3 Algebraic Models (Discrete/State Time)

In recent years, methods from algebra, and discrete mathematics play an important role in systems biology, through the use of discrete dynamical models and the use of theoretical concepts for their analyzes. We are going to give a brief review of two algebraic methodologies for systems biology: *Theory of Chemical Organizations* and *Petri Nets* (PNs) models. We will explain PNs because its widespread use and application as well as Organization theory which is new and growing fast approach.

A.3.1 Theory of Chemical Organizations

The theory of chemical organizations (Dittrich and Speroni di Fenizio, 2006) provides a new method to analyze complex reaction networks. Extending ideas

by Fontana and Buss (1994), one main objective is to determine combinations of network species that are more likely to be present over long periods of (simulation) time than others. Such sets of species are called organizations. To be an organization, a species set has to fulfill two properties (for review see Kaleta et al. (2007).

Algebraic closure and self-maintenance. The first property – closure – ensures that given the molecular species of an organization, there is no reaction within the reaction network that could create a novel species not yet present in the organization. The second property – self-maintenance – guarantees that every molecular species that is consumed within the organization can be recreated from organization species at a sufficient rate for its maintenance.

A rigorous link between organizations and the potential dynamics of a reaction system is provided by Theorem 1 from Ref. (Dittrich and Speroni di Fenizio, 2006): Assume that the dynamics is modeled as a "chemical" differential equation system $dx(t)/dt = \mathbf{S}v(x(t))$,(where S is a Stoichiometry matrix[1], and v is a flux[2] vector) then all steady states of the system are instances of organizations. In other words, the species with concentration levels greater than zero in a particular steady state are exactly those species contained in a corresponding organization. Note that organizations do not necessarily contain a steady state, as they can also embody growth in which species have increasing concentrations.

Organization theory is an efficient approach to analyze large scale network models. The theory handles a discrete time state, and has been applied in different areas (Centler, 2008). However, this theory is not able yet to include rates of a chemical reaction (fast, intermediate, slow,...) and inhibition rules. Future work needs for recognizing different types of steady states (e.g. find and handel chaotic behavior), or even include time. These more open question need to be addressed by the organization theory teams in the future. Finally, if you will try our MSAC models for instance with organization theory, we see only two organization, one for all species and one with very low number. It can give

[1] **Stoichiometry Matrix:** is the calculation of the quantities of reactants and products in a chemical reaction.

[2] **Flux:** is the speed of a chemical reaction

us qualitative behavior, or steady states. It is unable, yet, to reproduce any quantitative results. Thus, we are not going to use organization theory in this thesis.

A.3.2 Petri Nets

Petri nets (PNs) have been named after Carl Adam Petri who invented them early sixties (Petri, 1962). It provides a graphical notation with a formal mathematical semantics for modeling and reasoning about concurrent, asynchronous, distributed systems. A Petri net is a directed bipartite graph and consists of four basic components: places, which are denoted by circles; transitions denoted by rectangles; arcs denoted by arrows; and tokens denoted by black dots. An example of a Petri net for the template model is given in Figure A.2. The places, transitions and arcs describe the static structure of the Petri net. Each transition has a number of input places (places with an arc leading to the transition) and a number of output places (places with an arc leading to them from the transition). It normally views places as representing resources or conditions and transitions as representing actions or events. Note arcs that directly connect two transitions or two places are not allowed (Murata, 1989; Steggles et al., 2007).

Petri Nets of various different kinds have been used in several studies in systems biology, both as structural network models for qualitative analyzes and as quantitative models using high level nets (Pinney et al., 2003; Sackmann et al., 2006; Chaouiya, 2007).

These discrete-qualitative methods have the advantage that they only require information about the stoichiometry and reversibility of the constituent reactions, rather than relying on the availability of measurements of kinetic parameters. However, overcoming the combinatorial explosion associated with larger networks is recognized as a difficult challenge for these new approaches to networks analyzes.

Since our aim and interest is on quantitative approaches and therefore, we are not going to use PNs model. We show here an example of the template model (Figure A.2), in such an example and so for our models and in general for

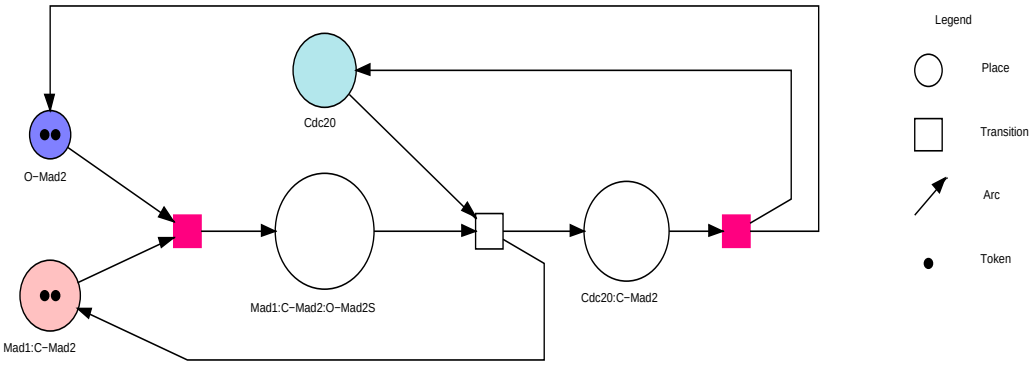

Figure A.2: Petri Net example: The Template model for Mad1 and Mad2 function of sequestering Cdc20 (for details see Chapter 3). We use colored Petri Net, e.g. red transition to emphasize the kinetochore effects (details in Chapter 3).

modelers, PNs is a good starting point to get an idea about the discrete dynamics or what could be expected from a dynamical model. In the following section, rich (continuous) dynamical modeling will be surveyed.

A.4 Time Dynamical Models

Understanding the dynamical behavior of a biological systems from the interaction of its molecular species is a rather difficult task (Bryja et al., 2004). A model based approach proposes a framework to express some hypotheses about a dynamical system and make some predictions out of it, in order to compare with experimental observations. Traditional approaches include differential equations (deterministic models) or stochastic processes (stochastic models).

A.4.1 Deterministic versus Stochastic (Probabilistic) Models

The most widespread formalism to model dynamical systems in science and engineering, ordinary differential equations (ODEs) have been widely used to analyze biological systems. The ODE formalism models the concentrations of

proteins, and other molecules by time-dependent variables with values contained in the set of nonnegative real numbers. Regulatory interactions take the form of functional and differential relations between the concentration variables.

Stochastic (or Probabilistic) modeling usually starts by describing real world objects on different spatial and temporal scales and uses different advanced mathematical approaches and techniques. It can be simple to reproduce the deterministic behavior (e.g. ODEs), or to bring more detailed modeling (interacting systems of individual agents or particles, random walks, random media).

Generally, stochastic kinetic models are more detailed. The disadvantage of a stochastic kinetic analyzes is that it can be computationally expensive, making such implementations impractical or impossible. A comparison between both approaches is shown in Table A.2.

Deterministic versus Stochastic models

- Deterministic approaches	- Stochastic approaches
- Less complicated.	- More complicated.
- Input determines unique output.	- Produce different results for the same input.
- Reproducible results/simulations.	- Include random influences.
- Easy to analyze.	- Rather difficult to analyze and usually averaged results of interest.
- Often good enough and secure.	- Could lead to a insecure sense.
- DEs methods require considerable mathematical skill and understanding (not common among biologists).	- Common and easy to impliment.
- Hard to capture noise or any stochasticity.	- Can be captured noise and stochasticity.
- In some cases, it can not (or hardly) simulated	- Can be always simulated.
- Required less knowledge.	- Required more knowledge
- Computationally less expensive.	- Computationally much more expensive.
⋮	⋮

Table A.2: Deterministic versus stochastic models: A comparison overview.

A.4.2 Multi-Scale Models

Typically, the same system can be modeled on different scales, and it is of crucial interest to study the interaction of different modeling approaches in systems biology. Practitioners even describe different scales of biological models, which are generally grouped into the three scaling categories: *macroscopic*[1], *mesoscopic*[2], and *microscopic*[3], (or concisely, as macro-, meso-, micro-, scales).

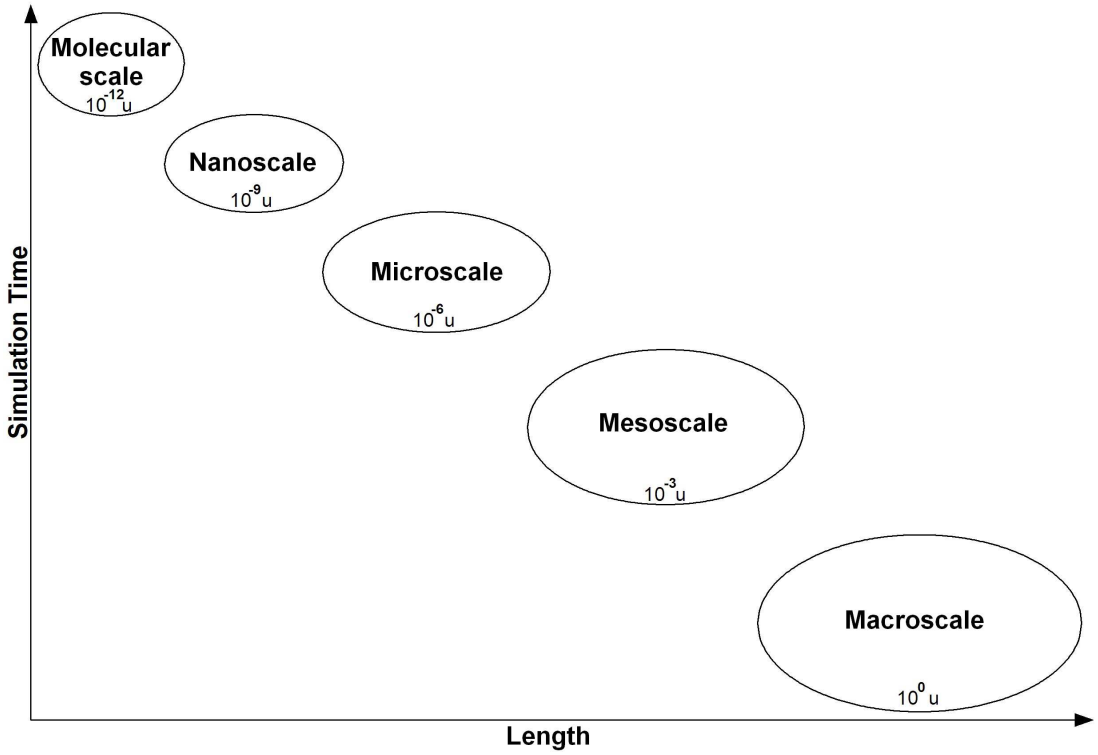

Figure A.3: Multi-scale modeling scheme in systems biology. Characterizing the simulation time and length scales. starting from Macroscale and ended with Molecular scale, where u is meter unit.

[1]The prefix "macro" comes from the Greek word, "mackros" that means long. Macroscopic objects are those that can easily be seen by humans.

[2]The prefix "meso" comes from the Greek word "mesos" meaning "intermediate".

[3]The prefix "Micro" comes from the Greek word "mikros" meaning small. In the everyday world the word microscopic is used to refer to objects that are too small for the unaided eye to see. People often think of bacteria or viruses when considering the microscopic world.

Macroscopic. The term "Macroscopic" is used to describe the largest scale of modeling. For example, dynamic of molecule concentrations mostly is represented in deterministic models (differential equations).

Advantages and disadvantages at macroscopic scales:
- Macroscopic model fails in small-length-scale regions.
- Microscopic details are usually not included.
- Lot of calculations but fast (should be carefully handel, e.g. stiffness systems).

Microscopic. Microscopic simulation models on the other hand are at the opposite end of the spectrum which is mostly stochastic models (e.g. interacting systems of individual agents or particles, random walks, random media).

Advantages and disadvantages at microscopic scales:
- Control over each component.
- Difficult implementation and tune.
- Most realistic.

Mesoscopic. Mesoscopic models fall between microscopic and macroscopic models. Dynamic of single molecules, without consideration of physical forces, mostly stochastic models.

Advantages and disadvantages at mesoscopic scales:
- Micro scale components deployed in a macro scale scenario.
- Better interactions tuning.
- Attributes of molecules are not consider.

One can start with macroscopic level (usually differential equations), for an overview of an essential continuous dynamics, then one moves to detailed microscopic level, the analysis of their long-time or average behavior and large deviations gives rise to models on the mesoscopic level. Analyzing these models on any level is a necessary prerequisite for their practical use.

We should emphasize that properties of a stochastic model could lead to a different behavior from that of a deterministic model for intracellular kinetics that initially

involved a low number of reactants. The reason might be due to the assumption of continuity of biochemical species in the deterministic model. In this thesis, quantitative modeling approach will be used. Additionally, stochastic effects will be examined.

A.5 Space Dynamical Models

Time dynamics can produce quantitative output for each time step. It can capture behavior, intrinsic properties, like bifurcation analyzes, robustness, etc, and even predict. Thus, it is widely used in systems biology. To keep going for deeper understanding of topological 'environment' (structure, diffusion, locations, binding sides) There are two disadvantages of space dynamical models. First, they need more kinetic knowledge, which are usually hard to get from the lab and not precise; second, it is computationally very expensive (consume very long time).

Classic spatial approaches use PDEs or SPDEs, which are able to acquire macroscopic details of a system for each time point and anywhere. Stochastic simulations (e.g. cellular automata, particles simulations) are used for capturing meso or microscopic levels.

A.6 Methods

"An idea which can be used once is a trick. If it can be used more than once it becomes a method." George Polya and Gabor Szego

Broadly speaking, we can divided methods into two categories our modeling approaches: Solvers (solving DEs mostly) and optimizations (parameters fitting). For solving DEs different, we used different methods base on the DEs type.

For ODEs, to solve the nonlinear systems of highly stiff ODEs, which arise in our optimization besides non stiff systems, a variety of computational approaches have been applied. In particular, we use high order (seven-eighth) Runge-Kutta (Fehlberg and Prince) formulas, a modified Rosenbrock formula, variable order

Adams-Bashforth-Moulton, an explicit Runge-Kutta, backward differentiation formulas, and an implicit Runge-Kutta formula. We switch between these methods automatically according to the system's stiffness state. We implemented our code in MATLAB. The numerical results were also validated Octave's (Eaton, 2008) ODEs solver (LSODE solver) and Copasi (Mendes group at VBI and Kummer group at EML research, 2008). For SDEs, the simulations were performed using standard numerical techniques for stochastic differential equations (including the strong implicit 1.5 order Runge-Kutta method, and the explicit Runge-Kutta method of order 1.5, Kloeden and Platen, 1999b). We implemented our code in (MATLAB , Matrix Labrotory) and/or Octave (Eaton, 2008). For PDEs in general use of Finite Element Methods (see tools example, COMSOL, 2008 and VCell, 2008).

Optimization methods for the estimation of unknown parameters are central and of great importance to this field of research. For this task, evolutionary approaches as well as deterministic algorithms have been applied to infer parameters in biochemical models. The nonlinear evolutionary optimization was usually validated with an independent evolutionary optimizer (Ibrahim et al., 2007). For optimization we applied the covariance matrix adaptation nonlinear evolutionary strategy (CMA-ES) (Hansen and Kern, 2004; Hansen et al., 2003), Quasi-Newton and sequential quadratic programming. We validate with Differential Evolution (DE) Storn and Price (1997). We encountered with problems in case of large search space. We demonstrate that parameter estimation can be efficiently and more accurately performed using scaled search steps (Rohn et al., 2008).

"Examples...show how difficult it often is for an experimenter to interpret his results without the aid of mathematics". Lord Rayleigh (1842 - 1919)
(Nobel Prize Laureate in Physics 1904)

"The great tragedy of Science the slaying of a beautiful hypothesis by an ugly fact". Thomas H. Huxley (1725-95)

Appendix B

Template-like models

B.1 ODEs of the Exchange model

$$\frac{\text{d[Mad1]}}{\text{dt}} = -\alpha_E.u[\text{Mad1}][\text{O-Mad2}] + k_{-2}[\text{Mad1:C-Mad2}] + k_3[\text{Mad1:C-Mad2}] - k_{-3}[\text{C-Mad2}][\text{Mad1}] \tag{B.1}$$

$$\frac{\text{d[O-Mad2]}}{\text{dt}} = -k_1[\text{O-Mad2}] + k_{-1}[\text{C-Mad2}] - \alpha_E.u[\text{Mad1}][\text{O-Mad2}] + k_{-2}[\text{Mad1:C-Mad2}] + \eta_E[\text{Cdc20:C-Mad2}] \tag{B.2}$$

$$\frac{\text{d[Mad1:C-Mad2]}}{\text{dt}} = \alpha_E.u[\text{Mad1}][\text{O-Mad2}] - k_{-2}[\text{Mad1:C-Mad2}] - k_3[\text{Mad1:C-Mad2}] + k_{-3}[\text{C-Mad2}][\text{Mad1}] \tag{B.3}$$

$$\frac{\text{d[C-Mad2]}}{\text{dt}} = k_1[\text{O-Mad2}] - k_{-1}[\text{C-Mad2}] + k_3[\text{Mad1:C-Mad2}] - k_{-3}[\text{C-Mad2}][\text{Mad1}] - k_E[\text{C-Mad2}][\text{Cdc20}] \tag{B.4}$$

$$\frac{\text{d[Cdc20]}}{\text{dt}} = -k_E[\text{C-Mad2}][\text{Cdc20}] + \eta_E[\text{Cdc20:C-Mad2}] \tag{B.5}$$

$$\frac{\text{d[Cdc20:C-Mad2]}}{\text{dt}} = k_E[\text{C-Mad2}][\text{Cdc20}] - \eta_E[\text{Cdc20:C-Mad2}] \tag{B.6}$$

B.2 ODEs of the Template model

$$\frac{\mathrm{d[Mad1{:}C{-}Mad2]}}{\mathrm{dt}} = -\alpha_T.u[\text{Mad1:C-Mad2}][\text{O-Mad2}] + \beta_T[\text{Mad1:C-Mad2:O-Mad2}^*] + \gamma_T.u[\text{Mad1:C-Mad2:O-Mad2}^*][\text{Cdc20}] \tag{B.7}$$

$$\frac{\mathrm{d[O{-}Mad2]}}{\mathrm{dt}} = -\alpha_T.u[\text{Mad1:C-Mad2}][\text{O-Mad2}] + \beta_T[\text{Mad1:C-Mad2:O-Mad2}^*] + \eta_T[\text{Cdc20:C-Mad2}] \tag{B.8}$$

$$\frac{\mathrm{d[Mad1{:}C{-}Mad2{:}O{-}Mad2^*]}}{\mathrm{dt}} = \alpha_T.u[\text{Mad1:C-Mad2}][\text{O-Mad2}] - \beta_T[\text{Mad1:C-Mad2:O-Mad2}^*] - \gamma_T.u[\text{Mad1:C-Mad2:O-Mad2}^*][\text{Cdc20}] \tag{B.9}$$

$$\frac{\mathrm{d[Cdc20]}}{\mathrm{dt}} = -\gamma_T.u[\text{Mad1:C-Mad2:O-Mad2}^*][\text{Cdc20}] + \eta_T[\text{Cdc20:C-Mad2}] \tag{B.10}$$

$$\frac{\mathrm{d[Cdc20{:}C{-}Mad2]}}{\mathrm{dt}} = \gamma_T.u[\text{Mad1:C-Mad2:O-Mad2}^*][\text{Cdc20}] - \eta_T[\text{Cdc20:C-Mad2}] \tag{B.11}$$

B.3 ODEs of the Template model with the Amplification effects

$$\frac{\mathrm{d[Mad1{:}C{-}Mad2]}}{\mathrm{dt}} = -\alpha_T.u[\text{Mad1:C-Mad2}][\text{O-Mad2}] + \beta_T[\text{Mad1:C-Mad2:O-Mad2}^*] + \gamma_T.u[\text{Mad1:C-Mad2:O-Mad2}^*][\text{Cdc20}] - k_4[\text{Cdc20:C-Mad2}][\text{O-Mad2}] + k_{-4}[\text{Cdc20:C-Mad2:O-Mad2}^*] \tag{B.12}$$

$$\frac{\mathrm{d[O{-}Mad2]}}{\mathrm{dt}} = -\alpha_T.u[\text{Mad1:C-Mad2}][\text{O-Mad2}] + \beta_T[\text{Mad1:C-Mad2:O-Mad2}^*] + \eta_T[\text{Cdc20:C-Mad2}] - k_4[\text{Cdc20:C-Mad2}][\text{O-Mad2}] + k_{-4}[\text{Cdc20:C-Mad2:O-Mad2}^*] \tag{B.13}$$

$$\frac{\mathrm{d[Mad1{:}C{-}Mad2{:}O{-}Mad2^*]}}{\mathrm{dt}} = \alpha_T.u[\text{Mad1:C-Mad2}][\text{O-Mad2}] - \beta_T[\text{Mad1:C-Mad2:O-Mad2}^*] - \gamma_T.u[\text{Mad1:C-Mad2:O-Mad2}^*][\text{Cdc20}] \tag{B.14}$$

$$\frac{\mathrm{d[Cdc20{:}C{-}Mad2{:}O{-}Mad2^*]}}{\mathrm{dt}} = k_4[\text{Cdc20:C-Mad2}][\text{O-Mad2}] - k_{-4}[\text{Cdc20:C-Mad2:O-Mad2}^*] - k_5[\text{Cdc20:C-Mad2:O-Mad2}^*][\text{Cdc20}] \tag{B.15}$$

$$\frac{\mathrm{d[Cdc20]}}{\mathrm{dt}} = -\gamma_T.u[\text{Mad1:C-Mad2:O-Mad2}^*][\text{Cdc20}] + \eta_T[\text{Cdc20:C-Mad2}] - k_5[\text{Cdc20:C-Mad2:O-Mad2}^*][\text{Cdc20}] \tag{B.16}$$

$$\frac{\mathrm{d[Cdc20{:}C{-}Mad2]}}{\mathrm{dt}} = \gamma_T.u[\text{Mad1:C-Mad2:O-Mad2}^*][\text{Cdc20}] - \eta_T[\text{Cdc20:C-Mad2}] - k_4[\text{Cdc20:C-Mad2}][\text{O-Mad2}] + k_{-4}[\text{Cdc20:C-Mad2:O-Mad2}^*] + 2k_5[\text{Cdc20:C-Mad2:O-Mad2}^*][\text{Cdc20}] \tag{B.17}$$

B.4 ODEs of of p31 effects on the Template model

$$\frac{\mathrm{d[Mad1{:}C{-}Mad2]}}{\mathrm{dt}} = -\alpha_T.u[\mathrm{Mad1{:}C{-}Mad2}][\mathrm{O{-}Mad2}] + \beta_T[\mathrm{Mad1{:}C{-}Mad2{:}O{-}Mad2^*}] + \gamma_T.u[\mathrm{Mad1{:}C{-}Mad2{:}O{-}Mad2^*}][\mathrm{Cdc20}] - \delta_T.v[\mathrm{Mad1{:}C{-}Mad2}][\mathrm{p31}] + \zeta_T[\mathrm{Mad1{:}C{-}Mad2{:}p31}] \tag{B.18}$$

$$\frac{\mathrm{d[O{-}Mad2]}}{\mathrm{dt}} = -\alpha_T.u[\mathrm{Mad1{:}C{-}Mad2}][\mathrm{O{-}Mad2}] + \beta_T[\mathrm{Mad1{:}C{-}Mad2{:}O{-}Mad2^*}] + \eta_T[\mathrm{Cdc20{:}C{-}Mad2}] \tag{B.19}$$

$$\frac{\mathrm{d[Mad1{:}C{-}Mad2{:}O{-}Mad2^*]}}{\mathrm{dt}} = \alpha_T.u[\mathrm{Mad1{:}C{-}Mad2}][\mathrm{O{-}Mad2}] - \beta_T[\mathrm{Mad1{:}C{-}Mad2{:}O{-}Mad2^*}] - \gamma_T.u[\mathrm{Mad1{:}C{-}Mad2{:}O{-}Mad2^*}][\mathrm{Cdc20}] \tag{B.20}$$

$$\frac{\mathrm{d[Cdc20]}}{\mathrm{dt}} = -\gamma_T.u[\mathrm{Mad1{:}C{-}Mad2{:}O{-}Mad2^*}][\mathrm{Cdc20}] + \eta_T[\mathrm{Cdc20{:}C{-}Mad2}] \tag{B.21}$$

$$\frac{\mathrm{d[Cdc20{:}C{-}Mad2]}}{\mathrm{dt}} = \gamma_T.u[\mathrm{Mad1{:}C{-}Mad2{:}O{-}Mad2^*}][\mathrm{Cdc20}] - \eta_T[\mathrm{Cdc20{:}C{-}Mad2}] \tag{B.22}$$

$$\frac{\mathrm{d[p31]}}{\mathrm{dt}} = -\delta_T.v[\mathrm{Mad1{:}C{-}Mad2}][\mathrm{p31}] + \zeta_T[\mathrm{Mad1{:}C{-}Mad2{:}p31}] \tag{B.23}$$

$$\frac{\mathrm{d[Mad1{:}C{-}Mad2{:}p31]}}{\mathrm{dt}} = \delta_T.v[\mathrm{Mad1{:}C{-}Mad2}][\mathrm{p31}] - \zeta_T[\mathrm{Mad1{:}C{-}Mad2{:}p31}] \tag{B.24}$$

B.5 ODEs of of p31 effects on the Template model with amplification

$$\frac{\mathrm{d[Mad1:C\text{-}Mad2]}}{\mathrm{dt}} = -\alpha_T.u[\text{Mad1:C-Mad2}][\text{O-Mad2}] + \beta_T[\text{Mad1:C-Mad2:O-Mad2}^*] + \gamma_T.u[\text{Mad1:C-Mad2:O-Mad2}^*][\text{Cdc20}] - k_4[\text{Cdc20:C-Mad2}][\text{O-Mad2}] + k_{-4}[\text{Cdc20:C-Mad2:O-Mad2}^*] - \delta_T.v[\text{Mad1:C-Mad2}][\text{p31}] + \zeta_T[\text{Mad1:C-Mad2:p31}] \quad \text{(B.25)}$$

$$\frac{\mathrm{d[O\text{-}Mad2]}}{\mathrm{dt}} = -\alpha_T.u[\text{Mad1:C-Mad2}][\text{O-Mad2}] + \beta_T[\text{Mad1:C-Mad2:O-Mad2}^*] + \eta_T[\text{Cdc20:C-Mad2}] - k_4[\text{Cdc20:C-Mad2}][\text{O-Mad2}] + k_{-4}[\text{Cdc20:C-Mad2:O-Mad2}^*] \quad \text{(B.26)}$$

$$\frac{\mathrm{d[Mad1:C\text{-}Mad2:O\text{-}Mad2^*]}}{\mathrm{dt}} = \alpha_T.u[\text{Mad1:C-Mad2}][\text{O-Mad2}] - \beta_T[\text{Mad1:C-Mad2:O-Mad2}^*] - \gamma_T.u[\text{Mad1:C-Mad2:O-Mad2}^*][\text{Cdc20}] \quad \text{(B.27)}$$

$$\frac{\mathrm{d[Cdc20:C\text{-}Mad2:O\text{-}Mad2^*]}}{\mathrm{dt}} = k_4[\text{Cdc20:C-Mad2}][\text{O-Mad2}] - k_{-4}[\text{Cdc20:C-Mad2:O-Mad2}^*] - k_5[\text{Cdc20:C-Mad2:O-Mad2}^*][\text{Cdc20}] \quad \text{(B.28)}$$

$$\frac{\mathrm{d[Cdc20]}}{\mathrm{dt}} = -\gamma_T.u[\text{Mad1:C-Mad2:O-Mad2}^*][\text{Cdc20}] + \eta_T[\text{Cdc20:C-Mad2}] - k_5[\text{Cdc20:C-Mad2:O-Mad2}^*][\text{Cdc20}] \quad \text{(B.29)}$$

$$\frac{\mathrm{d[Cdc20:C\text{-}Mad2]}}{\mathrm{dt}} = \gamma_T.u[\text{Mad1:C-Mad2:O-Mad2}^*][\text{Cdc20}] - \eta_T[\text{Cdc20:C-Mad2}] - k_4[\text{Cdc20:C-Mad2}][\text{O-Mad2}] + k_{-4}[\text{Cdc20:C-Mad2:O-Mad2}^*] + 2k_5[\text{Cdc20:C-Mad2:O-Mad2}^*][\text{Cdc20}] - \xi_T.v[\text{Cdc20:C-Mad2}][\text{p31}] + \sigma_T[\text{Cdc20:C-Mad2:p31}] \quad \text{(B.30)}$$

$$\frac{\mathrm{d[p31]}}{\mathrm{dt}} = -\delta_T.v[\text{Mad1:C-Mad2}][\text{p31}] + \zeta_T[\text{Mad1:C-Mad2:p31}] - \xi_T.v[\text{Cdc20:C-Mad2}][\text{p31}] + \sigma_T[\text{Cdc20:C-Mad2:p31}] \quad \text{(B.31)}$$

$$\frac{\mathrm{d[Mad1:C\text{-}Mad2:p31]}}{\mathrm{dt}} = \delta_T.v[\text{Mad1:C-Mad2}][\text{p31}] - \zeta_T[\text{Mad1:C-Mad2:p31}] \quad \text{(B.32)}$$

$$\frac{\mathrm{d[Cdc20:C\text{-}Mad2:p31]}}{\mathrm{dt}} = \xi_T.v[\text{Cdc20:C-Mad2}][\text{p31}] - \sigma_T[\text{Cdc20:C-Mad2:p31}] \quad \text{(B.33)}$$

B.6 Materials, Methods, and Optimization

The objective function $f(P)$ assigns a quality (i.e., a positive real number) to a given set of parameters P. In our case, the parameters are the reaction constants. In order to fit the parameters with respect to the observed qualitative function of the $^{\mathrm{M}}$SAC control, we use the Cdc20 concentration before and after kinetochore

attachment as a criterion. In each single simulation experiment, we simulate two phases of the spindle attachment status. Our simulation begins in the kinetochore unattached case (phase 1), until equilibrium is reached, then it continues in the attached state (phase 2), again, until steady state conditions are met. We measure the Cdc20 concentration at the end of each phase i, when all concentrations have reached steady state, and compare it with a user given value A_i, which describes the experimentally observed behavior. The two difference values are combined linearly:

$$f(P) = W_1([\text{Cdc20}]_{\text{Unattached}} - A_1)^2 + W_2([\text{Cdc20}]_{\text{Attached}} - A_2)^2$$

where W_1, and W_2 are the weights which were 10, and 1 respectively. A_1, and A_2 are the desired phase levels, which we set 0 and 0.01, respectively.

For optimization we applied the covariance matrix adaptation nonlinear evolution strategy (CMA-ES) Hansen and Kern (2004), Quasi-Newton and sequential quadratic programming. To solve the nonlinear systems of highly stiff ODEs, which arise in our optimization besides non stiff systems, a variety of computational approaches have been applied. In particular, we use high order (seven-eighth) Runge-Kutta (Fehlberg and Prince) formulas, a modified Rosenbrock formula, variable order Adams-Bashforth-Moulton, an explicit Runge-Kutta, backward differentiation formulas, and an implicit Runge-Kutta formula. We switch between these methods automatically according to the system's stiffness state. We implemented our code in MATLAB. The numerical results were also validated with Copasi. The nonlinear evolutionary optimization was validated with an independent evolutionary optimizer.

"As far as the laws of mathematics refer to reality, they are not certain; and as far as they are certain, they do not refer to reality". Albert Einstein (1779 - 1955)

"If you don't fail regularly you are not trying hard enough things". Ivan Sutherland (1938-)

Appendix C

MCC formation models

C.1 MCC "kinetochore dependent model"

$$\frac{\mathrm{d[Mad1:C\text{-}Mad2]}}{\mathrm{dt}} = -k_1.u[\mathrm{Mad1:C\text{-}Mad2}][\mathrm{O\text{-}Mad2}] + k_{-1}[\mathrm{Mad1:C\text{-}Mad2:O\text{-}Mad2^*}] + k_2.u[\mathrm{Mad1:C\text{-}Mad2:O\text{-}Mad2^*}][\mathrm{Cdc20}] \quad \text{(C.1)}$$

$$\frac{\mathrm{d[O\text{-}Mad2]}}{\mathrm{dt}} = -k_1.u[\mathrm{Mad1:C\text{-}Mad2}][\mathrm{O\text{-}Mad2}] + k_{-1}[\mathrm{Mad1:C\text{-}Mad2:O\text{-}Mad2^*}] + k_3[\mathrm{Cdc20:C\text{-}Mad2}] - k_6[\mathrm{Cdc20}][\mathrm{O\text{-}Mad2}] \quad \text{(C.2)}$$

$$\frac{\mathrm{d[Mad1:C\text{-}Mad2:O\text{-}Mad2^*]}}{\mathrm{dt}} = k_1.u[\mathrm{Mad1:C\text{-}Mad2}][\mathrm{O\text{-}Mad2}] - k_{-1}[\mathrm{Mad1:C\text{-}Mad2:O\text{-}Mad2^*}] - k_2.u[\mathrm{Mad1:C\text{-}Mad2:O\text{-}Mad2^*}][\mathrm{Cdc20}] \quad \text{(C.3)}$$

$$\frac{\mathrm{d[Cdc20]}}{\mathrm{dt}} = -k_2.u[\mathrm{Mad1:C\text{-}Mad2:O\text{-}Mad2^*}][\mathrm{Cdc20}] + k_3[\mathrm{Cdc20:C\text{-}Mad2}] - k_5.u[\mathrm{Cdc20}][\mathrm{Bub3:BubR1}] + k_{-5}[\mathrm{Bub3:BubR1:Cdc20}] - k_6[\mathrm{Cdc20}][\mathrm{O\text{-}Mad2}] \quad \text{(C.4)}$$

$$\frac{\mathrm{d[Cdc20:C\text{-}Mad2]}}{\mathrm{dt}} = k_2.u[\mathrm{Mad1:C\text{-}Mad2:O\text{-}Mad2^*}][\mathrm{Cdc20}] - k_3[\mathrm{Cdc20:C\text{-}Mad2}] - k_4.u[\mathrm{Cdc20:C\text{-}Mad2}][\mathrm{Bub3:BubR1}] + k_{-4}[\mathrm{MCC}] + k_6[\mathrm{Cdc20}][\mathrm{O\text{-}Mad2}] \quad \text{(C.5)}$$

$$\frac{\mathrm{d[Bub3:BubR1]}}{\mathrm{dt}} = -k_4.u[\mathrm{Cdc20:C\text{-}Mad2}][\mathrm{Bub3:BubR1}] + k_{-4}[\mathrm{MCC}] - k_5.u[\mathrm{Cdc20}][\mathrm{Bub3:BubR1}] + k_{-5}[\mathrm{Bub3:BubR1:Cdc20}] \quad \text{(C.6)}$$

$$\frac{\mathrm{d[MCC]}}{\mathrm{dt}} = +k_4.u[\mathrm{Cdc20:C\text{-}Mad2}][\mathrm{Bub3:BubR1}] - k_{-4}[\mathrm{MCC}] \quad \text{(C.7)}$$

$$\frac{\mathrm{d[Bub3:BubR1:Cdc20]}}{\mathrm{dt}} = k_5.u[\mathrm{Cdc20}][\mathrm{Bub3:BubR1}] - k_{-5}[\mathrm{Bub3:BubR1:Cdc20}] \quad \text{(C.8)}$$

C.2 Amplification effects

$$\frac{\mathrm{d}[\text{Mad1:C-Mad2}]}{\mathrm{dt}} = -k_1.u[\text{Mad1:C-Mad2}][\text{O-Mad2}] + k_{-1}[\text{Mad1:C-Mad2:O-Mad2}^*] + k_2.u[\text{Mad1:C-Mad2:O-Mad2}^*][\text{Cdc20}] \tag{C.9}$$

$$\frac{\mathrm{d}[\text{O-Mad2}]}{\mathrm{dt}} = -k_1.u[\text{Mad1:C-Mad2}][\text{O-Mad2}] + k_{-1}[\text{Mad1:C-Mad2:O-Mad2}^*] + k_3[\text{Cdc20:C-Mad2}] - k_6[\text{Cdc20}][\text{O-Mad2}] - k_7[\text{Cdc20:C-Mad2}][\text{O-Mad2}] + k_{-7}[\text{Cdc20:C-Mad2:O-Mad2}^*] \tag{C.10}$$

$$\frac{\mathrm{d}[\text{Mad1:C-Mad2:O-Mad2}^*]}{\mathrm{dt}} = k_1.u[\text{Mad1:C-Mad2}][\text{O-Mad2}] - k_{-1}[\text{Mad1:C-Mad2:O-Mad2}^*] - k_2.u[\text{Mad1:C-Mad2:O-Mad2}^*][\text{Cdc20}] \tag{C.11}$$

$$\frac{\mathrm{d}[\text{Cdc20}]}{\mathrm{dt}} = -k_2.u[\text{Mad1:C-Mad2:O-Mad2}^*][\text{Cdc20}] + k_3[\text{Cdc20:C-Mad2}] - k_5.u[\text{Cdc20}][\text{Bub3:BubR1}] + k_{-5}[\text{Bub3:BubR1:Cdc20}] - k_6[\text{Cdc20}][\text{O-Mad2}] - k_8[\text{Cdc20:C-Mad2:O-Mad2}^*][\text{Cdc20}] \tag{C.12}$$

$$\frac{\mathrm{d}[\text{Cdc20:C-Mad2}]}{\mathrm{dt}} = k_2.u[\text{Mad1:C-Mad2:O-Mad2}^*][\text{Cdc20}] - k_3[\text{Cdc20:C-Mad2}] - k_4.u[\text{Cdc20:C-Mad2}][\text{Bub3:BubR1}] + k_{-4}[\text{MCC}] + k_6[\text{Cdc20}][\text{O-Mad2}] - k_7[\text{Cdc20:C-Mad2}][\text{O-Mad2}] + k_{-7}[\text{Cdc20:C-Mad2:O-Mad2}^*] + 2k_8[\text{Cdc20:C-Mad2:O-Mad2}^*][\text{Cdc20}] \tag{C.13}$$

$$\frac{\mathrm{d}[\text{Bub3:BubR1}]}{\mathrm{dt}} = -k_4.u[\text{Cdc20:C-Mad2}][\text{Bub3:BubR1}] + k_{-4}[\text{MCC}] - k_5.u[\text{Cdc20}][\text{Bub3:BubR1}] + k_{-5}[\text{Bub3:BubR1:Cdc20}] \tag{C.14}$$

$$\frac{\mathrm{d}[\text{MCC}]}{\mathrm{dt}} = +k_4.u[\text{Cdc20:C-Mad2}][\text{Bub3:BubR1}] - k_{-4}[\text{MCC}] \tag{C.15}$$

$$\frac{\mathrm{d}[\text{Bub3:BubR1:Cdc20}]}{\mathrm{dt}} = k_5.u[\text{Cdc20}][\text{Bub3:BubR1}] - k_{-5}[\text{Bub3:BubR1:Cdc20}] \tag{C.16}$$

$$\frac{\mathrm{d}[\text{Cdc20:C-Mad2:O-Mad2}^*]}{\mathrm{dt}} = +k_7[\text{Cdc20:C-Mad2}][\text{O-Mad2}] - k_{-7}[\text{Cdc20:C-Mad2:O-Mad2}^*] - k_8[\text{Cdc20:C-Mad2:O-Mad2}^*][\text{Cdc20}] \tag{C.17}$$

C.3 p31$^{\text{comet}}$ contribution

$$\frac{\mathrm{d[Mad1:C\text{-}Mad2]}}{\mathrm{dt}} = -k_1[\text{Mad1:C-Mad2}][\text{O-Mad2}] + k_{-1}[\text{Mad1:C-Mad2:O-Mad2}^*] + k_2[\text{Mad1:C-Mad2:O-Mad2}^*][\text{Cdc20}] - k_{7p}.v[\text{Mad1:C-Mad2}][\text{p31}^{\text{comet}}] + k_{-7p}[\text{Mad1:C-Mad2:p31}^{\text{comet}}] \quad \text{(C.18)}$$

$$\frac{\mathrm{d[O\text{-}Mad2]}}{\mathrm{dt}} = -k_1[\text{Mad1:C-Mad2}][\text{O-Mad2}] + k_{-1}[\text{Mad1:C-Mad2:O-Mad2}^*] + k_3[\text{Cdc20:C-Mad2}] - k_6[\text{Cdc20}][\text{O-Mad2}] \quad \text{(C.19)}$$

$$\frac{\mathrm{d[Mad1:C\text{-}Mad2:O\text{-}Mad2^*]}}{\mathrm{dt}} = k_1[\text{Mad1:C-Mad2}][\text{O-Mad2}] - k_{-1}[\text{Mad1:C-Mad2:O-Mad2}^*] - k_2[\text{Mad1:C-Mad2:O-Mad2}^*][\text{Cdc20}] \quad \text{(C.20)}$$

$$\frac{\mathrm{d[Cdc20]}}{\mathrm{dt}} = -k_2[\text{Mad1:C-Mad2:O-Mad2}^*][\text{Cdc20}] + k_3[\text{Cdc20:C-Mad2}] - k_5.u[\text{Cdc20}][\text{Bub3:BubR1}] + k_{-5}[\text{Bub3:BubR1:Cdc20}] - k_6[\text{Cdc20}][\text{O-Mad2}] \quad \text{(C.21)}$$

$$\frac{\mathrm{d[Cdc20:C\text{-}Mad2]}}{\mathrm{dt}} = k_2[\text{Mad1:C-Mad2:O-Mad2}^*][\text{Cdc20}] - k_3[\text{Cdc20:C-Mad2}] - k_4.u[\text{Cdc20:C-Mad2}][\text{Bub3:BubR1}] + k_{-4}[\text{MCC}] + k_6[\text{Cdc20}][\text{O-Mad2}] - k_{8p}.v[\text{Cdc20:C-Mad2}][\text{p31}^{\text{comet}}] + k_{-8p}[\text{Cdc20:C-Mad2:p31}^{\text{comet}}] \quad \text{(C.22)}$$

$$\frac{\mathrm{d[Bub3:BubR1]}}{\mathrm{dt}} = -k_4.u[\text{Cdc20:C-Mad2}][\text{Bub3:BubR1}] + k_{-4}[\text{MCC}] - k_5.u[\text{Cdc20}][\text{Bub3:BubR1}] + k_{-5}[\text{Bub3:BubR1:Cdc20}] \quad \text{(C.23)}$$

$$\frac{\mathrm{d[MCC]}}{\mathrm{dt}} = +k_4.u[\text{Cdc20:C-Mad2}][\text{Bub3:BubR1}] - k_{-4}[\text{MCC}] \quad \text{(C.24)}$$

$$\frac{\mathrm{d[Bub3:BubR1:Cdc20]}}{\mathrm{dt}} = k_5.u[\text{Cdc20}][\text{Bub3:BubR1}] - k_{-5}[\text{Bub3:BubR1:Cdc20}] \quad \text{(C.25)}$$

$$\frac{\mathrm{d[p31^{comet}]}}{\mathrm{dt}} = -k_{7p}.v[\text{Mad1:C-Mad2}][\text{p31}^{\text{comet}}] + k_{-7p}[\text{Mad1:C-Mad2:p31}^{\text{comet}}] - k_{8p}.v[\text{Cdc20:C-Mad2}][\text{p31}^{\text{comet}}] + k_{-8p}[\text{Cdc20:C-Mad2:p31}^{\text{comet}}] \quad \text{(C.26)}$$

$$\frac{\mathrm{d[Mad1:C\text{-}Mad2:p31^{comet}]}}{\mathrm{dt}} = k_{7p}.v[\text{Mad1:C-Mad2}][\text{p31}^{\text{comet}}] - k_{-7p}[\text{Mad1:C-Mad2:p31}^{\text{comet}}] \quad \text{(C.27)}$$

$$\frac{\mathrm{d[Cdc20:C\text{-}Mad2:p31^{comet}]}}{\mathrm{dt}} = k_{8p}.v[\text{Cdc20:C-Mad2}][\text{p31}^{\text{comet}}] - k_{-8p}[\text{Cdc20:C-Mad2:p31}^{\text{comet}}] \quad \text{(C.28)}$$

C.4 Fitness function

Same as in Appendix B.6.

"The great aim of education is not knowledge but action".

Herbert Spencer (1820 - 1903)

Appendix D

The Dissociation and the Convey Model

D.1 ODEs of the ^{M}SAC model Dissociation variant

◇ First (uncontrolled) case: u′= 1

◇ Second (controlled) case: u′= 1−u

where u = 1 for unattached kinetochore and u = 0 at the attached kinetochore.

$$\frac{d[\text{Mad1:C-Mad2}]}{dt} = -k_1.u[\text{Mad1:C-Mad2}][\text{O-Mad2}] + k_{-1}[\text{Mad1:C-Mad2:O-Mad2}^*] + k_2.u[\text{Mad1:C-Mad2:O-Mad2}^*][\text{Cdc20}] \quad (D.1)$$

$$\frac{d[\text{O-Mad2}]}{dt} = -k_1.u[\text{Mad1:C-Mad2}][\text{O-Mad2}] + k_{-1}[\text{Mad1:C-Mad2:O-Mad2}^*] + k_3[\text{Cdc20:C-Mad2}] - k_6[\text{Cdc20}][\text{O-Mad2}] \quad (D.2)$$

$$\frac{d[\text{Mad1:C-Mad2:O-Mad2}^*]}{dt} = k_1.u[\text{Mad1:C-Mad2}][\text{O-Mad2}] - k_{-1}[\text{Mad1:C-Mad2:O-Mad2}^*] - k_2.u[\text{Mad1:C-Mad2:O-Mad2}^*][\text{Cdc20}] \quad (D.3)$$

$$\frac{d[\text{Cdc20}]}{dt} = -k_2.u[\text{Mad1:C-Mad2:O-Mad2}^*][\text{Cdc20}] + k_3[\text{Cdc20:C-Mad2}] - k_5.u[\text{Cdc20}][\text{Bub3:BubR1}] + k_{-5}[\text{Bub3:BubR1:Cdc20}] - k_6[\text{Cdc20}][\text{O-Mad2}] - k_8[\text{APC}][\text{Cdc20}] + k_{-8}[\text{APC:Cdc20}] \quad (D.4)$$

$$\frac{d[\text{Cdc20:C-Mad2}]}{dt} = k_2.u[\text{Mad1:C-Mad2:O-Mad2}^*][\text{Cdc20}] - k_3[\text{Cdc20:C-Mad2}] - k_4.u[\text{Cdc20:C-Mad2}][\text{Bub3:BubR1}] + k_{-4}[\text{MCC}] + k_6[\text{Cdc20}][\text{O-Mad2}] \quad (D.5)$$

$$\frac{d[\text{Bub3:BubR1}]}{dt} = -k_4.u[\text{Cdc20:C-Mad2}][\text{Bub3:BubR1}] + k_{-4}[\text{MCC}] - k_5.u[\text{Cdc20}][\text{Bub3:BubR1}] + k_{-5}[\text{Bub3:BubR1:Cdc20}] \quad (D.6)$$

$$\frac{d[\text{MCC}]}{dt} = +k_4.u[\text{Cdc20:C-Mad2}][\text{Bub3:BubR1}] - k_{-4}[\text{MCC}] - k_7.u[\text{MCC}][\text{APC}] + k_{-7}.u'[\text{MCC:APC}] \quad (D.7)$$

$$\frac{d[\text{Bub3:BubR1:Cdc20}]}{dt} = k_5.u[\text{Cdc20}][\text{Bub3:BubR1}] - k_{-5}[\text{Bub3:BubR1:Cdc20}] \quad (D.8)$$

$$\frac{d[\text{APC}]}{dt} = -k_7.u[\text{MCC}][\text{APC}] + k_{-7}.u'[\text{MCC:APC}] - k_8[\text{APC}][\text{Cdc20}] + k_{-8}[\text{APC:Cdc20}] \quad (D.9)$$

$$\frac{d[\text{MCC:APC}]}{dt} = +k_7.u[\text{MCC}][\text{APC}] - k_{-7}.u'[\text{MCC:APC}] \quad (D.10)$$

$$\frac{d[\text{APC:Cdc20}]}{dt} = +k_8[\text{APC}][\text{Cdc20}] - k_{-8}[\text{APC:Cdc20}] \quad (D.11)$$

D.2 ODEs of the ᴹSAC model Convey variant

◇ First (uncontrolled) case: u′= 1

◇ Second (controlled) case: u′= 1−u

where u = 1 for unattached kinetochore and $u = 0$ at the attached kinetochore.

$$\frac{\mathrm{d[Mad1:C\text{-}Mad2]}}{\mathrm{dt}} = -\mathrm{k_1.u[Mad1:C\text{-}Mad2][O\text{-}Mad2]} + \mathrm{k_{-1}[Mad1:C\text{-}Mad2:O\text{-}Mad2^*]} + \mathrm{k_2.u[Mad1:C\text{-}Mad2:O\text{-}Mad2^*][Cdc20]} \tag{D.12}$$

$$\frac{\mathrm{d[O\text{-}Mad2]}}{\mathrm{dt}} = -\mathrm{k_1.u[Mad1:C\text{-}Mad2][O\text{-}Mad2]} + \mathrm{k_{-1}[Mad1:C\text{-}Mad2:O\text{-}Mad2^*]} + \mathrm{k_3[Cdc20:C\text{-}Mad2]} - \mathrm{k_6[Cdc20][O\text{-}Mad2]} + \mathrm{k_{-7}.u'[MCC:APC]} \tag{D.13}$$

$$\frac{\mathrm{d[Mad1:C\text{-}Mad2:O\text{-}Mad2^*]}}{\mathrm{dt}} = \mathrm{k_1.u[Mad1:C\text{-}Mad2][O\text{-}Mad2]} - \mathrm{k_{-1}[Mad1:C\text{-}Mad2:O\text{-}Mad2^*]} - \mathrm{k_2.u[Mad1:C\text{-}Mad2:O\text{-}Mad2^*][Cdc20]} \tag{D.14}$$

$$\frac{\mathrm{d[Cdc20]}}{\mathrm{dt}} = -\mathrm{k_2.u[Mad1:C\text{-}Mad2:O\text{-}Mad2^*][Cdc20]} + \mathrm{k_3[Cdc20:C\text{-}Mad2]} - \mathrm{k_5.u[Cdc20][Bub3:BubR1]} + \mathrm{k_{-5}[Bub3:BubR1:Cdc20]} - \mathrm{k_6[Cdc20][O\text{-}Mad2]} - \mathrm{k_8[APC][Cdc20]} + \mathrm{k_{-8}[APC:Cdc20]} \tag{D.15}$$

$$\frac{\mathrm{d[Cdc20:C\text{-}Mad2]}}{\mathrm{dt}} = \mathrm{k_2.u[Mad1:C\text{-}Mad2:O\text{-}Mad2^*][Cdc20]} - \mathrm{k_3[Cdc20:C\text{-}Mad2]} - \mathrm{k_4.u[Cdc20:C\text{-}Mad2][Bub3:BubR1]} + \mathrm{k_{-4}[MCC]} + \mathrm{k_6[Cdc20][O\text{-}Mad2]} \tag{D.16}$$

$$\frac{\mathrm{d[Bub3:BubR1]}}{\mathrm{dt}} = -\mathrm{k_4.u[Cdc20:C\text{-}Mad2][Bub3:BubR1]} + \mathrm{k_{-4}[MCC]} - \mathrm{k_5.u[Cdc20][Bub3:BubR1]} + \mathrm{k_{-5}[Bub3:BubR1:Cdc20]} + \mathrm{k_{-7}.u'[MCC:APC]} \tag{D.17}$$

$$\frac{\mathrm{d[MCC]}}{\mathrm{dt}} = +\mathrm{k_4.u[Cdc20:C\text{-}Mad2][Bub3:BubR1]} - \mathrm{k_{-4}[MCC]} - \mathrm{k_7.u[MCC][APC]} \tag{D.18}$$

$$\frac{\mathrm{d[Bub3:BubR1:Cdc20]}}{\mathrm{dt}} = \mathrm{k_5.u[Cdc20][Bub3:BubR1]} - \mathrm{k_{-5}[Bub3:BubR1:Cdc20]} \tag{D.19}$$

$$\frac{\mathrm{d[APC]}}{\mathrm{dt}} = -\mathrm{k_7.u[MCC][APC]} - \mathrm{k_8[APC][Cdc20]} + \mathrm{k_{-8}[APC:Cdc20]} \tag{D.20}$$

$$\frac{\mathrm{d[MCC:APC]}}{\mathrm{dt}} = +\mathrm{k_7.u[MCC][APC]} - \mathrm{k_{-7}.u'[MCC:APC]} \tag{D.21}$$

$$\frac{\mathrm{d[APC:Cdc20]}}{\mathrm{dt}} = +\mathrm{k_8[APC][Cdc20]} - \mathrm{k_{-8}[APC:Cdc20]} + \mathrm{k_{-7}.u'[MCC:APC]} \tag{D.22}$$

D.3 Optimization

The objective function $f(P)$ assigns a quality (i.e., a positive real number, P=(k_7, k_{-7},k_8, k_{-8})^T) to a given set of parameters P. In our case, the parameters are the reaction constants. In order to fit the parameters with respect to the observed qualitative function of the ^{M}SAC control, we use the APC:Cdc20 concentration before and after kinetochore attachment as a criterion. In each single simulation experiment, we simulate two phases of the spindle attachment status. Our simulation begins in the kinetochore unattached case (phase 1), until equilibrium is reached, then it continues in the attached state (phase 2), again, until steady state conditions are met. We measure the APC:Cdc20 concentration at the end of each phase i, when all concentrations have reached steady state, and compare it with a user given value A_i, which describes the experimentally observed behavior. The two difference values are combined linearly:

$$f(P) = W_1(\sum_{i=1}^{5} [\text{APC:Cdc20}]_{i,\text{Unattached}} - A_{1,i})^2 + W_2(\sum_{i=1}^{5} [\text{APC:Cdc20}]_{i,\text{Attached}} - A_{2,i})^2$$

where W_1, and W_2 are the weights which were 10, and 1 respectively. A_1, and A_2 are the desired phase levels for 5 different point at the beginning, and at the end of each phase (we set $A1, i = 0, 0, 0, 0, 0$ and $A_2, i = 0.001, 0.005, 0.01, 0.01, 0.01$ respectively).

For optimization Techniques and ODEs solvers see Appendix B.

"Gravitation cannot be held responsible for people falling in love. How on earth can you explain in terms of chemistry and physics so important a biological phenomenon as first love? Put your hand on a stove for a minute and it seems like an hour. Sit with that special girl for an hour and it seems like a minute. That's relativity".

Albert Einstein (1879 - 1955)

Appendix E

The Integrative Model of mSAC and EFM Mechanisms

E.1 ODEs of the integrative model of ᴹSAC (Dissociation variant) and EFM

$$\frac{d[\text{Mad1:C-Mad2}]}{dt} = -k_1.u[\text{Mad1:C-Mad2}][\text{O-Mad2}] + k_{-1}[\text{Mad1:C-Mad2:O-Mad2}^*] + k_2.u[\text{Mad1:C-Mad2:O-Mad2}^*][\text{Cdc20}] \tag{E.1}$$

$$\frac{d[\text{O-Mad2}]}{dt} = -k_1.u[\text{Mad1:C-Mad2}][\text{O-Mad2}] + k_{-1}[\text{Mad1:C-Mad2:O-Mad2}^*] + k_3[\text{Cdc20:C-Mad2}] - k_6[\text{Cdc20}][\text{O-Mad2}] \tag{E.2}$$

$$\frac{d[\text{Mad1:C-Mad2:O-Mad2}^*]}{dt} = k_1.u[\text{Mad1:C-Mad2}][\text{O-Mad2}] - k_{-1}[\text{Mad1:C-Mad2:O-Mad2}^*] - k_2.u[\text{Mad1:C-Mad2:O-Mad2}^*][\text{Cdc20}] \tag{E.3}$$

$$\frac{d[\text{Cdc20}]}{dt} = -k_2.u[\text{Mad1:C-Mad2:O-Mad2}^*][\text{Cdc20}] + k_3[\text{Cdc20:C-Mad2}] - k_5.u[\text{Cdc20}][\text{Bub3:BubR1}] + k_{-5}[\text{Bub3:BubR1:Cdc20}] - k_6[\text{Cdc20}][\text{O-Mad2}] - k_8[\text{APC}][\text{Cdc20}] + k_{-8}[\text{APC:Cdc20}] \tag{E.4}$$

$$\frac{d[\text{Cdc20:C-Mad2}]}{dt} = k_2.u[\text{Mad1:C-Mad2:O-Mad2}^*][\text{Cdc20}] - k_3[\text{Cdc20:C-Mad2}] - k_4.u[\text{Cdc20:C-Mad2}][\text{Bub3:BubR1}] + k_{-4}[\text{MCC}] + k_6[\text{Cdc20}][\text{O-Mad2}] \tag{E.5}$$

$$\frac{d[\text{Bub3:BubR1}]}{dt} = -k_4.u[\text{Cdc20:C-Mad2}][\text{Bub3:BubR1}] + k_{-4}[\text{MCC}] - k_5.u[\text{Cdc20}][\text{Bub3:BubR1}] + k_{-5}[\text{Bub3:BubR1:Cdc20}] \tag{E.6}$$

$$\frac{d[\text{MCC}]}{dt} = +k_4.u[\text{Cdc20:C-Mad2}][\text{Bub3:BubR1}] - k_{-4}[\text{MCC}] - k_7.u[\text{MCC}][\text{APC}] + k_{-7}.u'[\text{MCC:APC}] \tag{E.7}$$

$$\frac{d[\text{Bub3:BubR1:Cdc20}]}{dt} = k_5.u[\text{Cdc20}][\text{Bub3:BubR1}] - k_{-5}[\text{Bub3:BubR1:Cdc20}] \tag{E.8}$$

$$\frac{d[\text{APC}]}{dt} = -k_7.u[\text{MCC}][\text{APC}] + k_{-7}.u'[\text{MCC:APC}] - k_8[\text{APC}][\text{Cdc20}] + k_{-8}[\text{APC:Cdc20}] \tag{E.9}$$

$$\frac{d[\text{MCC:APC}]}{dt} = +k_7.u[\text{MCC}][\text{APC}] - k_{-7}.u'[\text{MCC:APC}] \tag{E.10}$$

$$\frac{d[\text{APC:Cdc20}]}{dt} = +k_8[\text{APC}][\text{Cdc20}] - k_{-8}[\text{APC:Cdc20}] + k_{14}[\text{APC:Cdc20}][\text{Cdh1}] \tag{E.11}$$

$$\frac{d[\text{APC:Cdh1}]}{dt} = +k_{14}[\text{APC:Cdc20}][\text{Cdh1}] \tag{E.12}$$

$$\frac{d[\text{Cdh1}]}{dt} = -k_{14}[\text{APC:Cdh1}][\text{Cdh1}] - k_{13}[\text{Cyclin B}]\frac{[\text{Cdh1}]}{k_{13M} + [\text{Cdh1}]} + k_{-13}[\text{Cdc14A*}]\frac{[\text{Cdh1}^P]}{k_{-13M} + [\text{Cdh1}^P]} \tag{E.13}$$

$$\frac{d[\text{Cdh1}]^P}{dt} = +k_{13}[\text{Cyclin B}]\frac{[\text{Cdh1}]}{k_{13M} + [\text{Cdh1}]} - k_{-13}[\text{Cdc14A*}]\frac{[\text{Cdh1}^P]}{k_{-13M} + [\text{Cdh1}^P]} \tag{E.14}$$

$$\frac{d[\text{Separase:Securin}]}{dt} = -k_9[\text{APC:Cdc20}][\text{Separase:Securin}] \tag{E.15}$$

$$\frac{d[\text{Separase}]}{dt} = +k_9[\text{APC:Cdc20}][\text{Separase:Securin}] \tag{E.16}$$

$$\frac{d[\text{Cyclin B}]}{dt} = +k_{11} - k_{10}[\text{APC:Cdc20}][\text{Cyclin B}] - k_{15}[\text{APC:Cdh1}][\text{Cyclin B}] \tag{E.17}$$

$$\frac{d[\text{Cdc14A}]}{dt} = +k_{12}[\text{Cdc14A*}] - k_{-12}[\text{Separase}]\frac{[\text{Cdc14A}]}{k_{-12M} + [\text{Cdc14A}]} \tag{E.18}$$

$$\frac{d[\text{Cdc14A*}]}{dt} = -k_{12}[\text{Cdc14A*}] + k_{-12}[\text{Separase}]\frac{[\text{Cdc14A}]}{k_{-12M} + [\text{Cdc14A}]} \tag{E.19}$$

E.2 ODEs of the integrative model of ᴹSAC (Convey variant) and EFM

$$\frac{\mathrm{d[Mad1:C\text{-}Mad2]}}{\mathrm{dt}} = -\mathrm{k_1}.\mathrm{u[Mad1:C\text{-}Mad2][O\text{-}Mad2]} + \mathrm{k_{-1}[Mad1:C\text{-}Mad2:O\text{-}Mad2^*]} + \mathrm{k_2}.\mathrm{u[Mad1:C\text{-}Mad2:O\text{-}Mad2^*][Cdc20]} \tag{E.20}$$

$$\frac{\mathrm{d[O\text{-}Mad2]}}{\mathrm{dt}} = -\mathrm{k_1}.\mathrm{u[Mad1:C\text{-}Mad2][O\text{-}Mad2]} + \mathrm{k_{-1}[Mad1:C\text{-}Mad2:O\text{-}Mad2^*]} + \mathrm{k_3[Cdc20:C\text{-}Mad2]} - \mathrm{k_6[Cdc20][O\text{-}Mad2]} + \mathrm{k_{-7}}.\mathrm{u'[MCC:APC]} \tag{E.21}$$

$$\frac{\mathrm{d[Mad1:C\text{-}Mad2:O\text{-}Mad2^*]}}{\mathrm{dt}} = \mathrm{k_1}.\mathrm{u[Mad1:C\text{-}Mad2][O\text{-}Mad2]} - \mathrm{k_{-1}[Mad1:C\text{-}Mad2:O\text{-}Mad2^*]} - \mathrm{k_2}.\mathrm{u[Mad1:C\text{-}Mad2:O\text{-}Mad2^*][Cdc20]} \tag{E.22}$$

$$\frac{\mathrm{d[Cdc20]}}{\mathrm{dt}} = -\mathrm{k_2}.\mathrm{u[Mad1:C\text{-}Mad2:O\text{-}Mad2^*][Cdc20]} + \mathrm{k_3[Cdc20:C\text{-}Mad2]} - \mathrm{k_5}.\mathrm{u[Cdc20][Bub3:BubR1]} + \mathrm{k_{-5}[Bub3:BubR1:Cdc20]} - \mathrm{k_6[Cdc20][O\text{-}Mad2]} - \mathrm{k_8[APC][Cdc20]} + \mathrm{k_{-8}[APC:Cdc20]} \tag{E.23}$$

$$\frac{\mathrm{d[Cdc20:C\text{-}Mad2]}}{\mathrm{dt}} = \mathrm{k_2}.\mathrm{u[Mad1:C\text{-}Mad2:O\text{-}Mad2^*][Cdc20]} - \mathrm{k_3[Cdc20:C\text{-}Mad2]} - \mathrm{k_4}.\mathrm{u[Cdc20:C\text{-}Mad2][Bub3:BubR1]} + \mathrm{k_{-4}[MCC]} + \mathrm{k_6[Cdc20][O\text{-}Mad2]} \tag{E.24}$$

$$\frac{\mathrm{d[Bub3:BubR1]}}{\mathrm{dt}} = -\mathrm{k_4}.\mathrm{u[Cdc20:C\text{-}Mad2][Bub3:BubR1]} + \mathrm{k_{-4}[MCC]} - \mathrm{k_5}.\mathrm{u[Cdc20][Bub3:BubR1]} + \mathrm{k_{-5}[Bub3:BubR1:Cdc20]} + \mathrm{k_{-7}}.\mathrm{u'[MCC:APC]} \tag{E.25}$$

$$\frac{\mathrm{d[MCC]}}{\mathrm{dt}} = +\mathrm{k_4}.\mathrm{u[Cdc20:C\text{-}Mad2][Bub3:BubR1]} - \mathrm{k_{-4}[MCC]} - \mathrm{k_7}.\mathrm{u[MCC][APC]} \tag{E.26}$$

$$\frac{\mathrm{d[Bub3:BubR1:Cdc20]}}{\mathrm{dt}} = \mathrm{k_5}.\mathrm{u[Cdc20][Bub3:BubR1]} - \mathrm{k_{-5}[Bub3:BubR1:Cdc20]} \tag{E.27}$$

$$\frac{\mathrm{d[APC]}}{\mathrm{dt}} = -\mathrm{k_7}.\mathrm{u[MCC][APC]} - \mathrm{k_8[APC][Cdc20]} + \mathrm{k_{-8}[APC:Cdc20]} \tag{E.28}$$

$$\frac{\mathrm{d[MCC:APC]}}{\mathrm{dt}} = +\mathrm{k_7}.\mathrm{u[MCC][APC]} - \mathrm{k_{-7}}.\mathrm{u'[MCC:APC]} \tag{E.29}$$

$$\frac{\mathrm{d[APC:Cdc20]}}{\mathrm{dt}} = +\mathrm{k_8[APC][Cdc20]} - \mathrm{k_{-8}[APC:Cdc20]} + \mathrm{k_{-7}}.\mathrm{u'[MCC:APC]} - \mathrm{k_{14}[APC:Cdc20][Cdh1]} \tag{E.30}$$

$$\frac{\mathrm{d[APC:Cdh1]}}{\mathrm{dt}} = +\mathrm{k_{14}[APC:Cdc20][Cdh1]} \tag{E.31}$$

$$\frac{\mathrm{d[Cdh1]}}{\mathrm{dt}} = -\mathrm{k_{14}[APC:Cdh1][Cdh1]} - \mathrm{k_{13}[Cyclin\ B]}\frac{\mathrm{[Cdh1]}}{\mathrm{k_{13M} + [Cdh1]}} + \mathrm{k_{-13}[Cdc14A^*]}\frac{\mathrm{[Cdh1^P]}}{\mathrm{k_{-13M} + [Cdh1^P]}} \tag{E.32}$$

$$\frac{\mathrm{d[Cdh1]^P}}{\mathrm{dt}} = +\mathrm{k_{13}[Cyclin\ B]}\frac{\mathrm{[Cdh1]}}{\mathrm{k_{13M} + [Cdh1]}} - \mathrm{k_{-13}[Cdc14A^*]}\frac{\mathrm{[Cdh1^P]}}{\mathrm{k_{-13M} + [Cdh1^P]}} \tag{E.33}$$

$$\frac{\mathrm{d[Separase:Securin]}}{\mathrm{dt}} = -\mathrm{k_9[APC:Cdc20][Separase:Securin]} \tag{E.34}$$

$$\frac{\mathrm{d[Separase]}}{\mathrm{dt}} = +\mathrm{k_9[APC:Cdc20][Separase:Securin]} \tag{E.35}$$

$$\frac{\mathrm{d[Cyclin\ B]}}{\mathrm{dt}} = +\mathrm{k_{11}} - \mathrm{k_{10}[APC:Cdc20][Cyclin\ B]} - \mathrm{k_{15}[APC:Cdh1][Cyclin\ B]} \tag{E.36}$$

$$\frac{\mathrm{d[Cdc14A]}}{\mathrm{dt}} = +\mathrm{k_{12}[Cdc14A^*]} - \mathrm{k_{-12}[Separase]}\frac{\mathrm{[Cdc14A]}}{\mathrm{k_{-12M} + [Cdc14A]}} \tag{E.37}$$

$$\frac{\mathrm{d[Cdc14A^*]}}{\mathrm{dt}} = -\mathrm{k_{12}[Cdc14A^*]} + \mathrm{k_{-12}[Separase]}\frac{\mathrm{[Cdc14A]}}{\mathrm{k_{-12M} + [Cdc14A]}} \tag{E.38}$$

E. THE INTEGRATIVE MODEL OF ^{M}SAC AND EFM MECHANISMS

References

Abrieu, A., Magnaghi-Jaulin, L., Kahana, J. A., Peter, M., Castro, A., Vigneron, S., Lorca, T., Cleveland, D. W., Labbe, J. C., 2001. Mps1 is a kinetochore-associated kinase essential for the vertebrate mitotic checkpoint. Cell 106 (1), 83–93.

Acquaviva, C., Herzog, F., Kraft, C., Pines, J., 2004. The anaphase promoting complex/cyclosome is recruited to centromeres by the spindle assembly checkpoint. Nat Cell Biol 6 (9), 892–8.

Alberts, B., Jonson, A., Lewis, J., Raff, M., Roberts, K., Walter, P., 2002. Molecular biology of the cell, 4th Edition. Garland Science ,USA.

Alexandru, G., Zachariae, W., Schleiffer, A., Nasmyth, K., 1999. Sister chromatid separation and chromosome re-duplication are regulated by different mechanisms in response to spindle damage. EMBO J 18 (10), 2707–21.

Aravind, L., Koonin, E. V., 1998. The HORMA domain: a common structural denominator in mitotic checkpoints, chromosome synapsis and DNA repair. Trends Biochem Sci. 23 (8), 284–6.

Aristarkhov, A., Eytan, E., Moghe, A., Admon, A., Hershko, A., Ruderman, J. V., April 1996. E2-c, a cyclin-selective ubiquitin carrier protein required for the destruction of mitotic cyclins. Proc. Natl. Acad. Sci. 93 (9), 4294–9.

Baker, D., Jeganathan, K., Cameron, J. D., Thompson, M., Jueja, S., Kopecka, A., Kumar, R., Jenkins, R. B., De Groen, P. C., Roche, P., Van Deursen, J., 2004. BubR1 insufficiency causes early onset of aging - associted phenotypes and infetility in mice. Natrure Genetics 36 (7), 744–49.

Barabási, A.-L., 2002. Linked: The New Science of Networks. Perseus, Cambridge, MA.

Barabási, A.-L., Oltvai, Z. N., 2004. Network biology: understanding the cell's functional organization. Nat Rev Genet 5 (2), 101–13.

Basu, J., Bousbaa, H., Logarinho, E., Li, Z., Williams, B. C., Lopes, C., Sunkel, C. E., Goldberg, M. L., 1999. Mutations in the essential spindle checkpoint gene bub1 cause chromosome missegregation and fail to block apoptosis in Drosophila. J Cell Biol 146 (1), 13–28.

Battogtokh, D., Tyson, J. J., 2004. Bifurcation analysis of a model of the budding yeast cell cycle. Chaos 14 (3), 653–61.

Bembenek, J., Yu, H., 2001a. Regulation of the anaphase-promoting complex by the dual specificity phosphatase human Cdc14a. J Biol Chem.

Bembenek, J., Yu, H., 2001b. Regulation of the anaphase-promoting complex by the dual specificity phosphatase human Cdc14a. J Biol Chem 276 (51), 48237–42.

Bharadwaj, R., Yu, H., 2004. The spindle checkpoint, aneuploidy, and cancer. Oncogene 23 (11), 2016–27.

Biggins, S., Murray, A. W., 2001. The budding yeast protein kinase Ipl1/Aurora allows the absence of tension to activate the spindle checkpoint. Genes Dev 15 (23), 3118–29.

Bloom, J., Cross, F. R., 2007. Multiple levels of cyclin specificity in cell-cycle control. Nat Rev Mol Cell Biol 8 (2), 149–60.

Blow, J. J., Tanaka, T. U., 2005. The chromosome cycle: coordinating replication and segregation. Second in the cycles review series. EMBO Rep 6 (11), 1028–34.

Bolanos-Garcia, V. M., Beaufils, S., Renault, A., Grossmann, J. G., Brewerton, S., Lee, M., Venkitaraman, A., Blundell, T. L., 2005. The conserved N-terminal region of the mitotic checkpoint protein BUBR1: a putative TPR motif of high surface activity. Biophys J 89 (4), 2640–9.

Boronat, S., Campbell, J. L., 2007. Mitotic Cdc6 stabilizes anaphase-promoting complex substrates by a partially Cdc28-independent mechanism, and this stabilization is suppressed by deletion of Cdc55. Mol Cell Biol 27 (3), 1158–71.

Bosl, W. J., Li, R., 2005. Mitotic-exit control as an evolved complex system. Cell 121 (3), 325–33.

Brady, D. M., Hardwick, K. G., 2000. Complex formation between Mad1p, Bub1p and Bub3p is crucial for spindle checkpoint function. Curr Biol 10 (11), 675–8.

Braunstein, I., Miniowitz, S., Moshe, Y., Hershko, A., 2007. Inhibitory factors associated with anaphase-promoting complex/cylosome in mitotic checkpoint. Proc Natl Acad Sci U S A 104 (12), 4870–5.

Bruggeman, F. J., 2007. Systems biology: at last an integrative wet and dry biology! Biological Theory 2 (2), 183188.

Bryja, V., Pachernik, J., Faldikova, L., Krejci, P., Pogue, R., Nevriva, I. I., Dvorak, P., Hampl, A., 2004. Complex qualitative models in biology : A new approach. Complexus 2, 140 151.

Buffin, E., Emre, D., Karess, R. E., 2007. Flies without a spindle checkpoint. Nat Cell Biol 9 (5), 565–72.

Burton, J. L., Solomon, M. J., 2007. Mad3p, a pseudosubstrate inhibitor of APCCdc20 in the spindle assembly checkpoint. Genes Dev 21 (6), 655–67.

Buschhorn, B. A., Peters, J.-M., 2006. How APC/C orders destruction. Nat Cell Biol 8 (3), 209–11.

Campbell, M. S., Chan, G. K., Yen, T. J., 2001. Mitotic checkpoint proteins HsMAD1 and HsMAD2 are associated with nuclear pore complexes in interphase. J Cell Sci 114 (Pt 5), 953–63.

Centler, F., Feb. 2008. Chemical organizations in natural reaction networks. Ph.D. thesis, Friedrich Schiller University Jena.

Chan, G. K., Jablonski, S. A., Starr, D. A., Goldberg, M. L., Yen, T. J., 2000. Human Zw10 and ROD are mitotic checkpoint proteins that bind to kinetochores. Nat Cell Biol 2 (12), 944–7.

Chan, G. K., Jablonski, S. A., Sudakin, V., Hittle, J. C., Yen, T. J., 1999. Human BUBR1 is a mitotic checkpoint kinase that monitors CENP-E functions at kinetochores and binds the cyclosome/APC. J Cell Biol 146 (5), 941–54.

Chan, G. K., Liu, S.-T., Yen, T. J., 2005. Kinetochore structure and function. Trends Cell Biol 15 (11), 589–98.

Chan, G. K., Schaar, B. T., Yen, T. J., 1998. Characterization of the kinetochore binding domain of CENP-E reveals interactions with the kinetochore proteins CENP-F and hBUBR1. J Cell Biol 143 (1), 49–63.

Chan, G. K., Yen, T. J., 2003. The mitotic checkpoint: a signaling pathway that allows a single unattached kinetochore to inhibit mitotic exit. Prog Cell Cycle Res 5, 431–9.

Chang, H.-Y., Levasseur, M., Jones, K. T., 2004. Degradation of APCcdc20 and APCcdh1 substrates during the second meiotic division in mouse eggs. J Cell Sci 117 (Pt 26), 6289–96.

Chang, L., Morrell, J. L., Feoktistova, A., Gould, K. L., 2001. Study of cyclin proteolysis in anaphase-promoting complex (APC) mutant cells reveals the requirement for APC function in the final steps of the fission yeast septation initiation network. Mol Cell Biol 21 (19), 6681–94.

Chaouiya, C., 2007. Petri net modelling of biological networks. Brief Bioinform 8 (4), 210–9.

Cheeseman, I. M., Anderson, S., Jwa, M., Green, E. M., seog Kang, J., 3rd Yates, J. R., Chan, C. S. M., Drubin, D. G., Barnes, G., 2002. Phospho-regulation of kinetochore-microtubule attachments by the Aurora kinase Ipl1p. Cell 111 (2), 163–72.

Chen, K. C., Calzone, L., Csikasz-Nagy, A., Cross, F. R., Novák, B., Tyson, J. J., 2004. Integrative analysis of cell cycle control in budding yeast. Mol Biol Cell 15 (8), 3841–62.

Chen, K.-C., Wang, T.-Y., Tseng, H.-H., Huang, C.-Y. F., Kao, C.-Y., 2005. A stochastic differential equation model for quantifying transcriptional regulatory network in Saccharomyces cerevisiae. Bioinformatics 21 (12), 2883–90.

Chen, R., Aug 2002a. BubR1 is essential for kinetochore localization of other spindle checkpoint proteins and its phosphorylation requires Mad1. J Cell Biol. 158 (3), 487–96.

Chen, R.-H., 2002b. BubR1 is essential for kinetochore localization of other spindle checkpoint proteins and its phosphorylation requires Mad1. J Cell Biol 158 (3), 487–96.

Chen, R.-H., Brady, D. M., Smith, D., Murray, A. W., Hardwick, K. G., 1999a. The spindle checkpoint of budding yeast depends on a tight complex between the Mad1 and Mad2 proteins. Mol. Biol. Cell 10, 2607–18.

Chen, R.-H., Brady, D. M., Smith, D., Murray, A. W., Hardwick, K. G., 1999b. The spindle checkpoint of budding yeast depends on a tight complex between the Mad1 and Mad2 proteins. Mol. Biol. Cell 10, 2607–18.

Chen, R.-H., Brady, D. M., Smith, D., Murray, A. W., Hardwick, K. G., 1999c. The spindle checkpoint of budding yeast depends on a tight complex between the Mad1 and Mad2 proteins. Mol. Biol. Cell 10, 2607–18.

Chen, R. H., Shevchenko, A., Mann, M., Murray, A. W., 1998. Spindle checkpoint protein Xmad1 recruits Xmad2 to unattached kinetochores. J Cell Biol 143 (2), 283–95.

Chung, E., Chen, R.-H., 2002. Spindle checkpoint requires Mad1-bound and Mad1-free Mad2. Mol Biol Cell 13 (5), 1501–11.

Chung, E., Chen, R.-H., 2003. Phosphorylation of Cdc20 is required for its inhibition by the spindle checkpoint. Nature Cell Biology 5, 748 – 753.

Ciliberto, A., Lukacs, A., Toth, A., Tyson, J. J., Novák, B., 2005. Rewiring the exit from mitosis. Cell Cycle 4 (8), 1107–12.

Cleveland, D. W., Mao, Y., Sullivan, K. F., 2003. Centromeres and kinetochores from epigenetics to mitotic checkpoint signaling. Cell 112 (4), 407–421.

Compton, D. A., 2006. Chromosomes walk the line. Nat Cell Biol 8 (4), 308–10.

COMSOL, 2008. FEMLAB: homepage. Retrieved January 29, 2008, from `http://www.comsol.com//`.

D'Amours, D., Amon, A., 2004. At the interface between signaling and executing anaphase–Cdc14 and the FEAR network. Genes Dev 18 (21), 2581–95.

D'Angiolella, V., Mari, C., Nocera, D., Rametti, L., Grieco, D., 2003. The spindle checkpoint requires cyclin-dependent kinase activity. Genes Dev 17 (20), 2520–5.

Davenport, J., Harris, L. D., Goorha, R., 2006. Spindle checkpoint function requires Mad2-dependent Cdc20 binding to the Mad3 homology domain of BubR1. Exp Cell Res 312 (10), 1831–42.

Dawson, I. A., Roth, S., Artavanis-Tsakonas, S., 1995. The Drosophila cell cycle gene fizzy is required for normal degradation of cyclins A and B during mitosis and has homology to the CDC20 gene of Saccharomyces cerevisiae. J Cell Biol 129 (3), 725–37.

de Jong, H., 2002. Modeling and simulation of genetic regulatory systems: a literature review. J Comput Biol 9 (1), 67–103.

DeAntoni, A., Pearson, C. G., Cimini, D., Canman, J. C., Sala, V., Nezi, L., Mapelli, M., Sironi, L., Faretta, M., Salmon, E. D., Musacchio, A., 2005a. The Mad1/Mad2 complex as a template for Mad2 activation in the spindle assembly checkpoint. Curr Biol 15 (3), 214–25.

DeAntoni, A., Sala, V., Musacchio, A., 2005b. Explaining the oligomerization properties of the spindle assembly checkpoint protein Mad2. Philos Trans R Soc Lond B Biol Sci 360 (1455), 637–47, discussion 447–8.

Diaz-Martinez, L. A., Yu, H., 2007. Running on a treadmill: dynamic inhibition of APC/C by the spindle checkpoint. Cell Div 2, 23.

Ditchfield, C., Johnson, V. L., Tighe, A., Ellston, R., Haworth, C., Johnson, T., Mortlock, A., Keen, N., Taylor, S. S., Apr 2003. Aurora B couples chromosome alignment with anaphase by targeting BubR1, Mad2, and Cenp-E to kinetochores. J Cell Biol. 161 (2), 267–80.

Dittrich, P., Speroni di Fenizio, P., 2006. Chemical organization theory. B. Math. Biol.In print.

Dobles, M., Liberal, V., Scott, M. L., Benezra, R., Sorger, P. K., 2000. Chromosome missegregation and apoptosis in mice lacking the mitotic checkpoint protein Mad2. Cell 101 (6), 635–45.

Doncic, A., Ben-Jacob, E., Barkai, N., 2005. Evaluating putative mechanisms of the mitotic spindle checkpoint. Proc Natl Acad Sci U S A 102 (18), 6332–7.

Doncic, A., Ben-Jacob, E., Barkai, N., 2006. Noise resistance in the spindle assembly checkpoint. Mol Syst Biol 2, 2006.0027.

Dube, P., Herzog, F., Gieffers, C., Sander, B., Riedel, D., Muller, S. A., Engel, A., Peters, J.-M., Stark, H., 2005. Localization of the coactivator Cdh1 and the cullin subunit Apc2 in a cryo-electron microscopy model of vertebrate APC/C. Mol Cell 20 (6), 867–79.

Ducat, D., Zheng, Y., 2004. Aurora kinases in spindle assembly and chromosome segregation. Exp Cell Res 301 (1), 60–7.

Eaton, J. W., 2008. Octave: homepage. Retrieved January 10, 2008, from `http://www.octave.org/`.

Esteban, V., Vazquez-Novelle, M. D., Calvo, E., Bueno, A., Sacristan, M. P., 2006. Human Cdc14A reverses CDK1 phosphorylation of Cdc25A on serines 115 and 320. Cell Cycle 5 (24), 2894–8.

Eytan, E., Moshe, Y., Braunstein, I., Hershko, A., 2006. Roles of the anaphase-promoting complex/cyclosome and of its activator Cdc20 in functional substrate binding. Proc Natl Acad Sci U S A 103 (7), 2081–6.

Fang, G., 2002. Checkpoint protein BubR1 acts synergistically with Mad2 to inhibit anaphase-promoting complex. Mol Biol Cell 13 (3), 755–66.

Fang, G., Yu, H., Kirschner, M. W., April 1998a. The checkpoint protein Mad2 and the mitotic regulator Cdc20 form a ternary complex with the anaphase-promoting complex to control anaphase initiation. Genes Dev 12 (12), 1871–1883.

Fang, G., Yu, H., Kirschner, M. W., 1998b. The checkpoint protein mad2 and the mitotic regulator cdc20 form a ternary complex with the anaphase-promoting complex to control anaphase initiation. Genes & Dev. 12, 1871–1883.

Fisk, H. A., Mattison, C. P., Winey, M., 2004. A field guide to the Mps1 family of protein kinases. Cell Cycle 3 (4), 439–42.

Fisk, H. A., Winey, M., 2001. The mouse Mps1p-like kinase regulates centrosome duplication. Cell 106 (1), 95–104.

Fisk, H. A., Winey, M., 2004. Spindle regulation: Mps1 flies into new areas. Curr Biol 14 (24), R1058–60.

Flemming, W., 1882. Zellsubstanz, Kern und Zelltheilung. F. C. W. Vogel, Leipzig.

Fontana, W., Buss, L. W., 1994. 'The arrival of the fittest': Towards a theory of biological organization. B. Math. Biol. 56, 1–64.

Fraschini, R., Beretta, A., Sironi, L., Musacchio, A., Lucchini, G., Piatti, S., 2001. Bub3 interaction with Mad2, Mad3 and Cdc20 is mediated by WD40 repeats and does not require intact kinetochores. EMBO J. 20 (23), 664859.

Garcia-Saez, I., Yen, T., Wade, R. H., Kozielski, F., 2004. Crystal structure of the motor domain of the human kinetochore protein CENP-E. J Mol Biol 340 (5), 1107–16.

Geymonat, M., Spanos, A., Walker, P. A., Johnston, L. H., Sedgwick, S. G., 2003. In vitro regulation of budding yeast Bfa1/Bub2 GAP activity by Cdc5. J Biol Chem 278 (17), 14591–4.

Gillespie, D. T., 2002. The chemical langevin and fokker-planck equations for the reversible isomerization reaction. J. Phys. Chem. A 106, 5063–5071.

Gillett, E. S., Espelin, C. W., Sorger, P. K., 2004. Spindle checkpoint proteins and chromosome-microtubule attachment in budding yeast. J Cell Biol 164 (4), 535–46.

Glotzer, M., Murray, A. W., Kirschner, M. W., 1991. Cyclin is degraded by the ubiquitin pathway. Nature 349 (6305), 132–8.

Goldbeter, A., 1991. A minimal cascade model for the mitotic oscillator involving cyclin and cdc2 kinase. Proc Natl Acad Sci U S A 88 (20), 9107–11.

Griffis, E. R., Stuurman, N., Vale, R. D., June 2007. J Cell Biol 177 (6), 1005–1015.

Gupta, A., Inaba, S., Wong, O. K., Fang, G., Liu, J., 2003. Breast cancer-specific gene 1 interacts with the mitotic checkpoint kinase BubR1. Oncogene 22 (48), 7593–9.

Habu, T., Kim, S. H., Weinstein, J., Matsumoto, T., 2002. Identification of a MAD2-binding protein, CMT2, and its role in mitosis. EMBO J 21 (23), 6419–28.

Hagan, I., Hayles, J., Nurse, P., 1988. Cloning and sequencing of the cyclin-related cdc13+ gene and a cytological study of its role in fission yeast mitosis. J Cell Sci 91 (Pt 4), 587–95.

Hagan, R. S., Sorger, P. K., 2005. Cell biology: the more MAD, the merrier. Nature 434 (7033), 575–7.

Hagting, A., Elzen, N. D., Vodermaier, H. C., Waizenegger, I. C., Peters, J.-M., Pines, J., 2002. Human securin proteolysis is controlled by the spindle checkpoint and reveals when the APC/C switches from activation by Cdc20 to Cdh1. J Cell Biol 157 (7), 1125–37.

Hanks, S., Coleman, K., Reid, S., Plaja, A., Firth, H., Fitzpatrick, D., Kidd, A., Mehes, K., Nash, R., Robin, N., Shannon, N., Tolmie, J., Swansbury, J., Irrthum, A., Douglas, J., Rahman, N., 2004. Constitutional aneuploidy and cancer predisposition caused by biallelic mutations in BUB1B. Nat Genet 36 (11), 1159–61.

Hansen, N., Kern, S., 2004. Evaluating the cma evolution strategy on multimodal test functions. In: Eighth International Conference on Parallel Problem Solving from Nature PPSN VIII. Springer. pp. 282–291.

Hansen, N., Muller, S. D., Koumoutsakos, P., 2003. Reducing the time complexity of the derandomized evolution strategy with covariance matrix adaptation (CMA-ES). Evol Comput 11 (1), 1–18.

Hardwick, K. G., 2005. Checkpoint signalling: Mad2 conformers and signal propagation. Curr Biol 15 (4), R122–4.

Hardwick, K. G., Johnston, R. C., Smith, D. L., Murray, A. W., March 2000. MAD3 encodes a novel component of the spindle checkpoint which interacts with Bub3p, Cdc20p, and Mad2p. The Journal of Cell Biology 148 (5), 871–882.

Hardwick, K. G., Murray, A. W., 1995. Madlp, a phosphoprotein component of the spindle assembly checkpoint in budding yeast. J Cell Biol 131 (3), 709–20.

Hardwick, K. G., Weiss, E., Luca, F. C., Winey, M., Murray, A. W., 1996. Activation of the budding yeast spindle assembly checkpoint without mitotic spindle disruption. Science 273 (5277), 953–6.

Harper, J. W., Burton, J. L., Solomon, M. J., 2002. The anaphase-promoting complex: it's not just for mitosis any more. Genes Dev 16 (17), 2179–206.

Hartwell, L. H., Culotti, J., Reid, B., 1970. Genetic control of the cell-division cycle in yeast. I. Detection of mutants. Proc Natl Acad Sci U S A 66 (2), 352–9.

Hartwell, L. H., Mortimer, R. K., Culotti, J., , Culotti, M., 1973. Genetic Control of the Cell Division Cycle in Yeast: V. Genetic Analysis of cdc Mutants. Genetics 74 (2), 267–286.

Hauf, S., Cole, R. W., LaTerra, S., Zimmer, C., Schnapp, G., Walter, R., Heckel, A., van Meel, J., Rieder, C. L., Peters, J.-M., Apr 2003. The small molecule hesperadin reveals a role for aurora b in correcting kinetochoremicrotubule attachment and in maintaining the spindle assembly checkpoint. J Cell Biol. 161 (2), 281–294.

He, X., Patterson, T. E., Sazer, S., 1997. The Schizosaccharomyces pombe spindle checkpoint protein mad2p blocks anaphase and genetically interacts with the anaphase-promoting complex. Proc Natl Acad Sci U S A 94 (15), 7965–70.

Heald, R., 2006. Cell biology. Serving up a plate of chromosomes. Science 311 (5759), 343–4.

Heinrich, R., Schuster, S., August 1996. The Regulation Of Cellular Systems. Springer.

Hershko, A., Ganoth, D., Sudakin, V., Dahan, A., Cohen, L., Luca, F., Ruderman, J., Eytan, E., Feb 1994. Components of a system that ligates cyclin to ubiquitin and their regulation by the protein kinase cdc2. J. Biol. Chem. 269 (7), 4940–6.

Hoffman, D. B., Pearson, C. G., Yen, T. J., Howell, B. J., Salmon, E. D., 2001. Microtubule-dependent changes in assembly of microtubule motor proteins and mitotic spindle checkpoint proteins at PtK1 kinetochores. Mol Biol Cell 12 (7), 1995–2009.

Holland, J. H., 1995. Hidden Order: How Adaptation Builds Complexity. Reading, MA: Addison-Wesley.

Hooke, R., Jeeves, T. A., 1961. " direct search" solution of numerical and statistical problems. J. ACM 8 (2), 212–229.

Howell, B., McEwen, B., Canman, J., Hoffman, D., Farrar, E., Rieder, C., Salmon, E., Dec 2001. Cytoplasmic dynein/dynactin drives kinetochore protein transport to the spindle poles and has a role in mitotic spindle checkpoint inactivation. J. Cell Biol. 155, 1159 – 1172.

Howell, B. J., Hoffman, D. B., Fang, G., Murray, A. W., Salmon, E. D., 2000a. Visualization of Mad2 dynamics at kinetochores, along spindle fibers, and at spindle poles in living cells. J Cell Biol 150 (6), 1233–50.

Howell, B. J., Hoffman, D. B., Fang, G., Murray, A. W., Salmon, E. D., 2000b. Visualization of Mad2 dynamics at kinetochores, along spindle fibers, and at spindle poles in living cells. J Cell Biol 150 (6), 1233–50.

Howell, B. J., Moree, B., Farrar, E. M., Stewart, S., Fang, G., Salmon, E. D., 2004. Spindle checkpoint protein dynamics at kinetochores in living cells. Curr Biol 14 (11), 953–64.

Hoyt, M., Totis, L., Roberts, B., Aug 1991. S. cerevisiae genes required for cell cycle arrest in response to loss of microtubule function. Cell 66 (3), 507–17.

Hoyt, M. A., 2001. A new view of the spindle checkpoint. J Cell Biol 154 (5), 909–11.

Hu, F., Elledge, S. J., 2002. Bub2 is a cell cycle regulated phospho-protein controlled by multiple checkpoints. Cell Cycle 1 (5), 351–5.

Huang, J. N., Park, I., Ellingson, E., Littlepage, L. E., Pellman, D., 2001. Activity of the APC(Cdh1) form of the anaphase-promoting complex persists until S phase and prevents the premature expression of Cdc20p. J Cell Biol 154 (1), 85–94.

Hwang, L. H., Lau, L. F., Smith, D. L., Mistrot, C. A., Hardwick, K. G., Hwang, E. S., Amon, A., Murray, A. W., 1998. Budding yeast Cdc20: a target of the spindle checkpoint. Science 279 (5353), 1041–4.

Ibrahim, B., Diekmann, S., Schmitt, E., Dittrich, P., Feb 2008a. *In-Silico* modeling of the mitotic spindle assembly checkpoint. PLoS ONE 3 (2), e1555.
URL `http://www.plosone.org/doi/pone.0001555`

Ibrahim, B., Dittrich, P., Diekmann, S., Schmitt, E., 2007. Stochastic effects in a compartmental model for mitotic checkpoint regulation. Journal of Integrative Bioinformatics 4 (3).

Ibrahim, B., Dittrich, P., Diekmann, S., Schmitt, E., 2008b. Mad2 binding is not sufficient for complete Cdc20 sequestering in mitotic transition control (an in silico study). Biophys Chem 134 (1-2), 93–100.

Ibrahim, B., Schmitt, E., Dittrich, P., Diekmann, S., 2008c. *In-silico* study of kinetochore control, amplification, and inhibition effects in MCC assemblySubmitted Paper.

Iwanaga, Y., Chi, Y.-H., Miyazato, A., Sheleg, S., Haller, K., Peloponese, J.-M. J., Li, Y., Ward, J. M., Benezra, R., Jeang, K.-T., 2007. Heterozygous deletion of mitotic arrest-deficient protein 1 (MAD1) increases the incidence of tumors in mice. Cancer Res 67 (1), 160–6.

Iwanaga, Y., Kasai, T., Kibler, K., Jeang, K.-T., 2002. Characterization of regions in hsMAD1 needed for binding hsMAD2. A polymorphic change in an hsMAD1 leucine zipper affects MAD1-MAD2 interaction and spindle checkpoint function. J Biol Chem 277 (34), 31005–13.

Jaspersen, S. L., Charles, J. F., Tinker-Kulberg, R. L., Morgan, D. O., 1998. A late mitotic regulatory network controlling cyclin destruction in Saccharomyces cerevisiae. Mol Biol Cell 9 (10), 2803–17.

Kaern, M., Elston, T. C., Blake, W. J., Collins, J. J., 2005. Stochasticity in gene expression: from theories to phenotypes. Nat Rev Genet 6 (6), 451–64.

Kaleta, C., Centler, F., di Fenizio, P. S., Dittrich, P., 2007. Phenotype prediction in regulated metabolic networks. BMC Bioinformatics.

Kalitsis, P., Earle, E., Fowler, K. J., Choo, K. H., 2000. Bub3 gene disruption in mice reveals essential mitotic spindle checkpoint function during early embryogenesis. Genes Dev 14 (18), 2277–82.

Kallio, M. J., Beardmore, V. A., Weinstein, J., Gorbsky, G. J., 2002a. Rapid microtubule-independent dynamics of Cdc20 at kinetochores and centrosomes in mammalian cells. J Cell Biol 158 (5), 841–7.

Kallio, M. J., McCleland, M. L., Stukenberg, P. T., Gorbsky, G. J., 2002b. Inhibition of aurora B kinase blocks chromosome segregation, overrides the spindle checkpoint, and perturbs microtubule dynamics in mitosis. Curr Biol 12 (11), 900–5.

Karess, R., 2005. Rod-Zw10-Zwilch: a key player in the spindle checkpoint. Trends Cell Biol 15 (7), 386–92.

Kepler, T. B., Elston, T. C., December 2001. Stochasticity in transcriptional regulation: Origins, consequences, and mathematical representations. Biophysical Journal 81, 3116–3136.

Kienitz, A., Vogel, C., Morales, I., Muller, R., Bastians, H., 2005. Partial down-regulation of MAD1 causes spindle checkpoint inactivation and aneuploidy, but does not confer resistance towards taxol. Oncogene 24 (26), 4301–10.

Kim, M., Kao, G. D., 2005. Newly identified roles for an old guardian: profound deficiency of the mitotic spindle checkpoint protein BubR1 leads to early aging and infertility. Cancer Biol Ther 4 (2), 164–5.

King, E. M. J., van der Sar, S. J. A., Hardwick, K. G., 2007. Mad3 KEN Boxes Mediate both Cdc20 and Mad3 Turnover, and Are Critical for the Spindle Checkpoint. PLoS ONE 2, e342.

King, R. W., Deshaies, R. J., Peters, J. M., Kirschner, M. W., 1996. How proteolysis drives the cell cycle. Science 274 (5293), 1652–9.

King, R. W., Peters, J. M., Tugendreich, S., Rolfe, M., Hieter, P., Kirschner, M. W., 1995. A 20S complex containing CDC27 and CDC16 catalyzes the mitosis-specific conjugation of ubiquitin to cyclin B. Cell 81 (2), 279–88.

Kitamura, K., Maekawa, H., Shimoda, C., 1998. Fission yeast Ste9, a homolog of Hct1/Cdh1 and Fizzy-related, is a novel negative regulator of cell cycle progression during G1-phase. Mol Biol Cell 9 (5), 1065–80.

Kitano, H., 2002a. Computational systems biology. Nature 420 (14), 206–10.

Kitano, H., 2002b. Systems biology: a brief overview. Science 295 (5560), 1662–4.

Kloeden, P. E., Platen, E., 1999a. Numerical solution of stochastic differential equations, corrected third printing. Edition. No. 23. Springer.

Kloeden, P. E., Platen, E., 1999b. Numerical solution of stochastic differential equations. Vol. 23 of Applications of Mathematics. Springer, Berlin.

Kops, G. J. P. L., Kim, Y., Weaver, B. A. A., Mao, Y., McLeod, I., 3rd Yates, J. R., Tagaya, M., Cleveland, D. W., 2005a. ZW10 links mitotic checkpoint signaling to the structural kinetochore. J Cell Biol 169 (1), 49–60.

Kops, G. J. P. L., Weaver, B. A. A., Cleveland, D. W., 2005b. On the road to cancer: aneuploidy and the mitotic checkpoint. Nat Rev Cancer 5 (10), 773–85.

Kramer, E. R., Scheuringer, N., Podtelejnikov, A. V., Mann, M., Peters, J. M., 2000. Mitotic regulation of the APC activator proteins CDC20 and CDH1. Mol Biol Cell 11 (5), 1555–69.

Krasinska, L., de Bettignies, G., Fisher, D., Abrieu, A., Fesquet, D., Morin, N., 2007. Regulation of multiple cell cycle events by Cdc14 homologues in vertebrates. Exp Cell Res 313 (6), 1225–39.

Lampson, M. A., Kapoor, T. M., 2005. The human mitotic checkpoint protein BubR1 regulates chromosome-spindle attachments. Nat Cell Biol 7 (1), 93–8.

Lampson, M. A., Renduchitala, K., Khodjakov, A., Kapoor, T. M., Feb 2004. Correcting improper chromosome-spindle attachments during cell division. Nature Cell Bio. 6, 232 – 237.

Lanzetti, L., Margaria, V., Melander, F., Virgili, L., Lee, M.-H., Bartek, J., Jensen, S., 2007. Regulation of the Rab5 GTPase-activating protein RN-tre by the dual specificity phosphatase Cdc14A in human cells. J Biol Chem 282 (20), 15258–70.

Larsen, N. A., Al-Bassam, J., Wei, R. R., Harrison, S. C., 2007. Structural analysis of Bub3 interactions in the mitotic spindle checkpoint. Proc Natl Acad Sci U S A 104 (4), 1201–6.

Lee, M. S., Spencer, F. A., 2004. Bipolar orientation of chromosomes in Saccharomyces cerevisiae is monitored by Mad1 and Mad2, but not by Mad3. Proc Natl Acad Sci U S A 101 (29), 10655–60.

Lee, S. E., Frenz, L. M., Wells, N. J., Johnson, A. L., Johnston, L. H., 2001. Order of function of the budding-yeast mitotic exit-network proteins Tem1, Cdc15, Mob1, Dbf2, and Cdc5. Curr Biol 11 (10), 784–8.

Lénárt, P., Peters, J.-M., June 2006. Checkpoint activation: Donot get mad too much. Curr Biol. 16 (11), R412–4.

Lenser, T., Hinze, T., Ibrahim, B., Dittrich, P., 2007. Towards evolutionary network reconstruction tools for systems biology. In: Marchiori, E., Moore, J. H., Rajapakse, J. C. (Eds.), EvoBIO. Vol. 4447 of Lecture Notes in Computer Science. Springer, pp. 132–142.

Levine, E., Hwa, T., May 2007. Stochastic fluctuations in metabolic pathways. PNAS 104 (22), 9224–9229.
URL http://dx.doi.org/10.1073/pnas.0610987104

Li, L., Ernsting, B. R., Wishart, M. J., Lohse, D. L., Dixon, J. E., 1997a. A family of putative tumor suppressors is structurally and functionally conserved in humans and yeast. J Biol Chem 272 (47), 29403–6.

Li, R., Murray, A. W., Aug 1991. Feedback control of mitosis in budding yeast. Cell 66 (3), 519–531.

Li, Y., Gorbea, C., Mahaffey, D., Rechsteiner, M., Benezra, R., 1997b. MAD2 associates with the cyclosome/anaphase-promoting complex and inhibits its activity. Proc Natl Acad Sci U S A 94 (23), 12431–6.

Liu, S.-T., Chan, G. K. T., Hittle, J. C., Fujii, G., Lees, E., Yen, T. J., 2003. Human MPS1 kinase is required for mitotic arrest induced by the loss of CENP-E from kinetochores. Mol Biol Cell 14 (4), 1638–51.

Liu, S.-T., Rattner, J. B., Jablonski, S. A., Yen, T. J., 2006. Mapping the assembly pathways that specify formation of the trilaminar kinetochore plates in human cells. J Cell Biol 175 (1), 41–53.

Luo, X., Fang, G., Coldiron, M., Lin, Y., Yu, H., Kirschner, M. W., Wagner, G., 2000a. Structure of the Mad2 spindle assembly checkpoint protein and its interaction with Cdc20. Nat Struct Biol 7 (3), 224–9.

Luo, X., Fang, G., Coldiron, M., Lin, Y., Yu, H., Kirschner, M. W., Wagner, G., 2000b. Structure of the Mad2 spindle assembly checkpoint protein and its interaction with Cdc20. Nat Struct Biol 7 (3), 224–9.

Luo, X., Tang, Z., Rizo, J., Yu, H., 2002. The Mad2 spindle checkpoint protein undergoes similar major conformational changes upon binding to either Mad1 or Cdc20. Mol Cell 9 (1), 59–71.

Luo, X., Tang, Z., Xia, G., Wassmann, K., Matsumoto, T., Rizo, J., Yu, H., 2004. The Mad2 spindle checkpoint protein has two distinct natively folded states. Nat Struct Mol Biol 11 (4), 338–45.

Luo, X., Yu, H., 2005. Purification and assay of Mad2: a two-state inhibitor of anaphase-promoting complex/cyclosome. Methods Enzymol 398, 246–55.

Maiato, H., DeLuca, J., Salmon, E. D., Earnshaw, W. C., 2004. The dynamic kinetochore-microtubule interface. Journal of Cell Science 117, 5461–5477.

Mao, Y., Abrieu, A., Cleveland, D. W., 2003. Activating and silencing the mitotic checkpoint through CENP-E-dependent activation/inactivation of BubR1. Cell 114 (1), 87–98.

Mao, Y., Desai, A., Cleveland, D. W., 2005. Microtubule capture by CENP-E silences BubR1-dependent mitotic checkpoint signaling. J Cell Biol 170 (6), 873–80.

Mapelli, M., Filipp, F. V., Rancati, G., Massimiliano, L., Nezi, L., Stier, G., Hagan, R. S., Confalonieri, S., Piatti, S., Sattler, M., Musacchio, A., 2006. Determinants of conformational dimerization of Mad2 and its inhibition by p31comet. EMBO J 25 (6), 1273–84.

Martin-Lluesma, S., Stucke, V. M., Nigg, E. A., 2002. Role of Hec1 in spindle checkpoint signaling and kinetochore recruitment of Mad1/Mad2. Science 297 (5590), 2267–70.

Martinu, L., Masuda-Robens, J. M., Robertson, S. E., Santy, L. C., Casanova, J. E., Chou, M. M., 2004. The TBC (Tre-2/Bub2/Cdc16) domain protein TRE17 regulates plasma membrane-endosomal trafficking through activation of Arf6. Mol Cell Biol 24 (22), 9752–62.

MATLAB (Matrix Labrotory), 2008. Mathworks: homepage. Retrieved January 20, 2008, from `http://www.mathworks.com/`.

May, K. M., Hardwick, K. G., 2006. The spindle checkpoint. J Cell Sci 119 (Pt 20), 4139–42.

Mayr, E., 1982. The Growth of Biological Thought. Cambridge, MA: Harvard University Press.

Melloy, P. G., Holloway, S. L., 2004. Changes in the localization of the Saccharomyces cerevisiae anaphase-promoting complex upon microtubule depolymerization and spindle checkpoint activation. Genetics 167 (3), 1079–94.

Mendes group at VBI, Kummer group at EML research, 2008. COPASI: homepage. Retrieved January 20, 2008, from `http://www.copasi.org/`.

Meraldi, P., Draviam, V. M., Sorger, P. K., July 2004. Timing and checkpoints in the regulation of mitotic progression. Cell 7 (1), 45–60.

Michel, L., Diaz-Rodriguez, E., Narayan, G., Hernando, E., Murty, V. V. V. S., Benezra, R., 2004. Complete loss of the tumor suppressor MAD2 causes premature cyclin B degradation and mitotic failure in human somatic cells. Proc Natl Acad Sci U S A 101 (13), 4459–64.

Michel, L. S., Liberal, V., Chatterjee, A., Kirchwegger, R., Pasche, B., Gerald, W., Dobles, M., Sorger, P. K., Murty, V. V., Benezra, R., 2001. MAD2 haplo-insufficiency causes premature anaphase and chromosome instability in mammalian cells. Nature 409 (6818), 355–9.

Millband, D. N., Hardwick, K. G., 2002. Fission yeast Mad3p is required for Mad2p to inhibit the anaphase-promoting complex and localizes to kinetochores in a Bub1p-, Bub3p-, and Mph1p-dependent manner. Mol Cell Biol 22 (8), 2728–42.

Minshull, J., Sun, H., Tonks, N. K., Murray, A. W., Nov. 1994. A MAP kinase-dependent spindle assembly checkpoint in Xenopus egg extracts. Cell 79 (3), 475–486.

Mondal, G., Roychoudhury, S., 2003. The spindle assembly checkpoint and its defects in human cancer. Int J Hum Genet 3 (2), 89–97.

Mondal, G., Sengupta, S., Panda, C. K., Gollin, S. M., Saunders, W. S., Roychoudhury, S., 2007a. Overexpression of Cdc20 leads to impairment of the spindle assembly checkpoint and aneuploidization in oral cancer. Carcinogenesis 28 (1), 81–92.

Mondal, G., Sengupta, S., Panda, C. K., Gollin, S. M., Saunders, W. S., Roychoudhury, S., 2007b. Overexpression of Cdc20 leads to impairment of the spindle assembly checkpoint and aneuploidization in oral cancer. Carcinogenesis 28 (1), 81–92.

Moore, J. D., Kirk, J. A., Hunt, T., 2003. Unmasking the S-phase-promoting potential of cyclin B1. Science 300 (5621), 987–90.

Morgan, D. O., 1999. Regulation of the APC and the exit from mitosis. Nature Cell Biology 1, E47–E53.

Morrow, C. J., Tighe, A., Johnson, V. L., Scott, M. I. F., Ditchfield, C., Taylor, S. S., 2005. Bub1 and aurora B cooperate to maintain BubR1-mediated inhibition of APC/CCdc20. J Cell Sci 118 (Pt 16), 3639–52.

Murata, T., Apr. 1989. Petri nets: Properties, analysis and applications. In: Proceedings of the IEEE. pp. 541–580, newsletterInfo: 33Published as Proceedings of the IEEE, volume 77, number 4.

Murata-Hori, M., li Wang, Y., 2002. The kinase activity of aurora B is required for kinetochore-microtubule interactions during mitosis. Curr Biol 12 (11), 894–9.

Musacchio, A., Hardwick, K. G., 2002. The spindle checkpoint: structural insights into dynamic signalling. Nat Rev Mol Cell Biol 3 (10), 731–41.

Musacchio, A., Salmon, E. D., 2007. The spindle-assembly checkpoint in space and time. Nat Rev Mol Cell Biol. 8, 379–393.

Nasmyth, K., 1993. Control of the yeast cell cycle by the cdc28 protein kinase. Curr Opin Cell Biol. 5 (2), 166–79.

Nasmyth, K., 2005. How do so few control so many? Cell 120 (6), 739–46.

Nasmyth, K., Peters, J. M., Uhlmann, F., 2000. Splitting the chromosome: cutting the ties that bind sister chromatids. Science 288 (5470), 1379–85.

Neumann, E., Garcia-Saez, I., DeBonis, S., Wade, R. H., Kozielski, F., Conway, J. F., 2006. Human kinetochore-associated kinesin CENP-E visualized at 17 A resolution bound to microtubules. J Mol Biol 362 (2), 203–11.

Nezi, L., Rancati, G., DeAntoni, A., Pasqualato, S., Piatti, S., Musacchio, A., 2006. Accumulation of Mad2-Cdc20 complex during spindle checkpoint activation requires binding of open and closed conformers of Mad2 in Saccharomyces cerevisiae. J Cell Biol 174 (1), 39–51.

Nicklas, R., Ward, S., Gorbsky, G., Aug 1995. Kinetochore chemistry is sensitive to tension and may link mitotic forces to a cell cycle checkpoint. J Cell Biol. 130 (4), 929–39.

Nicklas, R. B., Jan 1997. How cells get the right chromosomes. Science 275 (5300), 632 – 637.

Núñez, J. A., Marco, R. J. D., 2007. Technology and the foundations of biology. Biological Theory 2 (2), 194199.

Palframan, W. J., Meehl, J. B., Jaspersen, S. L., Winey, M., Murray, A. W., 2006. Anaphase inactivation of the spindle checkpoint. Science 313 (5787), 680–4.

Paliwal, S., Ma, L., Krishnan, J., Levchenko, A., Iglesias, P. A., August 2004. Responding to directional cues: a tale of two cells. IEEE Control Systems Magazine, 77–90.

Papin, J. A., Hunter, T., Palsson, B. O., Subramaniam, S., 2005. Reconstruction of cellular signalling networks and analysis of their properties. Nat Rev Mol Cell Biol 6 (2), 99–111.

Passmore, L. A., 2004a. The anaphase-promoting complex (APC): the sum of its parts? Biochem Soc Trans 32 (Pt 5), 724–7.

Passmore, L. A., 2004b. The anaphase-promoting complex (APC): the sum of its parts? Biochem Soc Trans 32 (Pt 5), 724–7.

Pereira, G., Manson, C., Grindlay, J., Schiebel, E., 2002. Regulation of the Bfa1p-Bub2p complex at spindle pole bodies by the cell cycle phosphatase Cdc14p. J Cell Biol 157 (3), 367–79.

Peters, J.-M., 2002. The anaphase-promoting complex: proteolysis in mitosis and beyond. Mol Cell 9 (5), 931–43.

Peters, J.-M., 2006. The anaphase promoting complex/cyclosome: a machine designed to destroy. Nat Rev Mol Cell Biol 7 (9), 644–56.

Petri, C. A., 1962. Kommunikation mit automaten. Ph. d. thesis., University of Bonn.

Pfleger, C. M., Kirschner, M. W., 2000a. The ken box: an APC recognition signal distinct from the D box targeted by Cdh1. Genes Dev. 14, 655–65.

Pfleger, C. M., Kirschner, M. W., 2000b. The KEN box: an APC recognition signal distinct from the D box targeted by Cdh1. Genes Dev 14 (6), 655–65.

Pfleger, C. M., Lee, E., Kirschner, M. W., 2001. Substrate recognition by the Cdc20 and Cdh1 components of the anaphase-promoting complex. Genes Dev 15 (18), 2396–407.

Pinney, J. W., Westhead, D. R., McConkey, G. A., 2003. Petri Net representations in systems biology. Biochem Soc Trans 31 (Pt 6), 1513–5.

Pinsky, B. A., Biggins, S., 2005. The spindle checkpoint: tension versus attachment. Trends Cell Biol 15 (9), 486–93.

Poddar, A., Stukenberg, P. T., Burke, D. J., 2005. Two complexes of spindle checkpoint proteins containing Cdc20 and Mad2 assemble during mitosis independently of the kinetochore in Saccharomyces cerevisiae. Eukaryot Cell 4 (5), 867–78.

Popper, K., 1935. Logik der Forschung. Schriften zur wissenschaftlichen Weltauffassung VI. Springer Verlag, Wien.

Prinz, S., Hwang, E. S., Visintin, R., Amon, A., 1998. The regulation of Cdc20 proteolysis reveals a role for APC components Cdc23 and Cdc27 during S phase and early mitosis. Curr Biol 8 (13), 750–60.

Qi, W., Yu, H., 2007. KEN-box-dependent degradation of the Bub1 spindle checkpoint kinase by the anaphase-promoting complex/cyclosome. J Biol Chem 282 (6), 3672–9.

Queralt, E., Lehane, C., Novák, B., Uhlmann, F., 2006. Downregulation of PP2A(Cdc55) phosphatase by separase initiates mitotic exit in budding yeast. Cell 125 (4), 719–32.

Raff, J. W., Jeffers, K., Huang, J.-Y., 2002. The roles of Fzy/Cdc20 and Fzr/Cdh1 in regulating the destruction of cyclin B in space and time. J Cell Biol 157 (7), 1139–49.

Rao, C. V., Wolf, D. M., Arkin, A. P., 2002. Control, exploitation and tolerance of intracellular noise. Nature 420 (6912), 231–7.

Reddy, S. K., Rape, M., Margansky, W. A., Kirschner, M. W., April 2007. Ubiquitination by the anaphase-promoting complex drives spindle checkpoint inactivation. Nature 446, 921–925.

Rohn, H., Ibrahim, B., Lenser, T., Hinze, T., Dittrich., P., 2008. Enhancing parameter estimation of biochemical networks by exponentially scaled search steps. In: Marchiori, E., Moore, J. H. (Eds.), Proceedings EvoBIO. Vol. 4973 of Series Lecture Notes in Computer Science. Springer, p. 177187.

Sackmann, A., Heiner, M., Koch, I., 2006. Application of Petri net based analysis techniques to signal transduction pathways. BMC Bioinformatics 7, 482.

Saffery, R., Irvine, D. V., Griffiths, B., Kalitsis, P., Choo, K. H., 2000a. Components of the human spindle checkpoint control mechanism localize specifically to the active centromere on dicentric chromosomes. Hum Genet 107 (4), 376–84.

Saffery, R., Irvine, D. V., Griffiths, B., Wordeman, L., Choo, K. A., 2000b. Human centromeres and neocentromeres show identical distribution pattern of >20 functionally important kinetochore-associated proteins. Hum. Mol. Genet. 9 (2), 175–85.

Schmidt, M., Medema, R. H., 2006. Exploiting the compromised spindle assembly checkpoint function of tumor cells: dawn on the horizon? Cell Cycle 5 (2), 159–63.

Scholey, J. M., Brust-Mascher, I., Mogilner, A., 2003. Cell division. Nature 422 (6933), 746–52.

Schwab, M., Lutum, A. S., Seufert, W., 1997. Yeast Hct1 is a regulator of Clb2 cyclin proteolysis. Cell 90 (4), 683–93.

Sear, R. P., Howard, M., 2006. Modeling dual pathways for the metazoan spindle assembly checkpoint. Proc Natl Acad Sci U S A 103 (45), 16758–63.

Seufert, W., Jentsch, S., Feb 1990. Ubiquitin-conjugating enzymes UBC4 and UBC5 mediate selective degradation of short-lived and abnormal proteins. EMBO J. 9 (2), 543–50.

Shah, J. V., Botvinick, E., Bonday, Z., Furnari, F., Berns, M., Cleveland, D. W., 2004. Dynamics of centromere and kinetochore proteins; implications for checkpoint signaling and silencing. Curr Biol 14 (11), 942–52.

Shannon, K. B., Canman, J. C., Salmon, E. D., 2002. Mad2 and BubR1 function in a single checkpoint pathway that responds to a loss of tension. Mol. Biol. Cell 13, 3706–19.

Sharp-Baker, H., Chen, R. H., 2001. Spindle checkpoint protein Bub1 is required for kinetochore localization of Mad1, Mad2, Bub3, and CENP-E, independently of its kinase activity. J Cell Biol 153 (6), 1239–50.

Shirayama, M., Toth, A., Galova, M., Nasmyth, K., 1999. APC(Cdc20) promotes exit from mitosis by destroying the anaphase inhibitor Pds1 and cyclin Clb5. Nature 402 (6758), 203–7.

Shou, W., Seol, J. H., Shevchenko, A., Baskerville, C., Moazed, D., Chen, Z. W., Jang, J., Shevchenko, A., Charbonneau, H., Deshaies, R. J., 1999. Exit from mitosis is triggered by Tem1-dependent release of the protein phosphatase Cdc14 from nucleolar RENT complex. Cell 97 (2), 233–44.

Sigrist, S. J., Lehner, C. F., 1997. Drosophila fizzy-related down-regulates mitotic cyclins and is required for cell proliferation arrest and entry into endocycles. Cell 90 (4), 671–81.

Sironi, L., Mapelli, M., Knapp, S., Antoni, A. D., Jeang, K.-T., Musacchio, A., 2002. Crystal structure of the tetrameric Mad1-Mad2 core complex: implications of a 'safety belt' binding mechanism for the spindle checkpoint. EMBO J 21 (10), 2496–506.

Sironi, L., Melixetian, M., Faretta, M., Prosperini, E., Helin, K., Musacchio, A., 2001a. Mad2 binding to Mad1 and Cdc20, rather than oligomerization, is required for the spindle checkpoint. EMBO J 20 (22), 6371–82.

Sironi, L., Melixetian, M., Faretta, M., Prosperini, E., Helin, K., Musacchio, A., 2001b. Mad2 binding to Mad1 and Cdc20, rather than oligomerization, is required for the spindle checkpoint. EMBO J 20 (22), 6371–82.

Sklan, E. H., Serrano, R. L., Einav, S., Pfeffer, S. R., Lambright, D. G., Glenn, J. S., 2007. TBC1D20 is a Rab1 GTPase-activating protein that mediates hepatitis C virus replication. J Biol Chem 282 (50), 36354–61.

Sotillo, R., Hernando, E., Diaz-Rodriguez, E., Teruya-Feldstein, J., Cordon-Cardo, C., Lowe, S. W., Benezra, R., 2007. Mad2 overexpression promotes aneuploidy and tumorigenesis in mice. Cancer Cell 11 (1), 9–23.

Starr, D. A., Williams, B. C., Hays, T. S., Goldberg, M. L., 1998. ZW10 helps recruit dynactin and dynein to the kinetochore. J Cell Biol 142 (3), 763–74.

Steggles, L. J., Banks, R., Shaw, O., Wipat, A., 2007. Qualitatively modelling and analysing genetic regulatory networks: a Petri net approach. Bioinformatics 23 (3), 336–43.

Stegmeier, F., Amon, A., 2004. Closing mitosis: the functions of the Cdc14 phosphatase and its regulation. Annu Rev Genet 38, 203–32.

Stegmeier, F., Rape, M., Draviam, V. M., Nalepa, G., Sowa, M. E., Ang, X. L., 3rd McDonald, E. R., Li, M. Z., Hannon, G. J., Sorger, P. K., Kirschner, M. W., Harper, J. W., Elledge, S. J., 2007. Anaphase initiation is regulated by antagonistic ubiquitination and deubiquitination activities. Nature 446 (7138), 876–81.

Stegmeier, F., Visintin, R., Amon, A., 2002. Separase, polo kinase, the kinetochore protein Slk19, and Spo12 function in a network that controls Cdc14 localization during early anaphase. Cell 108 (2), 207–20.

Steuer, R., 2004. Effects of stochasticity in models of the cell cycle: from quantized cycle times to noise-induced oscillations. J Theor Biol 228 (3), 293–301.

Steuer, R., Zhou, C., Kurths, J., 2003. Constructive effects of fluctuations in genetic and biochemical regulatory systems. Biosystems 72 (3), 241–51.

Steuerwald, N., 2005. Meiotic spindle checkpoints for assessment of aneuploid oocytes. Cytogenet Genome Res 111 (3-4), 256–9.

Storn, R., Price, K., 1997. Differential evolution - a simple and efficient heuristic for global optimization over continuous spaces. J. of Global Optimization 11 (4), 341–359.

Stucke, V. M., Baumann, C., Nigg, E. A., 2004. Kinetochore localization and microtubule interaction of the human spindle checkpoint kinase Mps1. Chromosoma 113 (1), 1–15.

Stucke, V. M., Sillje, H. H. W., Arnaud, L., Nigg, E. A., 2002. Human Mps1 kinase is required for the spindle assembly checkpoint but not for centrosome duplication. EMBO J 21 (7), 1723–32.

Su, T. T., Sprenger, F., DiGregorio, P. J., Campbell, S. D., O'Farrell, P. H., 1998. Exit from mitosis in Drosophila syncytial embryos requires proteolysis and cyclin degradation, and is associated with localized dephosphorylation. Genes Dev 12 (10), 1495–503.

Sudakin, V., Chan, G. K., Yen, T. J., Sep 2001. Checkpoint inhibition of the APC/C in hela cells is mediated by a complex of BubR1, Bub3, Cdc20, and Mad2. J Cell Biol 154 (5), 925–936.

Sudakin, V., Ganoth, D., Dahan, A., Heller, H., Hershko, J., Luca, F. C., Ruderman, J. V., Hershko, A., 1995. The cyclosome, a large complex containing cyclin-selective ubiquitin ligase activity, targets cyclins for destruction at the end of mitosis. Mol Biol Cell 6 (2), 185–97.

Sudo, T., Ota, Y., Kotani, S., Nakao, M., Takami, Y., Takeda, S., Saya, H., 2001. Activation of Cdh1-dependent APC is required for G1 cell cycle arrest and DNA damage-induced G2 checkpoint in vertebrate cells. EMBO J 20 (22), 6499–508.

Sullivan, M., Uhlmann, F., 2003. A non-proteolytic function of separase links the onset of anaphase to mitotic exit. Nat Cell Biol 5 (3), 249–54.

Tan, A. L. C., Rida, P. C. G., Surana, U., 2005. Essential tension and constructive destruction: the spindle checkpoint and its regulatory links with mitotic exit. Biochem J 386 (Pt 1), 1–13.

Tanaka, T. U., Rachidi, N., Janke, C., Pereira, G., Galova, M., Schiebel, E., Stark, M. J. R., Nasmyth, K., Feb 2002. Evidence that the Ipl1-Sli15 (Aurora Kinase-INCENP) complex promotes chromosome bi-orientation by altering kinetochore-spindle pole connections. Cell 108 (3), 317–329.

Tang, Z., Bharadwaj, R., Li, B., Yu, H., 2001. Mad2-Independent inhibition of APCCdc20 by the mitotic checkpoint protein BubR1. Dev Cell 1 (2), 227–37.

Tang, Z., Shu, H., Oncel, D., Chen, S., Yu, H., 2004. Phosphorylation of Cdc20 by Bub1 provides a catalytic mechanism for APC/C inhibition by the spindle checkpoint. Mol Cell 16 (3), 387–97.

Taylor, S. S., 1999. Chromosome segregation: dual control ensures fidelity. Curr Biol 9 (15), R562–4.

Taylor, S. S., Ha, E., McKeon, F., 1998a. The human homologue of Bub3 is required for kinetochore localization of Bub1 and a Mad3/Bub1-related protein kinase. J Cell Biol 142 (1), 1–11.

Taylor, S. S., Ha, E., McKeon, F., 1998b. The human homologue of Bub3 is required for kinetochore localization of Bub1 and a Mad3/Bub1-related protein kinase. The Journal of Cell Biology 142, 111.

Taylor, S. S., Hussein, D., Wang, Y., Elderkin, S., Morrow, C. J., 2001. Kinetochore localisation and phosphorylation of the mitotic checkpoint components Bub1 and BubR1 are differentially regulated by spindle events in human cells. J Cell Sci 114 (24), 4385–95.

Taylor, S. S., Scott, M. I. F., Holland, A. J., 2004. The spindle checkpoint: a quality control mechanism which ensures accurate chromosome segregation. Chromosome Res 12 (6), 599–616.

Thornton, B. R., Ng, T. M., Matyskiela, M. E., Carroll, C. W., Morgan, D. O., Toczyski, D. P., 2006. An architectural map of the anaphase-promoting complex. Genes Dev 20 (4), 449–60.

Thorwarth, D., Eschmann, S. M., Paulsen, F., Alber, M., 2005. A kinetic model for dynamic [18F]-Fmiso PET data to analyse tumour hypoxia. Physics in Medicine an d Biology 50, 2209–2224.

Toth, A., Queralt, E., Uhlmann, F., Novák, B., 2007. Mitotic exit in two dimensions. J Theor Biol 248 (3), 560–73.

Townsley, F. M., Aristarkhov, A., Beck, S., Hershko, A., Ruderman, J. V., March 1997. Dominant-negative cyclin-selective ubiquitin carrier protein E2-C/UbcH10 blocks cells in metaphase. Proc. Natl. Acad. Sci. USA 94, 2362–67.

Tyson, J. J., 1991. Modeling the cell division cycle: cdc2 and cyclin interactions. Proc Natl Acad Sci U S A 88 (16), 7328–32.

Uhlmann, F., Lottspeich, F., Nasmyth, K., 1999. Sister-chromatid separation at anaphase onset is promoted by cleavage of the cohesin subunit Scc1. Nature 400 (6739), 37–42.

Vazquez-Novelle, M. D., Esteban, V., Bueno, A., Sacristan, M. P., 2005. Functional homology among human and fission yeast Cdc14 phosphatases. J Biol Chem 280 (32), 29144–50.

VCell, 2008. VCell: homepage. Retrieved January 23, 2008, from `http://www.vcell.org//`.

Vigneron, S., Prieto, S., Bernis, C., Labbe, J.-C., Castro, A., Lorca, T., 2004. Kinetochore localization of spindle checkpoint proteins: who controls whom? Mol Biol Cell 15 (10), 4584–96.

Vink, M., Simonetta, M., Transidico, P., Ferrari, K., Mapelli, M., Antoni, A. D., Massimiliano, L., Ciliberto, A., Faretta, M., Salmon, E. D., Musacchio, A., 2006. In vitro FRAP identifies the minimal requirements for Mad2 kinetochore dynamics. Curr Biol 16 (8), 755–66.

Visintin, R., Hwang, E. S., Amon, A., 1999. Cfi1 prevents premature exit from mitosis by anchoring Cdc14 phosphatase in the nucleolus. Nature 398 (6730), 818–23.

von Bertalanffy, L., 1968. General System Theory: Foundations,Development, Applications. New York: Braziller.

Wang, H., Hu, X., Ding, X., Dou, Z., Yang, Z., Shaw, A. W., Teng, M., Cleveland, D. W., Goldberg, M. L., Niu, L., Yao, X., 2004a. Human zwint-1 specifies localization of zeste white 10 to kinetochores and is essential for mitotic checkpoint signaling. J Biol Chem. 279 (52), 5459054598.

Wang, Q., Liu, T., Fang, Y., Xie, S., Huang, X., Mahmood, R., Ramaswamy, G., Sakamoto, K. M., Darzynkiewicz, Z., Xu, M., Dai, W., 2004b. BUBR1 deficiency results in abnormal megakaryopoiesis. Blood 103 (4), 1278–85.

Wang, X., Babu, J. R., Harden, J. M., Jablonski, S. A., Gazi, M. H., Lingle, W. L., De Groen, P. C., Yen, T. J., Van Deursen, J. M., 2001. The mitotic checkpoint protein hBUB3 and the mRNA export factor hRAE1 interact with GLE2p-binding sequence (GLEBS)-containing proteins. J Biol Chem 276 (28), 26559–67.

Wassmann, K., Liberal, V., Benezra, R., 2003. Mad2 phosphorylation regulates its association with Mad1 and the APC/C. EMBO J 22 (4), 797–806.

Weaver, B. A. A., Cleveland, D. W., 2005. Decoding the links between mitosis, cancer, and chemotherapy: The mitotic checkpoint, adaptation, and cell death. Cancer Cell 8 (1), 7–12.

Weinstein, J., Jacobsen, F. W., Hsu-Chen, J., Wu, T., Baum, L. G., 1994. A novel mammalian protein, p55CDC, present in dividing cells is associated with protein kinase activity and has homology to the Saccharomyces cerevisiae cell division cycle proteins Cdc20 and Cdc4. Mol Cell Biol 14 (5), 3350–63.

Wiener, N., 1948. Cybernetics. Cambridge, MA: MIT Press.

Williams, B. C., Li, Z., Liu, S., Williams, E. V., Leung, G., Yen, T. J., Goldberg, M. L., 2003. Zwilch, a new component of the ZW10/ROD complex required for kinetochore functions. Mol Biol Cell 14 (4), 1379–91.

Wolfe, B. A., McDonald, W. H., 3rd Yates, J. R., Gould, K. L., 2006. Phospho-regulation of the Cdc14/Clp1 phosphatase delays late mitotic events in S. pombe. Dev Cell 11 (3), 423–30.

Xia, G., Luo, X., Habu, T., Rizo, J., Matsumoto, T., Yu, H., 2004. Conformation-specific binding of p31(comet) antagonizes the function of Mad2 in the spindle checkpoint. EMBO J 23 (15), 3133–43.

Yamaguchi, S., Decottignies, A., Nurse, P., 2003. Function of Cdc2p-dependent Bub1p phosphorylation and Bub1p kinase activity in the mitotic and meiotic spindle checkpoint. EMBO J 22 (5), 1075–87.

Yamaguchi, S., Murakami, H., Okayama, H., 1997. A WD repeat protein controls the cell cycle and differentiation by negatively regulating Cdc2/B-type cyclin complexes. Mol Biol Cell 8 (12), 2475–86.

Yamano, H., Gannon, J., Mahbubani, H., Hunt, T., 2004. Cell cycle-regulated recognition of the destruction box of cyclin B by the APC/C in Xenopus egg extracts. Mol Cell 13 (1), 137–47.

Yanagida, M., 2000. Cell cycle mechanisms of sister chromatid separation; roles of Cut1/separin and Cut2/securin. Genes Cells 5 (1), 1–8.

Yang, M., Li, B., Tomchick, D. R., Machius, M., Rizo, J., Yu, H., Luo, X., 2007. p31(comet) Blocks Mad2 Activation through Structural Mimicry. Cell 131 (4), 744–55.

Yao, X., Abrieu, A., Zheng, Y., Sullivan, K. F., Cleveland, D. W., 2000. CENP-E forms a link between attachment of spindle microtubules to kinetochores and the mitotic checkpoint. Nat Cell Biol 2 (8), 484–91.

Yeong, F. M., Lim, H. H., Padmashree, C. G., Surana, U., 2000. Exit from mitosis in budding yeast: biphasic inactivation of the Cdc28-Clb2 mitotic kinase and the role of Cdc20. Mol Cell 5 (3), 501–11.

yong Huang, J., Raff, J. W., 2002. The dynamic localisation of the Drosophila APC/C: evidence for the existence of multiple complexes that perform distinct functions and are differentially localised. J Cell Sci 115 (Pt 14), 2847–56.

Yu, H., 2002. Regulation of APC-Cdc20 by the spindle checkpoint. Curr Opin Cell Biol 14 (6), 706–14.

Yu, H., 2006. Structural activation of Mad2 in the mitotic spindle checkpoint: the two-state Mad2 model versus the Mad2 template model. J Cell Biol 173 (2), 153–7.

Yu, H., 2007. Cdc20: a WD40 activator for a cell cycle degradation machine. Mol Cell 27 (1), 3–16.

Yu, H., King, R., Peters, J., Kirschner, M., Apr 1996. Identification of a novel ubiquitin-conjugating enzyme involved in mitotic cyclin degradation. Curr Biol. 6 (4), 455–66.

Zachariae, W., Schwab, M., Nasmyth, K., Seufert, W., 1998a. Control of cyclin ubiquitination by CDK-regulated binding of Hct1 to the anaphase promoting complex. Science 282 (5394), 1721–4.

Zachariae, W., Shevchenko, A., Andrews, P. D., Ciosk, R., Galova, M., Stark, M. J., Mann, M., Nasmyth, K., 1998b. Mass spectrometric analysis of the anaphase-promoting complex from yeast: identification of a subunit related to cullins. Science 279 (5354), 1216–9.

Zecevic, M., Catling, A. D., Eblen, S. T., Renzi, L., Hittle, J. C., Yen, T. J., Gorbsky, G. J., Weber, M. J., 1998. Active MAP kinase in mitosis: localization at kinetochores and association with the motor protein CENP-E. J Cell Biol 142 (6), 1547–58.

Zhang, Y., Lees, E., 2001a. Identification of an overlapping binding domain on Cdc20 for Mad2 and anaphase-promoting complex: model for spindle checkpoint regulation. Mol Cell Biol 21 (15), 5190–9.

Zhang, Y., Lees, E., 2001b. Identification of an overlapping binding domain on Cdc20 for Mad2 and anaphase-promoting complex: model for spindle checkpoint regulation. Mol Cell Biol 21 (15), 5190–9.

Zhou, Y., Ching, Y.-P., Ng, R. W. M., Jin, D.-Y., 2003. Differential expression, localization and activity of two alternatively spliced isoforms of human APC regulator CDH1. Biochem J 374 (Pt 2), 349–58.

Über den Autor

Lebenslauf und wissenschaftlicher Werdegang

Name: Bashar Ibrahim

Geburtsdatum: 28. August 1976

Geburtsort: Mosul, Irak

E-Mail: bininua@yahoo.com

Ausbildung

- Friedrich Schiller Universität Jena, Deutschland.
  Doktorand, Bioinformatik, April 2005 - September 2008
  Finanzierung: Deutscher Akademischer Austauschdienst (DAAD).
- Universität Kopenhagen, Dänemark.
  Bio-Math Summer School, August $3^{\text{rd}} - 16^{\text{th}}$, 2008.
  Finanzierung: Marie Curie
- Universität Trento, Italien.
  Computational and Systems Biology course (CoSBi), 10.-14. März 2008.
  Finanzierung: Microsoft research.
- Universität Graz, Österreich.
  School in Biomedical Modeling, 22. Juli bis 4. August 2007.
  Finanzierung: Marie Curie.
- RICAM & Johannes Kepler Universität, Linz, Österreich.
  EMS School Mathematics in Molecular Cell Biology, 9.-23. September 2006.
  Finanzierung: Lize Universität.
- Universität Southampton, Southampton, Großbritannien.
  School in Complexity Science, 9. März bis 12. April 2006.
  Finanzierung: EPSRC Großbritannien.
- InterDaF e.V. am Herder-Institut der Universität Leipzig, Deutschland.
  Sprachintensivkurs Deutsch, 4. Oktober 2004 bis 31. März 2005. Finanzierung: DAAD.
- Universität Mosul, Mosul, Irak.
  Master of Science (M.Sc.) mit Auszeichnung in Angewandter Mathematik, Juli 2000.
- Universität Mosul, Mosul, Irak.
  Bachelor of Science (B.Sc.) mit Auszeichnung in Mathematik, 1998.

Stipendium

Deutscher Akademischer Austauschdienst **Oktober 2004 - September 2008**

Forschungsinteressen

Systembiologie, Modellierung und Simulation, Spindelkontrollpunkt-Mechanismus, Endphase der Mitose, ODEs, SDEs, Reaktions-Diffusions-Systeme und Optimierungstechniken.

Akademische Erfahrungen

◇ Friedrich Schiller Universität Jena, Deutschland

-*Mitglied der Forschungsgruppe* **seit April 2005**

Biosystemanalyse. Einschließlich Promotion.

Leibniz-Institut für Altersforschung, Jena, Deutschland.

-*Forschungsprojekt*

Zusammenarbeit mit Humanbiologen, Modellierung des Zellzyklus.

◇ Fakultät der Wissenschaften, Al-Byda, Libyen.

Lehrtätigkeit **Oktober 2002 - Oktober 2004**

Beteiligung an Kursen im Grundstudium in gemeinschaftlicher Verantwortung für Vorlesung, Hausarbeiten und Bewertung.

◇ Fakultät für Mathematik und Informatik, Mosul, Irak.

Lehrtätigkeit **Oktober 2000 - Oktober 2002**

Beteiligung an Kursen im Grundstudium in gemeinschaftlicher Verantwortung für Vorlesung, Hausarbeiten und Bewertung.

Lehrerfahrung

Systembiologie des Zellzyklus

Beteiligung an der Betreuung von Diplomarbeiten

◇ Maiko Lohel, MSc. Bioinformatik (2008), Friedrich Schiller Universität Jena.

◇ Gerd Gruenert, MSc. Bioinformatik (2008), Friedrich Schiller Universität Jena.

◇ Margriet Palm, Engineer (2008), Eindhoven University of Technology, Niederlande.

◇ Sarah Werner, MSc. Bioinformatik (2007), Friedrich Schiller Universität Jena.

Veröffentlichungen

Peer-reviewed articles in international journals

◇ Ibrahim, B., Dittrich, P., Diekmann, S., Schmitt, E. Mad2 binding is not sufficient for complete Cdc20 sequestering (an *in-silico* study). BioPhy Chem. Journal, 134, 93-100., 2008.

◇ Ibrahim, B., Diekmann, S., Schmitt, E., Dittrich, P. *In-silico* Modeling of the Mitotic Spindle Assembly Checkpoint. PLoS ONE Journal, 3(2): e1555, 2008.

◇ Ibrahim, B., Schmitt, E., Dittrich, D., Diekmann, D. *In-silico* study of kinetochore control, amplification, and inhibition effects in MCC assembly. BioSystems Journal, 2008. (In press)

◇ Ibrahim, B, Dittrich, P., Diekmann, S., Schmitt, E. Stochastic effects in a compartmental model for mitotic checkpoint regulation. Journal of Integrative Bioinformatics, 4(3):66, 2007.

Peer-reviewed full articles in proceedings

◇ Rohn, H., Ibrahim, B., Lenser, T., Hinze, T., Dittrich., Enhancing Parameter Estimation of Biochemical Networks by Exponentially Scaled Search Steps. In: E. Marchiori and J. H. Moore (Eds.), Proceedings of the Sixth European Conference on Evolutionary Computation, Machine Learning and Data Mining in Bioinformatics (EvoBIO), Napoli, LNCS 4973, pp. 177-187, Springer Verlag, 2008.

◇ Lenser, T., Hinze, T., Ibrahim, B., Dittrich, P., Towards evolutionary network reconstruction tools for systems biology. In: E. Marchiori, J.H. Moore, J.C. Rajapakse (Eds.), Proceedings of the Fifth European Conference on Evolutionary Computation, Machine Learning and Data Mining in Bioinformatics (EvoBIO), Valencia, LNCS 4447, pp 132-142, Springer Verlag, 2007.

Posters

◇ Ibrahim, B., Schmitt, E., Diekmann, S., Dittrich, P. The "Convey" and the "Dissociation" model: Meta- to Anaphase Transition Control, CoSBi, March 10-14, 2008, Trento, Italy.

◇ Ibrahim, B., Schmitt, E., Diekmann, S., Dittrich, P. Modeling Mitosis Transition Controls, ECCS, October 1-5, 2007, Dresden, Germany.

◇ Dittrich, P., Hinze, T., Ibrahim, B., Lenser, T., Matsumaru, N. Hierarchically Evolvable Components for Complex Systems: Biologically Inspired Algorithmic Design ECCS, October 1-5, 2007, Dresden, Germany.

◇ Ibrahim, B., Schmitt, E., Diekmann, S., Dittrich, P. Neither Mad2 nor $p31^{comet}$ alone are sufficient for ^{M}SAC regulation. European Life Scientist Organization "ELSO", September 1-4, 2007, Dresden, Germany.

◇ Ibrahim, B., Schmitt, E., Diekmann, S., Dittrich, P. Modeling and simulation of the Mitotic Spindle Mechanism. Gold Springer Harbor Laboratory Computational Cell Biology, March 6-9, 2007, New York, USA.

Teilnahme an Konferenzen und Tagungen

2007

◇ European Life Scientist Organization “ELSO” , September 1-4, 2007, Dresden, Germany.

◇ Data Mining and Modeling in Systems Biology Workshop and Spring School, March 15-16, 2007, Jena, Germany.

2006

◇ Applications of Semantic Technologies Workshop, October 6, 2006, Dresden, Germany.

◇ Organic Computing Workshop, October 5, 2006, Dresden, Germany.

◇ International BCB - Workshop on Computational Proteomics, August 24-25, 2006, Berlin, Germany.

◇ 7^{th} German Workshop on Artificial Life “GWAL7”, July 26-28, 2006, Jena , Germany.

◇ International Conference on Systems Biology of Mammalian Cells “SBMC”, July 12-14 2006, Heidelberg, Germany.

2005

◇ International BCB - Workshop on Machine Learning in Bioinformatics, October 10, 2005, Berlin, Germany.

About the Author

Scientific Curriculum Vitae

Name: Bashar Ibrahim

Date of Birth: August 28, 1976

Place of Birth: Mosul, Iraq

Email: bininua@yahoo.com

Education

- Friedrich Schiller University Jena, Germany.
  Ph.D. Candidate, Bioinformatics, April 2005 - September 2008
  Financially supported by the German Academic Exchange Service (DAAD).
- University of Copenhagen, Denmark.
  Bio-Math Summer School, August $3^{rd} - 16^{th}$, 2008.
  Financially supported by Marie Curie
- University of Trento, Italy.
  Computational and Systems Biology course (CoSBi), March 10^{th}-14^{th}, 2008.
  Financially supported by Microsoft research.
- University of Graz, Austria.
  School in Biomedical Modeling, 22^{nd} July to August 4^{th}, 2007.
  Financially supported by Marie Curie
- RICAM & Johannes Kepler University, Linz, Austria.
  EMS School Mathematics in Molecular Cell Biology, September 9^{th}-23^{rd}, 2006.
  Financially supported by Lize University
- University of Southampton, Southampton, UK.
  School in Complexity Science, 9^{th} March to April 12^{th}, 2006.
  Financially supported by EPSRC UK
- InterDaF e.V. am Herder-Institut der Universität Leipzig, Germany.
  Intensive course in German language and culture, 4^{th} October 2004 to March 31^{th}, 2005. Financially supported by the DAAD
- University of Mosul, Mosul, Iraq.
  Master of Science (M.Sc.) with honor degree in Applied Mathematics, July 2000.
- University of Mosul, Mosul, Iraq.
  Bachelor of Science (B.Sc.) with honor degree in Mathematics, 1998.

Awarded Fellow

German Academic Exchange Service **October 2004 - September 2008**

Research Interests

Systems biology, modeling and simulation, spindle assembly checkpoint, exit from mitosis, ODEs, SDEs, reaction-diffusion system, and optimization techniques.

Academic Experience

◇ Friedrich Schiller University Jena, Germany

-Research group member **April, 2005 - present**

Bio Systems Analysis Group. Includes current Ph.D. research.

Leibniz Institute for Age Research"FLI"-Molecular Biology Group, Jena, Germany.

-Research Project

Collaboration research with human biology problems, modeling cell cycle.

◇ Faculty of Science, Al Byda, Libya.

Teaching Assistance **October, 2002 - October, 2004**

Co-taught undergraduate level courses. Shared responsibility for lectures, exams, homework assignments, and grades.

◇ Faculty of Mathematics and Computer Science, Mosul, Iraq.

Teaching Assistance **October, 2000 - October, 2002**

Co-taught undergraduate level course. Shared responsibility for lectures, exams, homework assignments, and grades.

Teaching

Systems Biology of the Cell Cycle

Thesis advisor or assist advisor

◇ Maiko Lohel, MSc. Bioinformatics (2008), Friedrich Schiller University Jena.

◇ Gerd Gruenert, MSc. Bioinformatics (2008), Friedrich Schiller University Jena.

◇ Margriet Palm, Engineer (2008), Eindhoven University of Technology, Holland.

◇ Sarah Werner, MSc. Bioinformatics (2007), Friedrich Schiller University Jena.

Publications

Peer-reviewed articles in international journals

◇ Ibrahim, B., Dittrich, P., Diekmann, S., Schmitt, E. Mad2 binding is not sufficient for complete Cdc20 sequestering (an *in-silico* study). BioPhy Chem. Journal, 134, 93-100., 2008.

◇ Ibrahim, B., Diekmann, S., Schmitt, E., Dittrich, P. *In-silico* Modeling of the Mitotic Spindle Assembly Checkpoint. PLoS ONE Journal, 3(2): e1555, 2008.

◇ Ibrahim, B., Schmitt, E., Dittrich, D., Diekmann, D. *In-silico* study of kinetochore control, amplification, and inhibition effects in MCC assembly. BioSystems Journal, 2008. (In press)

◇ Ibrahim, B, Dittrich, P., Diekmann, S., Schmitt, E. Stochastic effects in a compartmental model for mitotic checkpoint regulation. Journal of Integrative Bioinformatics, 4(3):66, 2007.

Peer-reviewed full articles in proceedings

◇ Rohn, H., Ibrahim, B., Lenser, T., Hinze, T., Dittrich., Enhancing Parameter Estimation of Biochemical Networks by Exponentially Scaled Search Steps. In: E. Marchiori and J. H. Moore (Eds.), Proceedings of the Sixth European Conference on Evolutionary Computation, Machine Learning and Data Mining in Bioinformatics (EvoBIO), Napoli, LNCS 4973, pp. 177-187, Springer Verlag, 2008.

◇ Lenser, T., Hinze, T., Ibrahim, B., Dittrich, P., Towards evolutionary network reconstruction tools for systems biology. In: E. Marchiori, J.H. Moore, J.C. Rajapakse (Eds.), Proceedings of the Fifth European Conference on Evolutionary Computation, Machine Learning and Data Mining in Bioinformatics (EvoBIO), Valencia, LNCS 4447, pp 132-142, Springer Verlag, 2007.

Posters

◇ Ibrahim, B., Schmitt, E., Diekmann, S., Dittrich, P. The "Convey" and the "Dissociation" model: Meta- to Anaphase Transition Control, CoSBi, March 10-14, 2008, Trento, Italy.

◇ Ibrahim, B., Schmitt, E., Diekmann, S., Dittrich, P. The "Convey" and the "Dissociation" model: Meta- to Anaphase Transition Control, CoSBi, March 10-14, 2008, Trento, Italy.

◇ Ibrahim, B., Schmitt, E., Diekmann, S., Dittrich, P. Modeling Mitosis Transition Controls, ECCS, October 1-5, 2007, Dresden, Germany.

◇ Dittrich, P., Hinze, T., Ibrahim, B., Lenser, T., Matsumaru, N. Hierarchically Evolvable Components for Complex Systems: Biologically Inspired Algorithmic Design ECCS, October 1-5, 2007, Dresden, Germany.

◇ Ibrahim, B., Schmitt, E., Diekmann, S., Dittrich, P. Neither Mad2 nor $p31^{comet}$ alone are sufficient for ^{M}SAC regulation. European Life Scientist Organization "ELSO", September 1-4, 2007, Dresden, Germany.

◇ Ibrahim, B., Schmitt, E., Diekmann, S., Dittrich, P. Modeling and simulation of the Mitotic Spindle Mechanism. Gold Springer Harbor Laboratory Computational Cell Biology, March 6-9, 2007, New York, USA.

Conferences and Workshops

2007

- European Life Scientist Organization "ELSO" , September 1-4, 2007, Dresden, Germany.
- Data Mining and Modeling in Systems Biology Workshop and Spring School, March 15-16, 2007, Jena, Germany.

2006

- Applications of Semantic Technologies Workshop, October 6, 2006, Dresden, Germany.
- Organic Computing Workshop, October 5, 2006, Dresden, Germany.
- International BCB - Workshop on Computational Proteomics, August 24-25, 2006, Berlin, Germany.
- 7^{th} German Workshop on Artificial Life "GWAL7", July 26-28, 2006, Jena , Germany.
- International Conference on Systems Biology of Mammalian Cells "SBMC", July 12-14 2006, Heidelberg, Germany.

2005

- International BCB - Workshop on Machine Learning in Bioinformatics, October 10, 2005, Berlin, Germany.

Erklärung

Ich erkläre, da ich die vorliegende Arbeit selbständig und nur unter Verwendung der angegebenen Quellen und Hilfsmittel angefertigt habe.

Bashar Ibrahim
Jena, 14. Mai 2008